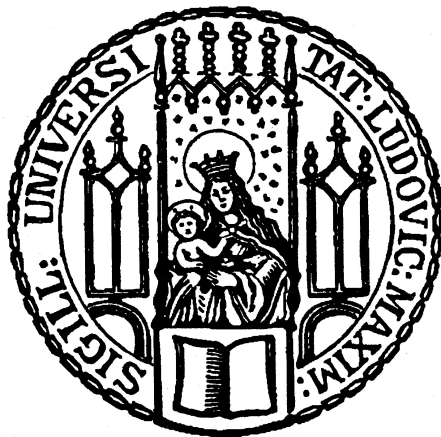# The persistence of memory

The effect of spaced training on memory and neuronal ensemble stability

ANNET GLAS

Dissertation der
Graduate School of Systemic Neurosciences
der Ludwig-Maximilians-Universität München

February 2021

Wetenschap is topsport.

— Cees Glas

ABSTRACT

Distributing learning in time has the remarkable ability to enhance memory in a wide range of species and behavioral paradigms, a phenomenon termed the spacing effect. An extensive body of scientific work provides insight into the molecular and cellular processes that underlie the spacing effect. However, it is unclear how trial spacing alters the activity of the neuronal populations that store a specific memory. With my work presented in this doctoral dissertation, I explored the relationship between trial spacing, memory strength, and the pattern of *in vivo* neuronal activity. To achieve this aim, I executed two initial studies to address two outstanding methodological concerns.

In the first study, I describe two nutritional restriction methods that balance mouse well-being and behavioral performance on an operant conditioning task. Nutritional restriction can be achieved by either food or fluid restriction and is typically necessary to ensure task engagement in mice. However, these procedures can have detrimental effects on mouse welfare if not executed diligently. I monitored the the effect of food or water restriction on mouse welfare as well as performance on a head-fixed two-choice visual discrimination task. In this study, both restriction regimen resulted in similar maximum learning performance while mouse discomfort was typically sub-threshold, providing a blueprint to the wider neuroscientific community to carry out similar experiments[1].

In the second study, I compare a novel *in vivo* microscopy technique with the current golden standard for *in vivo* imaging of individual neurons, which is two-photon microscopy. Imaging using a miniaturized epifluorescence microscope is an efficient and effective approach to image hundreds of neurons while a mouse is engaged in a freely moving behavioral task, but does not achieve the same lateral and axial resolution as two-photon imaging. I performed *in vivo* calcium imaging of mouse primary visual cortex neurons expressing genetically encoded calcium indicators using both microscopy techniques while mice were presented with drifting gratings. I demonstrated that the response properties and tuning features of mouse visual cortex neurons to gratings of different orientations were quantitatively comparable in spite of qualitative differences between the two imaging methods[2].

In the third and main study, I explore whether trial spacing affects memory strength and *in vivo* activity of a population of individual neocortical neurons. I addressed this question by examining two non-mutually exclusive hypotheses. Trial spacing could enhance the selective strengthening of the connections between neurons that store a preexisting memory. This would stabilize this neuronal ensemble, which would allow for more precise ensemble reactivation and thereby more effective memory retrieval. Alternatively, trial spacing could af-

fect the recruitment of additional neurons that store new information from subsequent trials. This would increase the size of the neuronal ensemble, which would make the stored memory more resilient to destabilization. To explore these hypotheses, I trained mice on an everyday memory task, a delayed matching-to-place task that instilled episodic-like memories. Trial spacing promoted memory retrieval, yet surprisingly impaired memory encoding. Simultaneously, I measured neuronal activity using a miniaturized microscope in the dorsomedial prefrontal cortex, a neocortical structure that stored these memories as evidenced by the amnesic effect of chemogenetic inhibition of the dorsomedial prefrontal cortex during training. Trial spacing promoted reactivation of the neuronal ensemble but did not affect the size of the neuronal ensemble, thereby providing the first direct observation of the effect of trial spacing on the activity of neurons in the intact mammalian brain.

In summary, the work presented in this doctoral dissertation used modern neuroscientific methods to study whether altered neuronal ensemble characteristics underlie the spacing effect, a phenomenon that was first described over a century ago.

CONTENTS

1

INTRODUCTION

Twenty two thousand eight hundred. An estimate of the number of hours an average doctoral candidate has spent learning in some form of classroom. If the purpose of education is to provide us with information that we will remember for the rest of our lives, we would hope that nearly twenty three thousand hours of learning turns us into walking encyclopedias. It does not. The reason is that memory is fascinatingly and frustratingly malleable. One piece of information can be acquired, stored, retrieved, updated, integrated, and seemingly lost only to resurface years later. If memory is so complex, is there a simple thing we could do to enhance it? Yes we can. In this doctoral dissertation I explore the neuronal foundations of the spacing effect, the longstanding observation that distributing learning over time strengthens memory in many contexts. I describe experiments that interrupt behavioral training of mice with the duration of an average lunch break and find that this simple manipulation strongly affects neuronal activity in a task-relevant brain area, the prefrontal cortex.

1.1   ON MEMORY ENHANCEMENT

1.1.1   *What is memory? Establishing sign posts and guard rails*

When surgeons removed both hippocampi of epilepsy patient H.M. in an attempt to relieve his seizures[3], his memory was severely compromised. H.M. was no longer able to acquire new declarative memories, e.g. information shared in a recent conversation, but could acquire new non-declarative memories, e.g. the skill to copy a complex figure. The descriptions of patient H.M. by Brenda Milner established a link between specific brain areas and specific memories. Since the 1950s, significant progress has been made in the understanding of the molecular, cellular, and circuit mechanisms that form the physical substrate of memory (for review see [4]). In parallel to the tens of thousands of studies on memory in general, a broad body of work has tested whether these mechanisms underlie the spacing effect, the observation that memory is strengthened by temporally distributed training[5]. This introduction will focus on those mechanisms that mediate both i) memory in general and ii) the memory-enhancing effect of spaced learning in particular. As such, its emphasis will mostly be on findings obtained in model organisms[6]. This will come at the cost of a thorough discussion of i) processes that mediate memory in general but have not (yet) been described to be altered by spaced learning and ii) findings on the spacing effect obtained in human subjects.

1.1.2   *What is memory? Key observations in synapses, cells, and circuits*

There is general scientific consensus that memories are stored as altered strength of a select subset of synaptic connections on specific neurons[7,8]. Within this framework, memory involves three main processes: encoding, consolidation, and retrieval (**Fig. 1**)[9,10]. During memory encoding (i.e. learning), a stimulus evokes a distinct neuronal firing pattern and creates an initial representation of the event. During memory consolidation, this representation is reinforced by synaptic plasticity, i.e. selective functional and structural alteration of the connectivity between the neurons that were activated during encoding. This process stores a representation of the memory in a defined neuronal population termed the neuronal ensemble. During memory retrieval, a relevant stimulus triggers reactivation of a pattern of neuronal firing that is reminiscent of the pattern during encoding. The distinct functional (i.e. molecular) and structural (i.e. morphological) changes that take place during encoding, consolidation, and retrieval are covered in more detail in the remainder of this chapter.
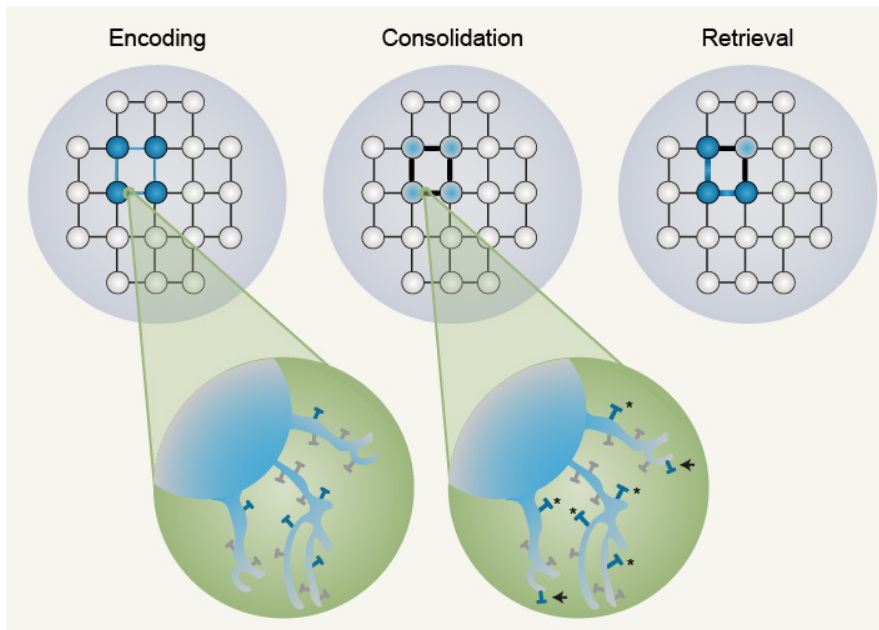
Figure 1 | Schematic of memory encoding, consolidation, and retrieval. During memory encoding (top left), a subset of synaptic connections (blue lines) on a subset of neurons (blue circles) becomes active. On pyramidal neurons, the post-synaptic compartments of synaptic connections typically reside on dendritic protrusions named spines (T-shapes; bottom left). During consolidation (top middle), functional and structural mechanisms can strengthen the synaptic connectivity within the subset of previously activated neurons (heavy black lines connecting grey-blue circles), termed the neuronal ensemble. The structural changes can involve growth of pre-existing spines (black asterisks) and sprouting of new spines (black arrows; bottom right). The altered synaptic connectivity is believed to be the physical substrate of a stored memory. During memory retrieval (top right), the neuronal ensemble reactivates in a pattern reminiscent of that observed during encoding (blue circles and lines).

One means to encode a memory is long-term potentiation (LTP) of certain synaptic connections, which alters the efficiency of synaptic transmission. LTP was first observed by Bliss & Lømo[11], who repetitively stimulated the perforant path, the synaptic input to the dentate gyrus in the hippocampal formation, and recorded the population response in the dentate gyrus. This stimulation produced a long-term increase in the population excitatory post-synaptic potential. LTP was later observed between pairs of neurons in rat hippocampal slices[12].

The molecular post-synaptic processes that underlie LTP can be subdivided into an early and a late phase (**Fig. 2**)[4,13]. The early phase of LTP ensures initial strengthening of pre-existing connections that were activated by a stimulus. During this process, activation of glutamatergic neurotransmitter receptors results in calcium-mediated activation of second messengers including calmodulin and Ca^{2+}/calmodulin-dependent protein kinase II (CaMKII)[14]. In turn, CaMKII signaling results in trafficking of pre-existing α-amino-3-hydroxy-5-methyl-4-isoxazolepropionic acid receptor (AMPAR) subunits from internal

stores to the synaptic membrane[15]. The first evidence that AMPAR distribution was altered by synaptic stimulation came from a study in which the fluorescent label green fluorescent protein (GFP) was attached to the AMPAR subunit GluR1[16]. Electrical stimulation of neurons that expressed GluR1-GFP resulted in delivery of AMPARs to the synaptic membrane[16]. In short, the early phase of LTP culminates in AMPAR insertion into the synapse, which enhances synaptic transmission between the neurons that were activated during memory encoding.
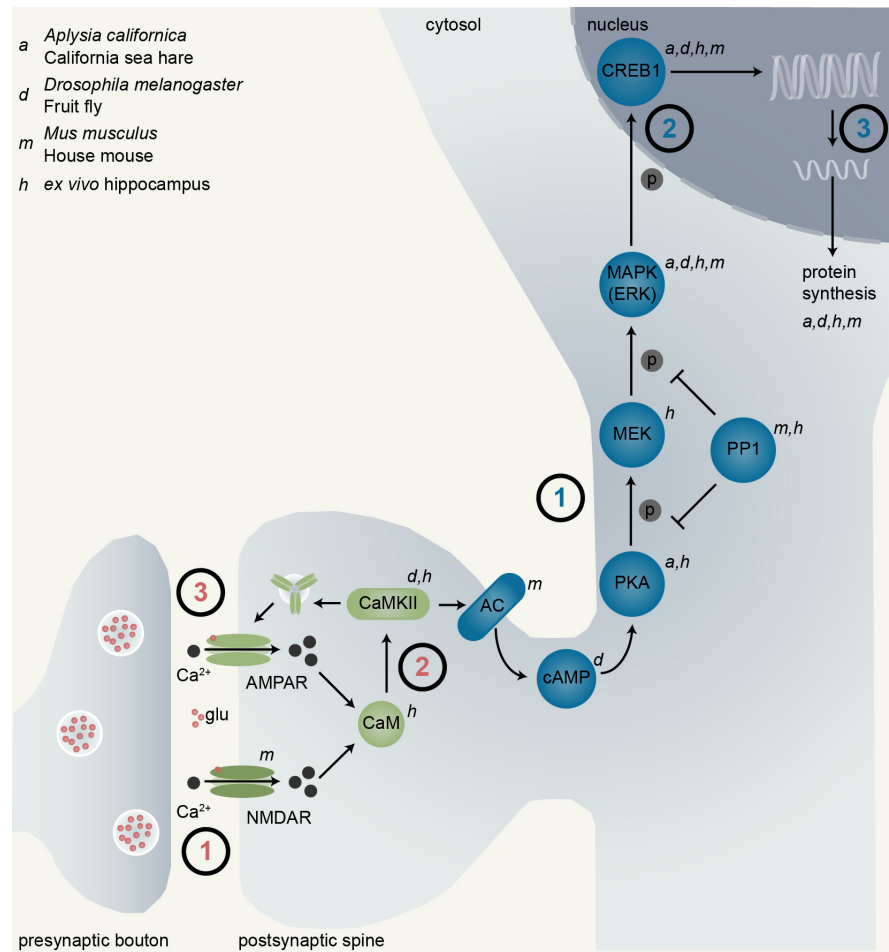
Figure 2 | Schematic of a post-synaptic intracellular signaling pathway that can induce long-term potentiation. Long-term potentiation depends on physiological changes in the post-synaptic neuron that result in increased synaptic transmission efficacy. Processes required for early phase LTP (red numbers) include neurotransmitter receptor activation (1), CaMKII activation (2), and AMPAR insertion (3). Additional processes required for late phase LTP (blue numbers) include activation of adenylyl cyclase and the MAPK pathway (1), activation of nuclear transcription factors, e.g. CREB1 (2), and expression of specific genes (3). Signaling molecules whose functioning has been described to mediate the spacing effect in the California sea hare (*Aplysia californica; a*), fruit fly (*Drosophila melanogaster; d*), house mouse (*Mus musculus; m*), and *ex vivo* slice preparations of the rodent hippocampus (*h*) are indicated and will be discussed in more detail in section 1.4.

The late phase of LTP enables long-term storage of memories by strengthening specific synaptic connections. A key hallmark of late phase LTP is that it requires synthesis of certain proteins (**Fig. 2**), as evidenced by a study that pharmacologically blocked transcription immediately after hippocampal stimulation and thereby prevented late LTP[17]. The signaling pathway that ultimately induces protein synthesis can be subdivided into four key intermediate steps. First, CaMKII activates adenylyl cyclase, an enzyme that converts ATP into cyclic adenosine monophosphate (cAMP). Second, cAMP recruits and activates kinases including protein kinase A (PKA), which triggers a molecular signaling cascade that ultimately results in mitogen-activated protein kinase (MAPK) activation[18]. Third, phosphorylated MAPK translocates to the nucleus and activates a series of transcription factors. One of these transcription factors is cAMP response element binding protein 1 (CREB1)[19], which binds to CREB1 response elements in the promoters of target genes. Fourth, CREB1-mediated protein synthesis results in differential expression of a wide variety of proteins[20]. These include a subset of transcription factors called immediate early genes, such as *c-Fos* and *Arc*, as well as genes that regulate experience-dependent cytoskeletal remodeling[20]. This final step in the late phase of LTP thereby links molecular alterations to morphological alterations that support long-term memory storage.

Late phase LTP modifies the morphology of dendritic spines, structures on pyramidal neurons that typically house an excitatory synapse. There are two classes of activity-dependent dendritic spine structural changes: sprouting of new dendritic spines or remodeling of pre-existing dendritic spines. In a seminal experiment, electrical stimulation of the hippocampal circuit resulted in emergence of new spines on the postsynaptic dendrite[21]. Furthermore, releasing glutamate near the spine head, thereby chemically stimulating the synapse, resulted in rapid growth of pre-existing small spines near the stimulation site[22]. Persistence of a subset of these structural changes for an extended period of time represents a morphological basis for long-term memory storage[23,24]. For example, certain new dendritic spines in the mouse visual cortex that were formed in response to monocular deprivation stabilize and survive beyond the deprivation period[25]. Conversely, shrinking recently potentiated spines disrupted memory, providing additional evidence that storage of memory depends on spine remodeling[26]. So far, the reviewed studies reveal that a synaptic signal can bring about parallel molecular and morphological changes that consolidate the memory and ensure stable, long-term memory storage.

For certain declarative memories, an additional consolidation phase takes place[27]. During a reorganization process termed systems consolidation[28], declarative memories that were initially stored in the hippocampus become less dependent on hippocampal activity over time. This insight was first affirmed by pioneering work by Milner[29], who described that hippocampal lesions lead to impaired encoding and retrieval of recent but not remote declarative memories.

If these previously hippocampus-dependent memories can still be retrieved, where do they reside in the brain? Generally, initially hippocampal-dependent memories transform and become integrated into neocortical networks. For example, one study described that remote spatial memories depended on prefrontal activity, while they initially depended on the hippocampal activity[30]. Furthermore, inhibition of the hippocampal projection to the prefrontal cortex disrupted remote but not recent fear memory[31], suggesting that associative memories likewise undergo systems consolidation.

Multiple lines of evidence suggest that systems consolidation primary occurs during slow-wave sleep[32]. During this phase, temporal firing sequences that were present during specific awake experiences can be replayed in both the neocortex and hippocampus in a coordinated fashion[33]. This finding indicates that simultaneous neocortical and hippocampal reactivation during slow-wave sleep contributes to systems consolidation. As such, systems consolidation stores a declarative memory in neuronal circuits with arguably more storage capacity than the hippocampus.

Once a memory is consolidated and stored, how can it be retrieved? Memory retrieval occurs when animals respond to certain cues based on previous experiences, but the interim chain of events remains largely unclear. What is apparent is that the pattern of neuronal activity during retrieval reactivates in a manner that mimics that generated during encoding[34]. Stronger memory retrieval correlated with an increased number of reactivated neurons that were originally activated during memory encoding[35]. A recent study established a causal link between neuronal reactivation and memory retrieval. Optogenetic activation of the specific subset of neurons that was active during learning resulted in memory retrieval in a novel context[36]. These findings indicate that reactivation of the neuronal ensemble that was active during memory encoding results in retrieval of a specific memory.

These studies, which span decades and represent merely the tip of the iceberg of memory research, establish a framework of how memories are encoded, consolidated, and retrieved. In this framework, a signal activates a subset of neurons that initially encode the memory. During memory consolidation, a signaling cascade ultimately alters gene expression and synaptic morphology and the memory is within a neuronal ensemble. Memory retrieval occurs when the neuronal ensemble reactivates in a pattern reminiscent of that during encoding. The efficacy with which these processes occur can govern how persistent memory is, which is the focal point of this doctoral dissertation.

1.1.3   *Interventions that enhance memory*

Since memory is vital for effective everyday functioning, strategies that can strengthen memory are of great interest. As such, the overarching aim of this doctoral dissertation is to study the neurobiological underpinnings of memory enhancement. Interventions that have

the potential to improve memory can be subdivided into electrical, chemical, and behavioral interventions (**Fig. 3**). The neurological underpinnings of certain behavioral interventions have been extensively studied. For example, both sleep and training using cognitive schemas can enhance memory, which has been attributed to increased systems consolidation[37,38]. These two examples will be discussed briefly below to provide a sense of how behavioral strategies can affect neuronal processing to bring about memory enhancement before taking a deep dive into the literature concerning the spacing effect.

Both chemical and electrical stimulation during sleep have been observed to further enhance memory consolidation[39,40]. Re-exposing individuals during slow-wave sleep with odors that were presented during learning activated the hippocampus and enhanced consolidation of hippocampus-dependent memories[40]. Furthermore, transcranial application of slow oscillating potentials to the frontal cortex of humans during slow-wave sleep increased the retention of hippocampus-dependent declarative memories[39]. These findings indicate that the memory consolidation during sleep, a physiological state that is vital for (systems) consolidation, can be augmented by external interventions.

A second context in which systems consolidation can be enhanced is when new knowledge is integrated into a "schema", a structure that organizes relevant prior knowledge[38]. Not every collection of information can function as a schema, as illustrated by the following experiment[41]. If subjects viewed the first part of a movie in the temporally correct order, their recognition of frames of the second part of the movie on the next day was improved[41]. Conversely, if the first part of the movie was temporally scrambled, recognition of the second part was reduced, suggesting that only structured prior knowledge could enhance memory formation.

Apart from human studies, schema learning has been studied using an elegant paradigm in rats. A schema of consistent paired-associates was created by training rats on a flavor-place association task across weeks[42]. A memory of an additional flavor-place association could be acquired within one trial if the flavor-place mapping was consistent, but not if the mapping changed on subsequent sessions. The new schema-dependent memory could be recalled if the hippocampus was lesioned 48 hours but not 3 hours post-training, which suggests that the memory is only initially hippocampus-dependent[42]. Pharmacological inhibition of the prefrontal cortex revealed that both encoding and retrieval of new, schema-dependent memories depended on activity of this neocortical area[43]. These findings demonstrate that learning in presence of a cognitive schema can result in accelerated systems consolidation.
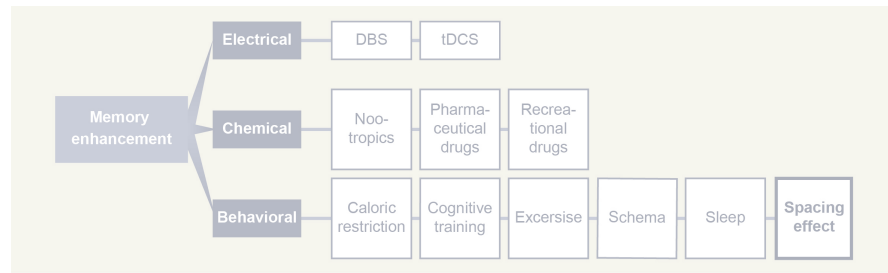
Figure 3 | Memory enhancement can be achieved by electrical, chemical and behavioral interventions. Electrical interventions include deep brain stimulation (DBS)[44] and transcranial direct current stimulation (tDCS)[45]. Chemical interventions include nootropic[46], pharmaceutical[47] and recreational drug[48] intake at appropriate dosages. Behavioral interventions include caloric restriction[48], cognitive training[49], physical exercise[50], schema learning[41,42], sleep[37], and temporally distributed learning (i.e. the spacing effect)[5], the last of which forms the focal point of this doctoral dissertation.

1.2   ON THE SPACING EFFECT

The first description of the beneficial effect of distributed learning came from Ebbinghaus[5], who performed extensive self-study on the subject. He repeatedly learned a set of nonsense syllables and varied the period between learning epochs. He next evaluated his memory for these syllables, and upon reviewing the retention efficacy he concluded:

"Sie macht die Annahme wahrscheinlich, dass bei einer größeren Anzahl von Wiederholungen eine angemessene Verteilung derselben über einen gewissen Zeitraum bedeutend vorteilhafter ist als ihre Kummulierung auf eine bestimmte Zeit"

Ebbinghaus | Über das Gedächtnis: Untersuchungen zur experimentellen Psychologie (1885)

Paraphrasing this statement, Ebbinghaus suggested that long-term memories are more successfully formed by an appropriate distribution of repetitions over a longer period of time than concentrating these repetitions within a shorter period of time. This effect turned out to be exceptionally ubiquitous as it has been described in non-human species including the nematode worm[51], wasp[52], cockroach[53], honey bee[54], pond snail[55], clawed frog[56], crab[57], zebra fish[58], rock dove[59], and domestic dog[60] (**Appendix 1**). This phenomenon is now termed the spacing effect: training with long intertrial intervals more effectively creates long-term memories than training with short or no intervals (i.e. massed training)[6,61].

1.2.1   *Models to study the spacing effect*

Three model systems have been studied most frequently to gain insight into the spacing effect (**Appendix 1**): the California sea hare (*Aplysia californica*), the fruit fly (*Drosophila melanogaster*), and the rodent, including the house mouse (*Mus musculus*) and brown rat (*Rattus norvegicus*; **Box 1**). The relative merits of these main models and their respective behavioral paradigms will be reviewed briefly in this section.

Box 1 | **Models to study the spacing effect**

Aplysia californica (California sea hare)
Siphon withdrawal reflex

Drosophila melanogaster (Fruit fly)
Aversive conditioning

Mus musculus (House mouse)
Rattus norvegicus (Brown rat)
Aversive conditioning
Optokinetic reflex adaptation
Spatial navigation
Object recognition
"Everyday" memory

The majority of studies on the spacing effect in the marine mollusk *Aplysia* characterize the habituation of the siphon withdrawal reflex: instead of withdrawing the siphon after a tactile stimulus, the mollusk no longer responds to this stimulus[62]. Long-term habituation can typically be induced by spaced but not massed training[63]. The key characteristic of *Aplysia* that makes it an attractive model organism is that its nervous system consists of only ~20,000 neuron that are generally large and easily identifiable[64].

Similar to the *Aplysia*, the fruit fly *Drosophila* is an attractive model to study the spacing effect in a relatively simple neuronal network. The main learning paradigm to examine the spacing effect in *Drosophila* is aversive olfactory conditioning, during which flies are presented with an odor and, shortly thereafter, an aversive shock stimulus. Flies express memory for the paired odor in a T-shaped maze by avoiding the arm where the odor is presented. Fear memory is generally more stable after spaced than massed training[65]. Major advantages of *Drosophila* as a model organism are the inexpensive husbandry, short generation time, and availability of diverse and well-developed genetic tools.

Rodents are an attractive model to study the spacing effect because of their relatively short evolutionary distance to humans as compared to *Aplysia* and *Drosophila*. Trial spacing has been observed to affect processing of motor, associative, spatial, and "episodic-like" memory in rodents[6]. Adaptation of the horizontal optokinetic response is a simple model of cerebellum-dependent motor learning[66]. In order to stabilize an image on the retina, the eye normally compensates for any horizontal motion in the visual field. If the visual field oscillates horizontally for a sustained period of time, this reflex adapts. This adaptation persists longer after spaced training[66].

Rodents acquire an associative memory upon paired presentation of an unconditioned stimulus, e.g. a foot shock, and a conditioned stimulus, e.g. a tone[67]. Presentation of the previously neutral conditioned stimulus in absence of the unconditioned stimulus can result in memory retrieval and a behavioral response of the rodent, e.g. freezing. If the conditioned stimulus is repeatedly presented in the absence

of the unconditioned stimulus, the rodent stops responding to the conditioned stimulus in a process termed extinction[68]. Fear processing depends on a distributed neuronal network, typically involving the amygdala, hippocampus, and prefrontal cortex. Both fear learning and fear extinction can be enhanced by spaced training[69–71].

The Morris water maze task is a hippocampus-dependent task on which rodents learn the location of a hidden platform[72]. Successful acquisition of spatial memory is evidenced by a shorter latency to reach the platform and increased dwell time near the platform. Spatial memory processing in rats has been reported to be enhanced by spaced training on the Morris water maze task[73], yet studies in mice have reported no such effects[74]. In summary, spaced training can enhance processing of motor, associative, and spatial memories in rodents.

1.2.2 *The spacing effect and episodic(-like) memory*

Before discussing how "episodic-like" memory can be enhanced by trial spacing in rodents, it is warranted to take a step back and describe the common denominators between human "episodic" and non-human "episodic-like" memory[75,76]. One critical similarity is that these memories form a single representation of a personally experienced event and its context, including information concerning the identity (the "what" component), location (the "where" component) or time (the "when" component) of the event. An example of a human episodic memory is the location ("where") of a parked car ("what") on a recent shopping trip ("when"). Some of the strongest evidence that certain memories in animals contain similar information comes from a study on scrub jays[77]. These birds can form remarkable memories that contain information about the content ("what"), location ("where") and freshness ("when") of food caches[77]. Scrub jays only searched for fresh worms shortly after caching, but abandoned the search if the intervening period was so long that the worms decayed[77]. In short, human episodic and non-human episodic-like memory contain similar information regarding the "what", "where," and/or "when" of an event.

A second critical similarity is that human episodic and non-human episodic-like memory share a neuronal basis. Specifically, both typically depend on hippocampal activity[75,78]. The case of patient H.M. provided seminal evidence that hippocampal damage can severely impair an individual's ability to process episodic memories[29]. Monkeys with hippocampal lesions are severely impaired at remembering recently learned episodic-like memories[79]. Similarly, hippocampal lesions impair episodic-like memory retrieval in rats[80,81]. Thus, biological parallels can be drawn between human episodic memories and non-human episodic-like memories since the latter captures components of "true" episodic memories and is supported by similar neuronal structures.

Given these similarities, why would non-human memories be described as "episodic-like" rather than "episodic"? In a seminal work, Tulving[76] suggested that humans can re-experience episodic memories by "mental time travel", which requires conscious awareness and communication using language. Since animals do not appear to possess language or consciousness similar to humans, their memories cannot be categorized as "episodic" by definition. This subjective definition of episodic memory is not universally shared. Most notably, Allen & Fortin[82] suggested that certain memories in humans, non-human mammals and birds share core properties and propose this is an evolutionarily conserved memory system. This doctoral dissertation takes a more conservative approach and labels memories in animals that contain "what", "where" and/or "when" information and depend on hippocampal processing as "episodic-like".

Rodent tasks that adhere to these two criteria are object exploration tasks, such as the object-in-place task or the novel object recognition task[83]. During these tasks, the rodent's preference for novelty is exploited to evaluate whether a rodent can recognize the old location ("where") or identity ("what") of an object. Thereby, the recency of an experience is weighed against another experience ("when"). Hippocampal damage impairs recognition on these tasks[84,85], satisfying the second criterion to label memories as episodic-like. Of particular interest for this discussion is that performance on object recognition tasks is improved by spaced training in mice[86] and rats[87]. These findings suggest that the spacing effect extends to episodic-like memory.

1.2.3   *Studying the spacing effect using the everyday memory task*

The "everyday memory" task instills memories in rodents that are best described as episodic-like. On this task, rodents need to remember the location ("where") of a buried food reward ("what") and distinguish this location from previously rewarded locations ("when")[88,89]. Efficient execution of the everyday memory task requires hippocampal activity, providing further indication that the formed memories are episodic-like[89]. Furthermore, interventions can enhance memory persistence on the everyday memory task, such as peri-encoding novelty, enhance hippocampal synaptic transmission[88–90]. Therefore, the everyday memory task fulfills the two criteria to label the memories it instills as episodic-like.

The everyday memory task functions as an appetitive, delayed matching-to-place task on which three key steps can be discerned. First, a food-restricted rodent (**Box 2**) needs to find a buried food reward and should remember where it was located in the arena. Second, the rodent is reintroduced to the arena after a delay period and should navigate back to the previously rewarded location to retrieve another food reward. Third, the location of the food reward is changed between each session so the rodent should memorize the new location[88,89]. In short, rodents have to flexibly encode and retrieve memories to effectively perform the everyday memory task.

Trial spacing can stabilize memories instilled by training on the everyday memory task[91]. Rats developed a longer lasting memory on the everyday memory task when encoding trials were spaced by 10 minutes. Conversely, multiple massed trials resulted in short-term but not long-term memory, suggesting that the spacing effects extends to episodic-like memory processing on the everyday memory task.

Box 2 | Motivational incentives on rodent behavioral tasks

Rodents need to be extrinsically motivated to engage with most behavioral tasks, including the everyday memory task. Appetitive reinforcement is typically delivered in the form of a food or fluid reward to a food- or fluid-restricted rodent. The decision to apply food or fluid restriction as a motivational incentive should be informed by i) the effect on rodent welfare and ii) the effect on in-task performance. These factors have not been extensively characterized, but a few studies suggest that fluid restriction results in better outcomes than food restriction[93-95]. First, food-restricted rats had increased serum corticosterone and open field activity as compared to fluid-restricted rats, suggesting that food-restricted rats experienced more physiological and behavioral stress[95]. Second, food-restricted mice had larger body weight fluctuations and poorer learning on an operant conditioning task as compared to fluid-restricted mice[94]. Third, moderate fluid restriction in mice did not strongly impair mouse welfare and motivated mice to perform over one hundred trials on an operant conditioning task[93]. In the same study, food restriction resulted in averse health outcomes before a similar weight reduction could be reached[93]. Given these findings, fluid restriction would be preferred over food restriction as a motivational incentive. However, food restriction has been used successfully to motivate mice and rats on the everyday memory task[91, 92] and ideally this experimental design would be mimicked in this doctoral dissertation. Therefore, the study described in chapter 2 of this doctoral dissertation established whether food restriction could be maintained across weeks of behavioral training without more strongly affecting mouse welfare than fluid restriction.

1.3   ON OPTIMIZING THE SPACING EFFECT

1.3.1   *One interval to rule them all: an impossible quest?*

Given that trial spacing generally enhances memory, can an "optimal" interval that most strongly supports long-term memory be discerned? Finding an "optimal" interval might prove difficult because of the great variability of species, behavioral paradigms, and experimental parameters that have been used in the over one hundred animal studies on the spacing effect (**Appendix 1**). Out of these studies, less than a quarter use more than two intervals. Therefore, three quarters of studies attest to the effectiveness of long intervals as compared to short intervals, but do not allow for an internal comparison of several spaced intervals. This internal comparison is vital as integrating the findings of multiple experiments is complex because of several factors, some of which are critical.

One critical factor is the strong positive correlation between the interval duration that most strongly supports memory and the retention period, i.e. the period between memory encoding and retrieval[96]. The longer the retention period, the longer the intertrial interval that supports strongest memory retrieval[96]. Most studies do not vary the retention period and instead compare the effect of intervals on memory retrieval after 24 hours. As a result, the reported optimal intervals might indeed be effective for training of shorter lasting memories, but not those that have to be retained over the course of a lifetime.

Another critical factor is that the duration of intervals greatly differs between studies (**Appendix 1**). The wide variety of interval durations result in a scattered collection of findings regarding the spacing effect that are difficult to parse. Furthermore, studied interval duration ranges between several seconds and several weeks, but typically the intervals do not extend beyond an hour. As such, the effect of longer intervals is underrepresented in the available data.

Species-based discrepancies in the spacing effect provide an additional factor that impedes the search for an optimal interval. One example comes from fear extinction studies, in which a particularly strong, massed extinction session instills a long-term safety memory in rats but not in mice[69,97]. Similarly, trial spacing on the Morris water maze task stabilizes spatial memory in rats but not mice[83,98–100]. These findings suggest that trial spacing on the same behavioral paradigm in different species can instill memories of distinctly different strength.

Another additional complicating factor is that even small alterations in the experimental design can have a strong impact on the resulting memory. This statement can be illustrated by a study that evaluated object location memory in mice[86]. When mice explored objects on three trials that each had a duration of 100 seconds, adding up to 5 minutes of total exploration time, a significant impact of trial spacing was observed. Mice formed long-term episodic-like memories when trials were spaced by 60 minutes. Either shorter spacing of 20 minutes, or longer spacing of 120 minutes, produced weaker memory, as anticipated by the spacing effect. However, when the total exploration time

was increased from 5 to 10 minutes, strong memories were created with any training protocol. These findings suggest that ceiling effects resulting from more intense training can mask the spacing effect. With these factors in mind, the next section will explore whether any optimal interval can be discerned.

1.3.2   *Quantifying the optimal interval: a dead end?*

As expected, the most precise statement regarding the "optimal" interval is admittedly rather vague and narrow in scope: there are typically strong differential effects on next-day memory strength when encoding trials are spaced on the timescale of tens of minutes. A seminal experiment that systematically characterized the effect of a range of intervals on aversive memory strength in *Drosophila* revealed that training with an interval of 15 minutes resulted in the strongest memory[101]. The memory was weaker after training with shorter intervals of either 1 or 5 minutes, or training with longer interval of either 20, 30, or 60 minutes, attesting to the strong modulating effect of trial spacing on the scale of minutes.

When reviewing the intervals reported in other studies, it becomes apparent that this 15 minute interval is by no means a general optimum. First, long-term fear memory in rats is stronger after training with an interval of 8 minutes than training with an interval of 3, 5, 10, 15, or 120 seconds, alluding to a shorter optimal interval[102]. Second, object location memory in mice is stronger after training with an interval of 60 minutes than training with an interval of 20 or 120 minutes, suggesting a hour-long interval enhances memory in a temporally precise manner[86]. The narrowness of this window has not been replicated in other studies: training rats with intervals ranging from 15 minutes to 7 hours has been described to produce stable next-day object location memory[87]. These results suggest that even when the animal model or the behavioral paradigm are similar, no "optimal" interval can be discerned.

1.3.3   *Qualifying the optimal interval: the Goldilocks principle*

Describing the general relationship between trial spacing and memory strength provides more insight into the spacing effect than focusing on any optimal interval. Similar to dose-response effects of pharmacological interventions on physiology, the duration-durability effects of trial spacing on memory strength could be captured in three main curve shapes, namely monotonically increasing, S-shaped, or inverted U-shaped (**Fig. 4**).
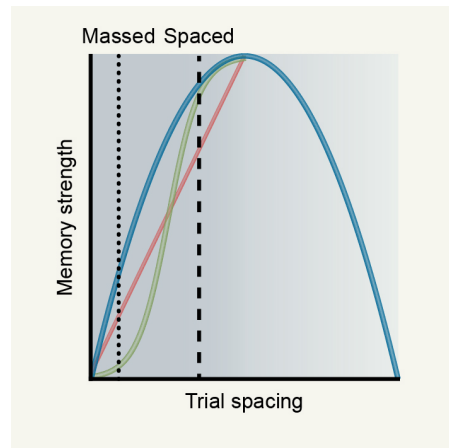
Figure 4 | Duration-durability curve. Generally, training with longer intervals ("spaced training", dashed line) creates stronger memories than training with shorter intervals ("massed training", dotted line). The duration-durability relationship could be described by a mono-tonically increasing (red)[102–106], S-shaped (green)[66,107], or inverted U-shaped (blue)[56,87,101,108–110] curve, of which the latter appears most biologically plausible.

Although frequently observed[102–106,111], a monotonically increasing curve appears biologically implausible. If memory strength could be indefinitely increased, this would suggest that there is no limiting factor in this process. However, synaptic competition for intracellular proteins has been observed when protein synthesis is not infinite[112], suggesting scarcity of resources (e.g. AMPARs or cytoskeletal proteins) that support functional and structural synaptic strengthening. An S-shaped curve appears equally implausible even though it has been described in a few studies[66,107]. When intervals are excessively long, memory traces could become labile as they have not been recently re-activated. Furthermore, whereas retrieval can promote consolidation of recent memories, it can destabilize remote memories[113], suggesting that long intervals are likely to result in passive or active forgetting.

If monotonically increasing and S-shaped curves are theoretically implausible, how can their observation be explained? The observations of monotonically increasing or S-shaped relationships can be most likely attributed to a lack of sampling of sufficiently long interval durations (**Fig. 4**). If long intervals are not studied, the detrimental or non-beneficial effects of these intervals cannot be observed. In short, neither a monotonically increasing nor an S-shaped curve corresponds to our understanding of memory processing.

The most prevalently observed and biologically plausible relationship between trial spacing and memory strength is an inverted U-shaped relationship (**Fig. 4**)[56,86,87,101,108–110]. This curve has three distinct parts: an initial upward slope, a peak, and a downward slope, which are compatible with our understanding of memory processing[114]. If the intervals are too short, the physiological processes resulting from the first event, e.g. molecular signaling and structural remodeling, are likely still unfolding. As a result, the second event

cannot support further synaptic strengthening at that moment. If the intervals are sufficiently long, the processes resulting from the first event will have completed, amongst which is a temporary increase in neuronal excitability. Therefore, a second event can more efficiently reactivate the same neuronal population[115] and contribute to memory strengthening. If the intervals are too long, intrinsic changes in neuronal excitability could reduce the probability that subsequent events stimulate the same neuronal ensemble[116]. Therefore, increasing trial spacing after an optimum duration would not have beneficial, but rather detrimental effects. Many of these theoretical predictions have been addressed in empirical experiments, as reviewed in the next section.

1.4   ON THE SYNAPTIC, CELLULAR, AND POPULATION MECHANISMS THAT MEDIATE THE SPACING EFFECT

The memory-enhancing effect of trial spacing could be based on neuronal mechanisms that are categorically distinct from those that take place during "regular" memory processing. Alternatively, trial spacing could strengthen memory by more efficiently executing the same processes that are required for memory processing in general, as described in section 1.1 of this introduction. Most evidence favors this second framework[6,61], and this section will therefore review how the synaptic, cellular and neuronal population mechanisms that underlie regular memory processing are enhanced by trial spacing.

1.4.1   *Effects of trial spacing on synaptic connections*

If the elementary building blocks of memories are synapses, trial spacing should enhance functional and structural strengthening of individual synaptic connections. Indeed, several studies conducted in the rodent hippocampal circuit indicate that spaced stimulation protocols can enhance the strength of synaptic transmission[107,109,117,118], which has been attributed to additional increased insertion of AMPARs[109]. As such, enhanced synaptic transmission could be a mechanism by which trial spacing enhances memory processing.

Spaced stimulation protocols have not only been observed to enhance synaptic transmission, they can also increase structural remodeling. One seminal study quantified the number of spines and dendritic protrusions on cultured rat hippocampal neurons providing a link between spaced training and strengthening of synapses[119]. Massed stimulation did not induce structural changes, whereas spaced stimulation induced sprouting of new protrusions from spines, some of which turned into new spine-like structures providing a link between spaced training and strengthening of synapses[119]. Similar results were obtained in a study that investigated how spaced training of mice on a cerebellum-dependent motor learning task affected synaptic morphology[103]. High-resolution imaging revealed that spaced motor training produced transient alterations in synapse size and number, which stabilized after 24 hours[103]. Massed training altered the synapse size and number as well, but these changes occurred slowly over the course of days rather than rapidly within 24 hours[103]. In summary, spaced stimulation has been demonstrated to enhance synaptic transmission as well as enlargement and formation of synapses, providing a link between spaced training and strengthening of synapses.

1.4.2 *Effects of trial spacing on cellular physiology*

The spacing effect is relatively well understood from a cellular perspective. At its core, trial spacing more effectively activates a cellular signaling pathway that mediates LTP (**Fig. 2**)[6]. This signaling pathway involves sequential activation of second messengers, kinases and phosphatases, including CaMKII, adenylyl cyclase, PKA, MEK, and MAPK. Ultimately, the transcription activator CREB1 is activated, which induces synthesis of proteins that support long-term memory. Enhanced activity of any of these molecular switches could ultimately result in more effective execution of this signaling pathway and more forcefully activate transcription[6].

The first insight that multiple molecules in this signaling pathway can be affected by spaced training came from a study that performed spaced stimulation of cultured rat hippocampal neurons[119]. A range of key signaling molecules were inhibited and the effect on activity-dependent biochemical changes was subsequently quantified[119]. The effect of spaced stimulation was blocked by application of inhibitors of calmodulin, CaMKII, Ras, and MEK, suggesting that any of these molecules could modify the effectiveness of spaced stimulation. Subsequent studies have described changes in the amount or the activity of each of the major molecules in this signaling pathway in more detail, as reviewed below.

CaMKII, adenylyl cyclase, and PKA are the first molecules that need to be activated to execute this pathway (**Fig. 2**). Whereas spaced training on an aversive olfactory conditioning task normally resulted in robust next-day memory in *Drosophila*, introduction of CaMKII hairpin RNA blocked long-term memory[120]. Conversely, CaMKII hairpin RNA did not disrupt memory induced by massed training, suggesting that short-term aversive memory did not require CaMKII signaling[120]. A downstream effector of CaMKII is adenylyl cyclase, which can be activated by the gene product of the *amnesiac* gene. Flies that express a mutated *amnesiac* gene do not form long-term memories upon spaced aversive olfactory conditioning, suggesting that adenylyl cyclase activity also mediates the spacing effect[121]. Moving down the cascade, adenylyl cyclase synthesizes cAMP, which activates PKA. Spaced serotonin application to *Aplysia* neuronal cultures reduced the activation of PKC, a negative regulator or PKA, thereby enhancing PKA activity[122]. Thus, CaMKII, adenylyl cyclase, and PKA signaling can be affected by trial spacing.

MAPK, a downstream target of PKA signaling, is another kinase whose signaling mediates long-term memory (**Fig. 2**)[123]. Increased MAPK phosphorylation has been observed upon spaced electrical stimulation of rat hippocampal slices[108], aversive olfactory conditioning using spaced intervals in *Drosophila*[124], and spaced training on the object-in-place task in mice[86]. Modifying the activity of positive and negative regulators of MAPK can also affect the efficacy of spaced training. Bilateral hippocampal infusion of a pharmacological inhibitor of MEK, a kinase that phosphorylates MAPK, inhibited the augmenting effect of spaced training on the object-in-place task in rats[87]. Overex-

pression of the *Drosophila* gene *corkscrew*, whose gene product acts as a positive regulator of MAPK signaling, improved long-term memory after massed aversive olfactory conditioning[124]. Conversely, activity of the phosphatase PP1, which reduces MAPK phosphorylation, is more strongly reduced after spaced training on the novel object recognition task in mice[125]. These findings suggest that MAPK activation is a lever in the molecular signaling cascade that can be pushed or pulled to strengthen or inhibit the effect of trial spacing on memory.

Spaced training also exerts its effects on the final step in the molecular signaling cascade, i.e. activation and signaling of the transcription factor CREB1. Repressing CREB1 function reduced long-term memory strength upon spaced aversive olfactory conditioning in *Drosophila*[121]. Furthermore, impaired memory in $CREB^{\alpha\Delta}$-knock-out mice was rectified by spaced aversive conditioning[102]. Conversely, increasing CREB1 expression using a viral vector significantly increased long-term memory after massed fear conditioning[102]. In summary, the studies described in this section illuminate how spaced training can more effectively trigger a molecular signaling pathway that supports long-term memory (**Fig. 2**).

Enhanced activation of the molecular signaling pathway ultimately results in enhanced protein synthesis, which is necessary for long-term memory. Studies in a variety of model systems have established a direct link between the memory-enhancing effect of trial spacing and protein synthesis by evaluating the effect of administration of anisomycin, an antibiotic that blocks protein synthesis. Anisomycin administration has been shown to prevent LTP maintenance upon spaced stimulation in rat hippocampal slices[117], impair habituation upon spaced serotonin application to sensory *Aplysia* neurons[122], and diminish the enhancing effects of spaced aversive olfactory conditioning in *Drosophila*[121]. These results suggest that protein synthesis is vital to sustain the enhanced long-term memory that results from spaced training. However, since anisomycin has an indiscriminant effect on protein synthesis, it remains mostly unclear which exact proteins are upregulated by spaced training. This issue has been addressed by genome-wide analysis of gene expression after massed and spaced training on the everyday memory task in rats, which revealed that mostly CREB1-target genes were upregulated[91]. These genes included those coding for proteins that regulate the aforementioned signaling pathway, protein-folding chaperones and the immediate early genes *Arc*, *c-Fos*, and several members of the *Egr* family of genes. In summary, a broad body of work indicates that spaced training results in stronger memories because it more efficiently activates a cellular signaling cascade that results in protein synthesis that support LTP.

1.4.3 *Effects of trial spacing on neuronal populations*

In contrast to the abundant evidence linking the spacing effect to altered synaptic and cellular signaling, there is limited understanding of how trial spacing affects the activity of neuronal populations. Some insights can be drawn from studies that performed *in vivo* calcium imaging during spaced aversive conditioning in *Drosophila*[121,126]. Here, spaced training resulted in a distinct activity pattern during memory encoding in neurons located in the mushroom body, a structure that mediates olfactory memory. This pattern was more conducive to long-term memory formation than that observed during massed training[126]. Furthermore, re-exposure of *Drosophila* to the memorized conditioned stimulus after spaced training resulted in a larger stimulus-induced response than massed training[121]. These results suggest that trial spacing affects *in vivo* neuronal activity during different phases of memory processing. Since calcium imaging of *Drosophila* cannot be executed repeatedly in the same subject, these results represent a snapshot but not a movie of how trial spacing affects memory-related neuronal activity. This doctoral dissertation therefore aims to bridge this gap in knowledge by testing how trial spacing affects memory processing in a neuronal population within the same subject.

1.4.4 *Hypotheses concerning the effect of spaced training on neuronal ensembles*

As of yet, no published studies have explored how trial spacing affects the activity of neuronal ensembles in the intact mammalian brain. Since memories are stored in neuronal ensembles, trial spacing could alter certain ensemble characteristics, including its size and its synaptic connectivity, which is discussed in more detail in this section.

One hypothesis is that spaced training could facilitate memory retrieval by increasing the neuronal ensemble size. In general, the strength of a memory correlates positively with the number of reactivated neurons, as was demonstrated by quantifying the number of reactivated neurons in the amygdala after a mouse retrieved a fear memory[35]. If the intervals between the trials are longer, the context of behavioral training, including external sensory cues, has typically altered more than when intervals are shorter. A representation including a wider variety of cues is likely represented by more neurons, thereby growing the neuronal ensemble. As a result, the number of cues that could (partially) reactivate the neuronal ensemble is larger and thereby increase the chance of successful memory retrieval. There are two main lines of evidence that support this hypothesis. In one experiment, exposing mice to a neutral context after aversive conditioning in another context resulted in aversive memory retrieval in the previously neutral context[116]. The linkage of these two distinct contextual memories only occurred when the exposures were several hours but not several days apart[116].

More critically, the size of the neuronal ensemble that was reactivated during retrieval of both memories was significantly larger when the memories were linked, suggesting that spacing of experiences can grow the neuronal ensemble dedicated to representing features of those experiences. Another experiment found that the number of neurons expressing CREB1, a marker of neuronal activity, was larger when training of mice on the novel object recognition task was spaced by 15 than 5 or 0 minutes[125]. This suggests that spacing experiences on the timescale of minutes increases the number of activated neurons. In short, one potential mechanism underlying the spacing effect is an expansion of the neuronal ensemble, which would bind a memory across diverse contexts.

Another alternative by which trial spacing could promote memory is strengthening of the synaptic connections within the neuronal ensemble. Repeated activation of the same neuronal population could induce several cycles of the canonical molecular signaling cascade (**Fig. 2**). This could strengthen the synaptic connections by inserting new AMPARs or inducing synapse growth[127]. Spaced training could promote selective reactivation of ensemble neurons, as their internal excitability should be increased from previous events in a time-dependent manner[128]. Thereby, memories from the individual trials could be more effectively allocated to the same neuronal ensemble during spaced training, severely strengthening the connections between ensemble but not non-ensemble neurons[127]. This would promote both memory persistence and probability of retrieval. Memory persistence would be increased because enhanced ensemble strength would render the stored memory more stable and more resilient to degradation. Memory retrieval would be more efficient because the activity of the neuronal ensemble during retrieval would more precisely mimic the activity pattern that was observed during encoding. In short, trial spacing could increase the neuronal ensemble size and/or connectivity, which would strengthen the ensemble and enhance memory.

In this doctoral dissertation, I choose to address these hypotheses experimentally by recording *in vivo* neuronal activity while mice perform the everyday memory task. That memory processing on the everyday memory task likely depends on multiple interconnected brain areas including the hippocampus[91], retrosplenial cortex[91], and the prefrontal cortex. The study described in chapter 4 of this dissertation specifically focuses on the prefrontal cortex, a brain area that mediates decision making and memory processing[129].

1.5 ON THE MOUSE MEDIAL PREFRONTAL CORTEX

An issue that has been debated for decades is whether the mouse has a prefrontal cortex (PFC), and, if so, which brain areas constitute the mouse PFC[130–133]. One approach to address the first part of the issue is based on anatomical homology, i.e. structural resemblance, between mouse and human. Brodmann[134] used a cytoarchitectural criterion and suggested that the hallmark of the human PFC was the presence of a distinct layer 4. However, mice do not share this characteristic[135], which would suggest that the mouse does not possess a PFC. Rose & Woolsey[132] challenged this idea and proposed another anatomical criterion to define the PFC. They argued that the PFC is that part of the frontal neocortex that receives projections from the mediodorsal nucleus of the thalamus. If this projection-based criterion is applied, all mammals (including mice) possess a PFC[132]. Opponents of this definition will argue that the thalamic-prefrontal projection pattern is not completely reciprocal, i.e. the PFC is also infiltrated by other thalamic nuclei, and the mediodorsal nucleus also projects to other areas[136]. Nevertheless, the projection-based definition is more attractive than the cytoarchitectural definition because it enables translation of similar functional findings obtained in similar brain areas from mouse to man. Therefore, although the debate continues[75,130], this dissertation argues that the mouse has a PFC, which can be delineated by the mediodorsal projection to the frontal neocortex.

This leads to the second part of the issue: which brain areas constitute the mouse PFC? The mediodorsal projection field in the mouse frontal neocortex encompasses mostly medial areas[136], including the anterior cingulate, prelimbic, and infralimbic area (**Fig. 5**). These areas are also considered to be part of the human PFC[131] and this dissertation will describe studies on these areas as studies in the mouse medial PFC (mPFC).
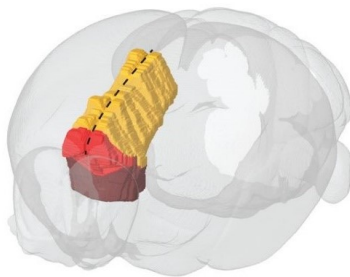

Figure 5 | Schematic of the mouse medial prefrontal cortex. The areas of the mouse brain (grey) that are generally believed to make up the mouse medial prefrontal cortex are the anterior cingulate area (yellow), the prelimbic area (red), and the infralimbic area (dark red). Reprinted with permission from[130].

Even though the structural resemblance is limited, certain functions performed by mouse and human prefrontal areas bear a strong resemblance. Similar to the human dorsolateral PFC, the mouse mPFC is considered to be the main neuronal network that processes cognitive information[129]. As such, the mouse mPFC mediates attentional set-shifting[137], decision making[138], executive control[139], goal-directed behavior[140], inhibitory control[141], and working memory[142], similar to the human dorsolateral PFC[143].

The mouse is an attractive model to study PFC function mostly because of the availability of high-resolution recording methods, including electrophysiological and imaging methods (**Appendix 2**). These method provide new insights in to the neuronal basis of cognition that cannot be obtained from studies on the human PFC. For example, *in vivo* calcium imaging (**Box 3**) of prefrontal activity in head-fixed mice demonstrated that individual prefrontal neurons signal sensory, motor, and reward cues[140]. These signals were differentially represented by (subtypes of) inhibitory and pyramidal neurons, whose responses varied across the cortical layers[140]. These findings establish that prefrontal neurons form an intricate microcircuitry that is involved in a variety of computations.

Temporally precise perturbation of the mouse mPFC using optogenetic or chemogenetic tools provides evidence that the PFC is vitally important for cognitive functions. Two studies illustrate how perturbation methods illuminate the necessity for mPFC activity for working memory and flexible cognitive processing[137,144]. Working memory retains information from a recent event during a short delay period to subsequently make an appropriate behavioral response. The observation of persistent activity in the PFC during the delay period in monkeys and humans[145,146] stimulated the search for approaches that could determine whether delay activity is necessary for working memory or is just an epiphenomenon. Optogenetic activation or inhibition of mouse mPFC pyramidal neurons during the delay period impaired behavioral performance while the mouse acquired the task but not once performance had reached the asymptotic maximum[144]. This suggests that delay-period activity in the mPFC mediates working memory in novice mice, but that other brain regions perform this computation in well-trained mice. These results provide a causal link between persistent delay activity and working memory function.

Box 3 | *In vivo* study of neurons in the mouse neocortex

In this doctoral dissertation, I aim to establish a connection between altered *in vivo* neuronal activity and the spacing effect. Training mice on the everyday memory task and simultaneously recording from prefrontal neurons is an appropriate approach to achieve this aim. What remains is selection of an effective method to perform large-scale neuronal recordings in the prefrontal cortex of awake, behaving mice. Both electrical and optical recordings would be viable options and have been used successfully in the past (**Appendix 2**). However, the implant that is necessary to perform these recordings, e.g. a silicon probe for electrical recordings and a glass microprism for optical recordings, have varying degrees of durability [153, 156]. At the onset of the study described in chapter 4, electrical implants were not sufficiently stable over the course of months (however, see [147]), making *in vivo* imaging a more suitable approach.

In vivo imaging is generally performed by recording from neurons that express a fluorescent calcium indicator [148]. The recorded fluorescence fluctuations approximate the intracellular calcium concentration and thereby the underlying firing pattern of the neuron. The current indicators of choice are genetically-encoded calcium indicators such as GCaMP6, which can be stably expressed by hundreds of neurons for an extended period of time [149]. These features make *in vivo* calcium imaging an attractive method to repeatedly study neuronal activity on the everyday memory task.

Two main microscopy methods allow *in vivo* calcium imaging with neuronal resolution in the awake, behaving mouse [150]. A typical benchtop two-photon microscope allows imaging of somata and subcellular structures in head-fixed mice [151, 155]. Conversely, a typical epifluorescence miniaturized microscope allows imaging of somata in freely moving mice [152]. Since the everyday memory task has been conducted in freely moving rodents, using miniaturized microscopy would be desirable. At the onset of experimentation, two-photon miniaturized microscopes [157] were not available and therefore a conventional miniaturized microscope was selected.

Conventional miniaturized microscopes do suffer from one potential caveat. That is, they typically use epifluorescent illumination and therefore collect photons from a considerably larger volume than two-photon microscopes. This results in a higher background fluorescence, lower resolution and greater sensitivity to scattering [152]. Therefore, the signals recorded with miniaturized microscopes might not solely reflect the activity of one neuron, but rather activity from an aggregate of the neuron and its surrounding somata and neurites. Before selecting the miniaturized microscope to record prefrontal activity on the everyday memory task, this methodological concern should be addressed. Therefore, the study described in chapter 3 of this doctoral dissertation describes a direct, *in vivo* comparison between recordings obtained with a typical benchtop two-photon microscope and a miniaturized microscope.

The role of the mPFC in flexible cognitive processing has been studied by training mice on a rule switching task[137]. On this task, a cue during the delay period signaled whether the mouse had to attend a visual or auditory target. The mPFC neuronal responses were both cue-selective and rule-selective (i.e. cue non-selective)[137]. Furthermore, optogenetic perturbation revealed that this rule selectivity was mediated by afferent connections from the mediodorsal thalamic nucleus. These selected studies illustrate that the mouse is an attractive model to study the wide range of cognitive processes that depend on PFC activity.

The mPFC performs many of its cognitive functions in conjunction with the hippocampus. One observation of coordinated hippocampal and prefrontal activity was made while mice were trained on a delayed non-matching-to-place task that evaluated spatial working memory performance[142]. Inhibition of hippocampal projections in the mPFC impaired encoding but not retrieval of spatial cues, suggesting that hippocampal activity aids in updating of relevant information. In line with this observation, hippocampal activity leads prefrontal activity in rats during a context-guided memory task[158]. On this task, the rat had to explore a context to find a goal object, from which it could retrieve a reward. Once the rat entered the context, hippocampal activity preceded mPFC activity upon context entry. This directionality was reversed upon onset of object sampling[158]. Furthermore, whereas associative flavor-place memories are initially stored in the hippocampus, they are subsequently stored in the mPFC upon systems consolidation[43]. These studies demonstrate that the mPFC predominantly exerts cognitive control over memory processing, whereas the hippocampal network stores the spatiotemporal context of the memory[75].

1.6 AIMS OF THE DOCTORAL DISSERTATION

The overarching aim of this doctoral dissertation was to establish whether and how neuronal population activity relates to the enhancing effect of trial spacing on memory. To achieve this aim, two initial studies were performed to clarify two outstanding methodological concerns.

The first study aimed to establish how the well-being and behavioral performance of mice were influenced by chronic, mild nutritional restriction. To this end, mice were restricted in either their food or their fluid uptake across months, during which mouse welfare was manually and automatically monitored and mice were trained on an operant conditioning task. The results of this study were published as "*Food and water restriction lead to differential learning behaviors in a head-fixed two-choice visual discrimination task for mice*" in the journal PLOS ONE and reprinted in this dissertation in chapter 2.

The second study aimed to establish whether the qualitative differences in two microscopes, i.e. a benchtop two-photon and a miniaturized epifluorescence microscope, result in quantitative differences in the recorded stimulus-induced neuronal responses. The well-characterized response properties of visual cortex neurons to gratings of different orientations were used as a model of stimulus-induced neuronal activity[159]. *In vivo* calcium imaging recordings obtained with both microscopes were analyzed to evaluate quantitative differences in the orientation tuning of individual neurons. The results of this study were published as "*Benchmarking miniaturized microscopy against two-photon calcium imaging using single-cell orientation tuning in mouse visual cortex*" in the journal PLOS ONE and reprinted in this dissertation in chapter 3.

The third and main study aimed to establish whether trial spacing on the everyday memory task affects neuronal ensemble activity. To this end, mice were trained across months on the everyday memory task and the effect of trial spacing on memory encoding and retrieval was quantified. Chemogenetic inactivation and calcium imaging of the dmPFC was performed in a subset of experiments, evaluating whether and how the dmPFC mediates behavioral performance. Finally, correlation and regression analysis established whether and how a population of dmPFC neurons altered its activity based on trial spacing. The results from this study titled "*Spaced training enhances memory and prefrontal ensemble stability in mice*" were made available as a preprint on *bioRxiv*, are currently under review for publication in the journal Current Biology, and are printed in this dissertation in chapter 4.

2

FOOD AND WATER RESTRICTION LEAD TO DIFFERENTIAL LEARNING BEHAVIORS IN A HEAD-FIXED TWO-CHOICE VISUAL DISCRIMINATION TASK FOR MICE

Declaration of author contributions

All listed authors contributed to this article: Pieter M. Goltstein, Sandra Reinert, Annet Glas, Tobias Bonhoeffer, and Mark Hübener.

Food and water restriction lead to differential learning behaviors in a head-fixed two-choice visual discrimination task for mice

Pieter M. Goltstein[1☯]*, **Sandra Reinert**[1,2☯], **Annet Glas**[1,2☯], **Tobias Bonhoeffer**[1], **Mark Hübener**[1]*

1 Max Planck Institute of Neurobiology, Martinsried, Germany, **2** Graduate School of Systemic Neurosciences, Martinsried, Germany

☯ These authors contributed equally to this work.
* goltstein@neuro.mpg.de (PG); mark@neuro.mpg.de (MH)

Abstract

Head-fixed behavioral tasks can provide important insights into cognitive processes in rodents. Despite the widespread use of this experimental approach, there is only limited knowledge of how differences in task parameters, such as motivational incentives, affect overall task performance. Here, we provide a detailed methodological description of the setup and procedures for training mice efficiently on a two-choice lick left/lick right visual discrimination task. We characterize the effects of two distinct restriction regimens, i.e. food and water restriction, on animal wellbeing, activity patterns, task acquisition, and performance. While we observed reduced behavioral activity during the period of food and water restriction, the average animal discomfort scores remained in the 'sub-threshold' and 'mild' categories throughout the experiment, irrespective of the restriction regimen. We found that the type of restriction significantly influenced specific aspects of task acquisition and engagement, i.e. the number of sessions until the learning criterion was reached and the number of trials performed per session, but it did not affect maximum learning curve performance. These results indicate that the choice of restriction paradigm does not strongly affect animal wellbeing, but it can have a significant effect on how mice perform in a task.

Introduction

Rodents, in particular rats and mice, have long been used in behavioral studies exploring the mechanisms underlying learning and memory [1,2]. Such experiments are particularly valuable when combined with simultaneous recordings from neurons involved in the task. Traditionally, this is done with extracellular recordings of single- or multi-unit activity, a technique that can easily be adopted to freely moving animals [3]. In some instances, however, it is desirable to carry out behavioral experiments in movement-restricted animals. Head-fixation in particular is indispensable under certain conditions, e.g. when precise control over sensory inputs is needed, or when the employed recording technique is sensitive to brain motion, like patch clamp recordings [4] and two-photon microscopy [5].

Head-fixed operant conditioning is now commonly used to train mice in diverse sensory detection- and discrimination tasks, as well as in virtual navigation experiments. Such tasks can be performed using various operant-stimulus modalities, e.g. visual [6], auditory [7], olfactory [8] or tactile [9]. The most widely used paradigm is the Go/No-Go task, in which the animal makes a choice by either performing or withholding from a certain behavior, such as a lick on a lick spout [9], a lever press [6] or running [10]. An important factor in behavioral training, especially with parallel neuronal recordings, is the ability to differentiate between the actual choice of a mouse and the mere level of motivation to participate in a task. Go/No-Go task designs lack the ability to precisely differentiate between an active No-Go (active withholding) and a passive No-Go, reflecting loss of motivation. Two-choice designs are therefore often more appropriate as they better allow discriminating between active choices of a mouse, e.g. licks left or right [9] or steering wheel movements to the left or right [11], and its task engagement (finished versus missed trials). Head-fixed paradigms also vary in the dimensionality of body movement that is permitted and measured. While some virtual reality approaches allow more degrees of freedom [12–14], it is common to restrict running to one dimension [10,15] or restrict body movement entirely by placing the animal in a narrow tube [9,16]. Beyond these, many more detailed parameters, e.g. setup design, training protocol, trial sequence and stimulus presentation can be adjusted to suit the specific experimental need.

The effect of such parameter choices on the outcome of a behavioral experiment is often not systematically explored and only occasionally reported in the literature. One such parameter is the choice of (naturalistic) motivational incentive. This can be appetitive (e.g. reward) or aversive (e.g. fear) and is commonly administered by delivery of food or water [9] or by delivery of mild shocks, respectively [17]. Animal behavior can also be motivated using targeted, optogenetic activation of dopaminergic circuits [11] or by circuits driving hunger or thirst [18]. Still, head-fixed learning paradigms mostly use food and water restriction, in part because it does not require additional optical equipment. While food and water restriction regimens are sometimes perceived as interchangeable, these two methods engage the animal's physiology differently [19,20], and hunger and thirst recruit different neuronal circuits [18,21,22]. Therefore, similar levels of food and water restriction, as usually measured by the animal's relative reduction in body weight, might affect task performance, task motivation and also animal welfare in a different manner [23].

This study provides a detailed description of the setup design and procedures to efficiently train mice using either food or water restriction on an appetitive operant visual discrimination task. We explicitly monitor animal welfare using measurements of body weight and a standardized scoring routine, as well as continuously recorded physical activity patterns from the home cage [24]. We demonstrate the sensitivity and reliability of our conditioning method by addressing how the choice for food or water restriction affects performance in head-fixed operant conditioning.

Methods

Animals

All procedures were performed in accordance with the institutional guidelines of the Max Planck Society and the local government (protocol number 55.2-1-54-2531-213-2015, approved by the Beratende Ethikkommission nach § 15 Tierschutzgesetz, Regierung von Oberbayern). Twelve male C57BL/6J mice (postnatal day 34) were individually housed in standard individually ventilated cages (IVC; Tecniplast GM500) and placed in a Digital Ventilated Rack (DVC, Tecniplast). Each cage was equipped with a dedicated electronic board (DVC board) composed of 12 electromagnetic field generating electrodes evenly positioned in a 4 by

3 grid underneath the entire cage floor area. Sensors measured activity at each electrode separately (4 Hz sampling frequency) and stored the data on a computer. Disturbances in the strength of the local electromagnetic field were used as proxy for a mouse's behavioral activity in the home cage (see Data analysis). All mice were kept on an inverted 12-h light, 12-h dark cycle with lights on at 22:00. Ambient temperature (21.0 ± 0.7 °C) and humidity (63 ± 2%) were kept constant. Water and standard chow (Altromin Spezialfutter GmbH, #1310) were provided to the mice *ad libitum* prior to behavioral experiments. Starting seven days before surgery, mice were handled and weighed daily by the same experimenters (two female, two male) that later also carried out behavioral training. After completion of behavioral procedures, mice were euthanized using CO_2 asphyxiation.

Surgical procedures

Mice were anesthetized with a mixture of fentanyl, midazolam and meditomidine in saline (0.05mg/kg, 5 mg/kg and 0.5 mg/kg respectively, injected i.p.) and sufficient depth of anesthesia was confirmed by absence of the pedal reflex. Eyes were covered with a thin layer of ophthalmic ointment (IsoptoMax). Lidocaine (0.2mg/ml) was applied onto the scalp for topical anesthesia and carprofen in saline (5mg/kg, injected s.c.) was administered for analgesia. The skull was exposed, dried and scraped with a scalpel to facilitate attachment of the head plate. The custom-designed head plate (Fig 1D; S1 File) was fixed in position, over the left parietal bone, using cyanoacrylate glue and subsequently secured with dental acrylic (Paladur). After surgery, mice were injected with a mixture of the antagonists naloxone, flumazenil and atipamezole in saline (1.2 mg/kg, 0.5 mg/kg and 2.5mg/kg respectively, injected s.c.) and left to recover under a heat lamp. For post-operative analgesia, mice received carprofen (5mg/kg, injected s.c.) for three subsequent days.
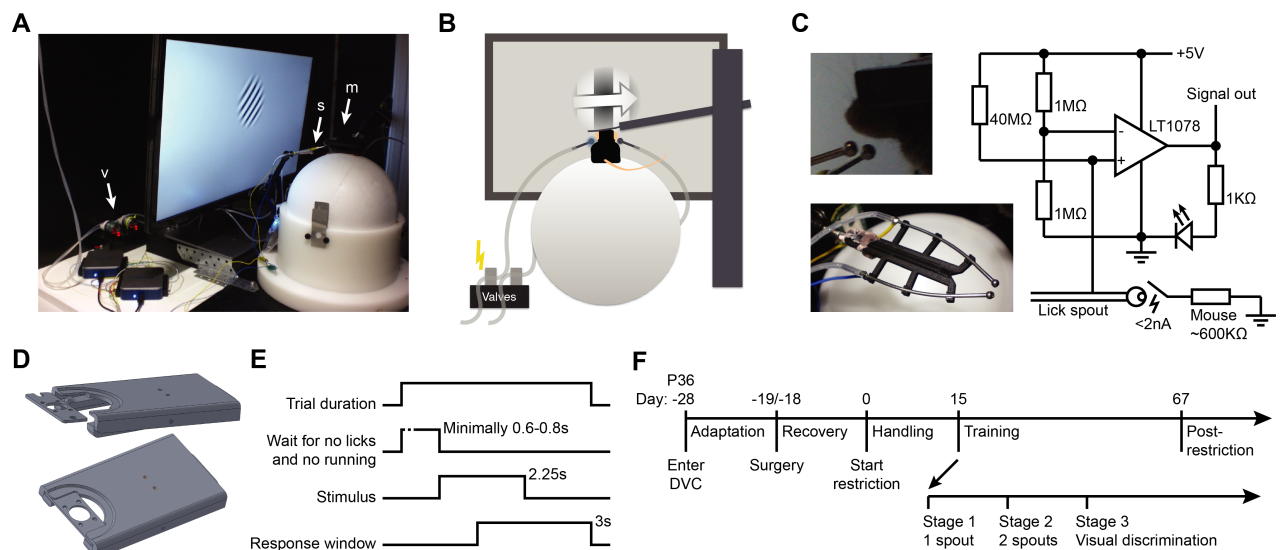
Fig 1. Behavioral apparatus and training protocol. A. Setup used for head-fixed visual conditioning. Arrow 'm' points to a head-fixed mouse, resting on a Styrofoam ball, in front of a centrally positioned monitor and the two lick spouts (arrow 's'). Arrow 'v' indicates the pinch valves for reward delivery. B. Schematic of the behavioral setup as seen from behind. C. Lick detection. Top left: Position of dual lick spouts in front of the mouse. Bottom left: Photo of fully assembled 3D printed lick spout holder. Right: Electrical circuit for contact/lick detection on a single lick spout. D. 3D renderings of head-bar and head-bar holder. E. Temporal sequence of within-trial phases. Reward is delivered immediately upon the first (correct) lick in the response window. F. Overall experimental timeline depicting main experimental and training stages.

Food and water restriction

Mice were randomly assigned to either the food-restricted or the water-restricted group. The period of restricted access to food or water was started 18–19 days after surgery. Animals were transferred to novel cages immediately before food or water restriction started.

At the start of water access restriction, mice were initially provided with 50% of the average *ad libitum* water intake per day (50% was on average 1.57 ml in our facility). The water ration was provided in the home cage using the nozzle of a standard water bottle that was closed off at the back using red tape. From the fourth day onwards, the water ration was first offered in a hand-held syringe during handling, with any remaining volume supplied in the home cage. In parallel, when a mouse reached the target weight of 85% of the initially measured *ad libitum* weight (reference weight), the daily volume of water supplement was individually adjusted in order to maintain the target weight. As precaution, a minimum daily ration was set to 25% of the *ad libitum* intake. However, the daily supplemented amount was only rarely as low as 25% of *ad libitum* intake. Water-restricted animals had *ad libitum* access to food throughout the experiment.

Food access was restricted according to the following procedure. On the first day, mice received the minimum ration size of 2.0 g standard chow (3.279 kcal/g) in their home cage. Subsequently, the daily ration was adjusted per mouse in order to keep its weight at 85% of the reference weight, while staying above the minimum ration weight of 2.0 g. From day four untill day seven, mice were fed unflavored soymilk (Alpro) from a handheld syringe during handling. However, we noted that mice were not particularly motivated to drink regular soymilk (average consumed volume per mouse; day 5: 0.58 ml; day 6: 0.63 ml; day 7: 0.51 ml). Thus, on days eight and nine we offered sweetened soymilk (Alpro), which did not increase the consumed volume (average consumed volume per mouse; day 8: 0.51 ml; day 9: 0.38 ml). Finally, from the tenth day until the end of the experiment we used infant formula soymilk (SMA Wysoy)[10]. The infant formula soymilk was prepared by adding lukewarm water to a falcon tube containing 10–12 ml of soymilk powder until the total volume of the suspension reached 30–34 ml. We immediately noticed a difference in consumption behavior when providing mice with infant formula soymilk (average consumed volume per mouse; day 7: 0.73 ml; day 8: 1.29 ml; day 9: 0.99 ml; day 10: 1.73 ml; day 11: 1.71 ml). The daily food ration of each mouse was reduced by an amount that matched the caloric content of the consumed volume of soymilk (0.67 kcal/ml). Food-restricted animals had *ad libitum* access to water during the entire experiment.

Animal welfare assessment

Daily welfare assessment involved scoring mice on five different aspects of wellbeing using individual scoresheets [9]. Scores on 'Activity and behavior' ranked an animal's behavior in the home cage from normal, active (0), via reduced activity (1), only moves when touched (2) to lethargy (3). 'Look/posture' indicated the condition of the fur and the posture of the mouse, ranging from normal (0) to arched back and very shaggy fur (3). 'Urine/feces' was scored as indication of eating, drinking and associated physiological processes, ranging from normal (0), via reduced amounts (1) to none (2). 'Body condition' indicated the shape and outline of the mouse's body and spine according to Ullman-Culleré & Foltz [25], ranging from normal (0), via underweight (1) to emaciated (2). 'Signs of dehydration' were assessed using skin turgor, ranging from none (0), via light (1), moderate (2), to strong (3). Finally, the cumulative score across all aspects was used to judge the overall wellbeing of the animal into four discomfort categories named according to the European Union based legislation. A discomfort score of zero was interpreted as 'sub-threshold discomfort', one as 'mild discomfort', between two and four as 'moderate discomfort' and higher than four as 'severe discomfort'.

Apparatus for visual discrimination learning

Visual discrimination learning was carried out in custom-built setups that were placed in 75 x 75 x 75 cm boxes, providing a semi-enclosed environment (Fig 1A and 1B). The apparatus consisted of a head-plate holder, a spherical treadmill, a computer monitor, two lick spouts (16 Gauge, 3mm tip-diameter reusable feeding needles, Fine Science Tools) with lick detectors, tubes and valves to supply liquid reward. The treadmill was made of an airflow-supported Styrofoam ball [26] and restricted to forward and backward motion by a pin pushed into the side of the ball. An optical sensor, extracted from a computer mouse (G502, Logitech), tracked rotation of the ball using a custom-written LabVIEW (National Instruments) program. The mouse was head-fixed on the ball using a surgically implanted aluminum head plate, clamped into a custom-designed holder (S1 File). The head plate holder employed a (simplified) system of kinematic mounts to ensure reproducible positioning of the animal's head within the apparatus (Fig 1D; S1 File; [27]). Visual stimuli were presented on a gamma corrected computer monitor (Dell P2414H; resolution: 1920 by 1080 pixels; width: 52.8 cm; height 29.6 cm; maximum luminance: 182.3 Cd/m^2). The monitor was positioned in front of the mouse at a distance of 18 cm and centered at 0 degrees azimuth and elevation. The box was illuminated by red LEDs (630 nm), and a webcam (Logitech F100) was used to observe the mouse and setup within the enclosed space.

The two steel lick spouts were mounted on a custom 3D-printed holder that allowed fine adjustment of the space between the lick spout nozzles (S2 File). The lick spouts were positioned in front of the animals' mouth using a movable arm (Fig 1C, left panels). Care was taken to place the lick spout well within the reach of the tongue, which is especially important in the first pre-training sessions. Precise central positioning of the lick spouts with respect to the animal's mouth was critical; asymmetrical placement sometimes biased mice to make more licks on the closer spout. Each lick spout was connected to a custom-made lick detection circuit based on Weijnen [28] and Slotnick [29]. The circuit registered a voltage drop on the non-inverting high impedance input of an operational amplifier (LT1079CN; Linear Technologies) when the mouse short-circuited the input by licking on the spout (Fig 1C, right panel). The inverting input was connected to a voltage divider such that an individual lick triggered a strong discrete voltage drop in the amplifier output. The non-inverting and inverting inputs of the circuit could be switched in order for the circuit to report licks by voltage peaks. However, the described arrangement allows detecting whether the circuit is switched on from the baseline circuit output voltage.

Liquid reward was supplied through the lick spout by gravitational flow, operated using full opening pinch valves (NResearch Inc.). Valves were individually calibrated to supply drops of approximately 8 μl, which required valve-open durations of roughly 50 ms for water and approximately 75 ms for soymilk. Tubing was pressure-flushed with distilled water after each behavioral training session to prevent clogging. Signals from the lick detectors, the optical speed sensor and other triggers were recorded with two USB multifunction input/output devices (USB6001, National Instruments). The first device was used for closed loop control of the setup using a custom-written behavioral-training program (Matlab, Mathworks). The second device passively recorded all sensor signals at 500 Hz using a custom-written data-acquisition program (LabVIEW, National Instruments), which allowed for more precise offline analysis of behavioral parameters (see Data analysis).

Habituation and pre-training for head-fixed two-choice operant conditioning

Behavioral procedures were carried out six times per week between 14:00 and 18:00. In a two-week period prior to head-fixed operant training, mice were habituated to the

experimental procedures. Each habituation session lasted 10 to 15 minutes during which the mouse was (1) held in the experimenter's gloved hands, (2) placed on the surface of a Styrofoam ball, (3) fed water or soymilk through a syringe and (4) accustomed to brief head fixation by holding the head plate manually for a few seconds. In this specific experiment animals were habituated for a period of two weeks because we tested different variants of soymilk (see above). However, mice typically accustom to these procedures in three to four days.

In order to shape animals for the head-fixed visual two-alternative choice task, we implemented two stages of head-fixed pre-training. The first stage familiarized animals with the association between timed licks and liquid reward from a single lick spout. To this end, animals were exposed to the trial sequence (Fig 1E), but in absence of visual stimulus presentation. Each trial started with an inter-trial interval of 2.0 s, after which the mouse was required to withhold licking and cease running (velocity below 1 cm/s) for a duration of at least 0.6 s to 0.8 s (varied per trial in order to prevent mice from learning a fixed timing sequence). When this requirement was met, the trial proceeded with the visual stimulus period. In pre-training stage 1 and 2 no actual visual stimulus was presented in this period, the screen remained blank. After 1.0 s from the onset of the visual stimulus period, the mouse could make a lick on the fluid spout in order to receive a single drop (approximately 8 µl) of water or soymilk. This period, during which a lick on the spout initiated reward delivery (named 'response window'), lasted initially 15.0 s and was gradually reduced to 5.0 s in subsequent pre-training sessions. At the start of the training sessions, a few drops were given by manual activation of the valves in order to motivate the mouse to lick for reward and to adjust the lick spout's positioning relative to the mouth and tongue. Mice proceeded to the second pre-training stage when they performed about 50 rewarded trials per training session on two consecutive days.

In pre-training stage 2 the trial sequence remained the same, except that now two lick spouts were positioned in front of the animal. On each trial, only a single lick spout was selected as active, and only a lick on this spout, during the response window, triggered reward delivery. Licks on the non-active spout were recorded but did not abort the remaining period of the trial/response window. The distance between the left and right lick spout was initially set to 1.0 to 1.5 mm. Later-on in pre-training stage 2, the inter-spout distance was increased to approximately 3.0–4.0 mm, the inter-trial interval was increased to 4.0 s and the response window duration was reduced to 4.0 s. Mice proceeded to the visual discrimination task when, in pre-training stage 2, animals performed a minimum of 50 trials per session and consumed drops without a strong preference for one of the two lick spouts.

Side bias correction strategy

Mice tend to develop a strategy of responding with a majority of the licks on only one of the two lick spouts (i.e. they showed a 'side-bias'), which we aimed to prevent using the following strategy. On each trial, we drew a random number r between -1 and +1. If this number was above an adjustable threshold t_b (bias-threshold), the next trial would give reward on the left spout, otherwise it would give reward on the right lick spout (Eq 1).

$$Next\ trial, side = (r > t_b \rightarrow Left) \land (r \leq t_b \rightarrow Right)$$ Eq 1

The value of the threshold t_b was calculated using the outcome of the last 20 non-missed trials where $n_{correct\ left}$ and $n_{correct\ right}$ were the total number of trials in which the first lick in the response window was on the correct spout, and $n_{total\ left}$ and $n_{total\ right}$ were the total number of

presented 'left trials' and 'right trials' within the 20-trial period (Eq 2).

$$t_b = \min\left\{m, \max\left\{-m, \left(\left(\frac{n_{correct\ left}}{n_{total\ left}}\right) - \left(\frac{c_{correct\ right}}{n_{total\ right}}\right)\right)\right\}\right\} \qquad \text{Eq 2}$$

The value of m instated a minimum probability for either stimulus to be selected by bounding the value of t_b to the range $-m$ to $+m$. Thus, when a mouse would only lick on the left lick spout, the value of t_b would approximate m, reducing the chance that the next trial would be a 'left trial' to minimally $0.5 - {}^m/_2$ and increasing the chance that the next trial would be a 'right trial' to maximally $0.5 + {}^m/_2$. As a result, mice were presented with more trials on the non-preferred lick spout (i.e. right), gradually and eventually altering the mouse's preference until it was balanced between spouts. The side-bias correction algorithm was active in pre-training stage 2 and during the first 5 to 7 training sessions of the visual discrimination stage.

Head-fixed visual two-choice operant conditioning

Two choice (lick left/lick right) operant conditioning featured visual stimuli consisting of sinusoidal gratings, drifting at 1.5 cycles/s. For each mouse, one stimulus was assigned to indicate 'lick left' and another to indicate 'lick right'. These two stimuli were chosen such that each had one of two orientations that differed by 90 degrees, and each had either a low or a high spatial frequency (0.04 or 0.1221 cycles/degree). Selection of stimulus orientation and spatial frequency was counterbalanced across animals. Full contrast stimuli were presented in a 37 degree diameter circular area, centered at 10 degrees elevation and 0 degrees azimuth and blended within an annulus of 4 degrees width into an equiluminant grey background (total stimulus diameter including blended surround was 45 degrees).

Visual discrimination training followed the same basic trial structure as described above (Fig 1E), with the main addition that now a visual stimulus was presented for 2.25 s. The response window (3.0 s duration) started 1.0 s after stimulus onset. During the response window, a lick on the correct spout triggered reward delivery, while a lick on the incorrect spout caused a time-out. On rewarded/correct trials, stimulus presentation was continued for the full 2.25 s. On incorrect trials, the stimulus was replaced by a narrow horizontal black bar spanning the width of the display, presented for the duration of the time-out (2.5 s). Stimulus presentation or time-out was followed by an inter-trial interval of 5.0 s. Licks during the inter-trial interval and in the 1.0 s period between stimulus onset and response window onset (called 'grace period') [9] did not change the trial flow. In order to facilitate exploration and motivation, time-outs were not implemented in the first three training sessions. Therefore, in these initial sessions, an incorrect lick did not abort the response window and the mouse could still obtain a reward by subsequently licking on the correct spout.

Data analysis

Experimental and behavioral parameters such as the timing of licks, timing of drops, running speed, stimulus onset and other triggers were extracted from the passive data-recorder at 2 ms temporal resolution (LabVIEW, National Instruments) and analyzed using custom-written Matlab (Mathworks) and Python routines.

Continuous home cage activity patterns were calculated from the 12 sensors of the DVC system using a custom analysis program (written in Python). Each sensor provided a constant signal (4 Hz), which dropped when a mouse moved near/over it. The variance of the sensor signal was calculated within time bins of 1 minute and subsequently averaged across sensors, resulting in a minute-by-minute indication of average home cage activity per single housed

animal. Per mouse/cage, outlying values (>95 percentile) were clipped to the value of the 95th percentile; these outliers often coincided with cage removal from or insertion into the rack. Next, all data points were normalized per mouse/cage (by division) to the 85th percentile of all values recorded during baseline periods (the 7 day period before surgery and the 14 day period before food/water restriction).

Learning performance was calculated as fraction of correct trials per session and evaluated across training sessions. The resulting learning curve was fit with a sigmoidal curve ([Eq 3](#)) where x was the average fraction correct trials per session, and parameters y_0 (minimum of curve), c (maximum of curve relative to y_0), k (steepness) and x_0 (time point of maximum steepness) were estimated using least squares fitting.

$$Fitted\ curve = y_0 + \frac{c}{1 + e^{-k(x-x_0)}}$$
<div align="right">Eq 3</div>

Latency to learning was determined as the number of sessions until an animal exceeded the criterion of 66% correct trials. The behavioral threshold of 66% correct trials was determined based on prior experience. The probability of detecting a single false-positive behavioral threshold crossing across the 23 sessions of the learning curve was 0.001 (assuming 100 trials per session). Maximum learning curve performance was estimated per mouse from the maximum of the individually fitted learning curve. This measure approximates the average level of performance that mice reached after 23 training sessions, independent of the latency to criterion. The total amount of water or soymilk that a mouse consumed during the task was computed from the number of drops that the mouse received. Data are presented as mean ±SD unless mentioned otherwise. Between-group statistical comparisons were carried out using a Mann-Whitney U test.

Results

Adaptation to reversed day/night cycle, surgery and recovery

Four weeks before starting food or water restriction, C57Bl/6j mice were transferred from a local animal breeding facility into individual 24hr/day activity monitoring cages (DVC, see [Methods](#)) that were kept in an animal holding room with a reversed day/night cycle. After an adaptation period of 9 to 10 days, the 12 animals with the highest bodyweight were randomly assigned to two experimental groups (food or water restriction, n = 6 each), implanted with a head-bar and subsequently allowed to recover until the start of the experiment. The four remaining mice (having the lowest body weight on the two surgery days) were not implanted and were left kept in their home cage throughout the experiment. While all implanted animals showed a reduction in body weight on the days immediately following surgery, both experimental groups recovered within seven days to a body weight that was comparable to the non-implanted group ([Fig 2A](#)).

Animal wellbeing during food or water restriction

The *ad libitum* reference weight of all mice was taken at 14:00 on day zero, after which food or water restriction was started (see [Methods](#)). The body weight of each mouse was maintained at around 85% of the individual *ad libitum* reference in all mice throughout the period of restricted food or water access ([Fig 2A and 2B](#)). All animals received a daily individually calibrated supplement of solid food (chow) or water (see [Methods](#); [Fig 2C](#)) in addition to any soymilk or water they obtained during handling or training ([Fig 2D](#)).

Daily discomfort scores were assessed from the day of the surgery until 10 days after the end of food/water restriction ([Fig 2E](#), solid lines). In addition, the institutes animal welfare
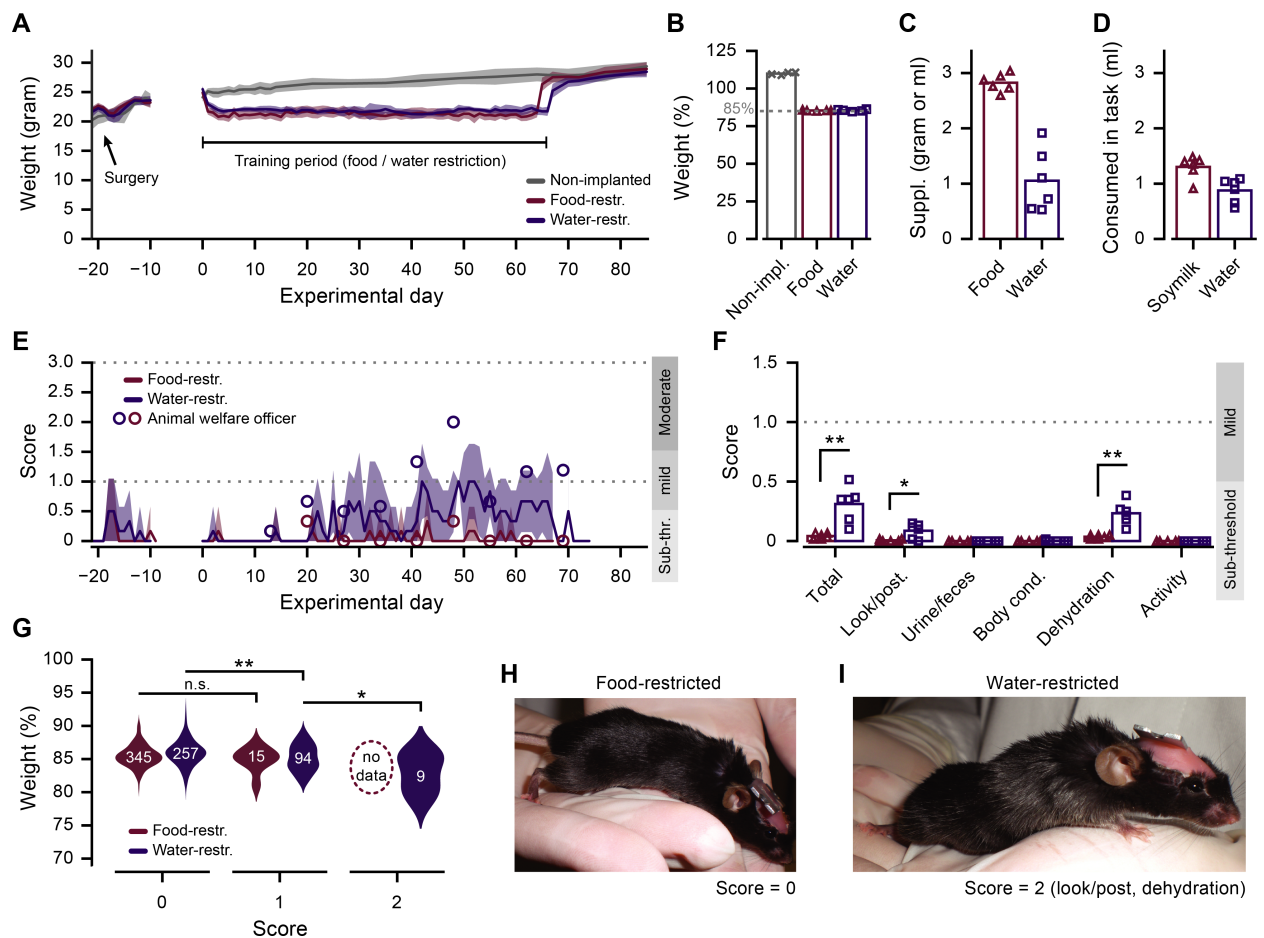
Fig 2. Animal weights and discomfort scores. A. Mean (±SD) daily weight of each experimental group across the entire experiment (gray: non-implanted, n = 4; red: food-restricted, n = 6; blue: water-restricted, n = 6). B. Average weight, in percentage of reference weight, throughout the period of food or water restriction. C. Amount of supplemented food (red) or water (blue) given (average of entire training period). D. Amount of soymilk (red) or water (blue) earned during training (average of entire training period). E. Mean (±SD) daily score of food (red) and water (blue) restricted mice over the entire experiment. Circles indicate scores as judged by the animal welfare officer. F. Daily score averaged across the period of food/water restriction. Total score is the sum across all five individual scores (look/posture, urine/feces, body condition, dehydration signs, activity; MWU test, *p = 0.018, ** p = 0.002). G. Distribution of daily measured weight as a function of the daily determined discomfort score for food- and water-restricted mice (MWU test, *p = 0.016, ** p = 0.002). Numbers in distribution plots indicate n in individual daily measurements. H. Example photo of food-restricted mouse (discomfort score 0, 'sub-threshold'). I. Example photo of water-restricted mouse (discomfort score, total = 2, 'moderate'; look/posture = 1; dehydration signs = 1). All panels: grey crosses (non-implanted), red triangles (food-restricted) and blue squares (water-restricted) indicate averages for individual animals.

officer assessed scores weekly, each Monday at 09:00, during the period of food/water restriction (Fig 2E, circles). The daily assessment of discomfort during the course of the experiment ranged mostly from 'sub-threshold' to 'mild', but individual scores very occasionally exceeded into the 'moderate' range. Signs of discomfort were most often observed in the post-surgery period and from the third week of food/water restriction onwards (Fig 2E).

The average score during the period of food/water restriction remained well below the cut-off for 'moderate' discomfort (Fig 2F). However, the food-restricted group had significantly lower total scores compared to the water-restricted group (total: food-restricted, score = 0.04 ±0.02; water-restricted, score = 0.31±0.13; MWU test, p = 0.002; n = 12 mice). This difference was mostly caused by observations of mild skin turgor (signs of dehydration: food-restricted, score = 0.04±0.01; water-restricted, score = 0.23±0.09; MWU test, p = 0.002; n = 12 mice) and

slightly erected, shaggy fur (look/posture: food-restricted, score = 0.01±0.01; water-restricted, score = 0.09±0.06; MWU test, p = 0.018; n = 12 mice). Scores on the other aspects did not exceed zero, except for a single occurrence of a score for the body condition of a water-restricted mouse.

The body weight of water-restricted mice with a total score above zero was on average significantly lower than that of mice with a zero score (score 0: 85.9±1.9%; score 1: 85.2±2.0%; score 2: 82.9±2.8%; MWU test; 0 vs. 1, p = 0.002; 1 vs. 2, p = 0.012; n = 360 scores; Fig 2G). This relation did not hold for food-restricted animals, probably because of the overall very low occurrence of >0 scores in this group (score 0: 85.5±1.6%; score 1: 84.9±1.7%; MWU test; 0 vs. 1, p = 0.30; n = 360 scores). In general, it is important to note that the differences between scores can be quite subtle, as is illustrated in Fig 2H and 2I, depicting a mouse with a score of 0 next to another one that had a total score of 2 (look/posture = 1; signs of dehydration = 1).

Continuous monitoring of physical activity in the home cage

While the discomfort score featured an instantaneous assessment of physical activity of the mice (activity and behavior), this could not be assessed without disturbing the mice in the first place. In order to measure activity of mice during the entire 24-hour cycle, we recorded the activity of each mouse in its home cage. Individual measurements were normalized to baseline activity as observed before the start of food/water restriction (see Methods; Fig 3A). These continuous readings were sensitive enough to measure the gradual adaptation to the reversed day/night cycle during the first seven days of the experiment (Fig 3B) and alterations to the day/night rhythm during the first two days after head-bar implantation surgery (Fig 3C).

Continuous home-cage activity recordings allowed us to monitor both the acute and long-term effects of restricted access to food or water. During the first few hours after restriction commenced, both experimental groups showed increased activity as compared to the non-implanted (non-restricted) group, which might be explained by the change into a novel cage (Fig 3D). On the following days, water-restricted animals showed a gradual decline in their daily activity, while food-restricted mice initially increased their home cage activity (Fig 3D). This initial increase in activity could indicate food-seeking/digging behaviors, before the animal learns that such efforts go unrewarded.

Across the entire duration of restriction, both food- and water-restricted mice showed reduced activity in the (active) daily light-off period (10:00–22:00, excluding the period during which training was typically done), as compared to their respective baseline levels before restriction had started (food-restricted: baseline = 0.62±0.16; training = 0.42±0.12; MWU test, p = 0.015; n = 6 mice; water-restricted: baseline = 0.47±0.04; training = 0.25±0.04; MWU test, p = 0.003; n = 6 mice; Fig 3E and 3F). This reduction in activity, relative to baseline activity, was not significantly different between food- and water-restricted mice (food-restricted: activity percentage of baseline = 68.0%±14.6%; water-restricted: activity percentage of baseline = 53.6%±5.9%; MWU test, p = 0.0641; n = 12 mice). Finally, in the post-restriction period, during which food and water was available *ad libitum* again, the average daily activity returned to levels that were comparable to the pre-training baseline (food-restricted: post-restriction = 0.73±0.19; water-restricted: post-restriction = 0.45±0.07; Fig 3F). Thus, by using continuous home-cage recordings we observed that food and water restriction induced a reversible reduction of overall activity levels that went undetected using the instantaneous scoring method.

Operant behavior and task-motivation

To compare how well the method of food and water restriction motivated mice to work for reward in a behavioral paradigm, we compared the total number of completed trials that mice
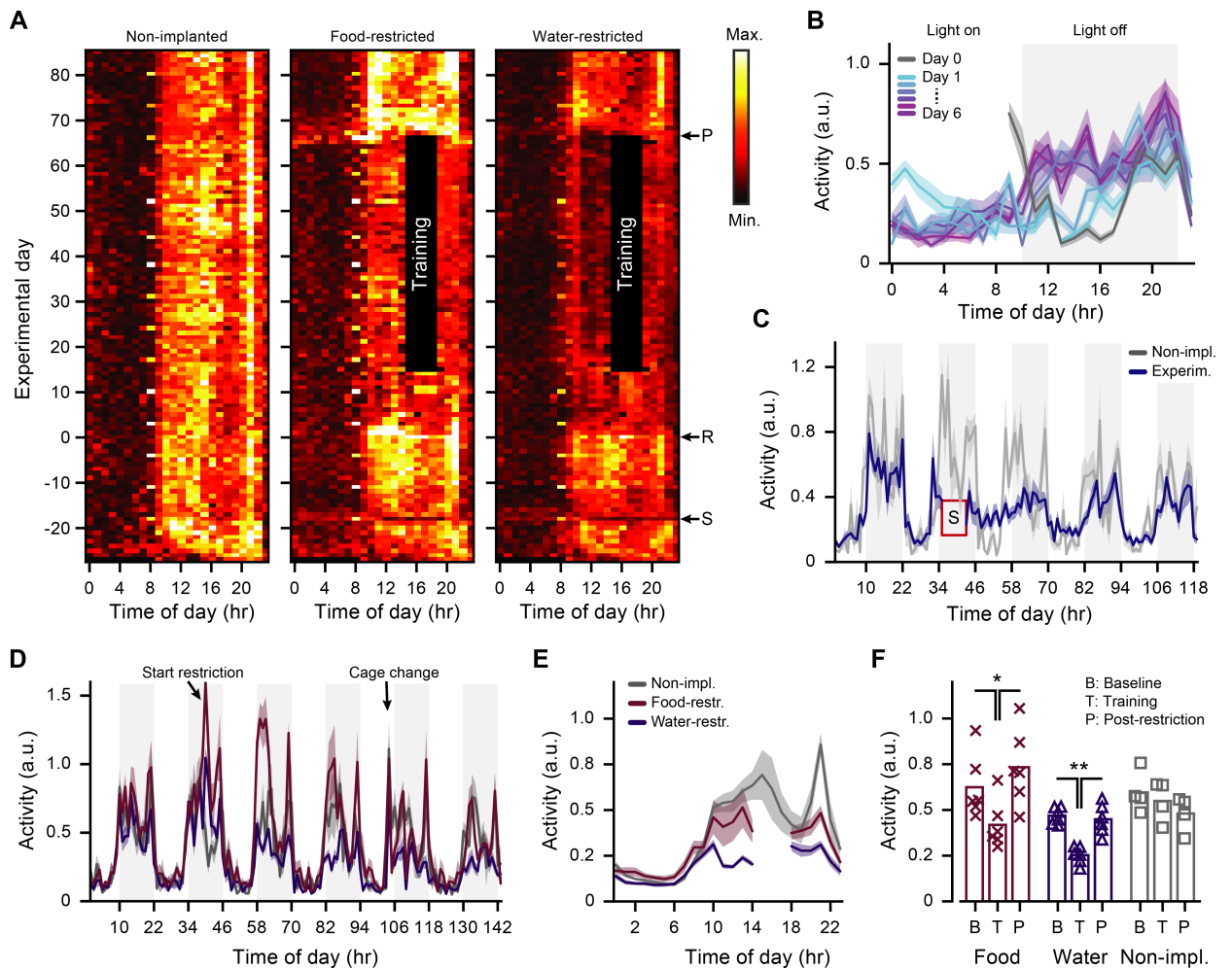
Fig 3. Continuous monitoring of physical activity in the home cage. A. Heat maps depicting baseline-normalized physical activity per hour (x-axis) throughout the days of the experiment (y-axis) as measured in the home cage, averaged across the non-implanted and experimental groups separately. Arrows: 'S' indicates the two days on which surgeries were performed; 'R' the day on which food or water restriction started; 'P' start of the post-training period (note that the food-restricted group received *ad libitum* access to food from two days before this post-training period). Cage changes can be identified as single bright data points, weekly reoccurring at 08:00. B. Hourly averaged (±SEM) home cage activity for the first seven days of adaptation to the reversed day/night cycle. C. Hourly averaged (±SEM) activity centered on the day of head bar implantation (blue, experimental group) or a matched day for animals that did not receive a head bar (gray, non-implanted group). D. Six days of average hourly home cage activity (mean±SEM), starting one day before onset of food or water restriction. E. Average (±SEM) 24hr home cage activity pattern throughout the entire period of training. Data of the experimental groups during the period of training (14:00–18:00) were left out. F. Mean (±SEM) home cage activity in the (active) light-off period (training period excluded). 'B': Baseline period, day -14 to 0. 'T': Training period, day 1 to 66. 'P': Post-restriction period, day 67 to 85. Crosses, triangle and squares indicate data points from individual mice (* MWU test, p<0.02; ** MWU test, p = 0.003).

https://doi.org/10.1371/journal.pone.0204066.g003

did in the pre-training stages (where every finished trial resulted in delivery of 8 µl soymilk or water). In pre-training stage 1, and (to a lesser extent) in pre-training stage 2, food-restricted mice executed significantly more trials compared to water-restricted animals (pre-training 1, # trials, food-restricted: 226±57; water-restricted: 45±21; MWU test, p = 0.003; pre-training 2, # trials, food-restricted: 237±84; water-restricted: 119±38; MWU test, p = 0.023; n = 12 mice; Fig 4F). As a direct consequence of this difference in total trial number, water-restricted mice required more pre-training stage 1 and pre-training stage 2 sessions to reach criterion compared to food-restricted animals. While we have no clear explanation for this, we noted that in subsequent experiments in our laboratory using water-restriction mice needed fewer pre-
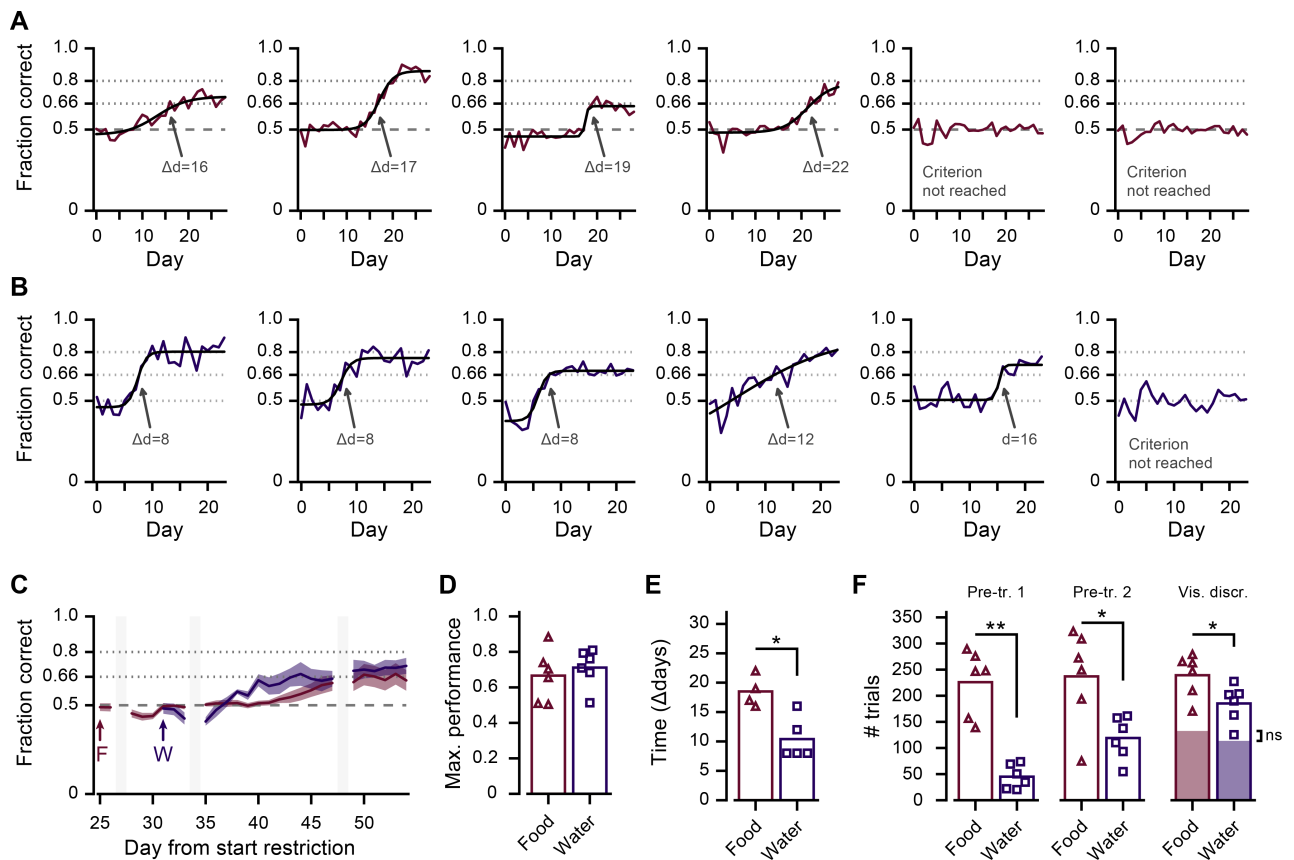
Fig 4. Visual discrimination in a head-fixed two-choice task. A, B. Learning curves of food (A) and water (B) restricted mice. Red and blue lines show the day-to-day performance for each animal, starting at the first day of visual discrimination learning. Black curve is a sigmoidal fit to data from animals that reached criterion (>66% correct). Gray arrows indicate the day on which mice reached criterion. C. Mean (±SEM) learning curve of all food- (red) and water- (blue) restricted mice in the overall experimental timeline. 'F' and 'W' indicate start days of training food- and water-restricted mice. Gray bars denote days without training. D. Maximum learning curve performance, determined by the sigmoidal fit in the time period during which mice were trained (as shown in A and B). E. Average number of days until criterion (>66% correct) was reached (MWU test, *p = 0.038). F. Average number of trials that mice performed per day in each of the training stages ('Pre-tr 1': pre-training stage 1, 1 lick spout; 'Pre-tr 2': pre-training stage 2, 2 lick spouts; 'Vis. Discr.': visual discrimination task (training stage 3); MWU test, ns: not significant, *p = 0.023, **p = 0.003). The red/blue shaded area in bars of the visual discrimination stage indicates the fraction of rewarded (correct) trials.

training sessions (three to five pre-training stage 1 and two to four pre-training stage 2 sessions). This indicates that potentially subtle changes in procedures, e.g. the experimenters becoming more experienced with the sub-millimeter positioning of the lick spouts, or only a single experimenter carrying out mouse handling and training, can reduce the number of pre-training sessions that water-restricted mice need.

In the final training stage (visual discrimination) the difference between the two groups was less pronounced, even-though food-restricted mice still performed a significantly larger number of trials compared to water-restricted mice (total # trials, food-restricted: 239±38; water-restricted: 185±33; MWU test, p = 0.023; Fig 4F). However, when only considering the trials in which mice made a correct choice, and thus received the soymilk or water reward, food- and water-restricted animals performed approximately equal numbers (Rewarded/correct # trials, Food-restricted: 132±26; Water-restricted: 114±28; MWU test, p = 0.149; n = 12 mice; Fig 4F).

The fact that water-restricted mice performed a lower number of trials throughout all training stages could indicate an overall lower motivation to work for water reward. Alternatively,

water-restricted mice might satiate faster from water compared to how fast food-restricted mice satiate from soymilk, and therefore completed fewer trials. Anticipatory licking is a reward-oriented behavior that is related to task-motivation and that can be computed for individual trials [30]. By counting anticipatory licks in a 1 s period from stimulus onset until the response window started (Fig 1E) and averaging over only trials in which animals produced an operant response, we approximated task-motivation independent of satiation. This measure showed that during the final training sessions of the experiment, both food- and water-restricted mice made roughly 3 anticipatory licks per single trial (anticipatory # licks, last 10 sessions, food-restricted: 2.79±1.21; water-restricted: 2.93±0.42; MWU test, p = 0.189; n = 12 mice). However, during the first training sessions of the visual discrimination stage (stage 3), food-restricted mice systematically made fewer anticipatory licks compared to water-restricted mice (anticipatory # licks, first 10 sessions, food-restricted: 1.73±0.90; water-restricted: 3.30 ±0.91; MWU test, p = 0.015; n = 12 mice). This argues that the lower number of trials that water-restricted mice performed in each training stage did not reflect reduced motivation to lick for reward. Quite the opposite: the results rather suggest that water-restricted mice were even more motivated, but probably satiated faster compared to food-restricted animals.

To confirm that satiation is an important factor in task-motivation, we tested whether there was a correlation between the relative weight of a mouse and its behavioral drive. We found that the daily measurement of relative body weight significantly predicted the number of trials that a mouse would perform in the training session of the same day (Correlation of percentage body weight and total number of trials, z-scored per mouse; food-restricted: r = -0.22, p = 0.005; water-restricted: r = -0.47, p = $3.2 \cdot 10^{-10}$). In summary, food and water restriction can both be used to motivate animals in an operant task, but the total number of trials that mice perform depends on the restriction paradigm.

Operant learning and performance

To test for differences in operant learning, mice were trained to discriminate visual patterns in the two-choice head-fixed lick left/lick right task. Out of twelve mice, four food-restricted and five water-restricted mice reached the performance criterion of 66% correct trials on a given day (Fig 4A and 4B). For all mice, maximum learning curve performance was estimated from the fitted learning curve on the last day of training and did not differ between groups (Maximum of fitted learning curve, food-restricted: 0.67±0.13; water-restricted: 0.71±0.10; MWU test, p = 0.189; n = 12 mice; Fig 4C and 4D). However, water-restricted mice reached the criterion of 66% correct trials significantly faster compared to food-restricted mice (food-restricted, Δdays = 18.5±2.3; water-restricted, Δdays = 10.4±3.2; MWU test, p = 0.038; n = 9 mice; Fig 4C and 4E). This difference did not depend on the exact value of the threshold. A similar difference was observed with a higher threshold (70%, as in Guo et al., 2014; food-restricted, Δdays = 21.0±2.9; water-restricted, Δdays = 11.0±3.0; MWU test, p = 0.033; n = 9 mice) as well as with a lower threshold (60%; food-restricted, Δdays = 17.3±1.9; water-restricted, Δdays = 5.8 ±2.4; MWU test, p = 0.003; n = 10 mice). Also, using an altogether different method of quantifying whether the learning criterion was reached, the number of training sessions to reach the point of maximum steepness of the sigmoid fitted learning curve, we observed that water-restricted mice learned faster (food-restricted, Δdays = 18.0±2.8; water-restricted, Δdays = 7.8 ±4.8; MWU test, p = 0.046; n = 9 mice).

To investigate whether motivational state or satiation could explain the difference in speed of learning, we tested whether either the average relative weight-loss of a mouse, or the average number of anticipatory licks in 10 pre-learning sessions, predicted the number of sessions needed to reach learning criterion. However, neither variable correlated significantly with

learning speed (correlation of percentage body weight and time to reach criterion, z-scored per condition: r = 0.11, p = 0.77; correlation of # of anticipatory licks and time to reach criterion, z-scored per condition: r = -0.54, p = 0.14; n = 9 mice). Additionally, we tested whether day-to-day fluctuations in relative body weight predicted task performance on the corresponding day (in mice that performed above criterion), which also did not correlate significantly in either the food- or water-restricted group (correlation of session-wise percentage body weight and performance, z-scored per mouse; food-restricted: r = -0.19, p = 0.28, n = 34 sessions; water-restricted: r = 0.11, p = 0.43, n = 58 sessions).

Another factor that may influence learning is general locomotor activity such as wheel-running in the home cage [31]. However, while food and water restriction both led to an overall reduction of home cage activity (Fig 3F), we observed that the most active mice actually took the longest to reach criterion (correlation of mean DVC activity and time to reach criterion, z-scored per condition: r = 0.82, p = 0.0069; n = 9 mice). In contrast to home-cage activity, we noted a large difference in the amount of running that the two groups of mice did during the visual discrimination task. Here, the water-restricted group ran about double the distance of the food-restricted group (distance ran per training session, food-restricted: 33±11 m; water-restricted: 66±24 m; MWU test, p = 0.023; n = 12 mice). Still, day-to-day differences in the amount of in-task running did not predict the performance on the visual discrimination task in either group (correlation of distance ran and performance, z-scored per mouse; food-restricted: r = 0.19, p = 0.28, n = 34 training sessions; water-restricted: r = 0.05, p = 0.72, n = 54 training sessions), and neither did the overall amount of in-task running predict the speed of learning (correlation in-task distance ran and time to reach criterion, z-scored per condition: r = -0.16, p = 0.67; n = 9 mice). Thus, parameters associated with motivational-state and physical activity provided a poor prediction of learning speed or task performance and do not likely explain the difference in time to reach learning criterion of food- and water-restricted mice.

Discussion

This study provides a detailed behavioral protocol for training mice in a fast and reliable way on a head-fixed two-alternative choice visual discrimination task. Our results show that most of the animals that were trained on the protocol learned discriminating visual stimuli within two or three weeks from the start of visual conditioning. An important aim of this study was to utilize the welfare- and behavioral read-outs of our training protocol to contrast two commonly used methods for motivating animals in head-fixed behavioral paradigms, i.e. food restriction with soymilk reward and water restriction with water reward. Using either method, the animals could be motivated to perform the task at or above criterion, without exceeding the 'mild' discomfort category, even for prolonged periods. However, we did observe specific differences in welfare assessment and in task performance, such as time to reach criterion and number of performed trials, which should be considered when selecting the restriction method.

Operant behavior

Throughout the training stages, there was a systematic difference in the number of trials that water- and food-restricted mice performed per session. In pre-training stage 1 and 2, food-restricted mice consumed larger volumes of soymilk than water-restricted mice consumed water. Furthermore, food-restricted animals proceeded faster through the pre-training stages than water-restricted mice. These differences might be explained by water-restricted mice satiating faster than food-restricted mice, since the 8-microliter water reward equaled on average 0.43% of the daily water intake in our experiment (1.93 ml), and the 8-microliter soymilk reward provided only 0.05% of the daily caloric food intake in this study (11.15 kcal). However,

in pre-training 1 sessions water-restricted mice performed on average only 50 trials, which is approximately only 25% of their daily water ration. Possibly, water-restricted mice already satiate after 40–50 drops and only through experiencing multiple pre-training sessions learn to obtain more water than they acutely need. On the other hand, Guo et al. [9] observed that water-restricted mice performed more trials when sucrose was added to the water reward. Similarly, in our experiment we noted that water-restricted mice after reaching criterion performed more trials when provided with soymilk reward compared to the usual water reward (data not shown). Therefore, soymilk reward may have had additional motivating or appetitive aspects compared to plain water reward. Possibly, this is related to the nutrients and flavor that soymilk contains. Alternatively, it is conceivable that the smell of reward (soymilk) coming directly from the lick spouts made it easier for food-restricted (soymilk rewarded) mice to learn the initial behavior of licking for reward.

Despite water-restricted mice performing fewer trials per session, they were on average faster in reaching the learning criterion (independent of which exact criterion we used). Throughout the experiment, we aimed for keeping the motivational state of individual animals comparable by maintaining the relative weight of each animal at 85% of the *ad libitum* measured reference value. In addition, we excluded that the difference in learning speed correlated with parameters reflecting task-motivation in this study. One remaining explanation could be that, as described above, the 8-microliter water drop might have been subjectively perceived as a larger reward compared to a soymilk drop of the same volume, thus providing a greater learning incentive for water-restricted mice. Moreover, there are fundamental differences in the neural circuits that mediate hunger and thirst [22], asserting different effects on motivation and learning that could provide a stronger incentive for learning in one group compared to the other. Importantly, the speed of learning, maximum learning curve performance and success rate achieved using either restriction method in this study was similar to previously reported head-fixed operant conditioning paradigms, e.g. [6,9].

A final in-task difference between food- and water-restricted animals was the distance they ran on the Styrofoam ball during the period of behavioral training, with food-restricted mice running significantly less than water-restricted mice. While speculative, one possible explanation is that water-restricted mice are in a higher anticipation state during the task, as they receive relatively more of their daily water amount within-task compared to the relative caloric amount that food-restricted mice receive during the task, leading to hyperactive behavior [32]. Another explanation is that water-restricted mice spend more time running because they performed fewer trials in each training session and therefore had more time in which they were not task-engaged.

Welfare assessment

We aimed to facilitate the objective categorical distinction between methods of food and water restriction by maintaining mice in both conditions close to a body weight of 85% of their baseline reference. Still, there remained a limited amount of day-to-day and mouse-to-mouse variation of relative body weight within the protocol. These fluctuations correlated with the number of trials that mice performed in the behavioral task, showing that relative weight loss is a key factor in task-motivation. In case of water-restricted mice, relative weight loss also corresponded to the daily discomfort score (Fig 2G). One reason the absence of a correlation between relative weight loss and discomfort scores in food-restricted mice could be that this group had mostly discomfort scores of zero. Alternatively, it is conceivable that scores directly attributable to dehydration, such as skin tenting and fur appearance, were more sensitive or better observable compared to scores related to reduced food intake, such as the body condition score.

Although we only once observed reduced activity using the instantaneous scoring method, both food- and water-restricted mice showed less home-cage activity in the continuous home-cage recordings compared to their own baseline measurement. In food-restricted mice, the reduction in overall home-cage activity could reflect reduced food-seeking behavior. In water-restricted mice, the reduced home-cage activity might (in part) reflect a decrease in grooming behavior, which could be a factor contributing to their higher score on the parameter 'look/posture' in the overall health assessment. Indeed, water loss in the form of saliva used for grooming can account for up to one third of water loss in rodents that are not water-restricted [33]. It is possible that water-restricted mice conserve water by reducing the amount of grooming, leading to overall poorer fur appearance.

It should be noted that we did not assay the effect of food or water restriction on the mouse's physiology and neuronal circuitry, neither did we measure the effect of water restriction on food-intake behavior. In addition, the five scoring parameters may have differed in their sensitivity for detecting food- or water restriction associated discomfort. Therefore, we do not aim to draw conclusions from the differences in scores between restriction regimens observed in this study, but rather advise considering these results in the context of literature on food and water restriction procedures, e.g. [20,23,34,35]. Furthermore, the choice for setting a threshold at 85% of pre-restriction body weight is rather arbitrary. Other studies use different thresholds, either above or below 85%, and occasionally take into account the gradual increase in weight that would be observed in non-restricted mice, e.g. [6,36–38]. Still, these methods do not consider that there may be individual variation in how mice adapt to chronic water restriction [35,39]. Therefore, in our opinion, the best method would be to set the threshold for continuation of an experiment entailing food or water restriction using the measure of discomfort directly, as for instance described in Guo et al. [9], and monitor the relative weight of the animals as an indication, but not as threshold.

Practical considerations

In the last two decades, the mouse has gained increasing attention in neuroscience as a versatile research model that can be adopted for studying sensory processing, learning and memory, decision making and motor behavior under both healthy and diseased conditions. Our behavioral protocol and conditioning task for training head-fixed mice can be readily combined with *in vivo* recording techniques such as intracellular patch clamp recordings [40], two-photon microscopy [13], but also with newly developed techniques for single cell control of neuronal activity patterns [41]. The two-choice lick left / lick right task can be easily adapted to include other sensory modalities, or expanded for the study of higher cognitive functions, making it a useful tool for studying mouse behavior in general. In addition, the in-task differences we observed between food- and water-restricted animals can be exploited in order to suit the specific behavioral requirements. Finally, we showed that the use of a continuous home-cage monitoring system allows expanding the quantification of animal wellbeing to include an objective measure of overall activity, which allows observing light-cycle adaptation, post-surgery recovery and effects of food and water restriction without disturbing the animals. Behavioral paradigms will likely always require precise fine-tuning of a large, mostly un-documented parameter space. The methods and procedures described in this study are intended to guide this process to smoother convergence while improving animal wellbeing.

Supporting information

S1 File. Head bar holder design. These files contain the designs of the head bar and of the components necessary for building the head bar holder. The files were produced in

SolidWorks (Dassault Systèmes) and can also be viewed using the free program eDrawings
(http://www.edrawingsviewer.com).
(ZIP)

S2 File. Lick spout holder design. This file contains the design of the 3D printable lick spout
holder. It was produced and can be opened using the online service TinkerCat (https://www.
tinkercad.com). The file can also be opened with the free program eDrawings (http://www.
edrawingsviewer.com) as well as with most software delivered with 3D printers.
(STL)

Author Contributions

Conceptualization: Pieter M. Goltstein, Sandra Reinert, Annet Glas, Tobias Bonhoeffer, Mark
Hübener.

Formal analysis: Pieter M. Goltstein.

Funding acquisition: Tobias Bonhoeffer, Mark Hübener.

Investigation: Pieter M. Goltstein, Sandra Reinert, Annet Glas, Mark Hübener.

Methodology: Pieter M. Goltstein, Sandra Reinert, Annet Glas.

Writing – original draft: Pieter M. Goltstein, Sandra Reinert, Annet Glas, Tobias Bonhoeffer,
Mark Hübener.

Writing – review & editing: Pieter M. Goltstein, Sandra Reinert, Annet Glas, Tobias Bonhoeffer, Mark Hübener.

References

1. Skinner BF. The behavior of organisms: An experimental analysis. New York: Appleton-Century;
1938.

2. Stone CP, Darrow CW, Landis C, Heath LL. Studies in the dynamics of behavior. Chicago: University
of Chicago Press; 1932.

3. O'Keefe J, Dostrovsky J. The hippocampus as a spatial map. Preliminary evidence from unit activity in
the freely-moving rat. Brain Res. 1971; 34: 171–175. PMID: 5124915

4. Harvey CD, Collman F, Dombeck DA, Tank DW. Intracellular dynamics of hippocampal place cells during virtual navigation. Nature. 2009; 461: 941–946. https://doi.org/10.1038/nature08499 PMID:
19829374

5. O'Connor DH, Peron SP, Huber D, Svoboda K. Neural activity in barrel cortex underlying vibrissa-based object localization in mice. Neuron. 2010; 67: 1048–1061. https://doi.org/10.1016/j.neuron.2010.
08.026 PMID: 20869600

6. Histed MH, Carvalho LA, Maunsell JH. Psychophysical measurement of contrast sensitivity in the
behaving mouse. J Neurophysiol. 2012; 107: 758–765. https://doi.org/10.1152/jn.00609.2011 PMID:
22049334

7. Sanders JI, Kepecs A. Choice ball: a response interface for two-choice psychometric discrimination in
head-fixed mice. J Neurophysiol. 2012; 108: 3416–3423. https://doi.org/10.1152/jn.00669.2012 PMID:
23019000

8. Abraham NM, Guerin D, Bhaukaurally K, Carleton A. Similar odor discrimination behavior in head-restrained and freely moving mice. PLoS One. 2012; 7: e51789. https://doi.org/10.1371/journal.pone.
0051789 PMID: 23272168

9. Guo ZV, Hires SA, Li N, O'Connor DH, Komiyama T, Ophir E, et al. Procedures for behavioral experiments in head-fixed mice. PLoS One. 2014; 9: e88678. https://doi.org/10.1371/journal.pone.0088678
PMID: 24520413

10. Poort J, Khan AG, Pachitariu M, Nemri A, Orsolic I, Krupic J, et al. Learning Enhances Sensory and Multiple Non-sensory Representations in Primary Visual Cortex. Neuron. 2015; 86: 1478–1490. https://doi.
org/10.1016/j.neuron.2015.05.037 PMID: 26051421

11. Burgess CP, Lak A, Steinmetz NA, Zatka-Haas P, Bai Reddy C, Jacobs EAK, et al. High-Yield Methods for Accurate Two-Alternative Visual Psychophysics in Head-Fixed Mice. Cell Rep. 2017; 20: 2513–2524. https://doi.org/10.1016/j.celrep.2017.08.047 PMID: 28877482

12. Aronov D, Tank DW. Engagement of Neural Circuits Underlying 2D Spatial Navigation in a Rodent Virtual Reality System. Neuron. 2014; 84: 442–456. https://doi.org/10.1016/j.neuron.2014.08.042 PMID: 25374363

13. Dombeck DA, Khabbaz AN, Collman F, Adelman TL, Tank DW. Imaging large-scale neural activity with cellular resolution in awake, mobile mice. Neuron. 2007; 56: 43–57. https://doi.org/10.1016/j.neuron.2007.08.003 PMID: 17920014

14. Harvey CD, Coen P, Tank DW. Choice-specific sequences in parietal cortex during a virtual-navigation decision task. Nature. 2012; 484: 62–68. https://doi.org/10.1038/nature10918 PMID: 22419153

15. Keller GB, Bonhoeffer T, Hübener M. Sensorimotor mismatch signals in primary visual cortex of the behaving mouse. Neuron. 2012; 74: 809–815. https://doi.org/10.1016/j.neuron.2012.03.040 PMID: 22681686

16. Andermann ML, Kerlin AM, Reid RC. Chronic cellular imaging of mouse visual cortex during operant behavior and passive viewing. Front Cell Neurosci. 2010; 4: 3. https://doi.org/10.3389/fncel.2010.00003 PMID: 20407583

17. Makino H, Komiyama T. Learning enhances the relative impact of top-down processing in the visual cortex. Nat Neurosci. 2015; 18: 1116–1122. https://doi.org/10.1038/nn.4061 PMID: 26167904

18. Allen WE, DeNardo LA, Chen MZ, Liu CD, Loh KM, Fenno LE, et al. Thirst-associated preoptic neurons encode an aversive motivational drive. Science. 2017; 357: 1149–1155. https://doi.org/10.1126/science.aan6747 PMID: 28912243

19. Heiderstadt KM, McLaughlin RM, Wright DC, Walker SE, Gomez-Sanchez CE. The effect of chronic food and water restriction on open-field behaviour and serum corticosterone levels in rats. Lab Anim. 2000; 34: 20–28. https://doi.org/10.1258/002367700780578028 PMID: 10759363

20. Toth LA, Gardiner TW. Food and water restriction protocols: physiological and behavioral considerations. Contemp Top Lab Anim Sci. 2000; 39: 9–17.

21. Krashes MJ, Shah BP, Madara JC, Olson DP, Strochlic DE, Garfield AS, et al. An excitatory paraventricular nucleus to AgRP neuron circuit that drives hunger. Nature. 2014; 507: 238–242. https://doi.org/10.1038/nature12956 PMID: 24487620

22. Jourjine N, Mullaney BC, Mann K, Scott K. Coupled Sensing of Hunger and Thirst Signals Balances Sugar and Water Consumption. Cell. 2016; 166: 855–866. https://doi.org/10.1016/j.cell.2016.06.046 PMID: 27477513

23. Tucci V, Hardy A, Nolan PM. A comparison of physiological and behavioural parameters in C57BL/6J mice undergoing food or water restriction regimes. Behav Brain Res. 2006; 173: 22–29. https://doi.org/10.1016/j.bbr.2006.05.031 PMID: 16870275

24. Giles JM, Whitaker JW, Moy SS, Fletcher CA. Effect of Environmental Enrichment on Aggression in BALB/cJ and BALB/cByJ Mice Monitored by Using an Automated System. J Am Assoc Lab Anim Sci. 2018; https://doi.org/10.30802/AALAS-JAALAS-17-000122 [Epub ahead of print]. PMID: 29669621

25. Ullman-Culleré MH, Foltz CJ. Body condition scoring: a rapid and accurate method for assessing health status in mice. Lab Anim Sci. 1999; 49: 319–323. PMID: 10403450

26. Hölscher C, Schnee A, Dahmen H, Setia L, Mallot HA. Rats are able to navigate in virtual environments. J Exp Biol. 2005; 208: 561–569. https://doi.org/10.1242/jeb.01371 PMID: 15671344

27. Scott BB, Brody CD, Tank DW. Cellular resolution functional imaging in behaving rats using voluntary head restraint. Neuron. 2013; 80: 371–384. https://doi.org/10.1016/j.neuron.2013.08.002 PMID: 24055015

28. Weijnen JA. Lick sensors as tools in behavioral and neuroscience research. Physiol Behav. 1989; 46: 923–928. PMID: 2634256

29. Slotnick B. A simple 2-transistor touch or lick detector circuit. J Exp Anal Behav. 2009; 91: 253–255. https://doi.org/10.1901/jeab.2009.91-253 PMID: 19794837

30. DeBold RC, Miller NE, Jensen DD. Effect of Strength of Drive Determined by a New Technique for Appetitive Classical Conditioning of Rats. J Comp Physiol Psychol. 1965; 59: 102–108. PMID: 14282384

31. Li H, Liang A, Guan F, Fan R, Chi L, Yang B. Regular treadmill running improves spatial learning and memory performance in young mice through increased hippocampal neurogenesis and decreased stress. Brain Res. 2013; 1531: 1–8. https://doi.org/10.1016/j.brainres.2013.07.041 PMID: 23916669

32. Sherwin CM. Voluntary wheel running: a review and novel interpretation. Anim Behav. 1998; 56: 11–27. https://doi.org/10.1006/anbe.1998.0836 PMID: 9710457

33. Ritter RC, Epstein AN. Saliva lost by grooming: a major item in the rat's water economy. Behav Biol. 1974; 11: 581–585. PMID: 4415674

34. Haines H, Ciskowski C, Harms V. Acclimation to chronic water restriction in the wild house mouse Mus musculus. Physiological Zoology. 1973; 46: 110–128.

35. Rowland NE. Food or fluid restriction in common laboratory animals: balancing welfare considerations with scientific inquiry. Comp Med. 2007; 57: 149–160. PMID: 17536615

36. Busse L, Ayaz A, Dhruv NT, Katzner S, Saleem AB, Schölvinck ML, et al. The detection of visual contrast in the behaving mouse. J Neurosci. 2011; 31: 11351–11361. https://doi.org/10.1523/JNEUROSCI.6689-10.2011 PMID: 21813694

37. Montijn JS, Goltstein PM, Pennartz CM. Mouse V1 population correlates of visual detection rely on heterogeneity within neuronal response patterns. Elife. 2015; 4: e10163. https://doi.org/10.7554/eLife.10163 PMID: 26646184

38. Jurjut O, Georgieva P, Busse L, Katzner S. Learning enhances sensory processing in mouse V1 before improving behavior. J Neurosci. 2017; 37: 6460–6474. https://doi.org/10.1523/JNEUROSCI.3485-16.2017 PMID: 28559381

39. Bekkevold CM, Robertson KL, Reinhard MK, Battles AH, Rowland NE. Dehydration parameters and standards for laboratory mice. J Am Assoc Lab Anim Sci. 2013; 52: 233–239. PMID: 23849404

40. Komai S, Denk W, Osten P, Brecht M, Margrie TW. Two-photon targeted patching (TPTP) in vivo. Nat Protoc. 2006; 1: 647–652. https://doi.org/10.1038/nprot.2006.100 PMID: 17406293

41. Mardinly AR, Oldenburg IA, Pégard NC, Sridharan S, Lyall EH, Chesnov K, et al. Precise multimodal optical control of neural ensemble activity. Nat Neurosci. 2018; 21: 881–893. https://doi.org/10.1038/s41593-018-0139-8 PMID: 29713079

3

BENCHMARKING MINIATURIZED MICROSCOPY AGAINST TWO-PHOTON CALCIUM IMAGING USING SINGLE-CELL ORIENTATION TUNING IN MOUSE VISUAL CORTEX

Declaration of author contributions

Benchmarking miniaturized microscopy against two-photon calcium imaging using single-cell orientation tuning in mouse visual cortex

Annet Glas[1,2], Mark Hübener[1], Tobias Bonhoeffer[1], Pieter M. Goltstein[1]*

1 Max Planck Institute of Neurobiology, Martinsried, Germany, **2** Graduate School of Systemic Neurosciences, Martinsried, Germany

* goltstein@neuro.mpg.de

Abstract

Miniaturized microscopes are lightweight imaging devices that allow optical recordings from neurons in freely moving animals over the course of weeks. Despite their ubiquitous use, individual neuronal responses measured with these microscopes have not been directly compared to those obtained with established *in vivo* imaging techniques such as bench-top two-photon microscopes. To achieve this, we performed calcium imaging in mouse primary visual cortex while presenting animals with drifting gratings. We identified the same neurons in image stacks acquired with both microscopy methods and quantified orientation tuning of individual neurons. The response amplitude and signal-to-noise ratio of calcium transients recorded upon visual stimulation were highly correlated between both microscopy methods, although influenced by neuropil contamination in miniaturized microscopy. Tuning properties, calculated for individual orientation tuned neurons, were strongly correlated between imaging techniques. Thus, neuronal tuning features measured with a miniaturized microscope are quantitatively similar to those obtained with a two-photon microscope.

Introduction

In recent years, the arsenal of imaging techniques for neuroscience has been supplemented with miniaturized microscopes, of which several versions are currently available [1–3]. Miniaturized microscopes allow simultaneous, functional imaging of hundreds of neurons in a variety of brain areas in freely moving animals as small as a mouse over extended periods of time [2,4–6]. Key merits of miniaturized microscopes as compared to benchtop microscopes are the ability for head-mounting and their low cost [1]. These qualities make miniaturized fluorescence microscopy a valuable complementary method to other *in vivo* imaging techniques [2]. A trade-off compared to two-photon microscopes is the lack of optical sectioning, resulting in poorer lateral and axial resolution due to out-of-focus fluorescence. In addition, conventional miniaturized microscopes have a reduced ability for imaging deeper in the tissue, which is inherent to single-photon versus two-photon illumination wavelengths (for an in-depth

technical comparison and a guide to imaging platform selection, see [5]). Together, these factors prevent *in vivo* imaging of sub-cellular structures such as dendritic spines as of yet [2]. On the positive side, miniaturized microscopy does enable chronic imaging of neurons and circuits in behavioral paradigms that require minimally constrained movement of the animal, and it has even been used as an alternative to functional two-photon imaging in head-fixed paradigms [7].

Despite the increasing use of miniaturized microscopy, signal amplitudes and neuronal tuning properties obtained with miniaturized microscope imaging have not been directly compared to those assessed with established *in vivo* imaging methods. Receptive field properties of neurons in primary visual cortex (V1) provide a suitable model for a direct comparison between both methods. Responses of visual cortex neurons to drifting gratings of particular orientations have been extensively investigated (e.g. [8,9]). Individual neurons respond selectively to gratings of particular orientations and their preferred orientation remains largely stable across longer periods of time [9–12]. Here, we perform *in vivo* miniaturized and two-photon microscopy of neurons in V1 of anesthetized mice presented with moving gratings. We identify the same neurons with both microscopy techniques, and quantify the similarity in response properties of matched neurons.

Materials and methods

Animals

All procedures were performed in accordance with the institutional guidelines of the Max Planck Society and the local government (approved by the Beratende Ethikkommission nach § 15 Tierschutzgesetz, Regierung von Oberbayern, Germany). Eight female C57BL/6J mice (~P60 on day of surgery) were individually housed in ventilated cages and kept on an inverted 12-h light, 12-h dark cycle with lights on at 10 AM. Ambient temperature (~22˚C) and humidity (~55%) were kept constant. Water and standard chow were available ad libitum.

Surgery

Mice were anesthetized with a mixture of fentanyl, midazolam, and medetomidine (FMM; 0.05 mg kg^{-1}, 5 mg kg^{-1}, and 0.5 mg kg^{-1} respectively, injected i.p.) and depth of anesthesia was monitored throughout the procedure by observation of the breathing rate and absence of a pedal reflex. Mice were placed in a stereotaxic apparatus (Neurostar) equipped with a thermal blanket (Harvard Apparatus). Eyes were covered with a thin layer of ophthalmic ointment. Lidocaine (0.2 mg ml^{-1}) was sprayed onto the scalp for topical analgesia and carprofen (5 mg kg^{-1}, injected s.c.) was administered for analgesia. The skull was exposed, dried and scraped with a scalpel. A custom-designed aluminum head bar was positioned using cyanoacrylate glue and subsequently covered with dental acrylic (Paladur). The location of V1 was verified using intrinsic signal imaging [13, 14] and a 4 mm circular craniotomy was created centered over V1. To sparsely label a population of V1 excitatory neurons, mice were injected with a viral vector mixture consisting of AAV2/1 CamKII0.4-Cre (1.15·10^{10} GC ml^{-1}, Penn Vector Core) and AAV2/1 hSyn-flex-GCaMP6s (7.26·10^{12} GC ml^{-1}, Penn Vector Core). At each injection site, 125 nl of viral vector was injected using a beveled glass pipette (30 µm outer diameter) at an injection speed of 25 nl min-1. The glass pipette was slowly retracted 10 min after initial placement. Upon injection, the craniotomy was covered with a circular cover glass (4 mm, Warner Instruments), which was glued in place using cyanoacrylate gel and subsequently cemented with dental acrylic. After surgery, mice were injected with a mixture of antagonists (naloxone, flumazenil, and atipamezole; 1.2 mg kg^{-1}, 0.5 mg kg^{-1}, and 2.5 mg kg^{-1}respectively, injected s.c.) and left to recover under a heat lamp. Carprofen (5 mg kg^{-1}, injected s.c.) was

given on the three following days. Imaging experiments were conducted at least two weeks after surgery.

Visual stimulation

Visual stimuli were displayed on a single LCD monitor (Dell P2717H; resolution: 1920 x 1080 pixels, width 60 cm, height 34 cm), with the center placed at roughly 45˚ azimuth and 12 cm from the animal's eye. To assess orientation tuning, we presented full-screen square wave gratings (8 directions, 45˚ spacing) with a spatial frequency of 0.04 cycles per degree and a temporal frequency of 1.5 Hz. The stimulus set was flanked with a 30 s pre- and post-stimulation period. Each trial consisted of 3 s of moving grating, followed by 5 s of inter-trial interval during which a gray screen was presented. During both miniaturized and two-photon microscopy imaging sessions, the complete stimulus set was repeated five times, with a random order of directions in each repetition (trial). To avoid stimulus light leak during two-photon imaging, monitor illumination was shuttered during each scan-line and only turned on during the line-scanner turnaround period [15]. The space between the microscopy objective and cranial window was closed off using opaque tape.

Miniaturized microscopy

Images were acquired with a commercially available miniaturized microscope (Basic Fluorescence Microscopy System—Surface, Doric Lenses) at a frame rate of 20 Hz and a resolution of 630 x 630 pixels (field of view 1 x 1 mm; Table 1). Laser power under the objective lens (2x magnification, 0.5 NA) was <1 mW for all imaging experiments. The excitation wavelength was 458 nm. To minimize movement, the miniaturized microscope was mounted on a rigid holder (Doric Lenses) attached to an xyz translation stage (Luigs & Neumann). To characterize the imaging resolution of the microscope, a 3-dimensional volume (1 μm steps between

Table 1. Microscope specifications and imaging settings.

	Minaturized microscope	Two-photon microscope
Illumination method	Epifluorescence	Two-photon
Frame rate	10 Hz	10 Hz
Maximum frame rate	50 Hz (at 630 x 630 pixels)	30 Hz (at 750 x 800 pixels)
Lens numerical aperture	0.5 NA	0.8 NA
Lens magnification	2x	16x
Field-of-view	1 mm x 1 mm (630 pixels x 630 pixels)	300 x 320 μm (750 x 800 pixels)
Excitation wavelength	458 nm	910 nm
Excitation power	<1 mW	25 mW
Optical resolution (X)[a]	3.52 μm	0.59 μm
Optical resolution (Y)[a]	6.12 μm	0.57 μm
Optical resolution (Z)[a]	33.35 μm	2.78 μm
Photobleaching[b]	1.013 ± 0.019 a.u.	0.994 ± 0.004 a.u.
Movement correction	<1.6 μm (95th percentile)	<1.6 μm (95th percentile)

[a] The optical resolution was emperically obtained by calculating the full width at half maximum (FWHM) of a Gaussian-curve fitted intensity profile of a subresolution (0.2 μm diameter) fluorescent bead.

[b] Photobleaching was defined as the fraction average fluorescence in the 30 s post-stimulation period compared to the 30 seconds pre-stimulus period (5–6 minute interval). A value of 1.0 indicates no change.

imaging planes) of yellow-green fluorescent microbeads (diameter 0.2μm; Invitrogen) embedded in 1.5% weight/volume agarose gel (Sigma) was acquired at a frame rate of 5 Hz.

For miniaturized microscope imaging experiments, mice were anesthetized with FMM (0.04 mg kg^{-1}, 4 mg kg^{-1}, and 0.4 mg kg^{-1} respectively, injected i.p.) The miniaturized microscope was positioned above the cranial window and lowered until the cortical surface blood vessel pattern became visible. To facilitate identification of individual neurons across microscopy techniques, a 3-dimensional volume spanning a depth 250 μm was acquired at 5 μm intervals between imaging planes while no visual stimulus was presented. Subsequently, visual stimuli (see above) were presented during imaging. Per session, up to 10 imaging planes were recorded in layer 2/3 at 10 μm depth intervals. The onset of imaging was approximately 60 minutes after the administration of anesthesia, and the total duration of recording was typically under 75 minutes.

Two-photon microscopy

Two-photon imaging was performed on a custom-built two-photon laser-scanning microscope with a Mai Tai eHP Ti:Sapphire laser (Spectra-Physics) set to a wavelength of 910 nm and a Nikon water immersion objective (16x magnification, 0.8 NA; Table 1). Images were acquired with an image resolution of 750 x 800 pixels at a frame rate of 10 Hz. The field of view for functional imaging was 300 x 320 μm. Laser power under the objective was kept stable at 25 mW throughout the experiment. Imaging data were acquired using custom software written in LabVIEW (National Instruments). To characterize the imaging resolution of the microscope, a high-resolution 3-dimensional volume (0.5 μm steps between imaging planes) of yellow-green fluorescent microbeads (diameter 0.2μm; Invitrogen) embedded in 1.5% weight/volume agarose gel (Sigma) was acquired at a frame rate of 5 Hz.

Two-photon imaging experiments were conducted one week after the miniaturized microscope imaging session in one half of the animals (n = 4 mice) and one week before the miniaturized microscope imaging session in the other half (n = 4 mice; see Fig 1A). Mice were anesthetized with FMM (0.04 mg kg^{-1}, 4 mg kg^{-1} and 0.4 mg kg^{-1} respectively, injected i.p.). The imaging location of the previous miniaturized microscopy session was determined by comparing the blood-vessel pattern using a wide-field camera that was aligned with the two-photon microscope (Teledyne DALSA Inc.). Subsequently, the matched field of view was imaged with the two-photon microscope. Prior to functional imaging, a volume of 300 x 320 x 200 μm (xyz) was imaged at 1 μm intervals while no visual stimulus was presented. For functional imaging, the anesthetized animal was presented with visual stimuli (see above), repeated for up to six imaging planes with depth increments of 10 μm.

Immunohistochemistry

Mice were deeply anesthetized and transcardially perfused with 9.25% w/v sucrose in distilled water followed by 4% PFA in PBS. Brains were then dissected out and post-fixed in 4% PFA for one week at 4˚C. Coronal sections (50 μm) were cut on a microtome (Thermo Fisher Scientific) and were kept free-floating at 4˚C until further processing. Immunohistochemistry was carried out using the primary antibodies chicken anti-GFP (1:1000; Millipore) labeling GCaMP6s and rabbit anti-Homer3 (1:250; Synaptic Systems), which labels excitatory neurons. After washing, sections were incubated with species-specific secondary antibodies conjugated to Alexa Fluor 488 (1:200, Life Technologies) or Cy3 (1:200, Life Technologies) and mounted with mounting medium containing DAPI (Vectashield).

Images were acquired using a laser-scanning confocal microscope (Leica, TCS SP8), across serial optical sections (spaced at 1 μm) acquired with a 20x objective (0.75 NA) at a resolution
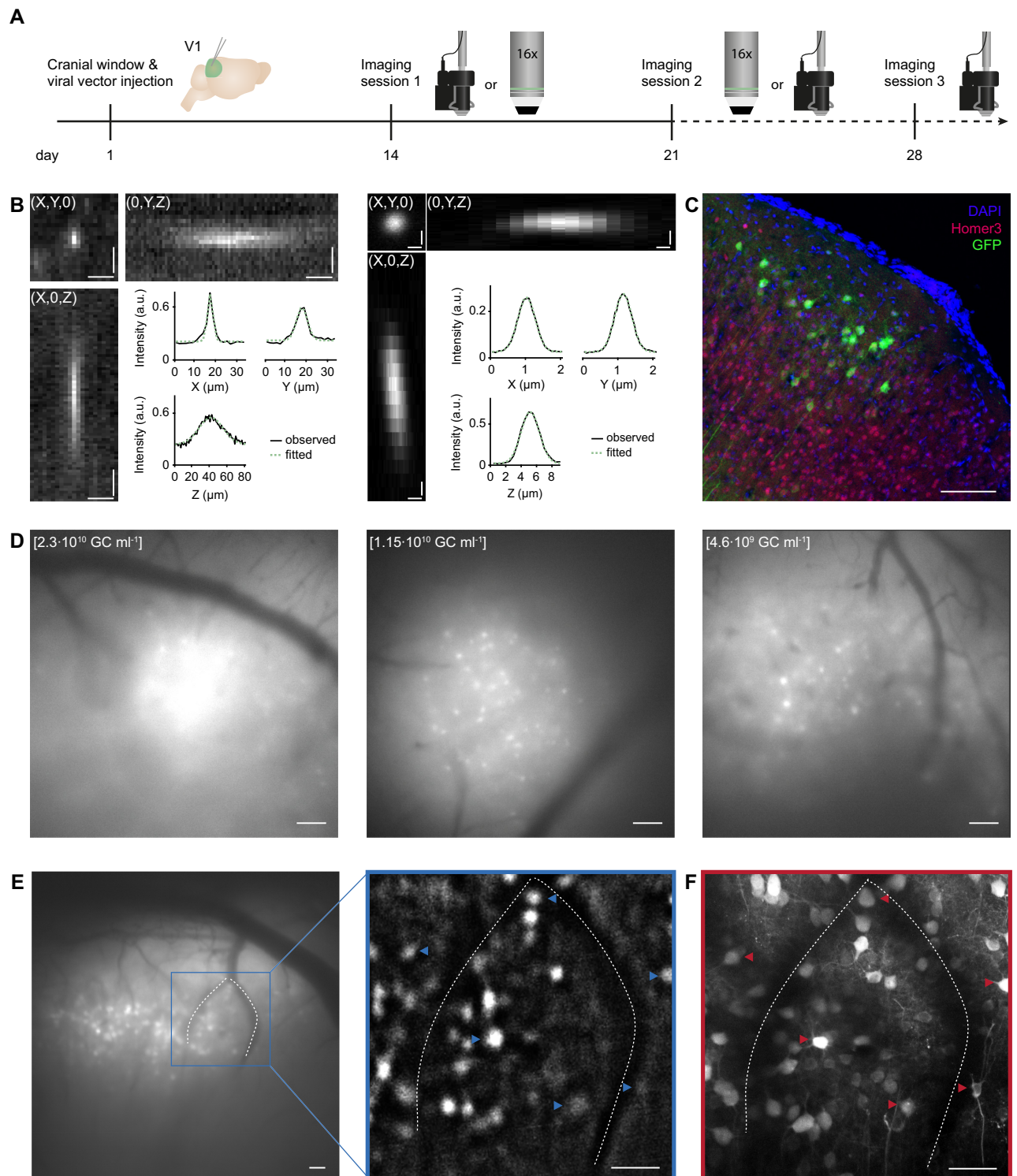
Fig 1. Matching neurons in images acquired with a miniaturized microscope and a two-photon microscope. A. Experimental timeline in days. Day 1: Cranial window implant and viral vector injection into visual cortex layer 2/3. Days 14 and 21: One miniature and one two-photon microscopy imaging session on either day (order was counterbalanced across animals). Day 28: Optional second miniature microscopy session. Icons at day 14, 21 and 28 illustrate a miniature microscope and a 16x two-photon microscope objective. B. Left: Projections of a three-dimensional stack of observed fluorescence from a sub-resolution fluorescent microbead acquired using a miniaturized microscope. Right: As in Left, but acquired using a two-photon microscope.

Insets depict observed (black solid line) and Gaussian-curve fitted (green dashed line) fluorescence intensity along each axis (X, Y and Z) separately. C. Immunohistochemical labeling of GCaMP6s-expressing excitatory layer 2/3 neurons (injection titer of $1.15 \cdot 10^{10}$ GC ml^{-1}). D. Example miniaturized microscopy images of V1 injected with different viral vector titers (left: $2.3 \cdot 10^{10}$ GC ml^{-1}; middle: $1.15 \cdot 10^{10}$ GC ml^{-1}; right: $4.6 \cdot 10^{9}$ GC ml^{-1}). E. Left: Miniaturized microscopy image prior to processing. Right: Magnified image after background-subtraction. Blood vessels (dotted lines) assist in matching neurons between microscopes (see panel F; examples of matched neurons are indicated with arrowheads). F. A collapsed volume as imaged with the two-photon microscope (100 planes, 1 μm spacing, projection along the axial axis). Scale bars, 10 μm (B, Left), 0.5 μm (B, Right), 100 μm (C,D), and 50 μm (E, F).

of 1024 x 1024 with a sequential scan using excitation lasers for DAPI (405 nm), Alexa488 (488 nm) and Cy3 (561 nm). Quantitative analysis was performed with the "Cell Counter" plug-in for ImageJ, by counting GFP expressing cells among Homer 3 expressing cells in cortical layer 2/3 (100–300 μm from the pial surface).

Analysis

Analysis of imaging data was performed using custom written routines in Matlab R2016b (Mathworks) and manual routines in the Fiji package of ImageJ (US National Institutes of Health) [16]. Small in-plane movement artefacts were corrected by aligning the images to a template [17]. Movement corrections were minor; frame displacements were smaller than 1.6 μm in 95% of miniaturized microscopy frames and in 95% of two-photon microscopy frames.

Next, to identify the same neurons imaged with both microscopes, images obtained with both microscopes were scaled to match pixel size and image orientation. Initial alignments were made based on the cell location relative to major landmarks such as blood vessels. Once two pairs of neurons were judged to be identical in both imaging planes, the images were aligned using an ImageJ plugin (Align Image by line ROI). Subsequently, other cell pairs were identified based on absolute distance relative to other cells and blood vessels.

Cellular fluorescence signals were calculated for each imaging frame by averaging across all pixels within manually drawn regions of interest (ROIs). Fluorescence signals from miniaturized microscope recordings were corrected for local neuropil contamination by subtracting the average fluorescence in a 27 μm ring (using a neuropil correction factor of 1.0) [18]. Because of the sparse labelling with GCaMP6, neuropil subtraction was not necessary for data acquired with the two-photon microscope (see also Results and Fig 2E). In addition, for a small subset of data constrained non-negative matrix factorization for endoscopic data (CNMF-E) [19] was applied to miniaturized microscopy imaging frames, using a Gaussian kernel width 3.17 μm, maximum soma diameter 23.8 μm, minimum local correlation 0.8, minimum peak-to-noise ratio 6, spatial overlap ratio 0.05 and temporal correlation 0.8. For comparison of calcium transients, we determined putative sources to be identical between the methods when the CNMF-E-detected seed pixel and manually detected center pixel were less than 10 μm apart, and if we could visually confirm similarity of the detected ROI contours. Next, ΔF/F calcium signals were quantified as relative increase in fluorescence over baseline, which was derived from the mean lowest 50% values in a 60 s sliding window [20]. In order to compare signal and noise amplitudes, miniaturized microscope data were resampled to the frame rate of the two-photon microscope (10 Hz). For each neuron, the signal amplitude was determined as the largest mean (across trials) response to any of the eight visual stimuli. Noise amplitude was calculated as the standard deviation of the ΔF/F values in the two-second period before stimulus presentation.

A neuron was defined as orientation tuned if it matched two criteria. First, the response to any of the eight movement directions was significantly different from any of the other
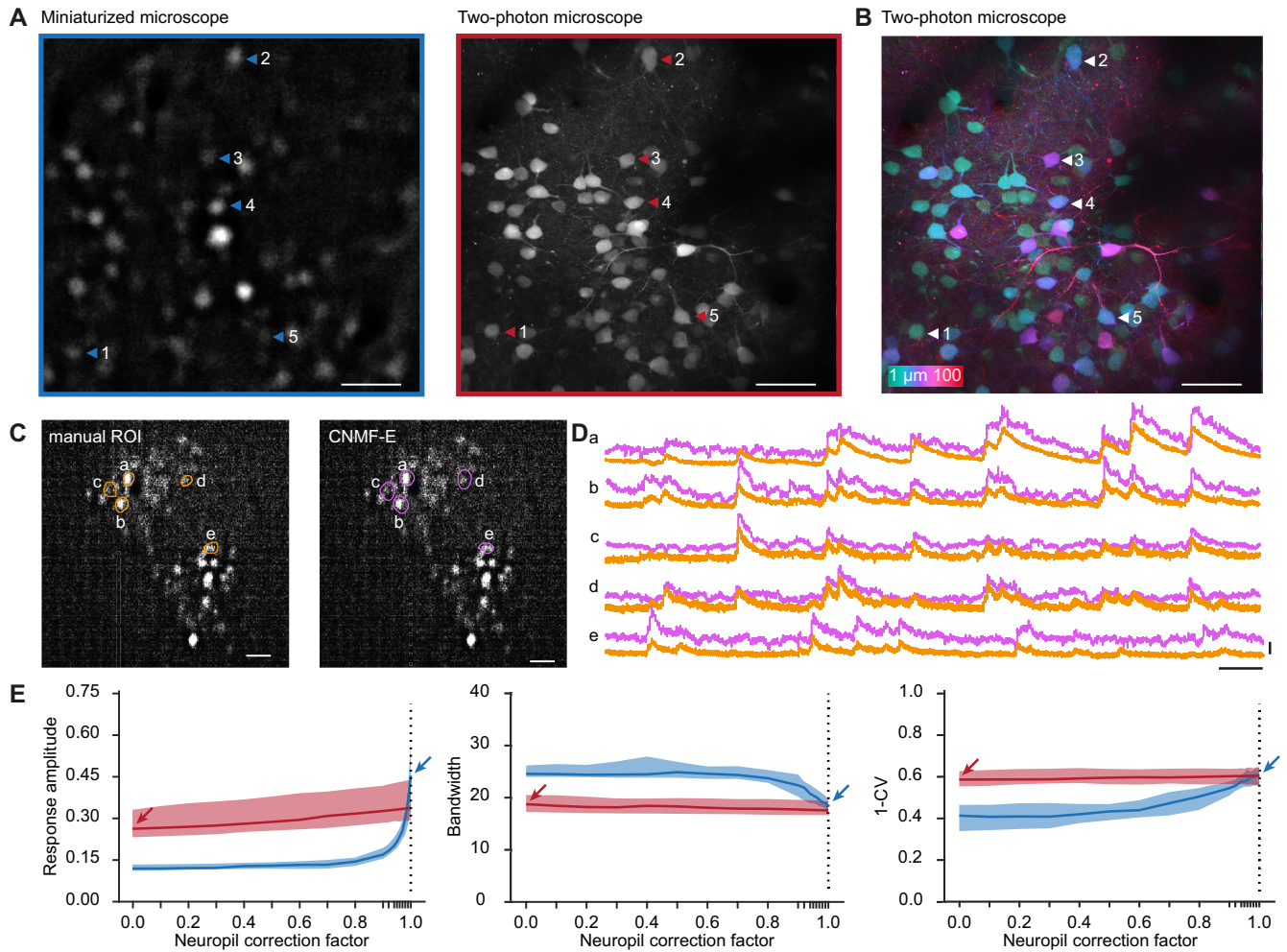
Fig 2. Imaging of visually evoked responses using a miniaturized microscope and a two-photon microscope. A. A background-subtracted image acquired with a miniaturized microscope (left) and a collapsed volume (100 planes, 1 μm spacing) acquired with a two-photon microscope (right). Example neurons matched across microscopes are indicated with arrowheads. B. Pixel-wise color-coded depth origin of the collapsed two-photon volume. C. Contours of neurons detected with either manual ROI selection (green, left) or CNMF-E (pink, right) within the same background-subtracted field of view recorded with a miniaturized microscope. D. Relative fluorescence changes (ΔF/F) of example neurons indicated in C. E. Median response amplitude (ΔF/F), bandwidth and global orientation selectivity index (1-CV) as a function of neuropil correction factor in recordings acquired from orientation tuned neurons using a miniaturized microscope (blue) and a two-photon microscope (red). Arrows indicate parameter values at the selected neuropil correction factor of miniature microscopy (blue) and two-photon microscopy (red). Colored shading indicates 95% confidence interval. Scale bars, 50 μm (A, B), 100 μm (C), 25 s (D, horizontal), 1 ΔF/F (D, vertical).

directions (p < 0.01), tested using the non-parametric Kruskal-Wallis test. Second, we excluded neurons of which the response to the preferred direction did not exceed the median response amplitude of the entire population of neurons (miniature microscope: 0.115 ΔF/F; two-photon microscope: 0.0525 ΔF/F; see Results and Fig 3B). Orientation tuning curves were constructed by averaging the response to each movement direction and fitted with a two peaked Gaussian curve [21]. Preferred orientation was defined as the maximum of the fitted curve, and the tuning curve bandwidth was defined as half width of the fitted curve at $1/\sqrt{2}$ maximum. To quantify global orientation selectivity, we determined the normalized length of the mean response vector (also referred to as 1-circular variance or 1-CV) [22].
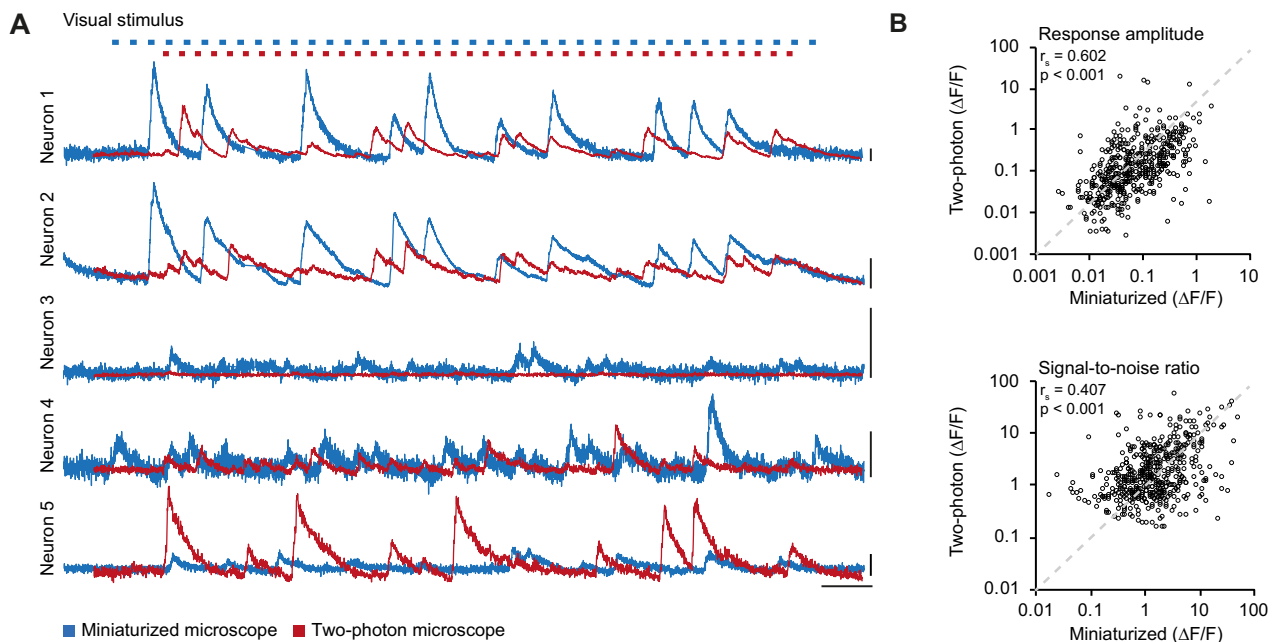
Fig 3. Calcium traces in miniaturized microscope and two-photon microscope recordings. A. Relative fluorescence changes (ΔF/F) for the five example neurons depicted in [Fig 2A and 2B](#) as recorded with a miniaturized microscope (blue) and a two-photon microscope (red) during visual stimulation. Top: Blue and red marks indicate stimulus presentation for miniaturized microscopy and two-photon microscopy, respectively. Stimuli were presented in a pseudo-randomized order that was unique for each experiment. B. Average ΔF/F response amplitude to the preferred stimulus ($p = 1.841 \cdot 10^{-49}$, Spearman's correlation) and ΔF/F signal-to-noise ratio of stimulus-induced calcium transients ($p = 6.348 \cdot 10^{-21}$, Spearman's correlation) of all matched neurons (488 neurons, n = 8 mice) in miniaturized microscope recordings plotted against the respective values in two-photon microscope recordings. Scale bars, 1 ΔF/F (A, vertical), and 25 s (A, horizontal).

https://doi.org/10.1371/journal.pone.0214954.g003

Statistics

Normality of distributions was verified using the Kolmogorov-Smirnov test. Similarity of two different distributions was analyzed with the two-sample Kolmogorov-Smirnov test. A Mann-Whitney U test was used to compare distribution medians (Mdn). The tuning features circular variance and bandwidth of individual neurons were compared by computing the Spearman correlation coefficient r_s between both microscopy techniques and the preferred orientation was compared using the circular correlation coefficient r_{circ} (The orientation space was remapped to the range of 0 to 2*pi for this purpose) [23]. 95% confidence intervals of the median ([Fig 2E](#)) were calculated using bootstrap resampling (bootstrap sample size: 84, number of re-samples: 10000). For all statistical tests, alpha was set at 0.05 and tests were conducted two-tailed.

Results

Identifying the same neurons across microscopy techniques

To compare evoked neuronal responses as obtained with a commercially available miniaturized microscope (Doric Lenses) and a custom-built two-photon microscope, we imaged V1 excitatory layer 2/3 neurons expressing the genetically encoded calcium indicator GCaMP6s while the anesthetized mice (n = 8) were presented with drifting square wave gratings ([Fig 1A](#)) [11]. The measured PSF (point spread function) of the miniaturized and two-photon microscopes confirmed the lower resolution of the miniaturized microscope, as well as the higher

background fluorescence (Fig 1B; Table 1). To minimize recording fluorescence from out-of-focus neurons, we used a dual viral vector intersectional approach and reduced the titer of the Cre-expressing viral vector, resulting in sparse labelling of neurons (see Methods; Fig 1D). Post-hoc immunohistochemical analysis revealed that $32.6 \pm 7.3\%$ of excitatory layer 2/3 neurons were labelled in the core of the bolus (injection titer of $1.15 \cdot 10^{10}$ GC ml^{-1}; Fig 1C). Using superficial blood vessels as landmarks, we centered the fields of view of both microscopes on the same location. To overcome the differences in optical sectioning of both microscopes, we compared a single, background-subtracted field of view recorded with the miniaturized microscope with a two-photon microscope stack, collapsed along the axial axis spanning a depth of 100 µm (Fig 1D and 1E). Upon completion of both imaging sessions, neurons were matched based on their position relative to blood vessels, other identified neurons and relative depth in the tissue (Fig 1D and 1E). The identification of neuronal pairs between miniaturized microscope and two-photon microscope recordings was verified by two independent observers using a subset of volumes. The same pairs were identified by the experimenter and observer 1 in 96.3% of identified pairs, and by the experimenter and observer 2 in 96.0% of identified pairs.

Extraction of stimulus-evoked responses of matched neurons

After careful, off-line matching of neurons across images, we were able to identify 488 neurons that were present in both fields of view (Fig 2A). This matching method allowed us to recognize a match for many, but not all neurons in the imaged planes. Of note, we found that the population of neurons detected in a single miniaturized microscopy imaging plane spanned over 70 µm in depth within the two-photon imaged volume (Fig 2B).

Before analyzing calcium activity from these neurons, we explored whether the obtained calcium transients were robust to the choice of signal extraction method. To this end, we extracted single cell calcium transients in a subset of miniaturized microscopy recordings by manual region of interest (ROI) selection [18], which involves outlining of the neurons' contours and direct surrounding by the experimenter (see Methods). We contrasted this to constrained nonnegative matrix factorization for microendoscopic data (CNMF-E) [19,24], which decomposes the recorded fluorescence into spatial footprints and temporal components modelling the calcium dynamics (Fig 2C and 2D). The obtained calcium transients were similar in both signal amplitude and transient kinetics (Fig 2D). However, source extraction methods often return spatial footprints that extend beyond the boundaries of visually identified neurons and tend to ignore cells that show only little calcium activity. Because re-identification of neurons across microscopy techniques relied on a direct comparison of morphological information, independent of calcium activity, we chose to quantify calcium traces and tuning properties using manual ROI selection.

An important step in the calculation of single cell calcium traces using manual ROI selection is to correct the contamination of cellular signals by out-of-focus fluorescence from the neuropil. The method, referred to as neuropil correction[18], measures neuropil fluorescence from an area directly surrounding the cell and subtracts the neuropil-signal time course, scaled by a factor (neuropil correction factor), from the signal measured within the outline of the cell. The rationale is that the signal measured within the cellular ROI is the linear sum of two signals: one truly generated in the ROI and one originating from tissue adjacent to the ROI (due to the limited axial and/or lateral resolution as well as tissue scattering). By choosing an appropriate neuropil correction factor, the contamination can be corrected by subtraction of the scaled neuropil time course. In our experiments, labeling of cortical cells was sparse, and we observed only a very small amount of neuropil fluorescence in the two-photon microscopy

recordings (Fig 2A, right panel). Hence, we chose to use a neuropil correction factor of 0.0 for these experiments. In contrast, miniaturized epifluorescence microscopy lacks optical sectioning, therefore we assumed that in those experiments virtually all of the signal originating from above and below an outlined neuron will mix into the measured neuronal signal, resulting in an estimated neuropil correction factor of 1.0.

In order to test whether our choice of neuropil correction factor for each method was appropriate, we varied the neuropil correction factor from 0.0 to 1.0 and investigated how three key parameters in this study changed as a result (the parameters were response amplitude, bandwidth and the global orientation selectivity index 1-circular variance (1-CV) of orientation tuned cells; see below and Methods for further explanation). The analysis showed that, in our two-photon microscopy recordings, these parameters altogether depended very little on the choice of neuropil correction factor (Fig 2E). This indicated that neuropil contamination was negligible, and it validated the choice for the value of 0.0 in two-photon microscopy recordings. However, in miniaturized microscopy recordings, all three parameters depended strongly on the neuropil contamination factor; signal amplitude and orientation selectivity (1-CV) increasing monotonically and bandwidth decreasing monotonically (Fig 2E). The curves for miniaturized and two-photon microscopy recordings intersected when the neuropil correction factor approximated the maximum value of 1.0, suggesting that the choice of neuropil correction factor in miniaturized microscopy recordings (1.0) is close to the optimal value.

Orientation tuned neurons show similar tuning properties in miniaturized microscope and two-photon microscope recordings

We extracted the calcium transients of all matched neurons and quantified the responses to visual stimulation (Fig 3A). Both the average response amplitude (r_s = 0.602, p = $1.841 \cdot 10^{-49}$, n = 488 neurons; Fig 3B) and the ΔF/F signal-to-noise ratio (r_s = 0.407, p = $6.348 \cdot 10^{-21}$, n = 488 neurons; Fig 3B) measured using the miniaturized microscope correlated strongly with the measurements recorded using the two-photon microscope. The median visually evoked response amplitude was significantly higher in miniaturized microscopy recordings (Mdn = 0.115) compared to two-photon microscopy recordings (Mdn = 0.0525, Wilcoxon test, T = 92271, p = $1.268 \cdot 10^{-25}$). In contrast, the median ΔF/F signal-to-noise ratio was significantly higher in two-photon microscopy recordings (Mdn = 1.432) compared to miniaturized microscopy recordings (Mdn = 1.339, Wilcoxon test, T = 69005, p = 0.003). Thus, while single-neuron visually driven fluorescence changes were strongly correlated between microscopes, the absolute values of response amplitude and signal-to-noise ratio were slightly different (this difference varies as function of the value of the neuropil correction factor; see Discussion and Fig 2E).

Many V1 neurons respond preferentially to moving gratings of specific orientations (Fig 4A) and their tuning features are relatively stable over the course of weeks [10,12], making this response property ideally suited for a direct comparison of the microscopy techniques. We averaged the calcium responses to the moving gratings of different directions and fitted the responses with a two-peaked Gaussian curve (Fig 4B). Out of 488 matched neurons, 194 were classified to be orientation tuned (see Methods) in miniaturized microscopy recordings, 133 in two-photon microscopy recordings, and 84 of these matched the criteria for being orientation tuned in both miniaturized and two-photon microscopy recordings (n = 7 mice; Fig 5A).

Key parameters of the tuning curves (preferred orientation, bandwidth, and global orientation selectivity, as described by 1-CV) were first determined for all neurons that were orientation tuned in each microscopy technique separately (Fig 5B). The overall distributions for
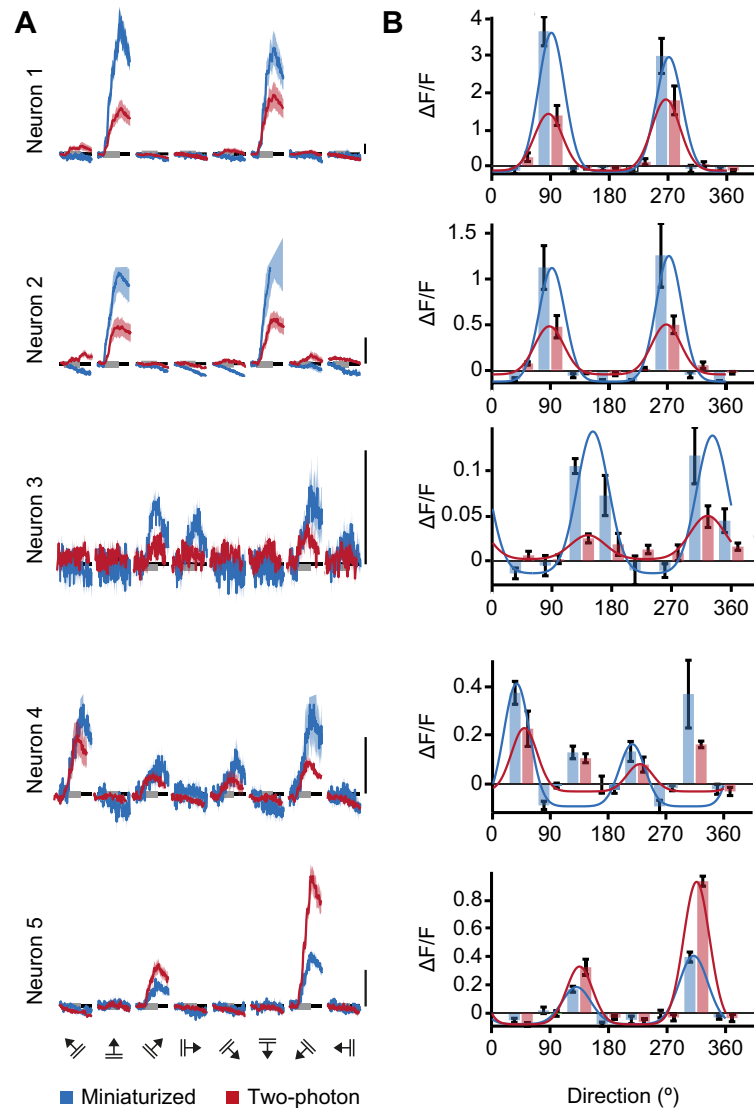
Fig 4. Orientation tuning curves of V1 neurons match between miniaturized microscopy and two-photon microscopy. A. A Calcium responses as acquired with a miniaturized microscope (blue) and a two-photon microscope (red) in response to drifting gratings (8 directions, 5 repetitions) of the five example neurons depicted in Fig 2A and 2B. B. Bars show the mean (± SEM) responses of the same neurons imaged with a miniaturized microscope (blue) and a two-photon microscope (red). Overlaid blue and red lines indicate the fitted tuning curves. Scale bars, 1 ΔF/F.

preferred orientation (two-sample Kolmogorov-Smirnov test, D = 0.073, p = 0.777) and 1-CV (two-sample Kolmogorov-Smirnov test, D = 0.071, p = 0.806) did not significantly differ between microscopy techniques ($n_{miniaturized}$ = 194, $n_{two\text{-}photon}$ = 133 in 7 mice). However, tuning curve bandwidth was distributed differently between microscopy techniques (two-sample Kolmogorov-Smirnov test, D = 0.168, p = 0.020). This observation indicates that orientation tuning in two-photon recordings appeared slightly broader, as evidenced by a larger median bandwidth ($Mdn_{miniaturized}$ = 18.9, $Mdn_{two\text{-}photon}$ = 19.8, Mann-Whitney U-test, U = 29919, p = 0.024), while median global orientation selectivity did not significantly differ (1-CV, $Mdn_{miniaturized}$ = 0.564, $Mdn_{two\text{-}photon}$ = 0.561, Mann-Whitney U-test, U = 32239, p = 0.61). However, the existence of a difference between the distribution-median of tuning curve
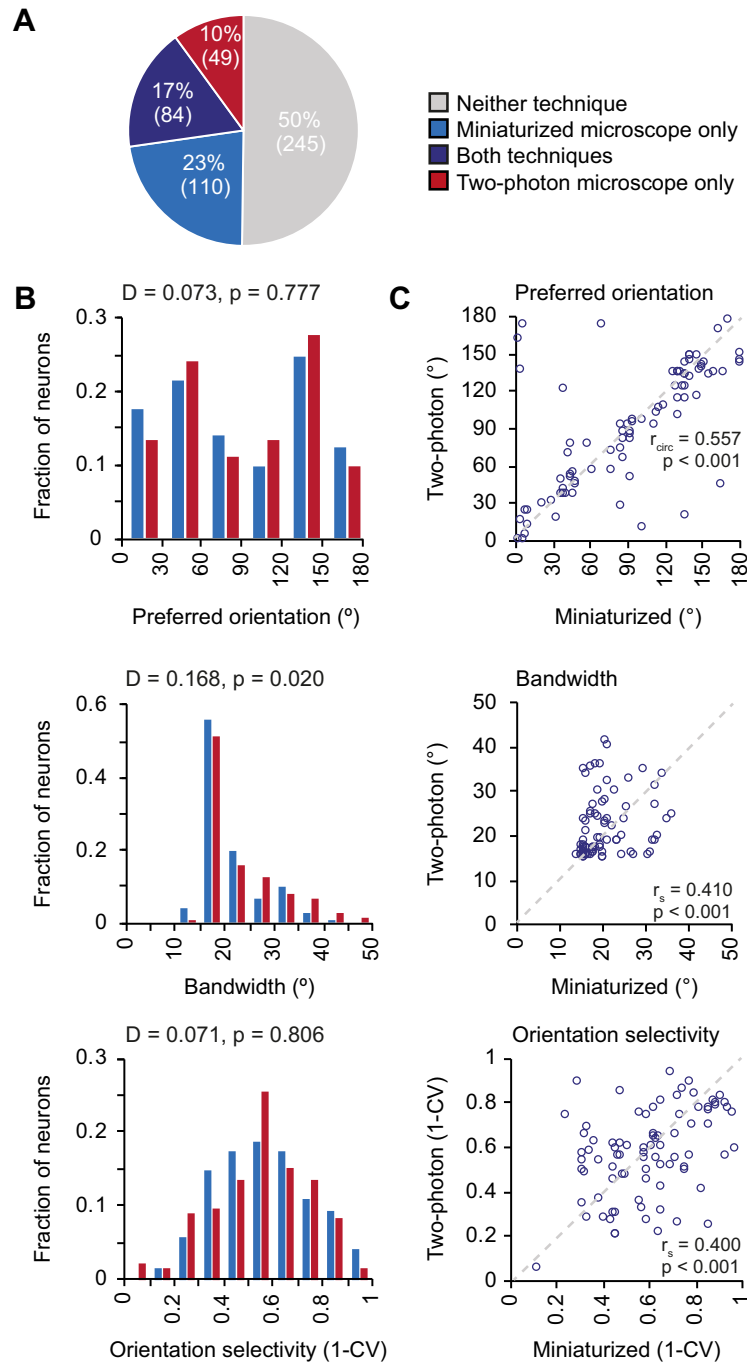
Fig 5. Orientation tuning properties of V1 neurons as imaged with a miniaturized microscope and a two-photon microscope. A. A Fractions of neurons that were classified as orientation tuned in miniaturized microscope recordings only (blue), using both microscopy techniques (purple), in two-photon microscope recordings only (red), or using neither microscopy technique (gray). B. Distribution of preferred orientation (p = 0.777, two-sample Kolmogorov-Smirnov test), bandwidth (p = 0.020, two-sample Kolmogorov-Smirnov test), and global orientation selectivity index 1-CV (p = 0.806, two-sample Kolmogorov-Smirnov test) for all neurons that were orientation tuned in recordings with a miniaturized microscope (blue bars, 194 neurons, n = 7 mice) or a two-photon microscope (red bars, 133 neurons, n = 6 mice). C. Preferred orientation (p = 2.02·10−6, circular correlation), bandwidth (p = 1.23·10−4, Spearman's correlation), and global orientation selectivity index 1-CV (p = 1.81·10−4, Spearman's correlation) for individual neurons (purple circles) that were orientation tuned using both microscopy techniques (84 neurons, n = 5 mice). The unity line is depicted as gray dashed line.

parameters depends on fine-tuning of the neuropil correction factor (see above, Discussion and Fig 2E).

To compare the tuning properties at the single neuron level, we limited the analysis to neurons that were classified orientation tuned with both microscopy techniques (n = 84 in 5 mice). Most importantly in the present context, the preferred orientation (r_{circ} = 0.557, p = 2.02·10–6), bandwidth (r_s = 0.410, p = 1.23·10^{-4}) and the global orientation selectivity index (1-CV; r_s = 0.400, p = 1.81·10^{-4}) of these individual neurons correlated significantly between recordings performed with both microscopes (n = 84 neurons; Fig 5C). As already quantified for the overall population, the average response amplitude across these orientation tuned neurons was again significantly higher in the miniaturized microscopy recordings (Mdn = 0.457) than in two-photon microscopy recordings (Mdn = 0.265, Wilcoxon test, T = 2913, p = 4.89·10^{-7}, n = 84 neurons). However, in this specific subset of neurons the ΔF/F signal-to-noise ratio was significantly higher in the two-photon microscopy recordings (Mdn = 7.137) compared to the miniaturized microscopy recordings (Mdn = 4.838, Wilcoxon test, T = 1066, p = 0.001, n = 84 neurons).

The effect of between-session variability on signal-amplitude and tuning properties

To test to which extent observed differences between microscopy techniques could be explained by test-retest variance, we performed a second miniaturized microscopy session spaced one week apart from the first miniaturized microscopy session in four mice (Fig 1A). In order to allow a direct comparison between this analysis and the results described above, we only considered neurons that were also observed in the accompanying two-photon microscopy session. As expected, both average response amplitude (r_s = 0.585, p = 4.78·10^{-18}, n = 181 neurons in 4 mice; Fig 6A) and the ΔF/F signal-to-noise ratio (r_s = 0.647, p = 6.45·10^{-23}, n = 181 neurons in 4 mice; Fig 6A) were strongly correlated between the two miniaturized microscopy sessions. When comparing the response amplitude correlation of two consecutive miniaturized microscopy sessions with the correlation between two sessions using the two different microscopes (Fig 3B versus Fig 6A), the correlation coefficient between these groups was not significantly different (Fisher's r-to-z transformation, z = 0.3, p = 0.382).

Finally, we assessed tuning curve parameters of neurons that were orientation tuned in both miniaturized microscopy sessions, as well as visually detected in the two-photon microscopy session (n = 49 in 3 mice). The preferred orientation (r_{circ} = 0.348, p = 0.018) and bandwidth (r_s = 0.319, p = 0.026) of these individual neurons correlated significantly between test-retest conditions (Fig 6B). However, the test-retest relationship between the global orientation selectivity index was not significant (1-CV; r s = 0.266, p = 0.065; Fig 6B), possibly because of the low number of neurons that could be included in this analysis.

Discussion

We used calcium imaging to measure visual response properties of V1 excitatory neurons with both a miniaturized microscope and a stationary two-photon microscope. The same neurons could be identified in images acquired with both microscopes. This was achieved by making use of sparse GCaMP6 labelling and volumetric structural imaging to overcome differences in optical sectioning between the two microscopy techniques. The amplitude and signal-to-noise ratio of visually evoked calcium transients of identical neurons were strongly correlated across imaging techniques and tuning features of orientation-tuned neurons recorded with the two microscopes were similar at the individual cell level. However, the population median of response and tuning parameters could be offset depending on the choice of neuropil
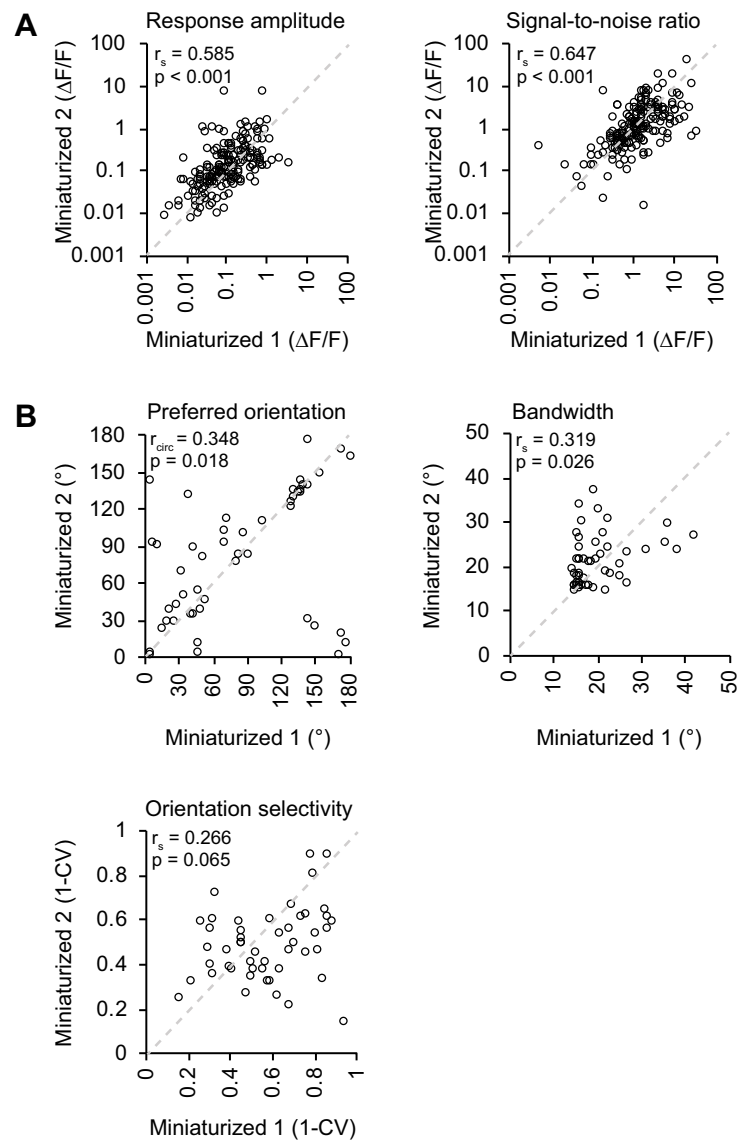
Fig 6. Effect of test-retest variability on recorded response properties in V1. A. A Average ΔF/F response amplitude to the preferred stimulus (p = 4.780·10−18, Spearman's correlation) and ΔF/F signal-to-noise ratio of stimulation-induced calcium transients (p = 6.451·10−23, Spearman's correlation) of matched neurons (181 neurons, n = 4 mice) in two consecutive miniaturized microscopy sessions (Miniaturized 1 and Miniaturized 2). B. Preferred orientation (p = 0.018, circular correlation), bandwidth (p = 0.026, Spearman's correlation), and global orientation selectivity index 1-CV (p = 0.065, Spearman's correlation) for individual neurons (black circles) that were orientation tuned during both consecutive microscopy sessions and visually detected in the two-photon microscopy session (49 neurons, n = 3 mice).

https://doi.org/10.1371/journal.pone.0214954.g006

correction factor that was applied to miniature microscopy data. The observed similarities were comparable to those between two consecutive miniaturized microscopy sessions. This suggests that the observed variability between microscopes is not larger than expected from miniature microscope test-retest variability. Overall, our results show that single-photon

miniaturized microscopy is a reliable method for recording functional properties of neurons in the visual cortex.

Influence of out-of-focus fluorescence

Although neuronal stimulus-induced calcium transients and orientation tuning features were strongly correlated between microscopy techniques at the single neuron level, we did observe certain differences when comparing the distributions of these features across the population of recorded neurons. The maximum amplitude of stimulus-induced calcium transients was larger in miniaturized microscope recordings, while the signal-to-noise ratio was lower. Furthermore, across the population of orientation-tuned neurons, local feature selectivity was slightly reduced as described by broader tuning curve bandwidths in recordings with the two-photon microscope.

Differences between the distributions of signal-to-noise ratio might be expected when comparing two imaging methods that differ vastly in the numbers of photons collected per neuron, e.g. using a CMOS sensor for miniaturized microscopy and a photomultiplier tube for two-photon microscopy. Moreover, differences in response amplitude and orientation selectivity can be attributed, at least in part, to the choice of the neuropil correction factor for analyzing miniaturized microscopy recordings. The curves describing the relationship between neuropil correction factor and ΔF/F response amplitude calculated for two-photon and miniaturized microscopy data intersect at a neuropil correction factor slightly smaller than 1.0 (see Fig 2E). Empirically, it can therefore be argued that for miniaturized microscopy a neuropil correction factor slightly below 1.0 should be employed, which is also theoretically evident: the neuropil signal is estimated by calculating the mean of all fluorescence in the cell-devoid region directly adjacent to an ROI (e.g. a neuron). On the other hand, the measured neuronal signal is the sum of the true neuronal signal from the cell body and the neuropil signal originating from within the ROI, not including any neuropil signal from the axial/lateral range in which the neuron's cell body was present. Thus, the intensity of neuropil signal bleeding into the neuronal signal is slightly lower than the intensity of neuropil signal measured in the area adjacent to the neuronal ROI. The optimal neuropil correction factor for an imaging method with poor optical sectioning (such as miniaturized microscopy) should therefore be just below 1.0, rather than exactly 1.0.

However, the empirically determined neuropil correction factor will depend on the density of neurons that expresses calcium indicator, and would have to be empirically verified for each preparation and tissue using a two-photon microscope, which is not practical for most studies. Therefore, for our purpose of verifying the general applicability of single cell calcium imaging using miniature microscopy, we think it is best to use the initial estimate of 1.0 as neuropil correction factor.

Comparison of source extraction methods

A key feature of our approach is the direct matching of the same neurons between microscopy techniques. The two techniques differ considerably in their ability for optical sectioning, with an increased probability that two neurons, located at different depths, cannot be separated using manual annotation methods in miniaturized microscopy recordings. Therefore it was important to obtain a sparse population of labelled neurons, which we achieved by titrating down the Cre-expressing viral vector. To extract calcium signals from both miniaturized microscopy and two-photon microscopy data, we chose a conventional method for extracting ΔF/F calcium activity, which uses the mean fluorescence signal from manually detected ROIs. This method facilitated a direct, morphology-based comparison of individual neurons

recorded with the two imaging techniques. When the experiment requires manually drawn ROIs, a more sophisticated approach to decontaminate neuropil signals is the FISSA toolbox, which delimits the local neuropil surrounding the soma and sequentially performs negative matrix factorization to isolate the fluorescence sources [25]. Additionally, there are alternative, activity-based automated ROI detection and source extraction methods that can be used for analyzing miniaturized microscopy and endoscopy data [19,26]. These methods have the advantage of allowing to demix activity patterns of overlapping sources (cells) that are often observed in more densely labelled preparations. In a subset of miniaturized microscopy recordings, we show that the calcium transients detected by an alternative source extraction method, CNMF-E [19], are similar to those that we detected using our manual ROI approach. We therefore expect that our conclusions extend to the use of this (and similar) source extraction and deconvolution method(s) that allow for recordings with denser labelling than reported here.

Session-to-session variability

Since the response properties of visual cortex cells are quite stable over time [10,12,27], we did not anticipate large differences in these properties to emerge within days. However, a portion of the variation in measured tuning properties between microscopy techniques might be ascribed to mere difference across time points, possibly relating to small fluctuations in anesthesia at the time of imaging. We conducted consecutive imaging sessions one week apart, with the first session performed two weeks after viral vector injection. We chose a one-week interval between imaging sessions to allow the animal to recover completely from anesthesia and to allow us to approximate the same anesthetic state in both experiments. Other forms of lightly dosed anesthesia, such as isoflurane, do not significantly alter V1 response properties as compared to awake animals [28]. However, we cannot exclude the possibility that fluctuations of fentanyl-based anesthesia can cause minor differences in orientation tuning between imaging sessions in our experiment. A study performed in awake experiments with minimal lag between imaging sessions might address these concerns but may at the same time suffer from other, e.g. state-dependent sources of inter-session variability [9,29].

Combining miniaturized and two-photon microscopy

The overall aim of our study was to quantitatively compare recordings obtained with miniaturized microscopy to those obtained with a conventional *in vivo* microscopy method such as two-photon microscopy. We report a high degree of similarity between these recordings, in spite of categorical differences between the two imaging methods [5, 30]. A promising future approach would be to make use of both microscopy methods in a single experimental design, optimally using their respective qualitative merits. Such an approach could involve imaging of a population of neurons with a miniaturized microscope while an animal engages in a freely moving task and subsequently characterizing structural changes in neurons implicated in the task with a two-photon microscope. An exciting new possibility is two-photon miniaturized microscopy [31], which allows functional imaging of single dendrites and dendritic spines in freely behaving animals. However, the currently smaller field of view reduces the number of somata that can be imaged at once, which makes identification of (sparse) task-related neurons and of large-scale population activity dynamics challenging with this method. The combination of single-photon miniaturized microscopy and two-photon microscopy thus provides a promising approach to disentangle the processes at the functional and structural level that underlie behavior in freely moving animals.

Acknowledgments

Author Contributions

Conceptualization: Annet Glas, Mark Hübener, Tobias Bonhoeffer, Pieter M. Goltstein.

Formal analysis: Annet Glas, Pieter M. Goltstein.

Investigation: Annet Glas.

Writing – original draft: Annet Glas, Mark Hübener, Tobias Bonhoeffer, Pieter M. Goltstein.

Writing – review & editing: Annet Glas, Mark Hübener, Tobias Bonhoeffer, Pieter M. Goltstein.

References

1. Cai DJ, Aharoni D, Shuman T, Shobe J, Biane J, Lou J, et al. A shared neural ensemble links distinct contextual memories encoded close in time. Nature. 2016; 534: 115–118. https://doi.org/10.1038/nature17955 PMID: 27251287

2. Ghosh KK, Burns LD, Cocker ED, Nimmerjahn A, Ziv Y, Gamal A El, et al. Miniaturized integration of a fluorescence microscope. Nat Methods. 2011; 8: 871–878. https://doi.org/10.1038/nmeth.1694 PMID: 21909102

3. Liberti WA, Markowitz JE, Perkins LN, Liberti DC, Leman DP, Guitchounts G, et al. Unstable neurons underlie a stable learned behavior. Nat Neurosci. 2016; 19: 1665–1671. https://doi.org/10.1038/nn.4405 PMID: 27723744

4. Betley JN, Xu S, Fang Z, Cao H, Gong R, Christopher J. Neurons for hunger and thirst transmit a negative-valence teaching signal. Nature. 2015; 521: 180–185. https://doi.org/10.1038/nature14416 PMID: 25915020

5. Yang W, Yuste R. In vivo imaging of neural activity. Nat Methods. 2017; 14: 349–359. https://doi.org/10.1038/nmeth.4230 PMID: 28362436

6. Ziv Y, Burns LD, Cocker ED, Hamel EO, Ghosh KK, Kitch LJ, et al. Long-term dynamics of CA1 hippocampal place codes. Nat Neurosci.2013; 16: 264–266. https://doi.org/10.1038/nn.3329 PMID: 23396101

7. Kamigaki T, Dan Y. Delay activity of specific prefrontal interneuron subtypes modulates memory-guided behavior. Nat Neurosci. 2017; 20: 854–863. https://doi.org/10.1038/nn.4554 PMID: 28436982

8. Hubel DH, Wiesel TN. Receptive fields, binocular interaction and functional architecture in the cat's visual cortex. J Physiol. 1962; 160: 106–154. PMID: 14449617

9. Niell CM, Stryker MP. Highly selective receptive fields in mouse visual cortex. J Neurosci. 2008; 28: 7520–7536. https://doi.org/10.1523/JNEUROSCI.0623-08.2008 PMID: 18650330

10. Mank M, Santos AF, Direnberger S, Mrsic-Flogel TD, Hofer SB, Stein V, et al. A genetically encoded calcium indicator for chronic in vivo two-photon imaging. Nat Methods. 2008; 5: 805–811. https://doi.org/10.1038/nmeth.1243 PMID: 19160515

11. Chen TW, Wardill TJ, Sun Y, Pulver SR, Renninger SL, Baohan A, et al. Ultrasensitive fluorescent proteins for imaging neuronal activity. Nature. 2013; 499: 295–300. https://doi.org/10.1038/nature12354 PMID: 23868258

12. Rose T, Jaepel J, Hübener M, Bonhoeffer T. Cell-specific restoration of stimulus preference after monocular deprivation in the visual cortex. Science. 2016; 352: 1319–1322. https://doi.org/10.1126/science.aad3358 PMID: 27284193

13. Schuett S, Bonhoeffer T, Hübener M. Mapping retinotopic structure in mouse visual cortex with optical imaging. J Neurosci. 2002; 22: 6549–6559. PMID: 12151534

14. Grinvald A, Bonhoeffer T. Optical imaging of electrical activity based on intrinsic signals and on voltage sensitive dyes. In: Toga AW, editor. Brain mapping; the methods. Academic Press Hardcover; 1996. pp. 55–97.

15. Leinweber M, Zmarz P, Buchmann P, Argast P, Hübener M, Bonhoeffer T, et al. Two-photon calcium imaging in mice navigating a virtual reality environment. J Vis Exp JoVE. 2014; 84: e50885.

16. Schindelin J, Arganda-Carreras I, Frise E, Kaynig V, Longair M, Pietzsch T, et al. Fiji: An open-source platform for biological-image analysis. Nat Methods. 2012; 9: 676–682. https://doi.org/10.1038/nmeth.2019 PMID: 22743772

17. Guizar-sicairos M, Thurman ST, Fienup JR. Efficient subpixel image registration algorithms. Optics Letters. 2008; 33: 156–158. PMID: 18197224

18. Kerlin AM, Andermann ML, Berezovskii VK, Reid RC. Broadly tuned response properties of diverse inhibitory neuron subtypes in mouse visual cortex. Neuron. 2010; 67: 858–871. https://doi.org/10.1016/j.neuron.2010.08.002 PMID: 20826316

19. Zhou P, Resendez SL, Rodriguez-Romaguera J, Jimenez JC, Neufeld SQ, Stuber GD, et al. Efficient and accurate extraction of in vivo calcium signals from microendoscopic video data. ELife. 2018; 7: e28728. https://doi.org/10.7554/eLife.28728 PMID: 29469809

20. Greenberg DS, Houweling AR, Kerr JND. Population imaging of ongoing neuronal activity in the visual cortex of awake rats. Nat Neurosci. 2008; 11: 749–751. https://doi.org/10.1038/nn.2140 PMID: 18552841

21. Mazurek M, Kager M, Van Hooser SD, Margolis DJ. Robust quantification of orientation selectivity and direction selectivity. Front Neural Circuits. 2014; 8: 1–17. https://doi.org/10.3389/fncir.2014.00001

22. Ringach DL, Shapley RM, Hawken MJ. Orientation selectivity in macaque V1: diversity and laminar dependence. J Neurosci. 2002; 22: 5639–5651. PMID: 12097515

23. Berens P. CircStat: a MATLAB toolbox for circular statistics. J. Stat. Softw. 2009; 31: 1–21.

24. Klaus A, Martins GJ, Paixao VB, Zhou P, Paninski L, Costa RM. The spatiotemporal organization of the striatum encodes action space. Neuron. 2017; 95: 1171–1180. https://doi.org/10.1016/j.neuron.2017.08.015 PMID: 28858619

25. Keemink S. W., Lowe S. C., Pakan J. M., Dylda E., van Rossum M. C., Rochefort N. L. FISSA: A neuropil decontamination toolbox for calcium imaging signals. Scientific reports. 2018; 8: 1–12. https://doi.org/10.1038/s41598-017-17765-5

26. Lu J, Li C, Singh-Alvarado J, Zhou ZC, Fröhlich F, Mooney R, et al. MIN1PIPE: A Miniscope 1-Photon-Based Calcium Imaging Signal Extraction Pipeline. Cell Rep. 2018; 23: 3673–3684. https://doi.org/10.1016/j.celrep.2018.05.062 PMID: 29925007

27. Poort J, Khan AG, Pachitariu M, Nemri A, Orsolic I, Krupic J, et al. Learning enhances sensory and multiple non-sensory representations in primary visual cortex. Neuron. 2015; 86: 1478–1490. https://doi.org/10.1016/j.neuron.2015.05.037 PMID: 26051421

28. Goltstein PM, Montijn JS, Pennartz CMA. Effects of isoflurane anesthesia on ensemble patterns of Ca2+ activity in mouse V1: reduced direction selectivity independent of increased correlations in cellular activity. PLoS One. 2015; 10: e0118277. https://doi.org/10.1371/journal.pone.0118277 PMID: 25706867

29. Polack PO, Friedman J, Golshani P. Cellular mechanisms of brain state-dependent gain modulation in visual cortex. Nat Neurosci. 2013; 16: 1331–1339. https://doi.org/10.1038/nn.3464 PMID: 23872595

30. Yu H., Senarathna J., Tyler B. M., Thakor N. V., Pathak A. P. Miniaturized optical neuroimaging in unrestrained animals. NeuroImage. 2015; 113, 397–406. https://doi.org/10.1016/j.neuroimage.2015.02.070 PMID: 25791782

31. Zong W, Wu R, Li M, Hu Y, Li Y, Li J, et al. Fast high-resolution miniature two-photon microscopy for brain imaging in freely behaving mice. Nat Methods. 2017; 14: 713–719. https://doi.org/10.1038/nmeth.4305 PMID: 28553965

4

SPACED TRAINING ENHANCES MEMORY AND PREFRONTAL ENSEMBLE STABILITY IN MICE

Declaration of author contributions

All listed authors contributed to this manuscript: Annet Glas, Mark Hübener, Tobias Bonhoeffer, and Pieter M. Goltstein.

All authors designed the study. Annet Glas acquired the data. Annet Glas and Pieter M. Goltstein analyzed the data. Tobias Bonhoeffer and Mark Hübener acquired funding. Annet Glas, Mark Hübener, Tobias Bonhoeffer, and Pieter M. Goltstein wrote the manuscript.

The results were published on the preprint server *bioRxiv* with the following reference: Glas, A., Hübener, M., Bonhoeffer, T., & Goltstein, P. M. Spaced training enhances memory and prefrontal ensemble stability in mice (2020). The manuscript is currently under review for publication in the journal Current Biology.

Spaced training enhances memory and prefrontal ensemble stability in mice

Annet Glas[1,2], Mark Hübener[1], Tobias Bonhoeffer[1], Pieter M. Goltstein[1]

Author Affiliations

[1] Max Planck Institute of Neurobiology, Am Klopferspitz 18, 82152, Martinsried, Germany

[2] Graduate School of Systemic Neurosciences, Großhaderner Straße 2, 82152, Martinsried, Germany

Lead Contact

Pieter M. Goltstein, goltstein@neuro.mpg.de

Summary

Memory is substantially improved when learning is distributed over time, an effect called "spacing effect". So far it has not been studied how spaced learning affects neuronal ensembles presumably underlying memory. In the present study, we investigate whether trial spacing increases the stability or size of neuronal ensembles. Mice were trained in the "everyday memory" task, an appetitive, naturalistic, delayed matching-to-place task. Spacing trials by 60 minutes produced more robust memories than training with shorter or longer intervals. c-Fos labeling and chemogenetic inactivation established the necessity of the dorsomedial prefrontal cortex (dmPFC) for successful memory storage. *In vivo* calcium imaging of excitatory dmPFC neurons revealed that longer trial spacing increased the similarity of the population activity pattern on subsequent encoding trials and upon retrieval. Conversely, trial spacing did not affect the size of the total neuronal ensemble or the size of subpopulations dedicated to specific task-related behaviors and events. Thus, spaced learning promotes reactivation of prefrontal neuronal ensembles processing episodic-like memories.

Introduction

Extending the period between individual learning events can considerably strengthen a memory and increase its lifespan, a phenomenon called the "spacing effect"[1]. This phenomenon has been described across a wide range of species, from mollusk to man[2]. In mice, spaced training can strengthen associative[3] episodic-like[4], motor[5], and spatial[6] memories. The effectiveness of spacing learning is thought to be mediated by molecular and synaptic processes[2], which involve activation and expression of key signaling proteins and transcription factors[2; 6; 7], leading to increased synaptic plasticity[5; 8]. It has not yet been studied, whether and how increasing the spacing of learning events affects neuronal ensembles representing an individual memory.

During a learning experience, a subset of neurons is activated as a result of their intrinsic excitability and external sensory drive[9; 10; 11; 12]. The memory itself is thought to be encoded by synaptic connections that are newly formed or strengthened within this neuronal ensemble[13; 14; 15]. Subsequently, memories can be consolidated by further functional and structural synaptic remodeling, enabling long-term retention[16; 17]. For retrieval of a memory, neurons that are part of the ensemble need to be reactivated in a pattern similar to that during memory encoding[11; 18; 19].

The working hypothesis for the present work is that the molecular and synaptic mechanisms underlying the spacing effect[2] can influence two characteristics of neuronal ensembles, i.e. the size or reactivation pattern of the ensemble, during memory encoding, storage, and retrieval. The reasoning is that when learning occurs over multiple optimally spaced trials, molecular signaling initiated in the first trial can extend the temporal window of enhanced neuronal excitability[10; 20] and thereby increase the likelihood of the same ensemble being reactivated in subsequent trials. As such, spaced training would more effectively strengthen the ensemble's internal synaptic connectivity[21; 22] and by local competitive circuit interactions result in a sparser, but more reliably activated assembly[23; 24; 25]. Sparseness would safeguard the specificity of the represented memory[26], while stronger connectivity would render the memory more resilient to homeostatic mechanisms that can result in forgetting[27] and thereby increase the probability of retrieval. Conversely, as the group of excitable neurons drifts over time[10], consecutive learning experiences could activate different sets of neurons. Spacing learning experiences over extended periods could therefore allocate a memory to overlapping sets of neurons[28]. Within this framework, the memory enhancing effect of spaced training could be mediated by representing a learning experience with a larger neuronal ensemble[4; 11].

To determine whether and how trial spacing changes the way neuronal ensembles represent learned experiences, we implemented the "everyday memory" task, a naturalistic delayed matching-to-place task[7]. The instilled episodic-like memories are typically forgotten within 24 hours, but spaced training reliably prolongs the period over which the memories can be retrieved[7].

Efficient execution of the everyday memory task relies on functions that have been attributed to the dorsal medial prefrontal cortex (dmPFC), including behavioral flexibility [29] and learning against a background of relevant prior knowledge [30]. Moreover, rodent prefrontal cortex is, in concert with hippocampus, involved in the encoding and retrieval of episodic-like memories [31; 32], providing an attractive system for examining the relation between neuronal ensemble activity and memory strength.

Here we report that trial spacing improves memory and is accompanied with enhanced reactivation of the neuronal ensembles in dmPFC. Increasing trial spacing in the everyday memory task enhanced memory retrieval, yet impaired memory encoding. *In vivo* calcium imaging with a miniaturized microscope revealed that trial spacing results in more similar reactivation of the ensemble between encoding trials and upon memory retrieval. Conversely, trial spacing did not affect the size of the ensemble, suggesting that trial spacing primarily affects the synaptic strength within the neuronal ensemble but not its size.

Results

Studying episodic-like memory in an "everyday memory" task.

We trained female mice (n = 20) in repeated sessions of an "everyday memory" task (see STAR Methods, **Figure 1A, B**) [7]. Each training session consisted of three encoding trials (ETs; separated by an "encoding intertrial interval") and three retrieval trials (RTs). During each encoding trial, mice entered the radial arm maze from a start box, explored the maze and retrieved a buried chocolate reward by digging in one of two available, odor-masked sandwells (i.e. the "rewarded" sandwell). Upon completion of the final encoding trial, mice were kept in their home cage for an extended delay period ("retrieval delay"), after which the three retrieval trials (RTs) were conducted. During retrieval trials, mice had to revisit the previously rewarded sandwell. Simultaneously, mice had to refrain from digging at the previously non-rewarded sandwell, as well as four new non-rewarded sandwells ("non-cued" sandwells). After each session, we changed the spatial configuration of the sandwells and the position of the start box. Consequently, mice had to relearn and remember a different rewarded location in each subsequent session. Performance in each trial was quantified as the number of incorrect sandwells the mouse dug in, relative to the total number of available sandwells.

We first characterized the conditions under which mice were able to successfully complete the task. Memory was only reliably retrieved after training with multiple encoding trials in which the rewarded location was kept constant (**Figure S1**).
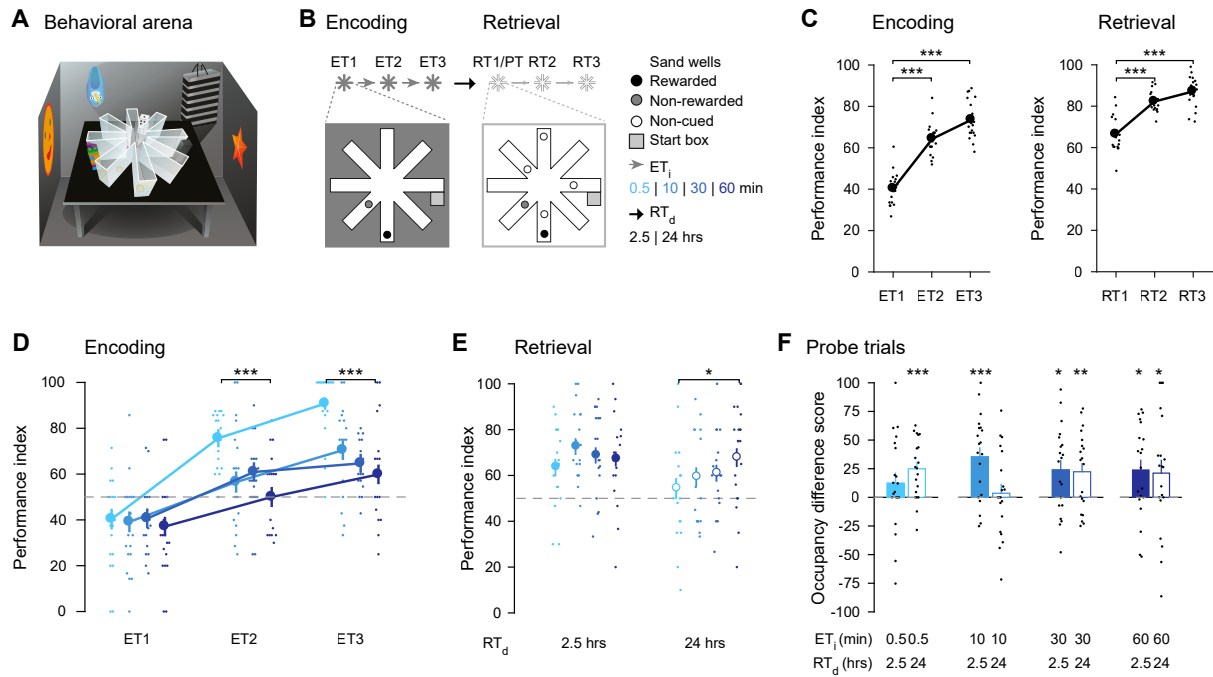
Figure 1. Trial spacing enhances memory retrieval, yet impairs memory encoding on the everyday memory task. A Schematic of behavioral training setup. **B** Schematic of session structure. Each session existed of a learning phase ("encoding", three trials separated by an "encoding intertrial interval" [ET_i]) and a memory phase ("retrieval", three trials), separated by a retrieval delay (RT_d). Occasionally, the first retrieval trial (RT1) was replaced with a probe trial (PT). The location of the sandwells and start box was altered on each session. **C** Performance improved across encoding and retrieval trials (one-way repeated measures [OWRM] ANOVA: $F_{5,90} = 111$, $p = 7.24 \cdot 10^{-37}$, Bonferroni post hoc tests: ET1 vs. ET2, $p = 1.22 \cdot 10^{-9}$; ET1 vs. ET3, $p = 2.27 \cdot 10^{-8}$; RT1 vs. RT2, $p = 1.10 \cdot 10^{-5}$; RT1 vs. RT2, $p = 3.00 \cdot 10^{-6}$, n = 19 mice). **D** Performance increased on subsequent encoding trials, but this enhancement was impaired by increasing the ET_i (two-way repeated measures [TWRM ANOVA]: trial number, $F_{2,108} = 111$, $p = 1.17 \cdot 10^{-15}$; ET_i, $F_{3,108} = 11.7$, $p = 6.00 \cdot 10^{-6}$; interaction, $F_{6,108} = 2.50$, $p = 0.027$, Bonferroni post hoc tests: 0.5 vs. 10 min, $p = 0.003$; 0.5 vs. 30 min, $p = 0.004$; 0.5 vs. 60 min, $p = 9.30 \cdot 10^{-5}$; ET1 vs. ET2, $p = 3.87 \cdot 10^{-10}$; ET1 vs. ET3, $p = 6.37 \cdot 10^{-9}$; ET2 vs. ET3, $p = 2.88 \cdot 10^{-4}$, n = 19 mice). **E** Increasing the ET_i did not alter performance on RT1 after a 2.5-hrs RT_d (OWRM ANOVA: $F_{3,54} = 1.58$, $p = 0.206$, n = 19 mice) yet did after 24 hrs (OWRM ANOVA: $F_{3,54} = 3.02$, $p = 0.038$, n = 19 mice). **F** Memory was not observed after 2.5 hrs if training was conducted with an ET_i of 0.5 min, but was after 24 hrs (one-sample t-test: ET_i 0.5 min, RT_d 2.5 hrs vs. chance: $t_{19} = 1.35$, $p = 0.194$; ET_i 0.5 min, RT_d 24 hrs vs. chance: $t_{19} = 4.27$, $p = 4.12 \cdot 10^{-4}$, n = 19 mice). Conversely, training with an ET_i of 10 min resulted in memory after 2.5 hrs, but not after 24 hrs (one-sample t-test: ET_i 10 min, RT_d 2.5 hrs vs. chance: $t_{19} = 4.30$, $p = 3.89 \cdot 10^{-4}$; ET_i 10 min, RT_d 24 hrs vs. chance: $t_{19} = 0.43$, $p = 0.675$, n = 19 mice). Memory was present and stable on probe trials conducted after training using a 30-min or 60-min ET_i (one-sample t-test: ET_i 30 min, RT_d 2.5 hrs vs. chance: $t_{19} = 2.83$, $p = 0.011$; ET_i 30 min, RT_d 24 hrs vs. chance: $t_{19} = 2.94$, $p = 0.008$; ET_i 60 min, RT_d 2.5 hrs vs. chance: $t_{19} = 2.63$, $p = 0.017$; ET_i 60 min, RT_d 2.5 hrs vs. chance: $t_{19} = 2.48$, $p = 0.023$, n = 19 mice). Filled dots indicate data from one mouse, circles and bars indicate mean ($\pm$ SEM) across mice, and gray dashed lines indicates chance level. * $p < 0.05$, ** $p < 0.01$, *** $p < 0.001$. See also Figures S1, S2, and S3.

Performance increased across subsequent encoding trials within sessions, as well as subsequent retrieval trials, verifying that mice can encode and retrieve memories in this task (**Figure 1C**). In addition, we studied the within- and between-session strategies that mice employ in this task. Altering the start box location between and after encoding trials confirmed that mice primarily used an allocentric (world-centered) rather than egocentric (body-centered) reference frame (**Figure S2A–D**)[33]. Within a session, mice revisited non-rewarded arms less than expected from chance (**Figure S2E**) and focused their search progressively closer to the rewarded arm (**Figure S2F**). Between sessions, the previous session's retrieval performance did not affect the next session's retrieval performance (**Figure S2G**), suggesting that a successfully stored memory did not interfere with learning of a new memory. From these analyses, we conclude that mice employ both a "within-session win-stay" and "between-session switch" strategy to optimize their task performance.

Increasing trial spacing enhances memory retrieval but impairs memory encoding.
To examine the influence of trial spacing on encoding and retrieval of episodic-like memory, we tested the effect of four encoding intertrial intervals: 30 s (i.e. "massed" training, 119 sessions), 10 min (115 sessions), 30 min (133 sessions), and 60 min (132 sessions; **Figure 1B**). To probe the effect of trial spacing on same- and next-day memory retrieval separately, we conducted retrieval trials after a retrieval delay of either 2.5 or 24 hrs. Performance was stable over months of training, allowing us to average a mouse's performance across sessions of the same encoding intertrial interval and retrieval delay.

We observed that performance in the second and third encoding trial was reduced when encoding intertrial intervals were extended (**Figure 1D**). In addition, memory retrieval after 24 hrs was improved when encoding intertrial intervals were longer, yet no effect was observed after 2.5 hrs (**Figure 1E**). This difference was not unexpected as trial spacing primarily affects less recent memories[2]. As a control, we compensated for impaired encoding by normalizing the performance in the first retrieval trial to the encoding performance in the final, third encoding trial ("retention"). Retention thereby addressed how much of the successfully encoded information persisted and subsequently could be retrieved. Memory retention positively correlated with encoding intertrial interval after both a 2.5 hrs and 24 hrs retrieval delay.

In a subset of sessions, we quantified the absolute strength of the memory by conducting a probe trial, which replaced the first retrieval trial. In these probe trials, the previously rewarded sandwell did not contain reward for the first minute of exploration. Absence of a reward during the probe trial did not discourage the mouse from revisiting the rewarded arm during the probe trials or on the subsequent retrieval trial. Memory in probe trials was quantified as the relative dig time at the rewarded sandwell, normalized to the total dig time at the rewarded and non-rewarded sandwell (termed the "occupancy difference score"). In sessions conducted with spaced encoding

intertrial intervals, we observed an inverted U-shaped effect of trial spacing on next-day memory. Specifically, mice that were trained using a 10 or 180 min encoding intertrial interval did not remember the rewarded location after 24 hrs (**Figure 1F, S2H**), while memories persisted after training with encoding intertrial intervals of 30 min or 60 min (**Figure 1F**). Unexpectedly, massed training did not result in same-day memory, but memory was observed after 24 hrs and was even still present after 48 hrs (see Discussion, **Figure 1F, S2H**).

Differences in trial spacing could affect a number of memory-related behavioral variables besides error-based performance: the latency to find the rewarded sandwell, distance traveled, running speed, relative dig time, and number of arm visits (**Figure S3**). In consecutive encoding trials, we observed a quantitative reduction in the variables that are indicative of exploration, i.e. latency, distance traveled, running speed, and number of arms visited. Conversely, we observed an increase in the relative dig time, a measure of exploitation of memory of the rewarded location. These results suggest that mice explored less and increasingly used their recollection of the rewarded sandwell location in subsequent encoding trials. Although there were incidental trials on which an effect of trial spacing was observed (**Figure S3**), we did not observe a systematic change in any of the behavioral variables resulting from trial spacing. We conclude that increased trial spacing enhances memory retrieval, independent of the impairing effect on memory encoding.

The dmPFC is activated and necessary during the everyday memory task.
To validate that training in the everyday memory task activates the dmPFC, we quantified neuronal activation resulting from training on the three encoding trials using expression of the immediate early gene c-Fos (**Figure 2A**). c-Fos expression in the dmPFC was increased after training as compared to handled or home cage controls (**Figure 2B, C**). However, the number of c-Fos-expressing neurons was similar after training spaced with any encoding intertrial interval. This suggests that trial spacing did not increase the number of activated neurons during memory encoding.

To establish a causal role of the dmPFC on the everyday memory task, and subsequently evaluate whether this role is attributable to a specific training regimen, we chemogenetically inhibited it. We bilaterally transduced excitatory dmPFC neurons with the inhibitory chemogenetic tool hM4D(Gi), which is activated by clozapine-*N*-oxide (CNO; **Figure 3A, B**) [34]. We first verified receptor function in dmPFC *ex vivo* electrophysiological recordings and established that CNO application to acute brain slices reduced the excitability of dmPFC neurons expressing hM4D(Gi) (**Figure S4A–C**). Next, we addressed the role of dmPFC activity during the everyday memory task using a full factorial 2^4 design (see STAR Methods; **Figure 3A**). In well-trained mice expressing either hM4D(Gi) (n = 7) or mCherry (n = 5), we injected either vehicle or CNO at either of two time points (i.e. before memory encoding or retrieval) using either of two encoding intervals (i.e. 0.5 min and 60 min; **Figure 3A**).
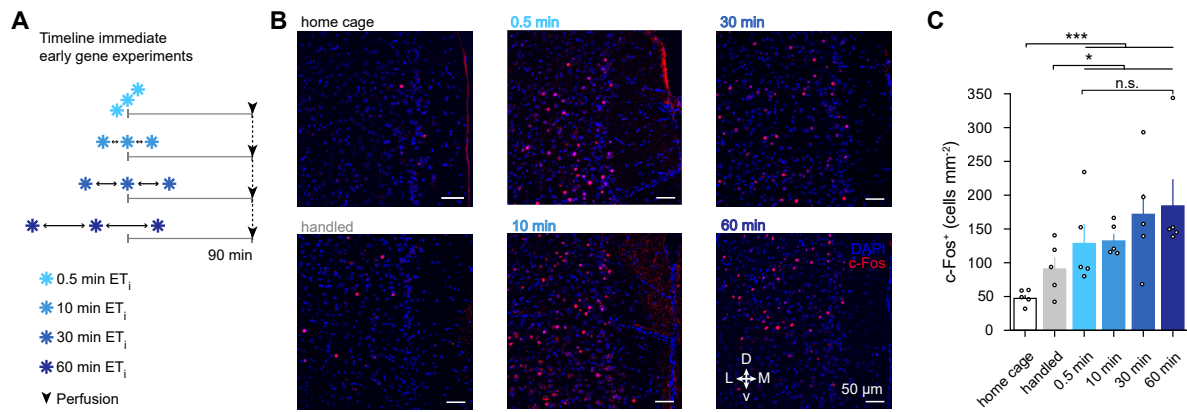
Figure 2. The dmPFC is activated by training on the everyday memory task, irrespective of trial spacing. A Timeline of behavioral procedures and tissue collection. **B** Representative images of c-Fos labeling in the dmPFC. **C** Training with any ET_i increased the number of cells expressing c-Fos as compared to home cage or handled controls (Kruskal-Wallis test: $H_2 = 15.8$, $p = 3.65 \cdot 10^{-4}$; Mann-Whitney U post hoc tests: training vs. home cage; training vs. home cage, $U = 0$, $p = 7.71 \cdot 10^{-4}$; training vs. handled, $U = 19$, $p = 0.013$, n = 5 mice per group). Increasing the ET_i did not alter the number of c-Fos-expressing cells (Kruskal-Wallis test: $H_3 = 1.19$, $p = 0.754$, n = 5 mice per group). Scale bar 50 µm (B). Bars indicate mean ($\pm$ SEM) across mice, black dots indicate data from a single mouse. * $p < 0.05$, *** $p < 0.001$, n.s. non-significant.

Robust bilateral viral vector expression was confirmed post hoc. Pooling data across time points and intervals showed that CNO-mediated inhibition impaired memory retrieval in hM4D(Gi)-expressing mice (**Figure 3C**). CNO application similarly reduced memory retrieval between individual time points and interval durations (**Figure 3D, E**). However, evaluating the individual time points and interval durations revealed that memory retrieval was only significantly influenced when the dmPFC was inhibited during spaced (i.e. 60 min) encoding. Overall, we conclude that memory storage requires dmPFC activation.
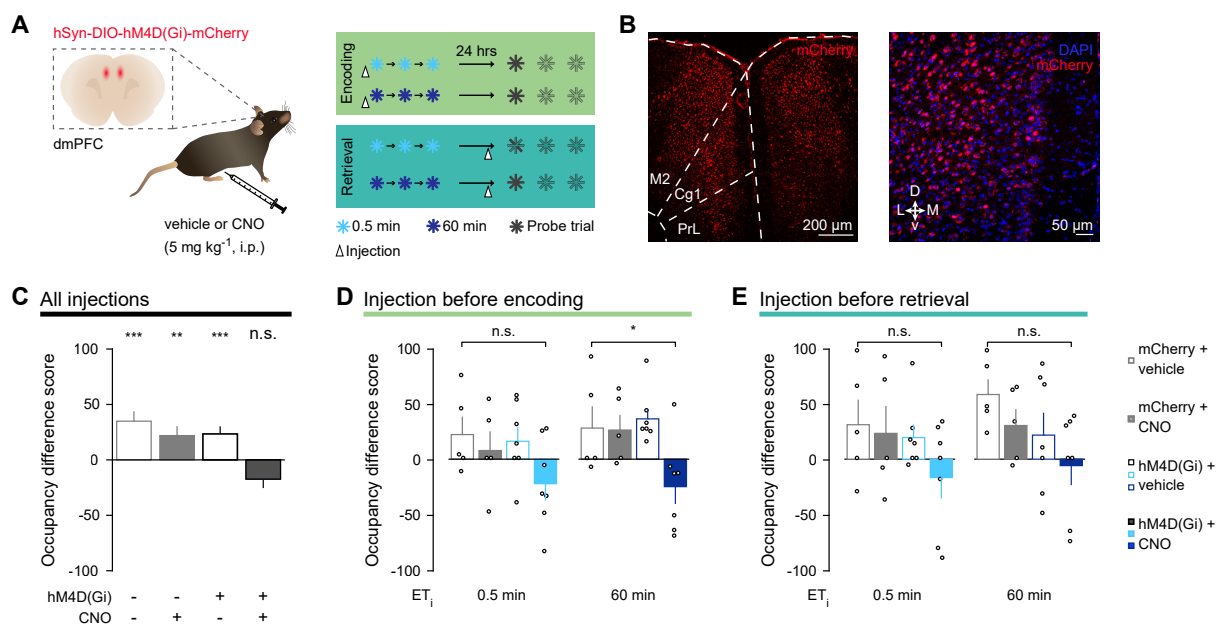
Figure 3. Chemogenetic inactivation of the dmPFC impairs episodic-like memory. Legend on next page.

A Chemogenetic silencing experiment. After bilateral transduction of the dmPFC with either mCherry (n = 5 mice) or hM4D(Gi) (n = 7 mice), mice were injected with vehicle or CNO during a subset of behavioral experiments. **B** Representative images of hM4D(Gi)-mCherry-expressing neurons in the dmPFC. **C** Memory on probe trials was impaired after silencing the dmPFC by injecting CNO into mice expressing hM4D(Gi)-mCherry (data pooled across injection time points and encoding intertrial intervals, TWRM ANOVA: drug, $F_{10,1} = 13.0$, $p = 7.73 \cdot 10^{-4}$; interaction, $F_{10,1} = 3.46$, $p = 0.069$, n = 12 mice; one-sample t-test: mCherry + vehicle vs. chance: $t_9 = 3.87$, $p = 5.13 \cdot 10^{-4}$; mCherry + CNO vs. chance: $t_9 = 2.56$, $p = 9.51 \cdot 10^{-3}$; hM4D(Gi) + vehicle vs. chance: $t_{11} = 3.45$, $p = 9.61 \cdot 10^{-4}$; hM4D(Gi) + CNO vs. chance: $t_{11} = -2.14$, $p = 0.979$, n = 12 mice). **D** Memory was significantly reduced after silencing the dmPFC using CNO during spaced encoding (ET_i 60 min [right]; TWRM ANOVA: drug, $F_{1,10} = 6.92$, $p = 0.026$; interaction, $F_{1,10} = 6.17$, $p = 0.032$, n = 12 mice) but not massed encoding (ET_i 0.5 min [left]; TWRM ANOVA: drug, $F_{1,10} = 2.41$, $p = 0.152$; interaction, $F_{1,10} = 0.50$, $p = 0.498$, n = 12 mice). **E** Same as in (**D**), for retrieval (TWRM ANOVA: ET_i 0.5 min [left]; drug, $F_{1,10} = 2.80$, $p = 0.125$; interaction, $F_{1,10} = 1.16$, $p = 0.307$; ET_i 60 min [right]; drug, $F_{1,10} = 2.09$, $p = 0.179$; interaction, $F_{1,10} = 0.00$, $p = 0.991$, n = 12 mice). Cg1: cingulate cortex, area 1, M2: secondary motor cortex, PrL: prelimbic cortex. Scale bars 200 μm (B, left), 50 μm (B, right). Bars indicate mean ($\pm$ SEM) across mice, black dots indicate data from a single mouse. * $p < 0.05$, ** $p < 0.01$, *** $p < 0.001$, n.s. non-significant. See also Figure S4.

Trial spacing increases the stability of the prefrontal cortex activation pattern.

The major aim of this study was to evaluate whether trial spacing stabilizes the activity patterns of the neuronal populations throughout a session, i.e. whether it facilitates reactivation of a similar neuronal ensemble in subsequent trials. To this end, we used *in vivo* calcium imaging to simultaneously measure the activity patterns of on average 210 ± 99 (SD) individual dmPFC neurons per session in freely-moving mice (n = 499 sessions across 19 mice; **Figure 4A, B**) [35]. We gained optical access to the dmPFC with an implanted microprism and used a Cre-dependent dual-virus method to label a sparse subset of neurons with the calcium indicator GCaMP6m (**Figure 4C, S4D–H**) [36]. To image GCaMP6m-expressing neurons, we used a miniaturized microscope (Doric Lenses) that clamped onto an implanted imaging cannula, thereby preventing notable alterations in the imaged field of view (**Figure S5A**). We ensured that carrying the miniaturized microscope did not hamper the mouse's motility in the radial arm maze (**Figure S4I, J**). Using the constrained nonnegative matrix factorization for microendoscopic data (CNMF-E) algorithm [37], we extracted neuronal calcium activity and used the deconvolved inferred spike rate for further analysis (see STAR Methods, **Figure S5B–E**). The number of identified neurons did not vary between experimental conditions. We next computed the probability of a neuron being active by comparing the inferred spike rate in each trial to the pre-trial baseline period, using temporal subsampling to control for session duration (p_{active}; see STAR Methods; **Figure 68A–C**). We subsequently concatenated these values into an ensemble response vector and stacked the single-trial ensemble response vectors into an ensemble response matrix (n neurons $\times$ 6 trials; **Figure 4D**). The Pearson correlation between the rows of this matrix was used as the sessions trial-to-trial ensemble stability measure (**Figure 4D**).

The ensemble correlation between the first and second encoding trial was enhanced when the intertrial interval was longer, establishing that the ensemble reactivated more precisely (**Figure 4E, F**). Furthermore, trial spacing increased the ensemble correlation between the third encoding trial and the first retrieval trial, suggesting that the population activity pattern present during learning

was more likely to be reactivated during retrieval (**Figure 4E, F**). The effect of trial spacing on ensemble correlation was not dependent on behavioral performance. As an alternative measure for similarity, we calculated the Euclidian distance between ensemble response vectors, which yielded similar results (**Figure S6D**). Overall, we find that increased trial spacing enhanced reactivation of the ensemble activity pattern instilled during encoding, while simultaneously strengthening memory retention.
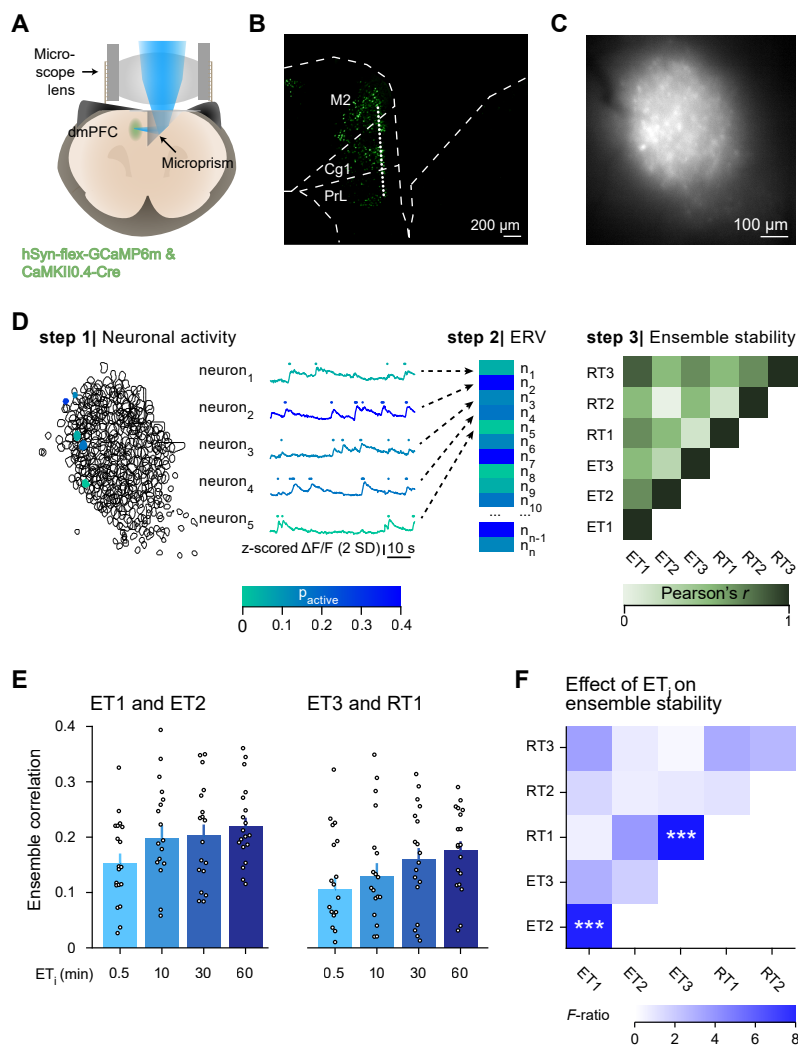
Figure 4. Trial spacing enhances ensemble stability, but not ensemble size. **A** Schematic of imaging preparation. **B** Approximate imaging plane (dotted line). **C** Sample microscopy frame. **D** Schematic showing the quantification of ensemble stability. Based on the deconvolved spiking activity (dots, calcium activity displayed as traces), the activity measure "p_{active}" was calculated for each neuron (step 1). For each trial, the "p_{active}" of individual neurons was concatenated into an ensemble response vector (ERV; step 2). The correlation between all ensemble response vectors of a session was used as a measure for ensemble stability (step 3). **E** Ensemble correlation between ET1 and ET2 (left) and between ET3 and RT1 (right). **F** Trial spacing enhanced the ensemble correlation between ET1 and ET2, as well as between ET3 and RT1 (OWRM ANOVA: ET1–ET2: $F_{3,54} = 6.98$, $p = 5.07 \cdot 10^{-4}$, Bonferroni post hoc tests: 0.5 vs. 10 min, $p = 3.16 \cdot 10^{-4}$; 0.5 vs. 60 min, $p = 2.04 \cdot 10^{-3}$; ET3–RT1: $F_{3,54} = 7.28$ $p = 3.72 \cdot 10^{-4}$, Bonferroni post hoc tests: 0.5 vs. 30 min, $p = 2.56 \cdot 10^{-3}$; 0.5 vs. 60 min, $p = 1.51 \cdot 10^{-3}$, n = 19 mice). Cg1: cingulate cortex, area 1, M2: secondary motor cortex, PrL: prelimbic cortex, SD: standard deviation. Scale bars: 200 µm (B), 100 µm (C). White lines indicate median across sessions, colored boxes indicate interquartile range, dots indicate data from a single mouse, averaged across sessions. *** p < 0.001. See also Figures S4, S5, and S6.

The size of the neuronal ensemble is not affected by trial spacing.

We evaluated whether trial spacing altered the size of the neuronal ensemble (**Figure 5A**). From the cumulative distribution of each trial's ensemble response vector, we inferred the active fraction within the neuronal population (i.e. the neuronal ensemble, $p_{active} > 0$) and the median activity of that population (**Figure 5A**). Interestingly, the neuronal ensembles became smaller across subsequent encoding and retrieval trials (i.e. first vs. second vs. third trial; **Figure 5B**). In addition, the median activity of the neuronal ensemble increased across subsequent trials (**Figure 5B**), indicating that the ensemble became sparser, yet the single neurons responded more strongly (see Discussion). However, neither ensemble size (i.e. the relative number of active neurons), nor its median activity was altered by trial spacing (**Figure 5B**).
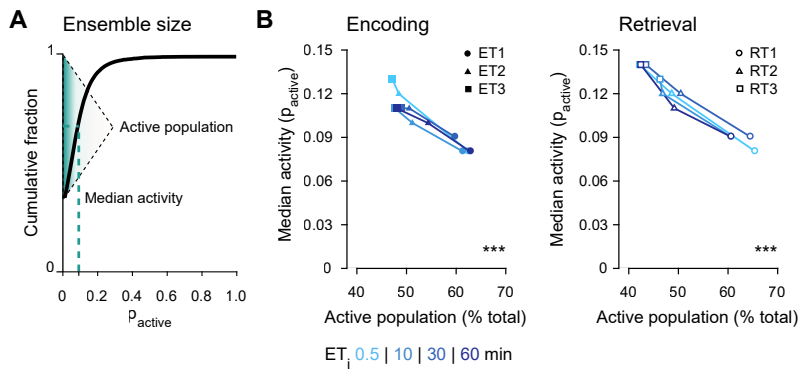
Figure 5. Trial spacing does not affect the size of the total neuronal ensemble. **A** Schematic showing the quantification of the total ensemble size. The size of the active population ($p_{active} > 0$) and its median activity were inferred from the cumulative distribution of the ensemble response vector. **G** The trial identity (i.e. first, second or third trial) but not the ETi affected the size of the active population (TWRM ANOVA: trial identity, $F_{5,270} = 61.4$, $p = 9.15 \cdot 10^{-27}$; ETi, $F_{3,270} = 2.28$, $p = 0.091$; Bonferroni post hoc tests for subsequent trials: ET1 vs. ET2, $p = 1.00 \cdot 10^{-6}$; RT1 vs. RT2, $p = 6.80 \cdot 10^{-8}$, n = 19 mice) and its median activity (TWRM ANOVA: trial identity, $F_{5,270} = 91.7$, $p = 9.57 \cdot 10^{-33}$; ETi, $F_{5,270} = 2.10$, $p = 0.111$; Bonferroni post hoc tests for subsequent trials: ET1 vs. ET2, $p = 3.12 \cdot 10^{-8}$; RT1 vs. RT2, $p = 9.90 \cdot 10^{-7}$; RT2 vs. RT3, $p = 0.004$, n = 19 mice). Data points indicate mean across mice. *** $p < 0.01$.

With the overall ensemble size remaining stable, the memory enhancing effect of trial spacing could be attributed to a shift in the fraction of neurons preferentially responding to task-related events. We identified eight task-related behavioral variables that correlated with reward, motor activity, and decision-making: reward onset, reward approach (i.e. the final entry into the arm containing the rewarded sandwell), acceleration, speed, digging onset, digging offset, entry into the center platform, and intra-arm turns. On first inspection, neuronal responses did not appear time-locked or consistently occurring with the onset of these defined behaviors (**Figure S5E**). This was likely related to the naturalistic character of the everyday memory task, in which the individual components that comprise a behavior can occur simultaneously, whereas these appear discrete in more controlled experimental settings.

To determine whether the activity of individual neurons was modulated by task-relevant behaviors, we implemented an encoding model (generalized linear model, GLM). The model fitted the eight aforementioned behavioral variables as time-varying predictors of a neuron's binarized inferred firing activity (**Figure 6A, B**, see STAR Methods) [39]. A neuron was classified as responsive to one of these behavioral variables if the weight of its corresponding time-varying predictor was significantly different from zero. Decoding performance was better upon training the encoding model with observed as compared to permuted inferred firing activity (**Figure 6C**). Across sessions, 22.7% of neurons were significantly modulated by at least one behavioral variable, most often reward onset, approach to reward, and digging onset (19.9%, 16.2%, and 18.1% of the population of modulated neurons, respectively; **Figure 6D**). This shows that dmPFC neuronal activity during the everyday memory task is modulated by specific behavioral variables.

However, trial spacing did not have a significant influence on the fractions of behaviorally modulated neurons, nor did the encoding performance or retrieval delay duration (**Figure 6E**). Firing modulation by all identified task-relevant behaviors did depend on session duration (**Figure 6E**), likely because an increased session duration inherently produces more neuronal spikes and therefore data for the GLM to fit. Furthermore, retrieval performance correlated with the fraction of neurons modulated by certain behavioral variables, i.e. running speed, reward approach, dig onset, dig offset, entry into the center platform, and intra-arm turns. Therefore, we conclude that a sparse population of dmPFC neurons encoded task-related behaviors similarly across experimental conditions and we did not find evidence of an effect of trial spacing on the number of neurons involved. Overall, trial spacing in the everyday memory task enhances ensemble stability but it does not affect ensemble size.
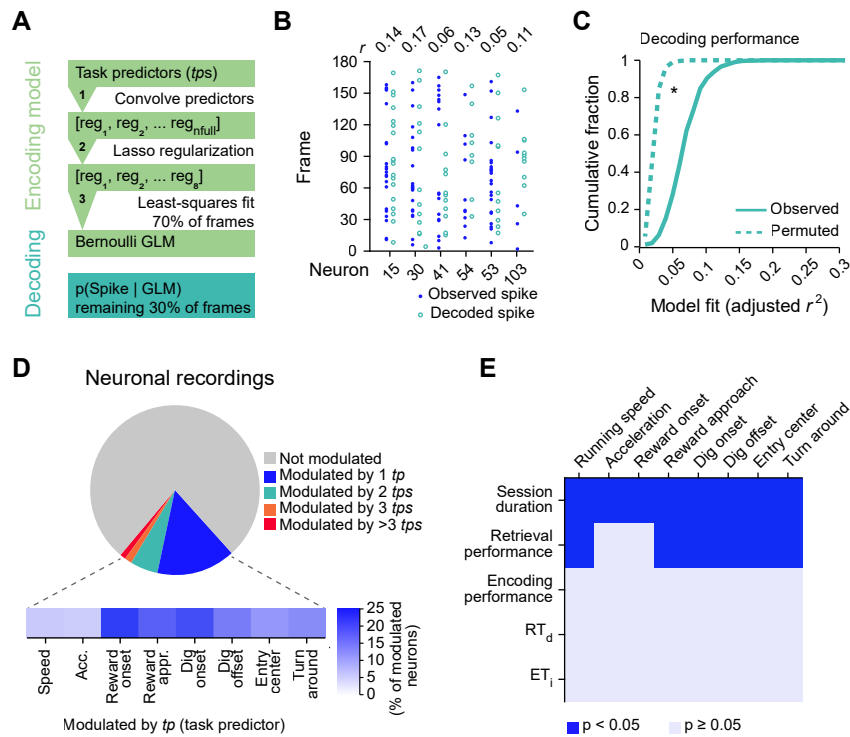
Figure 6. dmPFC neurons respond to multiple task-relevant behaviors irrespective of trial spacing. **A** Schematic of the generalized linear model to identify neurons whose firing was modulated by specific task-related behaviors and events. **B** Pearson's r between observed and decoded spikes of the test subset for six randomly selected neurons. **C** Decoding performance was significantly better for observed than permuted spiking activity (Kolmogorov-Smirnov test: observed vs. permuted, $D_{100} = 0.21$, $p = 0.021$). **D** Fractions of neurons (n = 105070 neurons from 499 sessions across 19 mice) that were modulated (top). Fractions of neurons modulated by the respective task predictor (bottom). **E** The effect of the five features session duration, performance on RT1 ("retrieval performance"), summed performance across ETs ("encoding performance"), ET_i, and RT_d, on the fraction of neurons modulated by the eight *tp*s. These five features differentially affected the fraction of neurons modulated by running speed (FW ANOVA: session duration [SeD], F = 121, p = $2.95 \cdot 10^{-25}$; retrieval performance [RP], $F_{5,810} = 3.05$, p = 0.01, n = 499 sessions), acceleration (FW ANOVA: SeD, F = 76.6, p = $3.43 \cdot 10^{-17}$, n = 499 sessions), reward onset (FW ANOVA: SeD, F = 67.7, p = $1.78 \cdot 10^{-15}$, n = 499 sessions), reward approach (FW ANOVA: SeD, F = 86.8, p = $4.14 \cdot 10^{-19}$; RP, $F_{5,810} = 6.37$, p = $1.00 \cdot 10^{-5}$, n = 499 sessions), dig onset (FW ANOVA: SeD, F = 121, p = $2.42 \cdot 10^{-25}$; RP, $F_{5,810} = 2.89$, p = 0.014, n = 499 sessions), dig offset (FW ANOVA: SeD, F = 129, p = $1.31 \cdot 10^{-26}$; RP, $F_{5,810} = 3.18$, p = 0.008, n = 499 sessions), entry into the center platform (FW ANOVA: SeD, F = 108, p = $5.89 \cdot 10^{-23}$; RP, $F_{5,810} = 7.74$, p = $5.10 \cdot 10^{-7}$, n = 499 sessions), and intra-arm turns (FW ANOVA: SeD, F = 86.8, p = $4.14 \cdot 10^{-19}$; RP, $F_{5,810} = 4.36$, p = $6.78 \cdot 10^{-4}$, n = 499 sessions). Only significant tests are reported. Acc: acceleration, appr: approach, GLM: generalized linear model, *tp*: task predictor, reg: regressor. * p < 0.05. See also Figure S5.

Discussion

We explored whether trial spacing strengthens memory by altering characteristics of the neuronal ensemble. We observed the behavioral effect of trial spacing on the everyday memory task and characterized the activity of prefrontal neurons that were necessary for task performance. During learning and upon memory retrieval, the ensemble activity pattern reactivated more precisely when trial spacing was increased. In contrast, trial spacing did not affect the overall size of the activated ensemble, nor the size of the subpopulations of neurons that responded to specific task-related behaviors. Our results suggest that more precise reactivation of the neuronal ensemble during spaced training strengthens connectivity that is conducive to memory retention and retrieval.

Spaced training strengthens memory.

Spaced training in the everyday memory task strengthens memory in rats[7] and we report the same in mice. Earlier studies investigating the effect of trial spacing on episodic-like memory in mice[6] and rats[40] have reported an inverted U-shaped relation, although the exact width and amplitude of the effect varied. Our study likewise reports an inverted U-shaped relation, as spacing trials at intervals of 60 min resulted in the strongest next-day (24 hrs) memory, while shorter (10 min and 30 min) and longer intervals (180 min) resulted in substantially poorer memory. The observed temporal window aligns with expectations from facilitated molecular signaling and synaptic physiology underlying the spacing effect[2; 6; 8].

As compared to spaced training, massed training in the everyday memory task affected memory in a rather complex manner. As expected, memory retrieval was poorer after massed training than after any spaced training regimen. Surprisingly, the ability to retrieve memory following massed training was better after 24 hrs, and even 48 hrs, as compared to 2.5 hrs. We propose that memory acquired during massed training might have only been stabilized after several hours. A similar phenomenon has been reported during massed motor learning in mice, in which both memory stabilization and concomitant synaptic remodeling occurred delayed as compared to spaced motor learning[5]. However, delayed memory stabilization was not observed in two earlier studies using the everyday memory task[7; 41]. This variation can possibly be attributed to methodological differences such as the animal model[7; 41], the number of encoding trials[41], navigational strategy[33], handling, or intertrial sleep epochs.

Prefrontal activity in the everyday memory task.

We focused our neuronal recordings and manipulations on the dmPFC. Activity of dmPFC neurons correlated with a range of task-relevant events on the everyday memory task, most notably reward (anticipation) and motor behavior, which is consistent with other reports in rodent PFC[38; 42]. We established a causal link between prefrontal activity and memory formation by chemogenetically

inactivating the dmPFC, which impaired next-day memory. This seemingly conflicts with reports that inactivation of prefrontal areas disrupts remote but not recent memories [43]. However, the early dependence of task-instilled memories on the dmPFC may have followed from accelerated systems consolidation, as observed in other behavioral paradigms where learning occurred within the context of relevant pre-existing knowledge [30].

Episodic-like memories formed in the everyday memory task unlikely depended solely on the dmPFC. Specifically the hippocampus [44] and retrosplenial cortex [45] have long been implicated in various forms of declarative memory. Indeed, the hippocampus and prefrontal cortex have been suggested to perform complementary roles in episodic-like memory processing [31; 46]. Furthermore, retrosplenial neurons form ensembles that stabilize during learning of spatial reference memory tasks [47] and the stability of these retrosplenial ensembles can predict memory retention [48]. Interestingly, a recent study shows that trial spacing upregulates a variety of genes, including immediate early genes, in both hippocampus and retrosplenial cortex in the rat [7]. Whether and how neuronal ensembles in the mouse hippocampus and retrosplenial cortex are affected by spaced training in the everyday memory task would be of interest for future investigation.

The spacing effect, synaptic strength, and memory stability.

Our experiments explored the possibility that trial spacing enhances memory by altering the size or stability of a neuronal ensemble. We quantified ensemble size using two distinct methods. First, we determined the neuronal ensemble size using calcium imaging of GCaMP6-expressing neurons, which closely reflects the temporal dynamics of neuronal firing throughout each trial [36]. This approach allowed for detecting both highly active and transiently activated neurons, while controlling for the influence of training duration on ensemble size by temporal subsampling. Second, we quantified ensemble size from the number of c-Fos-expressing neurons after a full encoding session. This method is more likely to only include strongly activated neurons that subsequently underwent plasticity implicated in long-term memory storage [49]. Despite the methodological differences between these approaches, both yielded similar results: the size of the active population was not influenced by trial spacing. This is in agreement with the previous observation that ensemble size is generally quite stable and is not strongly influenced by factors such as the type of memory and the strength of a memory [24].

Irrespective of trial spacing, behavioral training activated a progressively smaller population of neurons, whose activity was stronger than in previous trials. Sparsening of the neuronal ensemble can enhance memory selectivity, as for instance observed during *Drosophila* olfactory conditioning [26]. Several studies propose that this is the consequence of a competitive process [9; 24], in which highly excitable pyramidal neurons exclude less excitable neighboring pyramidal neurons from becoming part of the neuronal ensemble via local inhibition. A similar process might ensure ensemble sparsity

in the everyday memory task, thereby balancing memory fidelity with memory capacity [9].

The main consequence of trial spacing was that the neuronal ensemble reactivated in a pattern more reminiscent of previous learning experiences, corroborating theoretical predictions [50] and reports in human subjects [23]. Importantly, we established a relationship between trial spacing and ensemble stability, yet the question of whether the enhanced stability of the ensemble pattern is causal for the memory-enhancing effect of trial spacing remains unanswered. We suggest that more precise ensemble reactivation reflects specific synaptic processes that underlie memory formation [14]. One such process is CaMKII activation, which unfolds on a similar timescale as spacing-induced memory enhancement and has previously been implicated in the spacing effect [2]. A major outstanding question is whether these synaptic processes affect a random population of synapses or are confined to previously tagged synapses, as predicted by the synaptic tagging and capture theory [51]. This could be addressed using *in vivo* imaging of structure and function of individual spines during the everyday memory assay [52].

Overall, our data show that trial spacing increases the strength of connectivity within the ensemble, supposedly making memory more robust and increasing the probability of memory retrieval. Our findings provide the first direct description of how activity of the same neuronal population during memory encoding and retrieval mediates the spacing effect, a phenomenon originally described over a century ago [1].

Acknowledgments

Author Contributions

All authors designed the study. A. G. acquired the data. A. G. and P. G. analyzed the data. T. B. and M. H. acquired funding. All authors wrote the manuscript.

Declaration of Interests

The authors declare no competing interests.

STAR Methods

RESOURCE AVAILABILITY

Lead Contact

Further information and requests for resources and reagents should be directed to and will be fulfilled by the Lead Contact, Pieter M. Goltstein (goltstein@neuro.mpg.de).

Materials Availability

This study did not generate new unique reagents or mouse lines.

Data and Code Availability

Main datasets generated during this study will be made available at https://gin.g-node.org/pgoltstein/everyday-memory-spacingeffect-mpfc/. Imaging data are available in the form of data processed using the CNMF-e algorithm. Raw calcium imaging data have not been deposited in the repository because of file size, but are available upon reasonable request. Main code supporting this study will be made available at https://github.com/pgoltstein. Additional requests for data and code should be directed to the Lead Contact, Pieter M. Goltstein (goltstein@neuro.mpg.de).

EXPERIMENTAL MODEL AND SUBJECT DETAILS

Female adult C57BL/6NRj mice were used ($\sim$ postnatal day 90 at experimental onset). Mice were communally housed in standard, individually ventilated cages (2–3 mice per cage), enriched with a running wheel, tunnel and shelter. Mice were kept on an inverted 12-hrs light, 12-hrs dark cycle with lights on at 10 or 11 PM (winter and summer time, respectively) with constant ambient temperature ($\sim$22°C) and humidity ($\sim$55%). Water was always available ad libitum. Prior to behavioral experiments, standard chow was available ad libitum. From the start of behavioral experiments, mice were food-restricted to 85% of their free-feeding weight. Littermates were randomly assigned to experimental groups. All procedures were performed in accordance with the institutional guidelines of the Max Planck Society and the local government (Regierung von Oberbayern, Germany).

METHOD DETAILS

Surgical procedures

Mice were anesthetized with a mixture of fentanyl, midazolam and medetomidine in saline (FMM, 0.05 mg kg^{-1}, 5 mg kg^{-1}, and 0.5 mg kg^{-1} respectively, injected intraperitoneally). Lidocaine (10% w w^{-1}) was applied onto the scalp for topical anesthesia and carprofen (5 mg kg^{-1}, injected subcutaneously [s.c.]) was administered for analgesia. A head plate implantation was carried out as previously described [53]. For imaging experiments, a 3 mm circular craniotomy was created (cen-

tered at anteroposterior [AP] 2.0 mm, mediolateral [ML] 0.75 mm relative to bregma) [54] and a viral vector mixture of AAV2/1:CamKII0.4-Cre ($4.6 \cdot 10^9$ genome copies [GC] ml^{-1}), and AAV2/1:hSyn-flex-GCaMP6m ($3.2 \cdot 10^{12}$ GC ml^{-1}) was was unilaterally injected into the dmPFC at three injection sites along the anteroposterior axis (AP 1.6 mm, 2.0 mm, and 2.4 mm, ML 0.3 mm, dorsoventral [DV] -1.6 mm, 150 nl injection^{-1}, injection rate 25 nl min^{-1}). The left (n = 9 mice) or right (n = 10 mice) dmPFC was selected based on the superficial blood vessel pattern. Subsequently, a microprism implant (comprised of an aluminum-coated, right-angle microprism [1.5 mm side length] glued to a circular glass window [3.0 mm diameter]) was implanted by removing the dura over one hemisphere and lowering the microprism into the sagittal fissure, facing the other hemisphere [55]. For chemogenetic inactivation experiments, a viral vector mixture of AAV2/1:CamKII0.4-Cre ($2.1 \cdot 10^{11}$ GC ml^{-1}), and either AAV2/9:hSyn-DIO-mCherry ($2.1 \cdot 10^{12}$ GC ml^{-1}) or AAV2/9:hSyn-DIO-hM4D(Gi)-mCherry ($2.3 \cdot 10^{12}$ GC ml^{-1}) was bilaterally injected at two locations into the dmPFC (+2.5 mm AP, $\pm$0.3 mm ML, -1.0 mm DV, and +1.5 mm AP, $\pm$0.3 mm ML, -2.0 mm DV, relative to bregma; 150 nl injection^{-1}; injection rate 25 nl min^{-1}). Each viral vector injection was flanked by a 5 min pre- and post-injection period. After surgery, anesthetic agents were antagonized with a mixture of naloxone, flumazenil and atipamezole in saline (NFA, 1.2 mg kg^{-1}, 0.5 mg kg^{-1}, and 2.5 mg kg^{-1} respectively, injected s.c.). Mice received carprofen (5 mg kg^{-1}, injected s.c.) and dexamethasone (2 μg kg^{-1}, injected s.c.) for two subsequent days. For imaging experiments, a second procedure was carried out two weeks after microprism placement in which a miniaturized microscope lens and adjustment ring were lowered and subsequently glued and cemented over the microprism implant (field of view center approximately at AP 2.2 mm [$\pm$ 300 μm], DV -0.8 mm [$\pm$ 200 μm]).

Behavioral procedures

Mouse handling, habituation, training, and testing was performed similarly as previously described [7], with the main exception that training was conducted in a custom-made radial arm maze (**Figure 1A**). The maze was surrounded by multiple distal 3D cues and contained two proximal landmarks (**Figure 1A**). A remotely operated black Plexiglas start box was mounted at the end of one of the arms. The maze contained cutouts that contained either a sandwell (4 cm inner diameter, 4 cm depth, filled with sand and 5% w w^{-1} Garam Masala powder) or were covered by a white Plexiglas lid. The sandwells could not be seen from a distance from the mouse's perspective. The sandwells were subdivided in a center and surround compartment using semi-circular, perforated 3D-printed removable mesh cups. The surround compartment contained 20 chocolate-flavored pellets (97 mg, chocolate flavor) that served as masking odors and that were inaccessible to the mouse. During behavioral training, the rewarded sandwell contained one accessible chocolate-flavored pellet placed in the center compartment, 2 cm below the sand surface. In-between trials, all sandwells were refilled, any sand on the maze was brushed and vacuumed away, and all arms

were carefully wiped with 40% ethanol. At the end of each day, the maze was thoroughly cleaned using 80% ethanol. Behavioral training was recorded with an overhead video camera and the frame-by-frame position of the mouse was automatically annotated using custom-written Python and MATLAB routines.

Behavioral experiments were conducted approximately between 12:00 and 19:00 o'clock. During the first 7 days of the experiment, the mice were habituated to the maze, habituated to carrying the miniaturized microscope, and trained to dig for a chocolate pellet in the sandwells. During the main experimental phase, each session typically consisted of three encoding trials (ETs) and three retrieval trials (RTs; **Figure 1B**). The ETs had an encoding intertrial interval (ET_i) of either 30 s ("massed"), 10 min, 30 min, or 60 min (all "spaced") and the retrieval delay (RT_d) between the final ET and first RT was 2.5 hrs or 24 hrs (**Figure 1B**). All eight combinations of ET_i and RT_d formed one session block and blocks were repeated either three (n = 10 mice) or five (n = 10 mice) times. The ET_i, RT_d, start box location, and the order in which the mice were tested were randomized across sessions. For a given mouse, the location of and the egocentric path to the rewarded sandwell was randomized across sessions.

At the start of an encoding trial, the mouse was placed into the start box for 60 s. Subsequently, the experimenter would remotely open the start box and the mouse could explore the maze containing the rewarded and non-rewarded sandwell. Once a mouse found the buried pellet, the mouse was gently nudged and went back to the start box where it consumed the reward. In sessions with an ET_i of 30 s, the door of the start box was opened after 30 s and two more encoding trials were conducted. At the end of the final ET_i, the mouse was kept in the start box for 60 s and subsequently placed back in its home cage. In sessions with an ET_i longer than 30 s, mice were placed back in the home cage after 60 s and remained there during the ET_i, after which two more encoding trials were conducted. Retrieval trials were conducted either 2.5 or 24 hrs after completion of the third encoding trial. In retrieval trials, the maze contained six sandwells: the rewarded sandwell, the non-rewarded sandwell, and four unfamiliar non-rewarded sandwells ("non-cued sandwells"). Training was carried out the same way as in encoding trials, except that the interval between subsequent retrieval trials was kept constant at 30 s.

To evaluate memory acuity and strength with higher sensitivity, the first retrieval trial was occasionally replaced by a probe trial. A probe trial was conducted as a regular retrieval trail with the notable exception that the rewarded sandwell did not contain a reward for the first 60 s. After 60 s, the experimenter entered the maze room and placed one chocolate pellet in the sandwell. Probe trial sessions were interleaved with generally five but minimally two non-probe trial sessions.

After conclusion of the main behavioral training phase, several control experiments were conducted to evaluate whether mice could recall the rewarded location after a single encoding trial

(**Figure S1A**), whether mice used an egocentric (**Figure S2A**) or allocentric (**Figure S2C**) navigation strategy, and to confirm the absence of primacy or recency effects (**Figure S1D**).

Immediate early gene expression

Mice were pseudo-randomly assigned to one of six groups, ensuring that cohoused mice were equally distributed across conditions. These groups underwent behavioral training using an ET_i of 30 s, 10 min, 30 min, or 60 min (**Figure 2A**), were placed in the maze for 1 min without training ("handled control") or were merely handled ("home cage control"). Mice were kept in their home cage with litter mates and dim illumination after each encoding trial. Mice were perfused 90 min after handling (handled and home cage controls), after the start of ET2 (ET_i 30 s, 10 min, and 30 min), or 90 min after the middle of the interval between ET2 and ET3 (ET_i 60 min). As such, the time from ET3 to perfusion was 89 min, 80 min, 60 min, and 60 for the groups underwent behavioral training using an ET_i of 30 s, 10 min, 30 min, or 60 min, respectively.

Chemogenetic inactivation

For *ex vivo* slice electrophysiology, reagent and brain tissue preparation was carried out as previously described [56]. Intracellular patch-clamp recordings were made on visually identified neurons expressing mCherry. We performed intracellular patch-clamp recordings using electrodes (3–5 MΩ) filled with K-gluconate-based internal solution [56] under continuous perfusion of carbogenated recording aCSF [56] (1 ml min^{-1}). Electrical signals were acquired using an amplifier, post-amplified, low-pass filtered (3 kHz cut-off), noise-filtered, digitized at 10 kHz, and recorded. To determine the effect of CNO on intrinsic excitability and current-evoked excitability of dmPFC excitatory neurons, two current injection protocols were executed (protocol 1: step: -100 pA prepulse injection for 100 ms, 500-ms delay, current injection ranging from -450 pA to 450 pA at steps of 50 pA for 750 ms; each step separated by 10 s; protocol 2: step: -100 pA prepulse injection for 100 ms, 500-ms delay, current injection ranging from 0 pA to 150 pA at steps of 10 pA for 750 ms; each step separated by 10 s). To assess the influence of CNO on the resting membrane potential, it was measured at 1 Hz intervals starting 5 min prior to influx of 50 µM CNO in recording aCSF until 10 min post-influx. Subsequently, both aforementioned step protocols were performed again. Recordings were carried out up to 12 hrs post-preparation. Only neurons whose series resistance did not change more than 20% during the recording were included in analysis.

In vivo chemogenetic inactivation experiments followed a full factorial 2^4 design, with the four factors protein expression (mCherry or hM4D(Gi)-mCherry conjugate), injection substance (saline [vehicle] or CNO in saline), injection time point (before an encoding trial or before a retrieval trial), and the session's ET_i (0.5 min or 60 min). For chemogenetic inactivation, mice were injected intraperitoneally with either vehicle or CNO (5 mg kg^{-1}) 45 min before behavioral testing (**Figure 3A**). Sessions with injections were conducted between 38 and 71 days after viral vector injection

and were interleaved with at least two sessions without injections.

Histology and immunohistochemistry

Mice were deeply anesthetized with FMM and transcardially perfused with saline containing lidocaine and heparin (5 mg ml^{-1} and 2.8 mg ml^{-1}, respectively), followed by 4% PFA in PBS. Upon 72 hrs post-fixation in 4% PFA in PBS and cryoprotection in 30% sucrose for 72 hrs, brains were sectioned on a microtome (40 μm, coronal). For experiments quantifying immediate early gene expression, every 5th section containing dmPFC was stained for c-Fos (rabbit anti-c-Fos [1:1000], followed by goat anti-rabbit Cy3 [1:200]) and mounted with mounting medium containing DAPI. For experiments quantifying injury caused by microprism implantation, every 5th section containing dmPFC was stained for Iba1 (rabbit anti-Iba1 [1:1000], followed by goat anti-rabbit Cy3 [1:200]), or GFAP (chicken anti-GFAP [1:600], followed by goat anti-chicken Alexa 647 [1:200]), or Red TUNEL. Appropriate positive and negative controls were carried out for all stains.

For each slice containing the dmPFC (2.4 to 1.6 mm AP relative to bregma, 4 per mouse), five serial optical sections (spaced at 1 μm) of were acquired using a laser-scanning confocal microscope (TCS SP8, 20$\times$ NA 0.75 objective). Images had a resolution of 1024 $\times$ 1024 pixels (550 $\times$ 550 μm) and color channels were acquired sequentially using excitation lasers for DAPI (excitation at 405 nm, emission at 410–419 nm) and Cy3 (excitation at 561 nm, emission at 575–714 nm).

Miniaturized microscopy

Sessions with imaging were conducted between 20 and 98 days after viral vector injection. Images were acquired with a commercially available miniaturized microscope (Basic Fluorescence Microscopy System - Surface, Doric Lenses, excitation at 458/35 nm, emission at 525/40 nm) at a frame rate of 10 Hz and a resolution of 630 $\times$ 630 pixels (field of view 1 mm^2). Laser power under the objective lens (2$\times$ magnification, 0.5 NA) was <1 mW for all imaging experiments.

QUANTIFICATION AND STATISTICAL ANALYSIS

Behavioral analysis

For each ET and RT, the number of erroneous sandwell digs were manually counted. Of note, multiple dig periods at the same incorrect sandwell were scored as one error. For each trial, the performance index was calculated as ([error$_{max}$ − error$_{observed}$] / error$_{max}$ · 100%), with error$_{max}$ being 1 for ETs and 5 for RTs. Retention was quantified as the relative difference in the mean performance index of RT1 and ET3 for each individual mouse, across sessions of the same encoding intertrial interval and retrieval delay. For each probe trial, the time in the rewarded and non-rewarded arm was automatically recorded and behavioral videos were annotated frame-by-frame for position, speed, and distance to the nearest sandwell. Frames with mouse positions less than 1 cm from a sandwell and movement < 0.4 cm s^{-1} were labeled as dig frames. Performance on probe

trials was quantified as the relative time spent digging at the rewarded sandwell as compared to the total dig time at both the rewarded and non-rewarded sandwell, i.e. the occupancy difference score ($\text{dig}_{\text{rewarded}}$ / [$\text{dig}_{\text{rewarded}}$ + $\text{dig}_{\text{non-rewarded}}$]).

Immunohistochemical analysis

Post-processing was conducted using ImageJ [58]. Serial optical sections were collapsed into one image and subsequently processed using the function "Subtract background" (rolling ball radius 10, sliding paraboloid), "Enhance contrast" (normalize, 0.1% saturated pixels), and rescaling brightness to the range of 0% to 78% of maximum brightness. Subsequently, a blinded experimenter manually counted the number of immunopositive neurons for each photomicrograph. These counts were subsequently multiplied by 3.25 and averaged to yield one measurement per mouse.

Validation of microprism placement

For imaging experiments, the location of the microprism implant and viral vector transduction into the dmPFC were verified in coronal slices using a fluorescence microscope and compared to a reference atlas [59].

Image registration, motion correction, and source extraction

Timing of individual behavioral video and miniaturized microscopy frames was synchronized using data acquisition cards. Behavioral data were downsampled to fit the miniaturized microscope frame acquisition rate and imaging frames were spatially downsampled to 256×256 pixels. Using the NoRMCorre package [57], frames within a single recording were registered to each other, concatenated into a single stack per session, and re-aligned. Single neuron Ca^{2+} activity traces were extracted from the fluorescent imaging time series by applying constrained nonnegative matrix factorization for microendoscopic data (CNMF-E) [37]. Putative sources that had less than six transients during a session or whose transients, fitted with a single-term exponential, had an exponential decay factor was below -0.07 were removed. On average, we included 210 ± 99 neurons (mean $\pm$ SD) per session. All subsequent analyses were conducted using the deconvolved spike rate generated by the CNMF-E algorithm.

Quantification of neuronal activity spanning complete trials

To quantify the activity of a neuron during a trial, we used a probabilistic measure (p_{active}; **Figure S5A**). Trials were subdivided into the baseline and trial period. The baseline period was the 60-second period that the mouse spent in the start box prior to maze exploration. The trial period was the period from the first entry into the maze until 2 s after the mouse had retrieved the reward. Only trials with a minimum duration of 10 s were included in these analyses. To calculate p_{active}, we randomly selected a continuous, 5-second subsection from the baseline and trial period, thereby controlling for trial duration. The instantaneous inferred spike rate during both the baseline and

trial subsection was averaged across the subsection. The average baseline inferred spike rate was subtracted from the average trial inferred spike rate, yielding the observed "trial activity rate". Subsequently, the trial activity rate was calculated 1000× using permuted spike rate data, and the resulting permuted trial activity rates were stored in a 1000 × 1 vector. If the observed trial activity rate was larger than the 95th percentile of this vector, the neuron was labeled "active" for this particular 5-second subsection. The procedure outlined above was repeated 100 times for different, pseudo-randomly selected (i.e. non-duplicate) sections of baseline and trial periods. p_{active} was defined as the fraction of these 100 subsamples in which the neuron was labeled "active", and as such should be interpreted as the probability that a neuron was significantly more active during the trial compared to the baseline period. This procedure was repeated for all neurons and all trials, and the p_{active} values were concatenated into an N × 1 vector (N = neurons), which was termed the ensemble response vector. We calculated the Pearson correlation coefficient between the ensemble response vectors of the six trials in a session, which yielded the ensemble correlation matrix.

Generalized linear model (GLM) quantifying behavioral modulation of neuronal responses

A GLM was fitted to the spiking activity of single neurons to establish the predictive power of specific behavioral parameters (task predictors; *tp*s) for neuronal activity, similar to approaches taken in [39] (**Figure 6A**). The model incorporated the categorical task predictors running speed and running acceleration, and the continuous task predictors reward onset, reward anticipation (i.e. final entry into the rewarded arm), dig onset, dig offset, entry into the central platform, and intra-arm reversals of heading direction. Continuous task predictors were binned into 500 ms bins. Categorical task predictors were represented as boxcar functions [range 0,1], convolved with five evenly spaced Gaussian basis functions centered on the predictor onset (1.4 s half-width at half-height, peaks were spaced 2.5 s apart). Next, all predictors were rescaled to the range [0,1] and regularized using the MATLAB function "*lasso*" (specifiers: "*NumLambda*" 10, "*CV*" 10). Only regressors with non-zero regression coefficients at the minimum-deviance point were retained in the final, regularized model. The obtained regression coefficients were multiplied with the task predictor values and summed across temporally offset predictors of the same underlying task predictor. The regularized and deconvolved design matrix and a subsample of the neuron's inferred binarized spiking activity (70% of session's frames, downsampled to 2 Hz) were supplied to the MATLAB function "*fitglm*" (specifiers: "*modelspec*" linear, "*Distribution*" binomial, and "*link*" logit). When a resulting regression coefficient was significant on the t-test after Bonferroni correction, the neuron was labeled "modulated" by this task predictor. To quantify model fit, the GLM was fitted to a permuted spike trace using the previously defined task predictors. Model fit was quantified as the adjusted R^2 of the model fitted to the observed spiking trace. The model's decoding performance was quantified by correlating the observed spiking responses (remaining 30% of session's frames)

with the responses predicted by the GLM using the MATLAB function "*predict*".

Statistical analysis

All data are presented as mean ($\pm$ SEM) unless stated otherwise. Normality of distributions was assessed using the Kolmogorov-Smirnov test and appropriate parametric or non-parametric tests were used. Parametric analyses included the Student's t-test (test statistic t) and general linear models including one-way repeated measures (OWRM) or two-way repeated measures (TWRM) ANOVA (test statistic F) for data consisting of two groups or more than two groups, respectively. To analyze the fractions of responsive neurons as detected by the GLM approach, a four-way (FW) ANOVA with session duration as a covariate was conducted to evaluate main effects only. Non-parametric analyses for data consisting of two groups included the Kolmogorov-Smirnov test (test statistic D), the Mann-Whitney U test (test statistic U), Spearman correlation (test indicated by Spearman's rank correlation coefficient r_s) and the Wilcoxon's (matched-pairs) signed-rank test (test statistic *T*). The Kruskal-Wallis test (test statistic H) or Friedman's ANOVA (test statistic X^2) was used for non-parametric analyses for data consisting of more than two groups. For all statistical tests, alpha was set at 0.05 and tests were conducted two-tailed unless stated otherwise. In case of multiple comparisons, a Bonferroni alpha correction was applied.

References

1. Ebbinghaus, H. *Über das Gedächtnis: Untersuchungen zur experimentellen Psychologie.* (Berlin: Duncker & Humblot, 1885).

2. Smolen, P., Zhang, Y. & Byrne, J. H. The right time to learn: Mechanisms and optimization of spaced learning. *Nat. Rev. Neurosci.* **17**, 77–88 (2016).

3. Kogan, J. H. et al. Spaced training induces normal long-term memory in CREB mutant mice. *Curr. Biol.* **7**, 1–11 (1997).

4. Genoux, D. et al. Protein phosphatase 1 is a molecular constraint on learning and memory. *Nature* **418**, 970–975 (2002).

5. Aziz, W. et al. Distinct kinetics of synaptic structural plasticity, memory formation, and memory decay in massed and spaced learning. *Proc. Natl. Acad. Sci. U. S. A.* **111**, E194–E202 (2014).

6. Seese, R. R., Wang, K., Yao, Y. Q., Lynch, G. & Gall, C. M. Spaced training rescues memory and ERK1/2 signaling in fragile X syndrome model mice. *Proc. Natl. Acad. Sci. U. S. A.* **111**, 16907–16912 (2014).

7. Nonaka, M. et al. Everyday memory: towards a translationally effective method of modelling the encoding, forgetting and enhancement of memory. *Eur. J. Neurosci.* **46**, 1937–1953 (2017).

8. Kramár, E. A. et al. Synaptic evidence for the efficacy of spaced learning. *Proc. Natl. Acad. Sci. U. S. A.* **109**, 5121–5126 (2012).

9. Rao-Ruiz, P., Yu, J., Kushner, S. A., & Josselyn, S. A. Neuronal competition: Microcircuit mechanisms define the sparsity of the engram. *Curr. Opin. Neurobiol.* **54**, 163–170 (2019).

10. Silva, A. J., Zhou, Y., Rogerson, T., Shobe, J., & Balaji, J. Molecular and cellular approaches to memory allocation in neural circuits. *Science* **326**, 391–395 (2009).

11. Garner, A. R. et al. Generation of a synthetic memory trace. *Science* **335**, 1513–1516 (2012).

12. Rashid, A. J. et al. Competition between engrams influences fear memory formation and recall. *Science* **353**, 383–387 (2016).

13. Hebb, D. O. *The organization of behavior: A neuropsychological theory.* (New York: Wiley, 1949).

14. Holtmaat, A., & Caroni, P. Functional and structural underpinnings of neuronal assembly formation in learning. *Nat. Neurosci.* **19**, 1553–1562 (2016).

15. Engert, F., & Bonhoeffer, T. Dendritic spine changes associated with hippocampal long-term synaptic plasticity. *Nature* **399**, 66–70 (1999).

16. Nadel, L., & Moscovitch, M. Memory consolidation, retrograde amnesia and the hippocampal complex. *Curr. Opin. Neurobiol.* **7**, 217–227 (1997).

17. Tonegawa, S., Morrissey, M. D. & Kitamura, T. The role of engram cells in the systems consolidation of memory. *Nat. Rev. Neurosci.* **19**, 485–498 (2018).

18. Liu, X. et al. Optogenetic stimulation of a hippocampal engram activates fear memory recall. *Nature* **484**, 381–385 (2012).

19. Reijmers, L. G., Perkins, B. L., Matsuo, N., & Mayford, M. Localization of a stable neural correlate of associative memory. *Science* **317**, 1230–1233 (2007).

20. Pignatelli, M., et al. Engram cell excitability state determines the efficacy of memory retrieval. *Neuron* **101**, 274-284 (2019).

21. Kitamura, T. et al. Engrams and circuits crucial for systems consolidation of a memory. *Science* **356**, 73–78 (2017).

22. Choi, J. H. et al. Interregional synaptic maps among engram cells underlie memory formation. *Science* **360**, 430–435 (2018).

23. Feng, K. et al. Spaced learning enhances episodic memory by increasing neural pattern similarity across repetitions. *J. Neurosci.* **39**, 5351–5360 (2019).

24. Morrison, D. J. et al. Parvalbumin interneurons constrain the size of the lateral amygdala engram. *Neurobiol. Learn. Mem.* **135**, 91–99 (2016).

25. Gdalyahu, A. et al. Associative fear learning enhances sparse network coding in primary sensory cortex. *Neuron* **75**, 121–132 (2012).

26. Lin, A. C., Bygrave, A. M., De Calignon, A., Lee, T., & Miesenböck, G. Sparse, decorrelated odor coding in the mushroom body enhances learned odor discrimination. *Nat. Neurosci.* **17**, 559–568 (2014).

27. Vyazovskiy, V. V., Cirelli, C., Pfister-Genskow, M., Faraguna, U., & Tononi, G. Molecular and electrophysiological evidence for net synaptic potentiation in wake and depression in sleep. *Nat. Neurosci.* **11**, 200–208 (2008).

28. Cai, D. J. et al. A shared neural ensemble links distinct contextual memories encoded close in time. *Nature* **534**, 115–118 (2016).

29. de Bruin, J. P. C., Sànchez-Santed, F., Heinsbroek, R. P. W., Donker, A. & Postmes, P. A behavioural analysis of rats with damage to the medial prefrontal cortex using the Morris water maze: Evidence for behavioural flexibility, but not for impaired spatial navigation. *Brain Res.* **652**, 323–333 (1994).

30. Tse, D. et al. Schema-dependent gene activation and memory encoding in neocortex. *Science* **333**, 891–895 (2011).

31. Eichenbaum, H. Prefrontal-hippocampal interactions in episodic memory. *Nat. Rev. Neurosci.* **18**, 547–558 (2017).

32. Sekeres, M. J., Winocur, G., & Moscovitch, M. The hippocampus and related neocortical structures in memory transformation. *Neurosci. Lett.* **680**, 39–53 (2018).

33. Broadbent, N. et al. A stable home-base promotes allocentric memory representations of episodic-like everyday spatial memory. *Eur. J. Neurosci.* **51**, 1539–1558 (2020).

34. Armbruster, B. N., Li, X., Pausch, M. H., Herlitze, S. & Roth, B. L. Evolving the lock to fit the key to create a family of G protein-coupled receptors potently activated by an inert ligand. *Proc. Natl. Acad. Sci. U. S. A.* **104**, 5163–5168 (2007).

35. Ghosh, K. K. et al. Miniaturized integration of a fluorescence microscope. *Nat. Methods* **8**, 871–878 (2011).

36. Chen, T. W. et al. Ultrasensitive fluorescent proteins for imaging neuronal activity. *Nature* **499**, 295–300 (2013).

37. Zhou, P. et al. Efficient and accurate extraction of *in vivo* calcium signals from microendoscopic video data. *Elife* **7**, 1–37 (2018).

38. Pinto, L. & Dan, Y. Cell-type-specific activity in prefrontal cortex during goal-directed behavior. *Neuron* **87**, 437–450 (2015).

39. Runyan, C. A., Piasini, E., Panzeri, S. & Harvey, C. D. Distinct timescales of population coding across cortex. *Nature* **548**, 92–96 (2017).

40. Tintorelli, R. et al. Spatial-memory formation after spaced learning involves ERKs1/2 activation through a behavioral-tagging process. *Sci. Rep.* **10**, 1–11 (2020).

41. Takeuchi, T. et al. Locus coeruleus and dopaminergic consolidation of everyday memory. *Nature* **537**, 357–362 (2016).

42. Euston, D. R., Gruber, A. J. & McNaughton, B. L. The role of medial prefrontal cortex in memory and decision making. *Neuron* **76**, 1057–1070 (2012).

43. Maviel, T., Durkin, T. P., Menzaghi, F. & Bontempi, B. Sites of neocortical reorganization critical for remote spatial memory. *Science* **305**, 96–99 (2004).

44. Scoville, W. B., & Milner, B. Loss of recent memory after bilateral hippocampal lesions. *Journal of neurology, neurosurgery, and psychiatry* **20**, 11-21 (1957).

45. Maddock, R.J. The retrosplenial cortex and emotion: New insights from functional neuroimaging of the human brain. *Trends Neurosci.* **22**, 310–316 (1999).

46. Place, R., Farovik, A., Brockmann, M. & Eichenbaum, H. Bidirectional prefrontal-hippocampal interactions support context-guided memory. *Nat. Neurosci.* **19**, 992–994 (2016).

47. Czajkowski, R. et al. Encoding and storage of spatial information in the retrosplenial cortex. *Proc. Natl. Acad. Sci. U. S. A.* **111**, 8661–8666 (2014).

48. Milczarek, M. M., Vann, S. D. & Sengpiel, F. Spatial memory engram in the mouse retrosplenial cortex. *Curr. Biol.* **28**, 1975–1980 (2018).

49. Bullitt, E. Expression of c-fos-like protein as a marker for neuronal activity following noxious stimulation in the rat. *Journal of Comparative Neurology*, **296**, 517-530 (1990).

50. Hintzman, D. L., Summers, J. J., & Block, R. A. Spacing judgments as an index of study-phase retrieval. *J. Exp. Psychol. Hum. Learn. Mem.* **1**, 31–40 (1975).

51. Redondo, R. L., & Morris, R. G. M. Making memories last: The synaptic tagging and capture hypothesis. *Nat. Rev. Neurosci.* **12**, 17–30 (2011).

52. Zong, W. et al. Fast high-resolution miniature two-photon microscopy for brain imaging in freely behaving mice. *Nat. Methods* **14**, 713–719 (2017).

53. Glas, A., Hübener, M., Bonhoeffer, T., & Goltstein, P. M. Benchmarking miniaturized microscopy against two-photon calcium imaging using single-cell orientation tuning in mouse visual cortex. *PLOS ONE* **14**, 1-18 (2019).

54. Holtmaat, A. et al. Long-term, high-resolution imaging in the mouse neocortex through a chronic cranial window. *Nat. Protoc.* **4**, 1128–1144 (2009).

55. Low, R. J., Gu, Y. & Tank, D. W. Cellular resolution optical access to brain regions in fissures: Imaging medial prefrontal cortex and grid cells in entorhinal cortex. *Proc. Natl. Acad. Sci. U. S. A.* **111**, 18739–18744 (2014).

56. Weiler, S., Bauer, J., Hübener, M., Bonhoeffer, T., Rose, T., & Scheuss, V. High-yield *in vitro* recordings from neurons functionally characterized in vivo. *Nature protocols*, **13**, 127-1293 (2018).

57. Pnevmatikakis, E. A. & Giovannucci, A. NoRMCorre: An online algorithm for piecewise rigid motion correction of calcium imaging data. *J. Neurosci. Methods* **291**, 83–94 (2017).

58. Schindelin, J. et al. Fiji: An open-source platform for biological-image analysis. *Nat. Methods* **9**, 676–682 (2012).

59. Franklin, K. B. J. & Paxinos, G. The mouse brain in stereotaxic coordinates. (New York: Academic Press Hardcover, 2007).

Supplemental Information

Spaced training enhances memory and prefrontal ensemble stability in mice.

Annet Glas, Mark Hübener, Tobias Bonhoeffer, Pieter M. Goltstein

Supplemental Information includes:

Supplemental Figures 1–6

Supplemental Figures
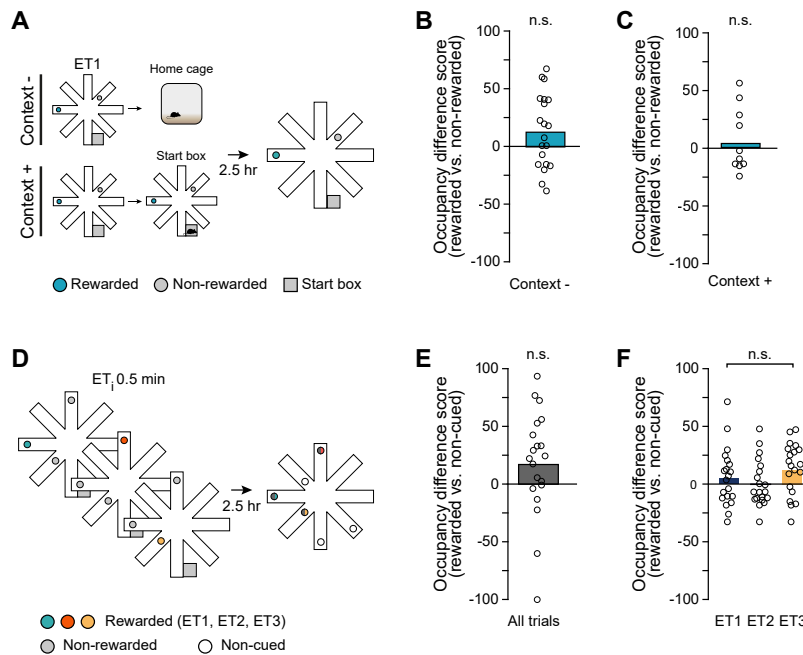
Supplemental Figure 1. Only congruent, multi-trial training resulted in memory on the every-day memory task. Related to Figure 1. A Single trial learning experiment. A single encoding trial was conducted, after which the mouse was kept in the home cage during the entire retrieval delay (no re-introduction: Context -), or briefly re-introduced into the start box (Context +). After a retrieval delay of 2.5 hrs, a probe trial was conducted, and the occupancy at the rewarded and non-rewarded sandwell was recorded. **B** Memory retrieval (occupancy difference) was not observed in the probe trial upon training with a single encoding trial without re-introduction (Wilcoxon signed-rank test: Context -, $T = 126$, p = 0.078, n = 20 mice). **C** Same as in (**B**) for a single encoding trial with re-introduction (Wilcoxon signed-rank test: Context +, $T = 29$, p = 0.922, n = 10 mice). **D** Incongruent learning experiment. On ET1, ET2, and ET3 (encoding intertrial interval [ET_i] 0.5 min), the location of the rewarded sandwell was altered. After a retrieval delay of 2.5 hrs, a probe trial was conducted. **E** Occupancy was similar for previously rewarded sandwells and all non-cued sandwells (Wilcoxon signed-rank test: rewarded vs. non-cued sandwells, $T = 155$, p = 0.062, n = 20 mice) **F** Occupancy was similar for all of the previously rewarded sandwells (Friedman's ANOVA: $X^2 = 2.03$, p = 0.363, n = 20 mice). Circles indicate data from each mouse and bars indicate population mean. n.s., non-significant.
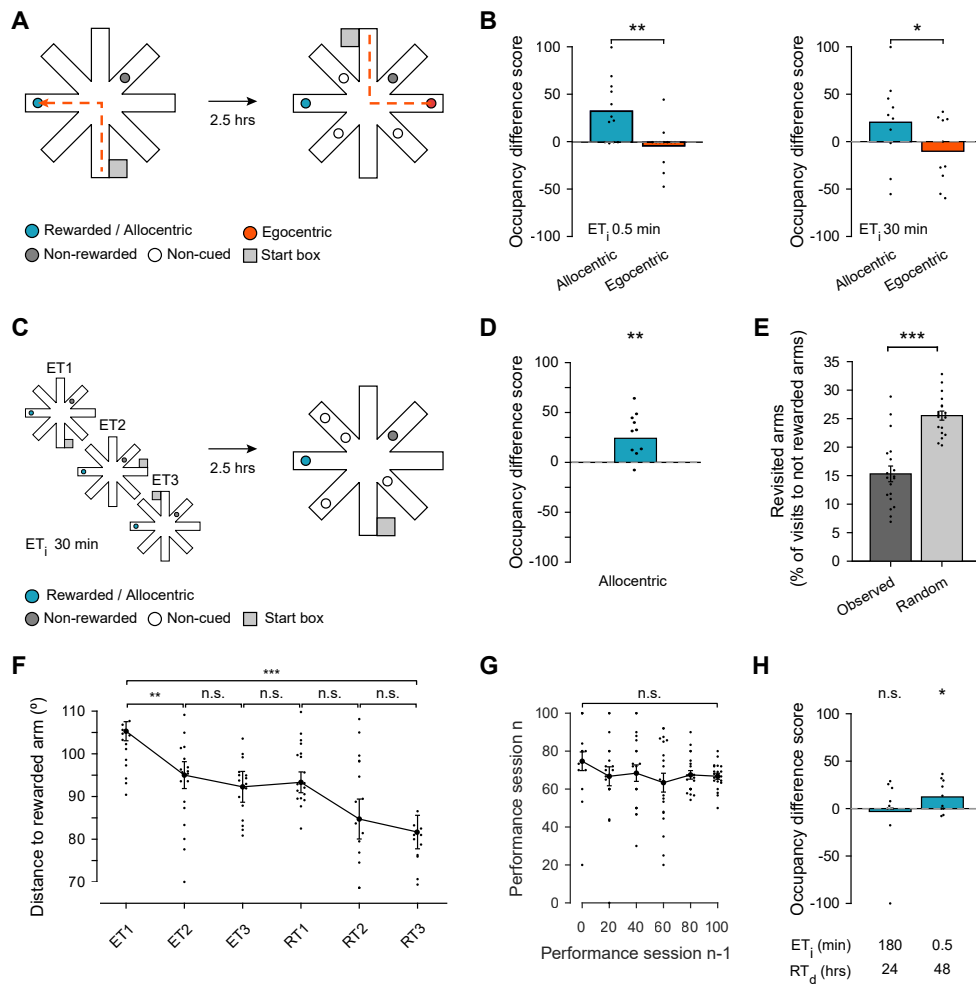
Supplemental Figure 2. Navigational strategies and extended delays on the everyday memory task. Related to Figure 1. A Navigational strategy experiment. Mice were trained on three encoding trials using either massed (ET_i 0.5 min) or spaced (ET_i 30 min) training. During the retrieval delay, the start box was placed at the opposite end of the maze, altering the path but not the location of the rewarded sandwell ("allocentric sandwell"). Egocentric spatial navigation would lead the mouse to a non-cued sandwell ("egocentric sandwell"). **B** The occupancy at the allocentric versus egocentric sandwell upon both massed (left; paired-sample t-test: $t_{11} = 3.69$, p = $3.59 \cdot 10^{-3}$, n = 12 mice) or upon spaced training (right; paired-sample t-test: $t_9 = 2.40$, p = 0.040, n = 10 mice). **C** Forced allocentric strategy experiment. The start box location was altered after each encoding trial (ET_i 30 min), enforcing allocentric navigation. **D** Occupancy at the rewarded sandwell (observed vs. chance [0]; one-sample t-test: $t_9 = 3.50$, p = 0.007, n = 10 mice). **E** The observed fraction of incorrect arm visits was lower than expected from chance (observed vs. random arm visits; paired-sample t-test: $t_{19} = -13.5$, p = $7.50 \cdot 10^{-11}$, n = 19 mice). **F** The mean angular distance of the arm the mouse was in, relative to the rewarded arm, decreased across trials (OWRM ANOVA: $F_{5,90} = 8.17$, p = $3.00 \cdot 10^{-6}$, Bonferroni post hoc tests: ET1 vs. ET2, $1.17 \cdot 10^{-3}$, n = 19 mice). **G** The performance in RT1 of the previous session did not affect that of the current session (OWRM ANOVA: $F_{5,90} = 0.61$, p = 0.695, n = 19 mice). **H** Occupancy at the rewarded sandwell upon training with an extended encoding intertrial interval (one-sample t-test: ET_i 180 min, RT_d 24 hrs; observed vs. chance [0], t_9 = -0.26, p = 0.799, n = 10 mice) or an extended retrieval delay (one-sample t-test: ET_i 0.5 min, RT_d 48 hrs; observed vs. chance [0]: $t_9 = 2.31$, p = 0.046, n = 10 mice). Filled dots indicate data from each mouse, circles indicate the population mean ± SEM, bars indicate population mean, error bars indicate SEM. n.s., non-significant, * p < 0.05, ** p < 0.01, *** p < 0.001.
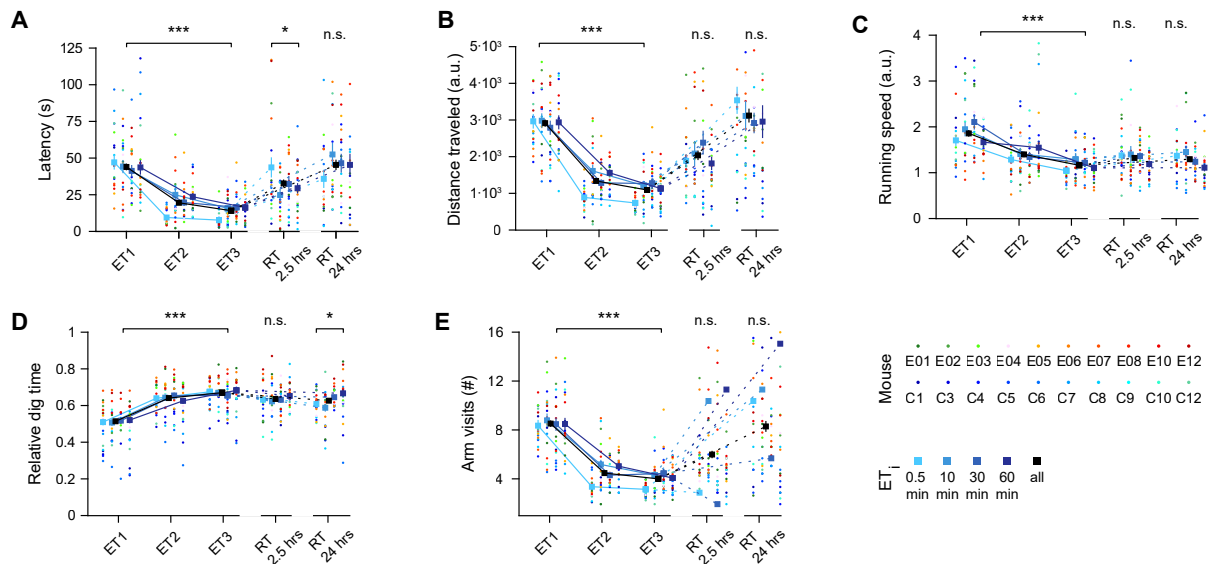
Supplemental Figure 3. Behavioral parameters of individual mice in the everyday memory task. Related to Figure 1. The mean values of individual mice (n = 19) are represented by colored dots and are sorted by the session's ET_i (0.5, 10, 30, or 60 min). The means for each trial, pooled across mice and ET_is, are represented by black lines and squares. **A** Latency to the rewarded arm on ET1, ET2, and ET3 ("consecutive encoding trials", TWRM ANOVA: encoding trial identity [ETID], $F_{2,108}$ = 71.5, p = $6.58 \cdot 10^{-13}$; ET_i, $F_{3,108}$ = 1.93, p = 0.137; Bonferroni post hoc test: ET1 vs. ET2, p = $2.00 \cdot 10^{-6}$; ET1 vs. ET3, p = $1.10 \cdot 10^{-7}$; ET2 vs. ET3, p = $1.14 \cdot 10^{-3}$; n = 19 mice) and the first retrieval trial (RT1) after a retrieval delay (RT_d) of 2.5 hrs (OWRM ANOVA: $F_{3,54}$ = 3.76, p = 0.016, n = 19 mice) or 24 hrs (OWRM ANOVA: $F_{3,54}$ = 1.16, p = 0.334, n = 19 mice). **B** Same as in (**A**), for the distance traveled (consecutive encoding trials: TWRM ANOVA: encoding trial identity [ETID], $F_{2,108}$ = 174, p = $1.29 \cdot 10^{-18}$; ET_i, $F_{3,108}$ = 3.08, p = 0.036; Bonferroni post hoc test: ET1 vs. ET2, p = $8.63 \cdot 10^{-10}$; ET1 vs. ET3, p = $1.11 \cdot 10^{-10}$; ET2 vs. ET3, p = 0.003; RT_d 2.5 hrs: OWRM ANOVA: $F_{3,54}$ = 1.51, p = 0.224; RT_d 24 hrs: OWRM ANOVA: $F_{3,54}$ = 0.564, p = 0.641, n = 19 mice). **C** Same as in (**A**), for the running speed (consecutive encoding trials: TWRM ANOVA: encoding trial identity [ETID], $F_{2,108}$ = 27.9, p = $6.88 \cdot 10^{-8}$; ET_i, $F_{3,108}$ = 2.60, p = 0.063; Bonferroni post hoc test: ET1 vs. ET2, p = 0.002; ET1 vs. ET3, p = $9.00 \cdot 10^{-6}$; ET2 vs. ET3, p = 0.007; RT_d 2.5 hrs: OWRM ANOVA: $F_{3,54}$ = 0.98, p = 0.410; RT_d 24 hrs: OWRM ANOVA: $F_{3,54}$ = 2.49, p = 0.074, n = 19 mice). **D** Same as in (**A**), for the relative dig time (consecutive encoding trials: TWRM ANOVA: encoding trial identity [ETID], $F_{2,108}$ = 73.2, p = $4.80 \cdot 10^{-13}$; ET_i, $F_{3,108}$ = 1.04, p = 0.384; Bonferroni post hoc test: ET1 vs. ET2, p = $1.37 \cdot 10^{-6}$; ET1 vs. ET3, p = $4.04 \cdot 10^{-8}$; RT_d 2.5 hrs: OWRM ANOVA: $F_{3,54}$ = 0.91, p = 0.445; RT_d 24 hrs: OWRM ANOVA: $F_{3,54}$ = 3.42, p = 0.024, n = 19 mice). **E** Same as in (**A**), for the number of arm visits (consecutive encoding trials: TWRM ANOVA: encoding trial identity [ETID], $F_{2,108}$ = 133, p = $7.80 \cdot 10^{-17}$; ET_i, $F_{3,108}$ = 3.84, p = 0.015; Bonferroni post hoc test: ET1 vs. ET2, p = $4.44 \cdot 10^{-9}$; ET1 vs. ET3, p = $8.85 \cdot 10^{-10}$; RT_d 2.5 hrs: OWRM ANOVA: $F_{3,54}$ = 1.59, p = 0.204; RT_d 24 hrs: OWRM ANOVA: $F_{3,54}$ = 1.03, p = 0.386, n = 19 mice). Squares indicate mean ± SEM across animals. n.s., non-significant, * p < 0.05 *** p < 0.001.
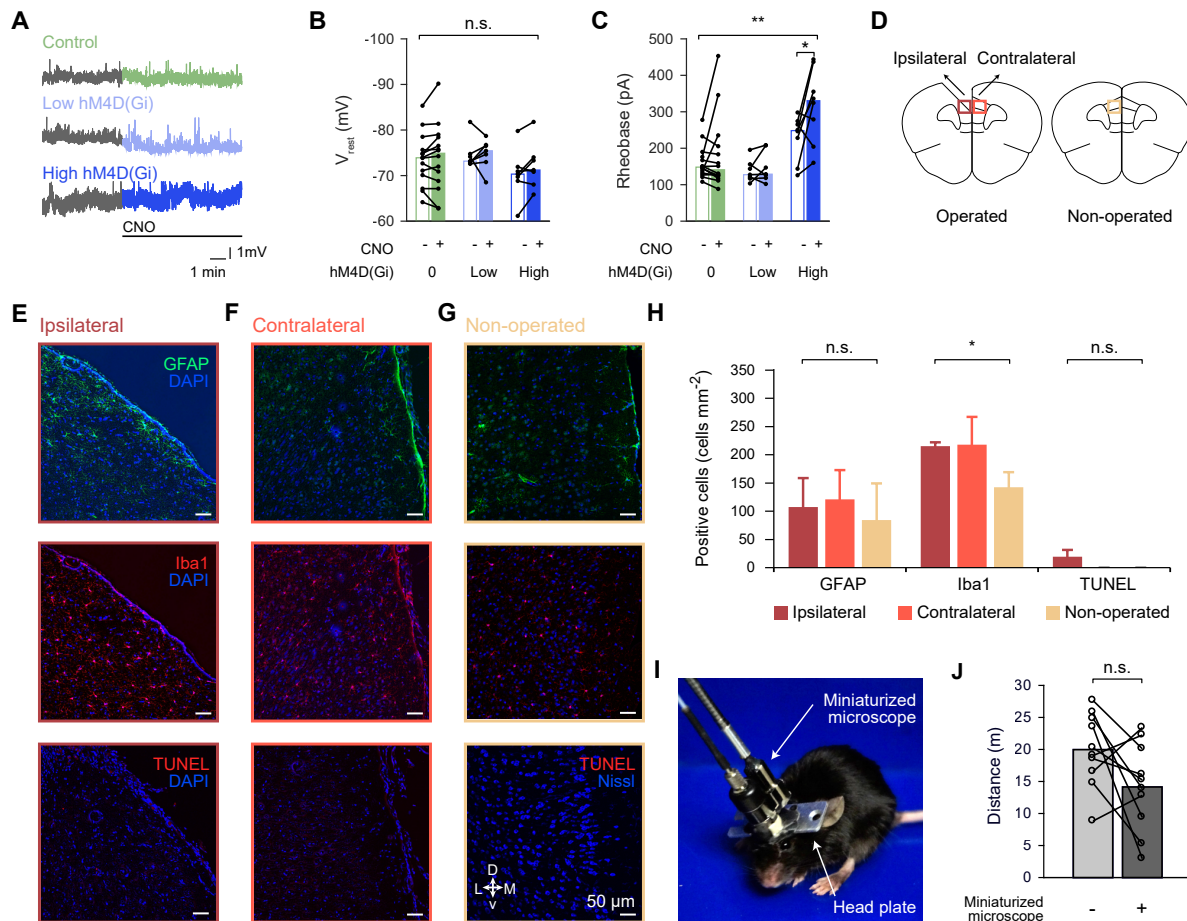
Supplemental Figure 4. Control experiments regarding chemogenetic inactivation and miniaturized microscope imaging of the dmPFC. Related to Figures 3 and 4. A Example *ex vivo* current-clamp recordings of the membrane potential of neurons not transduced (control; n = 14 neurons), transduced with a low titer (titer $2.3 \cdot 10^{10}$ GC ml^{-1}; n = 7 neurons), or transduced with a high titer (titer $2.3 \cdot 10^{12}$ GC ml^{-1}; n = 9 neurons) hM4D(Gi)-encoding AAV before and after clozapine-*N*-oxide (CNO) application. **B** CNO application did not affect the resting membrane potential (V_{rest}: TWRM ANOVA: CNO, $F_{1,25}$ = 2.38, p = 0.135, n = 28 neurons) **C** CNO application affected rheobase (TWRM ANOVA: CNO, $F_{1,25}$ = 8.16, p = 0.008, n = 28 neurons), post hoc analysis revealed an effect for high hM4D(Gi)-expressing neurons (paired-sample t-test: t_6 = -2.62, p = 0.034, n = 7 neurons). Recordings from an individual neuron (circles) are connected with lines, bars indicate population means. n.s., non-significant, * p < 0.05. **D** A subsection of the ipsilateral and contralateral dmPFC hemisphere of mice with (operated) or without (non-operated) a microprism implant was analyzed for markers of astrogliosis (GFAP expression), microgliosis (Iba1 expression) and apoptosis (TUNEL assay). **E–G** Representative micrographs of dmPFC sections from the ipsilateral hemisphere (**E**), contralateral hemisphere (**H**), and non-operated hemisphere (**G**) labeled with GFAP (top), Iba1 (middle), and TUNEL (bottom). **E** The number of GFAP-expressing (Kruskal-Wallis test: H_2 = 0.35, p = 0.840), Iba1-expressing (Kruskal-Wallis test: H_2 = 6.05, p = 0.049), and TUNEL-positive Kruskal-Wallis test: (H_2= 3.85, p = 0.146) cells in the ipsilateral (n = 4 mice), contralateral (n = 4 mice) and non-operated (n = 3 mice) hemispheres. **I** Mouse carrying a miniaturized microscope, mounted on a head plate implant. **J** The distance mice traveled was not significantly affected by carrying the miniaturized microscope (paired-sample t-test, t_9 = 1.92, p = 0.084, n = 10 mice). Recordings from individual neurons (filled circles) are connected with lines, bars indicate population means. Open circles indicate data from one mouse, bars indicate means. Scale bars 50 µm (**E–G**). n.s., non-significant, * p < 0.05, ** p < 0.01.
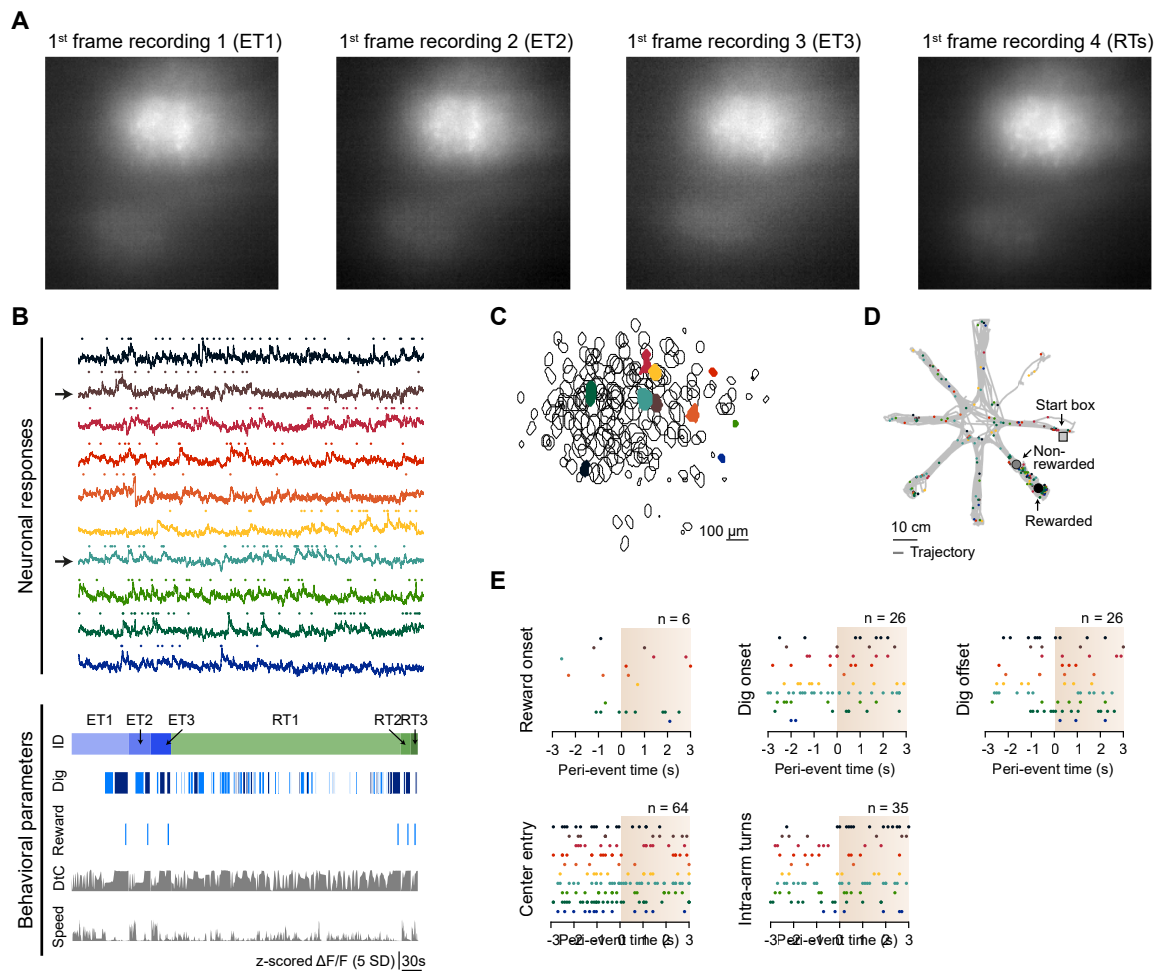
Supplemental Figure 5. *In vivo* **calcium imaging of dmPFC neuronal populations in the every-day memory task. Related to Figures 4 and 6. A** First microscopy frame from the first, second, third, and fourth recording comprising one behavioral session after concatenation of imaging data. **B** Responses of 10 example neurons (top) and behavioral parameters (bottom) during an example session. Two partially overlapping sources are indicated with an arrow. Behavioral parameters include digging at the rewarded (dark blue) and non-rewarded sandwell (blue), reward consumption ("Reward"), distance to center ("DtC"; max-normalized distance to the central platform), and running speed of the mouse ("Speed"). **C** Outlines of all neurons (black lines) in the field of view of the miniaturized microscope. Example neurons are indicated by color. **D** Locations where the example neurons fired along the mouse's trajectory from the start box via various arms to the non-rewarded sandwell and rewarded sandwell. **E** Peri-event responses of the example neurons, aligned to reward onset (n = 6 events), digging onset (n = 26 events), digging offset (n = 6 events), entry into the center platform (n = 64 events), and intra-arm turns (n = 35 events). Filled dots indicate spikes, color-coded by neuron identity. ID: trial identity SD: standard deviation. Scale bars: 30 s (**B**), 100 μm (**C**), 10 cm (**D**).
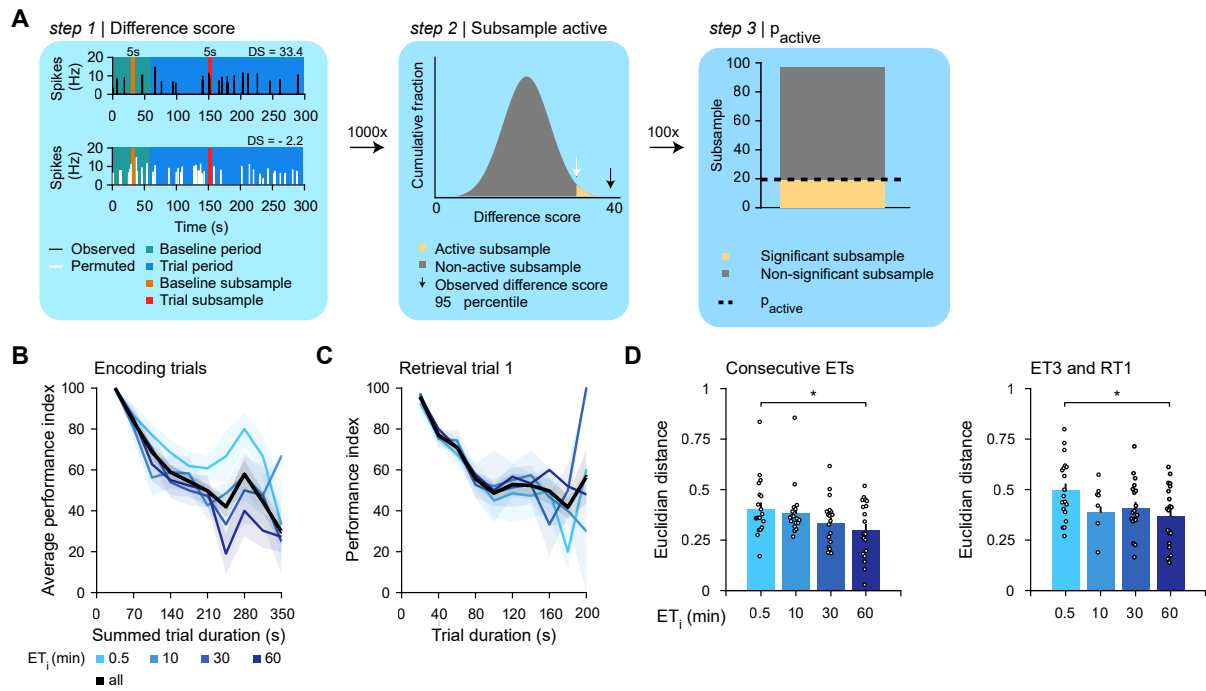
Supplemental Figure 6. Quantification of the activity and stability of a neuronal population. **Related to Figure 4.** **A** Approach to quantify neural activity (p_{active}) within a trial. Step 1: quantify difference score (DS) from 5-second subsample of inferred spiking activity. Step 2: permutation of spike trace, re-quantify DS. The neuron was qualified as active in this subsample when observed DS > 95th percentile of permuted DSs. Step 3: repeat steps 1 and 2 100 times with different baseline and trial subsamples. The sum of active subsamples, divided by 100, yielded the p_{active} for this neuron in this trial. **B** The behavioral performance on, and duration of, all encoding trials of a session, sorted by ET_i. Across all sessions, encoding trial duration correlated significantly with performance (Spearman correlation: $r_s = -0.40$, $p = 1.02 \cdot 10^{-20}$, $n = 499$ sessions). **C** As in (**A**), but for the first retrieval trial of a session (Spearman correlation: $r_s = -0.49$, $p = 6.59 \cdot 10^{-32}$, $n = 499$ sessions). **D** Euclidian distance of the ensemble response vectors, sorted by ET_i, between consecutive encoding trials (ET1, ET2, and ET3) and between ET3 and RT1 (consecutive ETs: OWRM ANOVA: ET_i, $F_{3,54} = 3.71$, $p = 0.017$; ET3–RT1: OWRM ANOVA: ET_i, $F_{3,54} = 5.97$, $p = 0.001$, Bonferroni post hoc tests: 0.5 vs. 10 min, $p = 0.009$; 0.5 vs. 30 min, $p = 0.017$; 0.5 vs. 60 min, $p = 0.011$, $n = 19$ mice). Circles dots indicate data from individual mice, bars indicate population means, lines and shaded area indicate mean and SEM, respectively. n.s., non-significant, * $p < 0.05$.

5

DISCUSSION

5.1 FOOD (OR WATER) FOR THOUGHT

FOOD AND WATER RESTRICTION LEAD TO DIFFERENTIAL LEARN-
ING BEHAVIORS IN A HEAD-FIXED TWO-CHOICE VISUAL DISCRIM-
INATION TASK FOR MICE

The aim of the study described in chapter 2 was to evaluate whether
two nutritional restriction paradigms differently affected mouse wel-
fare, circadian behavior, and task performance. Overall, food and fluid
(i.e. water) restriction influenced these factor similarly, but produced
distinct differences in in-task behavior. Both food and fluid restric-
tion to 85% of free-feeding weight were typically well-tolerated and
discomfort was subthreshold on most days. Furthermore, both food-
and fluid-restricted mice were less active in their home cage than
non-restricted mice, but the circadian activity pattern rectified once
restriction ended. Moreover, food- and fluid-restricted mice reached
similar maximum performance on a head-fixed two-choice visual dis-
crimination task. However, fluid-restricted mice required less training
sessions to acquire the task, whereas food-restricted mice performed
more trials. Taken together, these results indicate that food and fluid
restriction enforce strong task performance without severely affecting
mouse welfare.

5.1.1 *At one's pleasure or to one's benefit? Ensuring rodent welfare during nutritional restriction*

Laboratory rodents can be supplied with food and fluid by employing
either of two feeding schedules: unrestricted ("*ad libitum*") or restricted.
Major advantages of an *ad libitum* nutritional regimen are convenience
to husbandry staff and minimal risk of dehydration or malnourish-
ment. However, rodents have evolved to withstand environments in
which especially food is scarce. As a result, an *ad libitum*, or "at one's
pleasure", feeding regimen generally results in a strong increase in adi-
pose tissue in laboratory rodents as compared to wild conspecifics[237].
By most standards used in humans, the body fat percentage of labora-
tory rodents fed on an *ad libitum* schedule would be considered obese
and could lead to a reduced life expectancy[191]. So, although *ad libitum*
access to fluid supports rodent welfare, there are strong indicators
that an *ad libitum* feeding schedule has detrimental effects.

Scheduled access to food or water, thereby mildly nutritionally
restricting the mouse, is not harmful to mouse welfare if performed
according to the standards of good animal husbandry. Mice typically
adapt well to mild food restriction schedules, as long as water is freely

available and all essential nutrients are provided in the daily food supplement[238]. Caloric restriction has even been observed to promote rodent health[239]. Conversely, mild water restriction is not detrimental to mouse welfare if food is freely available and the relative humidity of the animal room is maintained at approximately 50%[93].

The effects of nutritional restriction on mouse physiology are modified by a wide range of factors, including sex, age, and physical activity. Male rodents are typically heavier than female rodents, whereas female rodents have a higher body fat content[237]. Furthermore, age correlates positively with body weight and adiposity in healthy rodents. Therefore, the sex and initial age of the rodent will influence its capacity to compensate for nutritional restriction with pre-existing fat stores. Physical activity has been observed to have beneficial effects on the adaptation to food restriction, as it results in a more stable weight and less fluctuation in the energy metabolism[240]. In summary, characteristics of the rodent on the onset of nutritional restriction modify its impact on welfare.

To mildly nutritionally restrict mice in the study described in chapter 2, age-matched male mice were given a daily supplement of food or water. This supplement was carefully calibrated based on recent weight alterations to maintain the weight to 85% of free-feeding weight, a calibration point that is typically well-tolerated across months[191]. Mouse welfare was safeguarded by continuous home cage monitoring and daily quantification of five key metrics relating to mouse physiology: body condition, look/posture, defecation, dehydration, and home cage activity. Consequently, mice were mostly kept at a sub-threshold discomfort level throughout the study.

Incidentally, fluid-restricted mice experienced "moderate" discomfort, which was not observed in food-restricted mice. This increased discomfort score was specifically the result of higher scores on the metrics "look/posture" and "dehydration". These metrics are arguably more affected by fluid than food restriction. The metric "look/posture" quantified fur smoothness, which fluid-restricted mice neglected by reduced grooming to conserve fluids. Conversely, food-restricted mice did not have a similar incentive to cease grooming. The metric "dehydration" quantified skin turgor, deterioration of which results from severe food restriction but only mild fluid restriction. Therefore, the incidental observation of "moderate" discomfort in fluid-restricted mice can be attributed to more sensitive measurement of the effects of fluid than food restriction. More broadly, these results indicate that in contrast to previous reports[93,94] (**Box 2**), rodent welfare is not necessarily more compromised by food than by fluid restriction.

5.1.2 *Nutritional restriction as a means to motivate mice on behavioral experiments*

Nutritional restriction has the dual benefit of motivating mice to engage with a behavioral task and standardizing the level of motivation between sessions and studies. However, restriction that is too mild or

too severe can have detrimental effects on research outcome[191]. On the one hand, excessively mild restriction might not motivate the rodent to engage with the behavioral task. As a result, the rodent might not learn the task or perform inconsistently[93]. On the other hand, excessively severe restriction negatively affects the rodent's ability to engage with the task. In the study described in chapter 2, rewarding food-restricted mice with soy milk or rewarding fluid-restricted mice with water provided sufficient motivational incentive to complete over one hundred trials per training session. Both restriction regimen motivated mice to perform an approximately equal numbers of correct trials on the final visual discrimination task, suggesting that both regimen can be used to successfully train mice.

Since the restriction paradigm did not affect maximum in-task performance, are food- and fluid-restriction interchangeable? This was not the case in the study described in chapter 2, since the paradigms modifies certain in-task outcomes that might make the one more appropriate than the other. Fluid-restricted mice reached the criterion in approximately half the time it took food-restricted mice. Fluid restriction would therefore be the method of choice if the researcher's main objective is to reduce the experiment duration. Conversely, food-restricted mice performed more than twice the number of trials during pre-training. For that reason, food restriction would be preferred for experiments that need a large number of pre-learning trials to characterize neuronal activity in different stages of learning[241]. Study-specific considerations should thus inform the decision to use food or fluid restriction as a motivational incentive.

5.1.3   *Replace, reduce, and refine*

To carry out animal experiments humanely and maintain societal acceptance of these experiments, three guiding principles have been defined: replace, reduce, and refine[242]. These principles reflect the aim to minimize animal discomfort by replacing animal with non-animal experimentation, reducing the number of animals per study, and refining the treatment of animals during experimental periods. This last factor can be operationalized by re-evaluating nutritional restriction, as described below.

In specific experimental situations, task engagement remains high with less severe food restriction, further minimizing the effect on rodent welfare. Combining a mild reduction in home-cage food availability with delivery of palatable, high-calorie food during behavioral training has been observed to lead to strong behavioral performance[243]. Anecdotal evidence from the study described in chapter 4 suggests that mice perform well on the everyday memory task when only restricted to 90% instead of 85% of free-feeding weight, potentially because the chocolate reward was highly palatable.

The intensity of fluid restriction can likewise be reduced in certain conditions. One method is to make the in-task fluid supplement more rewarding than the regular water reward, for example by adding

sucrose to the water[93] or replacing the water reward with a soy milk reward. Another method to reduce the impact of fluid restriction is to enforce it on fewer days, for example by combining free access to water on weekends with weekday water restriction[244]. This last method does have certain drawbacks. First, it severely reduced the number of completed trials on Monday and Tuesday[244]. Second, it resulted in large weight fluctuations, which have negative metabolic and health consequences in humans[245]. In short, nutritional restriction could be decreased in certain experimental situations by increasing the value of the in-task reward.

High task performance can even be achieved without nutritional restriction, particularly if the in-task reward is sufficiently attractive and the behavioral task is relatively undemanding[246]. For example, non-nutritionally restricted mice that received a sucrose solution after successful trials acquired a simple operant conditioning task and performed hundreds of trials[247]. A sucrose in-task reward likewise motivated mice to engage with a more demanding visual discrimination task if mice had home cage *ad libitum* access to acid water, likely resulting in self-restriction[244]. Although promising, behavioral training of non-restricted mice is probably only successful if the task is not too arduous.

5.1.4 *Conclusion and future directions*

The study described in chapter 2 established that food and fluid restriction of mice to 85% of their free-feeding weight promoted behavioral motivation without resulting in enduring adverse health effects. These results are encouraging for all major stakeholders involved. For researchers, mild nutritional restriction enables training of mice on non-trivial behavioral tasks, for example the everyday memory task as described in chapter 4. For members of animal ethics committees, which provide legal approval of animal experiments, these results demonstrate that mild nutritional restriction does not necessarily inflict harm on mice. For society at large, open-access publication of studies employing animal experiments provides a transparent account of these procedures and should aid in societal acceptance of animal experiments.

A challenge for the future is to find elegant methods to motivate mice on complex behavioral tasks without nutritional restriction. One such method might be optogenetic manipulation of neural motivational and/or reward circuits[169]. This would provide a more precise control over the rewarding effects of successful trial completion while reducing peripheral physiological effects. A potential disadvantage of the optogenetic approach is that most learning happens in response to relevant stimuli in the external world. Short-circuiting this interaction by omitting an external reward might not accurately reflect normal learning processes. Furthermore, as with any surgery, each researcher would have to gain experience with this procedure to acquire the desired competence. Therefore, while optogenetic manipulation might

become a customary method to motivate rodents in the future, it might not reduce the number of rodents used by individual researchers.

5.2 DAVID VERSUS GOLIATH

BENCHMARKING MINIATURIZED MICROSCOPY AGAINST TWO- PHOTON CALCIUM IMAGING USING SINGLE-CELL ORIENTATION TUNING IN MOUSE VISUAL CORTEX

The aim of the study described in chapter 3 was to benchmark recordings acquired with a miniaturized microscope against the gold standard in *in vivo* neuronal calcium imaging, which is two-photon microscopy[151,155]. To achieve this aim, an anesthetized mouse was presented with drifting gratings, which elicit orientation-dependent responses in a large population of mouse primary visual cortex neurons[159]. Primary visual cortex neurons were matched post-hoc between miniaturized microscope and two-photon microscope recordings using blood vessels as landmarks. Both techniques registered a proportional response amplitude and signal-to-noise ratio of stimulus-induced calcium transients. Furthermore, tuning properties of primary visual cortex neurons, including preferred orientation, tuning bandwidth, and orientation selectivity were highly correlated between recordings. These results suggest that recordings acquired with a miniaturized microscope and a two-photon microscope yield quantitatively similar neuronal tuning features, in spite of distinctive qualitative differences between the methods.

5.2.1 *Methodological improvements enable neuroscientific innovation*

"Optical methods will continue to revolutionize neuroscience and provide precise readout and manipulation of neural activity . . . and are likely to help decipher the neural code used by different nervous systems."

Yang & Yuste | Nature Methods (2017)

Advances in optical methods have enabled researchers to answer outstanding questions and provide novel insights. The study described in chapter 3 provided a benchmark for a novel light microscopy technique, which is *in vivo* neuronal imaging using a miniaturized epifluorescence microscope. Versions of this microscopy method have been successfully integrated into several scientific lines of inquiry[31,116]. This powerful optical tool can be even more effectively harnessed when used in parallel with other methodological advances, particularly in fluorescent indicators and source extraction methods.

5.2.1.1 *Advances in fluorescent indicators*

Neuronal activity can be measured *in vivo* by imaging fluorescent indicators, of which genetically encoded calcium indicators (GECIs), especially the GFP-based GCaMP construct, are currently the most attractive option[248]. GECIs reliably sense activity-induced calcium changes in (a population of) neurons and subcellular compartments[149].

Furthermore, GECIs can be introduced into specific brain areas by viral gene transfer using adeno-associated viruses, resulting in long-term, region-specific expression[149]. Specialized GECIs with improved biophysical properties, including the signal-to-noise ratio, rise and decay kinetics and dynamic range, better meet the requirements of individual imaging techniques[249]. In spite of their many advantages, GECIs have certain drawbacks[248]. GECI fluorescence scales non-linearly with the actual intracellular calcium concentration[250]. Furthermore, GECI dynamics are too slow to capture high-frequency firing[251]. Finally, GECIs function as calcium buffers and interact with native proteins, altering the calcium homeostasis of the neuron[252]. In short, GECIs are an effective tool to record from individual neurons, but there is an unmet demand for indicators with even more attractive features.

In contrast with confocal or two-photon microscopes, microscopes that use wide-field epifluorescent illumination, such as miniaturized microscopes, do not effectively block fluorescence that arises from the volume surrounding the neuron of interest. This volume, devoid of neurons and mostly comprised of axons and dendrites, forms the neuropil, whose activity co-fluctuates with that of the neuron of interest[253]. Several approaches can minimize the neuropil signal in the recording. Reducing the genome copies of the viral vector decreases the fluorescence intensity from neighboring structures. Granted that this approach reduces both the signal and the noise, it is applicable for GECIs that have strong stimulus-evoked fluorescence such as GCaMP6s. Furthermore, a dual vector approach using Cre-Lox recombination can restrict GECI expression to a subset of neurons. Combining these two approaches reduced the neuropil signal strongly in the study described in chapter 3 and enabled imaging of individual neurons. However, the contaminating signal from the neuropil still had a strong effect on the response amplitude in recordings obtained with a miniaturized microscope. Therefore, additional approaches to combat the contaminating neuropil signal are of interest.

One such approach is imaging of a GECI with a high signal-to-noise ratio and low baseline fluorescence, such as GCaMP7c[249]. GCaMP7c could be delivered using a viral vector, but this approach has a drawback particularly relevant for studies that span weeks or months. That is, the protein load can increase over weeks, become detrimental to neuronal health, and result in necrosis, leading to small but significant changes in the neuronal population that expresses GECIs. The protein level is more homogeneous and stable in transgenic mouse lines that express GECIs[254], which allow researchers to perform long-term imaging. Therefore, transgenic mice expressing GCaMP7c could facilitate long-term imaging with a miniaturized microscope. Before adopting such new transgenic mouse lines, it should be validated that the transgene does not affect electrical activity[255].

5.2.1.2   *Advances in source extraction methods*

Sources of activity in microscopy recordings can be segmented using a wide array of source extraction methods[256]. One approach is

a morphology-based method, in which stimulus-evoked signals in neurons are extracted by manually annotating the outline of a neuron in the recorded image. This approach was taken in chapter 3, primarily because it allowed matching of sources between microscopy recordings of different quality. To minimize the neuropil signal, the surround signal was completely subtracted from the source signal by delineating an annulus around the source and subsequently subtracting the mean of all fluorescence in the annulus from the somatic signal[210]. The drawbacks to this approach, most notably its labor intensity, were outweighed by its potential to match neurons across microscope modalities.

For studies that do not compare signals obtained with multiple imaging methods, automated approaches to detect sources of activity are more advantageous. These approaches utilize the sparse spatiotemporal activity pattern of neurons to disentangle activity components that co-fluctuate. Examples of automated approaches include approaches based on principal component analysis[257] or on (non-negative) matrix factorization, including constrained nonnegative matrix factorization for endoscopic data (CNMF-E)[211,258] and MIN1PIPE[218]. The major advantage of these approaches is that they can demix overlapping sources of activity, which is of particular interest for wide-field recordings in which fluorescence fluctuations in a single pixel could have originated from many sources. A drawback of activity-based automated approaches is that they cannot detect sources with a low signal-to-noise ratio. Furthermore, these automated methods are compute-intensive and benefit greatly from being run on a computer cluster if the recording is longer than $\sim$10 minutes. As computational costs have gone down in recent years, automated signal extraction methods become even more attractive than manual methods.

Taken these considerations into account, it appears that imaging of GCaMP7c-expressing neurons using a miniaturized microscope and subsequent extraction of sources using an automated approach could further increase the quantity of detected neurons in miniaturized microscopy recordings, as well as the quality of the extracted stimulus-evoked responses.

5.2.2 *Conclusion and future directions*

To assess the merits of novel methodologies in neuroscience, they should be benchmarked against the current gold standard. The study described in chapter 3 compared the signals acquired with a relatively novel imaging device, i.e. a miniaturized microscope, with those acquired with a well-established imaging device, i.e. a two-photon microscope. In spite of the qualitative differences between recordings obtained with these devices, the response properties that were quantified using these recordings were remarkably similar. These results confirmed the prediction that imaging with a miniaturized microscope is a valid approach to characterize the activity of hundreds of neurons *in vivo*.

Therefore, a miniaturized microscope was used to image the prefrontal cortex of mice performing the everyday memory task as reported in chapter 4 of this doctoral dissertation.

Miniaturized microscopes with additional features will enable researchers to answer additional questions. Three classes of these devices are miniaturized microscopes with dual wavelength illumination, wireless miniaturized microscopes, and miniaturized two-photon microscopes, which are attractive devices for specific applications as outlined below.

Miniaturized microscopes with two distinct illumination sources extend the range of studies that can be performed with miniaturized microscopes. A first class of studies would be those in which simultaneous manipulation and measurement of populations of neurons is needed[259]. This could be achieved by combining optogenetics with calcium imaging. Another situation in which a dual-color miniaturized microscope is needed is when measurements of two distinct neuronal populations are required. This could be achieved by recording from GECI with a different illumination wavelength, for example green-fluorescent GCaMP-expressing interneurons and red-fluorescent R-GECO-expressing pyramidal neurons[260].

Wireless miniaturized microscopes do not have a data acquisition cable and fiber-optic patch cord[261], which gives these devices distinct advantages and disadvantages. On the one hand, they enhance the mobility of a mouse, which is beneficial if the behavioral task demands the mouse to move over a long range, though narrow corridors, through tunnels, or into shelters. Furthermore, they allow more tilting head movements, which are necessary during many social interactions. Additionally, behavioral tracking of the mouse is facilitated since the outline of the mouse is not distorted by any cables. On the other hand, these devices are heavier than their cabled counterparts, mostly due to the internally housed battery. Furthermore, data storage is limited to the capacity of SD cards, limiting the duration of each individual imaging session to ∼20 minutes. Moreover, the field of view of the microscope cannot be compared to previously acquired recordings before starting another experiment and might therefore not be suitable for repeated characterization of the identical set of neurons. Despite these disadvantages, wireless miniaturized microscopes are an interesting tool to study behaviors that require complex movements.

Miniaturized two-photon imaging enables examination of subneuronal compartments such as neurites and synaptic structures during freely-moving behavior[262]. Furthermore, two-photon illumination minimizes out-of-focus fluorescence that impacts somatic fluorescence. Currently, two-photon miniaturized microscopes are not commercially available, are financially prohibitive and require significant expertise and skill to be installed and operated[157], but are likely to become more attractive in the near future. In conclusion, imaging using miniaturized microscopes is an attractive method to study individual neurons in the freely moving mouse across months and multiple methodological advances could further increase the applicability of this technique.

5.3 BRINGING ETHOLOGY TO THE LABORATORY

The central nervous system has evolved to allow animals to interact with and adapt to their natural environment. One means by which mice interact with their environment is by foraging for food. During foraging, mice have to balance two conflicting demands of feeding efficiently and avoiding predation[263]. As such, foraging requires mice to continuously update a variety of cues that influence decision making, including predation risk[264], habitat features[265], thermoregulation[266], hunger signals[267], and prior knowledge of food sources. Therefore, naturally occurring foraging behavior in mice is an interesting vehicle to study real-world decision-making[268].

5.3.1 *The ethological approach*

One approach to study foraging behavior is an ethological approach, in which behavior is studied under natural conditions in field experiments. There are clear advantages to this approach. It allows researchers to study those behaviors that have been refined by natural selection. Furthermore, field studies can uncover non-obvious behavioral repertoires and interactions between these behaviors. This last factor can also be perceived as a disadvantage of field studies. In the case of foraging behavior, stimuli that influence decision-making typically co-occur, making quantification of stimulus-response relationships complex[269]. Furthermore, most foraging is self-motivated and might happen at random times. Most critically, ethological approaches traditionally have focused on observing the behavior of mice without obtaining neuronal recordings[269]. To record from individual neurons in the field, the recording devices would have to be sturdy, have an internal power source, and send the recorded signals using telemetry[270,271]. To date, there are no devices available that meet these three criteria for mice. Therefore, approaches that combine field experiments with high-resolution neuronal recordings in mice are not yet feasible.

5.3.2 *The hybrid "neuroethological" approach*

How to capitalize on the advantages of the ethological approach while sidestepping the disadvantages? A common thread binding the studies described in this doctoral dissertation is that they adopted methods that mimicked aspects of the natural environment in the laboratory[272]. In the study described in chapter 4, mice were trained on the everyday memory task, in which mice forage for a food reward by revisiting previously rewarded locations[273,274]. Several features of the experimental design were inspired by ethological descriptions of mouse foraging behavior. First, the maze had narrow corridors to encourage mice to forage, which they are normally hesitant to do in open spaces because of predation risk[264]. Second, mice had to dig at sandwells that were sunken into the maze floor to retrieve a food reward, which bears

resemblance to foraging for food under leaves on the forest floor. The tenacity by which mice dug at a previously rewarded sandwell was used as a proxy for memory strength. Third, to prevent caching of the reward[274], the reward size per trial was kept small. Fourth, mice naturally use olfactory cues to forage[275], so several precautions were taken to prevent olfactory-based strategies that left mice solely relying on memory-based strategies. Finally, since self-motivated foraging would strongly increase the duration of individual trials, mice were additionally motivated to forage in the maze by scarcity of food in the home cage. Mice have adapted to withstand food scarcity[191], and the study described in chapter two demonstrated that 85% restriction to free-feeding weight was well tolerated[1]. These factors combined likely affected the high efficiency by which mice acquired the everyday memory task. In short, "hybrid" neuroethological approaches that take advantage of naturally occurring behaviors are an attractive method to study behavior in laboratories.

One advantage of experimentation in the laboratory is the comparative ease with which behavioral manipulation can be combined with neuronal recordings. In the case of the everyday memory task, the device recording the neuronal signals had to allow for freely moving behavior. This requirement is met by many electrophysiological recording devices[276], but these devices have the distinct disadvantage that they cannot faithfully record from the same source across long periods. So, the dynamics of individual neurons were instead recorded using a light-weight miniaturized microscope[152]. Miniaturized microscopes have several key advantages. They can record signals from individual neurons, which the study described in chapter 3 validated to be similar to those observed with two-photon microscopes[2]. Moreover, the miniaturized microscope minimally restrained mice on the everyday memory task as mice navigated narrow corridors and dug at sandwells. Finally, miniaturized microscopes are commercially available and do not need extensive experience to be operated. As such, miniaturized microscopes record from individual neurons while mice execute naturally-occurring behaviors, including foraging[277], social exploration[278], mating[279], and parental behavior.

5.3.3   *Future directions*

In the last fifteen years, "hybrid" neuroethological approaches have been increasingly adopted. This interest is at least partially due to technical and computational advances that allow better manipulation, measurement and modeling of naturalistic behaviors[280]. Naturally-occurring behaviors can now be studied using a combination of high-resolution neuronal recordings[152] and temporally precise, cell-type specific perturbation[281]. This trend might be taken one step further in the near future by analysis of naturally-occurring home cage behavior[269], which can be recorded using high-speed cameras and segmented using convolutional neural network-based approaches[282]. If microscopes can be further miniaturized and carried by mice for extended periods

of time, motives of co-occurring home cage behavior and neuronal activity might be discerned in the near future. These findings will be the first description of the neuroethology of laboratory mice.

5.4   THE PERSISTENCE OF MEMORY

SPACED TRAINING ENHANCES MEMORY AND PREFRONTAL ENSEMBLE STABILITY IN MICE

The aim of the study described in chapter 4 was to establish whether trial spacing produced a pattern of neuronal activity conducive to memory strengthening. The study specifically quantified whether the size or stability of a neuronal ensemble was increased by trial spacing, since both could contribute to strengthening of long-term memories (as described in **1.4.4**). To distinguish these possibilities, mice were trained across months on the everyday memory task, a delayed match-to-place task in which mice find and subsequently revisit a food source. Mice performed stably and strongly across dozens of sessions and trial spacing produced distinct differences in memory encoding and retrieval. On the one hand, trial spacing impaired memory encoding, which is a relatively uncommon observation. On the other hand, trial spacing promoted memory retrieval, which was predicted by the spacing effect. Neuronal measurements and manipulations were focused on the dmPFC, a neocortical structure whose role in mediating decision-making and memory processing has been well characterized[129]. Quantification of immediate early gene expression and chemogenetic inactivation established both a correlative and causative relationship between training on the everyday memory task and dmPFC activation. Spaced training reinstated the neuronal ensemble activity more faithfully in subsequent encoding trials and upon memory retrieval, but did not affect the size of the neuronal ensemble. These results provide the first characterization of the effect of trial spacing on activity of individual neurons in the intact mammalian brain.

5.4.1   *A temporal window for memory enhancement*

The effect of trial spacing on the everyday memory task was similar to that observed during other episodic-like memory tasks[86]. Specifically, memory retrieval was strongest after training with intervals of 60 minutes and training with shorter or longer intervals resulted in weaker retrieval. These results are reminiscent of the effect of trial spacing on the object recognition task, on which memory can be retrieved when training was spaced by 60 minutes but not 20 or 120 minutes[86]. These observations are consistent with the idea that trial spacing has an inverted U-shaped effect on memory strength (**Fig. 4**). The general concept of a temporal window of memory retrieval translates other species as well[110], but its width depends on the behavioral context.

Surprisingly, memory encoding was impaired by increasing trial spacing on the everyday memory task. Specifically, the shortest, "massed" interval, which was 30 seconds, resulted in better performance on the three encoding trials than intervals of 10, 30, or 60 minutes. This was unexpected, since trial spacing typically has not been reported

to affect encoding performance[283]. Neither spaced training on the Morris water maze task, nor spaced fear conditioning, nor spaced reflex conditioning alters the effectiveness of memory encoding in mice[103,284]. That being said, incidental reports of trial spacing affecting encoding performance do exist[285]. What might explain why not many studies describe an effect of trial spacing on memory encoding? A plausible explanation is that if the training paradigm is sufficiently strong, any training regimen enables memory formation. Many studies on the spacing effect train animals on a task until they have reached asymptotic maximum performance, which typically requires at least ten trials. However, in the study described in chapter 4, there were only three encoding trials, and the ceiling of performance had not yet been reached. This suggests that although rarely observed, trials spacing influences memory encoding in certain behavioral paradigms if performance has not reached it asymptotic maximum.

5.4.2 *Prefrontal representation of task-related behaviors*

The study described in chapter 4 characterized whether trial spacing affected neuronal activity on the everyday memory task. A first and straightforward approach to examine prefrontal neuronal activity was visualization of peri-event neuronal firing. However, the peri-event time histograms did not reveal reliable co-occurrence of firing and behavioral events. Another approach was therefore warranted and a generalized linear model (GLM) was selected. This model contained the binarized neuronal firing pattern from one session as the outcome variable, normalizing all firing to a value of one. This approach was motivated by the finding that spiking is sparse in the dmPFC and, consequently, the presence of any spike might be more meaningful than the spiking frequency. The GLM did not reveal a modulatory effect of trial spacing on the fraction of neurons that was modulated by task-related events. In other words, the number of neurons representing a given task-relevant event was not altered by trial spacing.

The GLM did provide valuable insight into event-related activity of prefrontal neurons during the everyday memory task. Approximately 15% of dorsomedial prefrontal neurons were significantly modulated by at least one of the eight predictors related to decision-related, motor-related, and reward-related behaviors. This fraction contrasts starkly with that reported in other studies, particularly one that performed *in vivo* calcium imaging in the mouse prefrontal cortex during an operant conditioning task[140]. Here, mice responded to a target stimulus by licking to obtain a water reward. Pyramidal neurons represented similar behaviors as described in the current study, yet the fraction of task-modulated neurons was approximately five times larger. Several factors likely contributed to this discrepancy, as outlined below.

One critical factor was that the type of training and task were dissimilar: training on the six, short trials that encompass the everyday memory task likely activated the dmPFC in a less forceful manner than training on over a hundred trials on a highly controlled (semi-)

artificial experimental paradigm. Therefore, training on the everyday memory task might not provide the GLM with enough event-related spiking to attribute a significant modulating effect to a behavioral predictor. Additionally, only neurons that fired could be perceived by the source extraction algorithm. As such, neurons whose fluorescence did not change during the session were not characterized, suggesting that the reported fractions might be an overestimation of the true fraction of modulated neurons. To balance this overestimation, there was no activity-based exclusion criterion to pre-select neurons. This contrasts with most other studies, which only analyze highly responsive neurons. These factors together contributed strongly to the discrepant reports on the fraction of prefrontal neurons modulated by in-task events.

The study described in chapter 4 did not further specify the dmPFC area in which the visualized neurons were located for several reasons. The major contributing factor was that this was the first examination of the role of the dmPFC on the everyday memory task. As such, the experiment was designed to prioritize imaging from a large number of prefrontal neurons over selectively imaging one subarea. Furthermore, there were no strong indications that one subarea would be most critical on the everyday memory task as all subareas have been reported to mediate task-relevant behaviors[286]. In short, the benefit of imaging many neurons outweighed the cost of reduced specificity.

To provide a coarse sense of which areas were imaged, post-hoc histological analysis revealed that neurons in the anterior cingulate, prelimbic, and premotor cortex expressed GCaMP6 and could therefore have been visualized. Given where the field-of-view of the miniaturized microscope was typically centered, approximately 50% of neurons were located in the anterior cingulate, 40% in the prelimbic and 10% in the premotor cortex. Future investigations could further disentangle the contribution of the individual dmPFC areas to performance on the everyday memory task.

5.4.3   *Repeated encoding and retrieval: Stabilizing a prefrontal neuronal ensemble*

The key insight from the study described in chapter 4 was that trial spacing increased the stability of the neuronal ensemble, i.e. the similarity of the neuronal activity pattern across subsequent trials. In order to reactivate the same pattern on subsequent trials, these trials likely activated a similar set of synaptic connections in the neuronal ensemble. This is plausible given the molecular processes that unfold on the timescale of tens of minutes in dendritic spines and the soma, as described below.

Local post-synaptic activity likely contributed to initial strengthening after the first encoding trial and tagged these synaptic connections for further strengthening on subsequent trials[287]. One insight into how synaptic strengthening is restricted to previously activated spines comes from an experiment that visualized synaptic CaMKII

activation[288]. Here, local synaptic stimulation resulted in transient activation of CaMKII in the stimulated spines, which remained confined to the spine and did not diffuse across the dendritic branch[288]. Confinement of other signaling molecules, including scaffolding proteins[287], potentially further contributed to local synaptic strengthening after the first encoding trial.

Beyond synaptic mechanisms, somatic signaling likely rendered these previously activated neurons more easily activated than their neighbors by subsequent learning events. Generally, training enhances neuronal excitability in previously activated neurons[289,290]. Training with appropriately spaced intervals can enhance neuronal excitability by more effectively activating intracellular signaling cascades that underlie synaptic strengthening[290]. One result of intracellular signaling might have been AMPAR insertion and spine remodeling, which occurs within an hour of synaptic stimulation[16,291,292]. These processes ensure that subsequent spaced encoding events affect a similar population of synaptic connections on a similar population of neurons. In summary, memory enhancement resulting from spacing the first three trials on the everyday memory task is the outcome of several interactive processes underlying memory encoding and retrieval.

5.4.4   *From mouse to man: Cognitive theories on the spacing effect*

The insights from studies in animals should be connected to the numerous studies on the spacing effect in humans to establish a common conceptual framework describing why trial spacing enhances memory. Three predominant cognitive theories have been postulated to explain the efficacy of spaced training in humans: the encoding variability theory, the deficient-processing theory, and study-phase retrieval theory[6]. The study described in chapter 4 provides evidence in favor and against these theories, as reviewed below.

The core concept of the encoding variability theory is that distributed learning enhances the relevance of the learned information in more situations. Spaced stimuli generally present themselves in different contexts, and the resulting memory traces include elements of these contexts. Therefore, more cues are likely to result in (partial) reactivation of these memory traces. The experimental foundation for the encoding variability theory was the observation that presenting human subjects with a different but not the same cue word before each word presentation enhanced retrieval[293]. Given the results of the study described in chapter 4 however, a dissimilar context does not appear to be a requirement for observation of the spacing effect. Conceding that neither events during the intertrial periods nor the internal state were tightly controlled, a key feature of the everyday memory task was its highly standardized training context across trials. The individual encoding trials were largely indistinguishable from each other, yet spaced training still strengthened memory. Therefore, the study described in chapter 4 does not provide strong evidence in favor of the encoding variability theory.

The deficient-processing theory suggests that massed training prevents efficient execution of cognitive processes during encoding and that this deficient processing can be rectified by spaced training[294]. This theory has been empirically addressed by training human subject on tasks that judge semantic information while measuring repetition suppression. Repetition suppression is the commonly observed phenomenon that stimulus-evoked neural activity is reduced when a stimulus is repeated[295]. The deficient-processing theory predicts that repetition suppression is stronger during massed training, since the context is more similar between stimuli[296]. This theory was upheld in multiple studies employing judgement tasks on faces[297] and words[298,299]. In these studies, enhanced repetition suppression upon massed training[297–299] has been observed in the task-relevant brain areas. These observations suggest that signal processing is enhanced in spaced as compared to massed training and affirm the deficient-processing theory.

Despite its merits, the deficient-processing theory cannot explain the findings of the study described in chapter 4. The most critical observation was that encoding was most successful upon massed training. Furthermore, there was no effect of trial spacing on repetition suppression, since neither the faction of active neurons nor the activity of this fraction was modulated by trial spacing. Repetition suppression was observed across trials, since the fraction of activated neurons decreased across encoding trials in a trial-spacing independent manner. However, this was (partially) counterbalanced by an increase of activity of the remaining active population. In short, the study in chapter 4 does not provide strong evidence in favor of the deficient processing theory.

The study-phase retrieval theory asserts that repeated memory retrieval underlies the spacing effect[300]. This theoretical framework is conceptually distinct from deficient-processing theory, which addresses the encoding component of memory processing. According to study-phase retrieval theory, the threshold for neuronal activation is raised as long as a stimulus is present and recovery begins when the stimulus disappears[294]. During this period, information from the previous trial is processed and the memory is stabilized. If the second stimulus comes quickly after the first, the recovery is still ongoing, the threshold for activation remains raised and the memory cannot be retrieved and reinforced. However, if the second stimulus is temporarily offset, the memory can be retrieved and reactivated, further strengthening the memory. In short, the study-phase retrieval theory suggests that spacing trials for a specific duration enhances the probability that a memory is reactivated and retrieved.

A key merit of the study-phase retrieval theory is that it predicted the observed inverted U-shaped relationship between trial spacing and memory strength. Neither the encoding variability nor the deficient-processing theory can explain why spacing exceeding an optimum interval would impair memory. The encoding variability theory would predict a monotonically increasing relationship between trial spacing and memory strength since context diversity increases with any

increase in trial spacing, thereby incorporating even more cues into the memory trace. The deficient-processing theory would predict an S-shaped relationship since the repetition suppression is negligible when stimuli are sufficiently spaced. As a result, the stimulus-induced neuronal activity not change beyond the optimum interval duration, neither enhancing nor impairing memory. According to study-phase retrieval theory, the neural alterations resulting from the first learning event are removed during excessively long intervals. This destabilizes the memory trace and prevents retrieval of the memory, resulting in an inverted U-shaped relationship between trial spacing and memory strength as observed in the study described in chapter 4.

The framework of study-phase retrieval theory also accommodates the main finding of the study described in chapter 4 regarding neuronal processing, which was that the neuronal activity pattern reactivated more precisely when training was spaced and mediated memory retrieval. Similar observations have been made in human subjects, in which successful episodic memory retrieval was associated with increased similarity of stimulus-induced neuronal patterns across trials[301]. Furthermore, spaced learning on a facial recognition task resulted in better memory retrieval, which was associated with higher spatiotemporal pattern similarity in the recorded EEG signal[297]. These observations attests to the idea that retrieval is generally more effective when neuronal representations are reinstated more faithfully, as suggested from the study-phase retrieval theory. In short, the findings of the study described in chapter 4 are best understood within the framework of the study-phase retrieval theory.

5.4.5 *Relevance of the spacing effect in the clinic and classroom*

The spacing effect has high translational potential, especially as an additional therapy to alleviate learning impairments in individuals with congenital intellectual disabilities, including those with Angelman, Down or fragile X syndrome. These disorders are characterized by abnormal synaptic signaling[302], which could be partially rectified by spaced training. Studies with genetic mouse models of the aforementioned intellectual disabilities have provided insight into how spaced training can rescue memory processing[86,303]. Trial spacing is by no means a panacea however: its effects depend on the nature of the memory and neuronal circuits involved[303]. For example, spaced training enhanced episodic-like memory processing in genetic mouse models of Down and fragile X syndrome[86,303], which was mediated by enhanced MAPK signaling[86]. Furthermore, spaced training promoted spatial memory acquisition in mouse models of Down and Angelman syndrome[303]. However, spaced training did not improve motor memory of Down or Angelman syndrome model mice. Future studies directly comparing the effect of massed versus spaced training on learning and memory retrieval of human patients would have to validate the therapeutic applicability and efficacy of spaced training.

The pedagogical relevance of spaced learning is generally better appreciated than its clinical relevance. The effects of spaced learning are dependent on the student's ability: whereas pupils with above average ability do not perform significantly better upon spaced instruction, pupils with below average ability or specific language impairments retain more knowledge if instruction is spaced[304,305]. The (above) average pupils are not negatively impacted by spaced instruction, most likely because of a ceiling effect. It is possible that, if a tasks is sufficiently challenging, even (above) average pupils benefit from spaced instruction. This suggests that spaced training is a beneficial strategy to standardize, or even increase, the effectiveness of pedagogical instruction.

As traditional teaching environments move online, it is beneficial to apply principles from the spacing effect while designing these platforms. Whereas temporal distribution of offline classes is typically restricted by teacher or resource availability, online classes can be accessed around the clock. The effectiveness of these courses benefit from measures that encourage spaced learning by users, as evidenced in certain massive online courses and language learning applications[306]. For example, students perform better on a massive open online course when learning time is distributed among more sessions[307]. Further, both memory encoding and retrieval improve if massive open online courses are modified to encourage or even enforce spaced learning[306,308]. Given these results, trial spacing should be implemented into pedagogical methods to optimize learning in the classroom and online.

5.4.6   *Future directions*

Many behavioral and neuronal features of the spacing effect are still unexplored, even though the spacing effect was first described over 135 years ago. Key questions that are still unanswered are whether memories acquired during spaced training are more resilient to disruption, whether irregular trial spacing could further enhance memory retrieval, whether longer trial spacing stabilizes memory over longer retrieval delays, and how subneuronal structures are affected by trial spacing.

Given that spaced training on the everyday memory task instills a stable next-day memory, how stable is this memory? One approach to assess this would be to evaluate memory retrieval after a longer retention period, for instance a week. However, this would only provide correlative but not causative evidence that memories are more stable if they result from spaced training. Causal evidence could be provided by evaluating to what degree memory can be reconsolidated 24 hours after training on the everyday memory task. Reconsolidation is a process that is triggered by retrieval of a previously acquired, stable memory, which can transiently destabilize the memory trace[309]. To re-stabilize the memory, a protein synthesis dependent process must take place, as evidenced by amnesia of a previously acquired

memory upon infusion of the protein synthesis inhibitor anisomycin briefly after memory retrieval[310]. This study paved the way into the investigation of the boundary conditions that influence reconsolidation. Generally, younger and weaker memories are more sensitive to a block of protein synthesis during reconsolidation than older and stronger memories[311–314]. These insights could be leveraged to address the stability of memories instilled by training on the everyday memory task. If anisomycin infusion into the dmPFC during next-day memory retrieval would destabilize memories formed during massed but not spaced training, this would suggest that massed training induces weaker memories than spaced training.

Could memory be improved further by training using irregularly spaced intervals, i.e. intervals of a different duration that are presented in a specific order? Irregular trial spacing enhances the interactions between key signaling proteins that underlie memory formation[6]. The only study to date evaluating the enhancing effect of irregular trial spacing combined computational modeling with empirical experimentation[315]. Rather than evaluating the mechanistic effects of training on a range of intervals, this study used computational modeling to propose an optimal training protocol. The model predicted that spacing five stimuli with 10, 10, 5, and 30 minutes would maximize interaction between PKA and MAPK and thereby increase the magnitude and duration of long-term synaptic facilitation[315]. Testing these predictions *in vivo* demonstrated that the irregularly spaced training protocol enhanced sensitization of the withdrawal reflex in *Aplysia* more than any regularly spaced training regimen[315]. Future studies using irregularly spaced intervals would have to demonstrate whether an irregularly spaced training protocol further improves the effect of trial spacing in mammals.

If the intended retention period is longer, should trial spacing be increased? In the version of the everyday memory task described in chapter 4, memory had to be retained for one day, which was optimally achieved by spacing encoding trials by one hour. Longstanding evidence points to a positive correlation between trial spacing and the memory retention period (reviewed in [283]). It is therefore likely that if the retention period on the everyday memory task would be extended to several days, trial spacing should be extended as well to produce longer lasting memories[96]. Testing this hypothesis would help bridge the gap between the typical retention period in animal studies, typically one day, the typical retention period in human studies, which can be several weeks, and the retention period in real-world situations, which can be decades.

Are dendritic spines more extensively remodeled by spaced training on the everyday memory task? This final question relates to several *in vitro* and *ex vivo* studies that have described how synaptic remodeling is affected by spaced training[66,103,107,119]. However, no *in vivo* studies directly quantify structural remodeling.

The effect of trial spacing on the everyday memory task on the dynamics of structural plasticity could be addressed by structural imaging of dendritic spines using miniaturized two-photon imaging[157]. This experiment would provide a first insight into how trial spacing affects synaptic remodeling in real time.

5.5 CONCLUSION AND EPILOGUE

In this doctoral dissertation, I demonstrate that trial spacing enhances ensemble reactivation on the everyday memory task. This work represents the first *in vivo* insight into the relationship between memory enhancement, trial spacing, and activity of individual neurons. The experiments providing these insights were realizable because of recent development of miniaturized microscopes. I argue that the memory-enhancing effect of the relatively simple act of distributing learning remains a fascinating area of study. In the future, pharmacology-based or technology-based approaches might enhance human memory beyond what is achievable by distributed learning, but the applicability of these approaches is currently highly speculative. Instead, distributed learning can bring about memory enhancement that would improve the everyday functioning of school-age children, aging individuals, and those who suffer from neurodevelopmental and neurodegenerative disorders. If these lofty goals are not met, distributed learning could at least enhance the amount of information that doctoral candidates retain from their thousands of hours of classroom education.

6

BIBLIOGRAPHY

1. Goltstein, P. M., Reinert, S., Glas, A., Bonhoeffer, T. & Hübener, M. Food and water restriction lead to differential learning behaviors in a head-fixed two-choice visual discrimination task for mice. *PLOS ONE* **13,** 1–19 (2018).

2. Glas, A., Hübener, M., Bonhoeffer, T. & Goltstein, P. M. Benchmarking miniaturized microscopy against two-photon calcium imaging using single-cell orientation tuning in mouse visual cortex. *PLOS ONE* **14,** 1–18 (2019).

3. Scoville, W. B. & Milner, B. Loss of recent memory after bilateral hippocampal lesions. *Journal of neurology, neurosurgery, and psychiatry* **20,** 11–21 (1957).

4. Asok, A., Leroy, F., Rayman, J. B. & Kandel, E. R. Molecular mechanisms of the memory trace. *Trends in Neurosciences* **42,** 14–22 (2019).

5. Ebbinghaus, H. *Über das Gedächtnis: Untersuchungen zur experimentellen Psychologie* (Duncker & Humblot, Berlin, 1885).

6. Smolen, P., Zhang, Y. & Byrne, J. H. The right time to learn: Mechanisms and optimization of spaced learning. *Nature Reviews Neuroscience* **17,** 77–88 (2016).

7. Konorski, J. *Conditioned reflexes and neuronal organization.* (Cambridge Univserity Press, Cambridge, 1948).

8. Hebb, D. O. *The organization of behavior: a neuropsychological theory* (Wiley, New York, 1949).

9. Josselyn, S. A., Köhler, S. & Frankland, P. W. Finding the engram. *Nature Reviews Neuroscience* **16,** 521–534 (2015).

10. Poo, M. M., Pignatelli, M, Ryan, T. J., Tonegawa, S, Bonhoeffer, T, *et al.* What is memory? The present state of the engram. *BMC Biology* **14,** 1–18 (2016).

11. Bliss, T. & Lømo, T. Long-lasting potentiation of synaptic transmission in the dentate area of the unanaesthetized rabbit following stimulation of the perforant path. *The Journal of Physiology* **232,** 331–356 (1973).

12. Malinow, R. Transmission between pairs of hippocampal slice neurons: quantal levels, oscillations, and LTP. *Science* **252,** 722–724 (1991).

13. Kandel, E. R., Dudai, Y. & Mayford, M. R. The molecular and systems biology of memory. *Cell* **157,** 163–186 (2014).

14. Hayashi, Y., Shi, S. H., Esteban, J. A., Piccini, A., Poncer, J. C., *et al.* Driving AMPA receptors into synapses by LTP and CaMKII: Requirement for GluR1 and PDZ domain interaction. *Science* **287,** 2262–2267 (2000).

15. Granger, A. J., Shi, Y., Lu, W., Cerpas, M. & Nicoll, R. A. LTP requires a reserve pool of glutamate receptors independent of subunit type. *Nature* **493,** 495–500 (2013).

16. Shi, S. H., Hayashi, Y., Petralia, R. S., Zaman, S. H., Wenthold, R. J., *et al.* Rapid spine delivery and redistribution of AMPA receptors after synaptic NMDA receptor activation. *Science* **284,** 1811–1816 (1999).

17. Nguyen, P. V., Abel, T. & Kandel, E. R. Requirement of a critical period of transcription for induction of a late phase of LTP. *Science* **265,** 1104–1107 (1994).

18. Frey, U., Huang, Y.-Y. & Kandel, E. R. Effects of cAMP simulate a late stage of LTP in hippocampal CA1 neurons. *Science* **260,** 1661–1664 (1993).

19. Bartsch, D., Casadio, A., Karl, K. A., Serodio, P. & Kandel, E. R. CREB1 encodes a nuclear activator, a repressor, and a cytoplasmic modulator that form a regulatory unit critical for long-term facilitation. *Cell* **95,** 211–223 (1998).

20. Rao-Ruiz, P., Couey, J. J., Marcelo, I. M., Bouwkamp, C. G., Slump, D. E., *et al.* Engram-specific transcriptome profiling of contextual memory consolidation. *Nature Communications* **10,** 1–14 (2019).

21. Engert, F. & Bonhoeffer, T. Dendritic spine changes associated with hippocampal long-term synaptic plasticity. *Nature* **399,** 66–70 (1999).

22. Matsuzaki, M., Honkura, N., Ellis-Davies, G. C. R. & Kasai, H. Structural basis of long-term potentiation in single dendritic spines. *Nature* **429,** 761–766 (2004).

23. Holtmaat, A., Wilbrecht, L., Knott, G. W., Welker, E. & Svoboda, K. Experience-dependent and cell-type-specific spine growth in the neocortex. *Nature* **441,** 979–983 (2006).

24. Yang, G., Pan, F. & Gan, W. B. Stably maintained dendritic spines are associated with lifelong memories. *Nature* **462,** 920–924 (2009).

25. Hofer, S. B., Mrsic-Flogel, T. D., Bonhoeffer, T. & Hübener, M. Experience leaves a lasting structural trace in cortical circuits. *Nature* **457,** 313–317 (2009).

26. Hayashi-Takagi, A., Yagishita, S., Nakamura, M., Shirai, F., Wu, Y. I., *et al.* Labelling and optical erasure of synaptic memory traces in the motor cortex. *Nature* **525,** 333–338 (2015).

27. Tonegawa, S., Morrissey, M. D. & Kitamura, T. The role of engram cells in the systems consolidation of memory. *Nature Reviews Neuroscience* **19,** 485–498 (2018).

28. Squire, L. Mechanisms of memory. *Science* **232,** 1612–1619 (1986).

29. Milner, B. & Penfield, W. *The effect of hippocampal lesions on recent memory.* in *Transactions of the American Neurological Association* (1955), 42–48.

30. Maviel, T., Durkin, T. P., Menzaghi, F. & Bontempi, B. Sites of neocortical reorganization critical for remote spatial memory. *Science* **305,** 96–99 (2004).

31. Kitamura, T., Ogawa, S. K., Roy, D. S., Okuyama, T., Morrissey, M. D., *et al.* Engrams and circuits crucial for systems consolidation of a memory. *Science* **356,** 73–78 (2017).

32. Wilson, M. A. & McNaughton, B. L. Reactivation of hippocampal ensemble memories during sleep. *Science* **265,** 676–679 (1994).

33. Ji, D. & Wilson, M. A. Coordinated memory replay in the visual cortex and hippocampus during sleep. *Nature Neuroscience* **10,** 100–107 (2007).

34. Nyberg, L., Habib, R., McIntosh, A. R. & Tulving, E. Reactivation of encoding-related brain activity during memory retrieval. *Proceedings of the National Academy of Sciences of the United States of America* **97,** 11120–11124 (2000).

35. Reijmers, L. G., Perkins, B. L., Matsuo, N. & Mayford, M. Localization of a stable neural correlate of associative memory. *Science* **317,** 1230–1233 (2007).

36. Liu, X., Ramirez, S., Pang, P. T., Puryear, C. B., Govindarajan, A, *et al.* Optogenetic stimulation of a hippocampal engram activates fear memory recall. *Nature* **484,** 381–385 (2012).

37. Diekelmann, S. & Born, J. The memory function of sleep. *Nature Reviews Neuroscience* **11,** 114–126 (2010).

38. Gilboa, A. & Marlatte, H. Neurobiology of schemas and schema-mediated memory. *Trends in Cognitive Sciences* **21,** 618–631 (2017).

39. Marshall, L., Helgadóttir, H., Mölle, M. & Born, J. Boosting slow oscillations during sleep potentiates memory. *Nature* **444,** 610–613 (2006).

40. Rasch, B., Büchel, C., Gais, S. & Born, J. Odor cues during slow-wave sleep prompt declarative memory consolidation. *Science* **315,** 1426–1429 (2007).

41. Van Kesteren, M. T. R., Fernández, G., Norris, D. G. & Hermans, E. J. Persistent schema-dependent hippocampal-neocortical connectivity during memory encoding and postencoding rest in humans. *Proceedings of the National Academy of Sciences of the United States of America* **107,** 7550–7555 (2010).

42. Tse, D., Langston, R. F., Kakeyama, M., Bethus, I., Spooner, P. A., *et al.* Schemas and memory consolidation. *Science* **316,** 76–82 (2007).

43. Tse, D., Takeuchi, T., Kakeyama, M., Kajii, Y., Okuno, H., *et al.* Schema-dependent gene activation and memory encoding in neocortex. *Science* **333,** 891–895 (2011).

44. Fregni, F., Boggio, P. S., Nitsche, M., Bermpohl, F., Antal, A., *et al.* Anodal transcranial direct current stimulation of prefrontal cortex enhances working memory. *Experimental Brain Research* **166,** 23–30 (2005).

45. Hamani, C., McAndrews, M. P., Cohn, M., Oh, M., Zumsteg, D., *et al.* Memory enhancement induced by hypothalamic/fornix deep brain stimulation. *Annals of Neurology* **63,** 119–123 (2008).

46. Fond, G., Micoulaud-Franchi, J. A., Brunel, L., Macgregor, A., Miot, S., *et al.* Innovative mechanisms of action for pharmaceutical cognitive enhancement: A systematic review. *Psychiatry Research* **229,** 12–20 (2015).

47. Malykh, A. G. & Sadaie, M. R. Piracetam and piracetam-like drugs: From basic science to novel clinical applications to CNS disorders. *Drugs* **70,** 287–312 (2010).

48. McGaugh, J. L. & Roozendaal, B. Drug enhancement of memory consolidation: Historical perspective and neurobiological implications. *Psychopharmacology* **202,** 3–14 (2009).

49. Witte, A. V., Fobker, M., Gellner, R., Knecht, S. & Flöel, A. Caloric restriction improves memory in elderly humans. *Proceedings of the National Academy of Sciences of the United States of America* **106,** 1255–1260 (2009).

50. Erickson, K. I., Voss, M. W., Prakash, R. S., Basak, C., Szabo, A., *et al.* Exercise training increases size of hippocampus and improves memory. *Proceedings of the National Academy of Sciences of the United States of America* **108,** 3017–3022 (2011).

51. Rose, J. K., Kaun, K. R. & Rankin, C. H. A new group-training procedure for habituation demonstrates that presynaptic glutamate release contributes to long-term memory in Caenorhabditis elegans. *Learning and Memory* **9,** 130–137 (2002).

52. Smid, H. M., Wang, G., Bukovinszky, T., Steidle, J. L., Bleeker, M. A., *et al.* Species-specific acquisition and consolidation of long-term memory in parasitic wasps. *Proceedings of the Royal Society B: Biological Sciences* **274,** 1539–1546 (2007).

53. Hosono, S., Matsumoto, Y. & Mizunami, M. Interaction of inhibitory and facilitatory effects of conditioning trials on long-term memory formation. *Learning and Memory* **23,** 669–678 (2016).

54. Menzel, R., Manz, G., Menzel, R. & Greggers, U. Massed and spaced learning in honeybees: The role of CS, US, the intertrial interval, and the test interval. *Learning and Memory* **8,** 198–208 (2001).

55. Sangha, S., Scheibenstock, A., Morrow, R. & Lukowiak, K. Extinction requires new RNA and protein synthesis and the soma of the cell right pedal dorsal 1 in Lymnaea stagnalis. *Journal of Neuroscience* **23,** 9842–9851 (2003).

56. Gong, L. Q., He, L. J., Dong, Z. Y., Lu, X. H., Poo, M. M., *et al.* Postinduction requirement of NMDA receptor activation for late-phase long-term potentiation of developing retinotectal synapses in vivo. *Journal of Neuroscience* **31,** 3328–3335 (2011).

57. Berón De Astrada, M. & Maldonado, H. Two related forms of long-term habituation in the crab Chasmagnathus are differentially affected by scopolamine. *Pharmacology Biochemistry and Behavior* **63,** 109–118 (1999).

58. Roberts, A., Reichl, J., Song, M., Dearinger, A., Moridzadeh, N., *et al.* Habituation of the C-start response in larval zebrafish exhibits several distinct phases and sensitivity to NMDA receptor blockade. *PLOS ONE* **6,** 1–10 (2011).

59. Roberts, W. A. Distribution of trials and intertrial retention in delayed matching to sample with pigeons. *Journal of Experimental Psychology: Animal Behavior Processes* **6,** 217–237 (1980).

60. Meyer, I. & Ladewig, J. The relationship between number of training sessions per week and learning in dogs. *Applied Animal Behaviour Science* **111,** 311–320 (2008).

61. Naqib, F., Sossin, W. S. & Farah, C. A. Molecular determinants of the spacing effect. *Neural Plasticity* **2012,** 1–8 (2012).

62. Carew, T. J., Pinsker, H. M. & Kandel, E. R. Long-term habituation of a defensive withdrawal reflex in Aplysia. *Science* **175,** 451–454 (1972).

63. Sutton, M. A., Ide, J., Masters, S. E. & Carew, T. J. Interaction between amount and pattern of training in the induction of intermediate- and long-term memory for sensitization in Aplysia. *Learning and Memory* **9,** 29–40 (2002).

64. Kandel, E. R. The molecular biology of memory storage: A dialogue between genes and synapses. *Science* **294,** 1030–1038 (2001).

65. Tully, T., Preat, T., Boynton, S. C. & Del Vecchio, M. Genetic dissection of consolidated memory in Drosophila. *Cell* **79,** 35–47 (1994).

66. Okamoto, T., Endo, S., Shirao, T. & Nagao, S. Role of cerebellar cortical protein synthesis in transfer of memory trace of cerebellum-dependent motor learning. *Journal of Neuroscience* **31,** 8958–8966 (2011).

67. Watson, J. & Rayner, R. Conditioned emotional reactions. *Journal of experimental psychology* **3,** 1–14 (1920).

68. Konorski, J. *Integrative activity of the brain; an interdisciplinary approach* (University of Chicago Press, Chicago, 1967).

69. Cain, C. K., Blouin, A. M. & Barad, M. Temporally massed CS presentations generate more fear extinction than spaced presentations. *Journal of Experimental Psychology: Animal Behavior Processes* **29,** 323–333 (2003).

70. Fanselow, M. S. & Tighe, T. J. Contextual conditioning with massed versus distributed unconditional stimuli in the absence of explicit conditional stimuli. *Journal of Experimental Psychology: Animal Behavior Processes* **14,** 187–199 (1988).

71. Davis, M. The role of the amygdala in fear and anxiety. *Annual Review of Neuroscience* **15,** 353–375 (1992).

72. Morris, R. G. Developments of a water-maze procedure for studying spatial learning in the rat. *Journal of Neuroscience Methods* **11,** 47–60 (1984).

73. Mandel, R. J., Gage, F. H. & Thal, L. J. Enhanced detection of nucleus basalis magnocellularis lesion-induced spatial learning deficit in rats by modification of training regimen. *Behavioural Brain Research* **31,** 221–229 (1989).

74. Upchurch, M. & Wehner, J. M. Effects of N-methyl-d-aspartate antagonism on spatial learning in mice. *Psychopharmacology* **100,** 209–214 (1990).

75. Eichenbaum, H. Prefrontal-hippocampal interactions in episodic memory. *Nature Reviews Neuroscience* **18,** 547–558 (2017).

76. Tulving, E. What is episodic memory? *Current directions in psychological science* **2,** 67–70 (1993).

77. Clayton, N. S. & Dickinson, A. Episodic-like memory during cache recovery by scrub jays. *Nature* **335,** 272–274 (1998).

78. Burgess, N., Maguire, E. A. & O'Keefe, J. The human hippocampus and spatial and episodic memory. *Neuron* **35,** 625–641 (2002).

79. Zola-Morgan, S. M. & Squire, L. R. The primate hippocampal formation: Evidence for a time-limited role in memory storage. *Science* **250,** 288–290 (1990).

80. Broadbent, N. J., Gaskin, S., Squire, L. R. & Clark, R. E. Object recognition memory and the rodent hippocampus. *Learning & Memory* **17,** 5–11 (2010).

81. Fortin, N. J., Wright, S. P. & Eichenbaum, H. Recollection-like memory retrieval in rats is dependent on the hippocampus. *Nature* **431,** 188–191 (2004).

82. Allen, T. A. & Fortin, N. J. The evolution of episodic memory. *Proceedings of the National Academy of Sciences of the United States of America* **110,** 10379–10386 (2013).

83. Bevins, R. A. & Besheer, J. Object recognition in rats and mice: A one-trial non-matching-to-sample learning task to study 'recognition memory'. *Nature protocols* **1,** 1306–1311 (2006).

84. Aggleton, J. P. & Brown, M. W. Episodic memory, amnesia, and the hippocampal-anterior thalamic axis. *Behavioral and Brain Sciences* **22,** 425–444 (1999).

85. Broadbent, N., Lumeij, L. B., Corcoles, M., Ayres, A. I., Bin Ibrahim, M. Z., *et al.* A stable home-base promotes allocentric memory representations of episodic-like everyday spatial memory. *European Journal of Neuroscience* **51,** 1539–1558 (2020).

86. Seese, R. R., Wang, K., Yao, Y. Q., Lynch, G. & Gall, C. M. Spaced training rescues memory and ERK1/2 signaling in fragile X syndrome model mice. *Proceedings of the National Academy of Sciences of the United States of America* **111,** 16907–16912 (2014).

87. Tintorelli, R., Budriesi, P., Villar, M. E., Marchal, P., da Cunha, P. L., *et al.* Spatial-memory formation after spaced learning involves ERKs1/2 activation through a behavioral-tagging process. *Scientific Reports* **10,** 1–11 (2020).

88. Takeuchi, T., Duszkiewicz, A. J., Sonneborn, A., Spooner, P. A., Yamasaki, M., *et al.* Locus coeruleus and dopaminergic consolidation of everyday memory. *Nature* **537,** 357–362 (2016).

89. Wang, S. H., Redondo, R. L. & Morris, R. G. M. Relevance of synaptic tagging and capture to the persistence of long-term potentiation and everyday spatial memory. *Proceedings of the National Academy of Sciences of the United States of America* **107,** 19537–19542 (2010).

90. Salvetti, B., Morris, R. G. & Wang, S. H. The role of rewarding and novel events in facilitating memory persistence in a separate spatial memory task. *Learning and Memory* **21,** 61–72 (2014).

91. Nonaka, M., Fitzpatrick, R., Lapira, J., Wheeler, D., Spooner, P. A., *et al.* Everyday memory: Towards a translationally effective method of modelling the encoding, forgetting and enhancement of memory. *European Journal of Neuroscience* **46,** 1937–1953 (2017).

92. Wang, S. H. & Morris, R. G. M. Hippocampal-neocortical interactions in memory formation, consolidation, and reconsolidation. *Annual review of psychology* **61,** 49–79 (2010).

93. Guo, Z. V., Hires, S. A., Li, N., O'Connor, D. H., Komiyama, T., *et al.* Procedures for behavioral experiments in head-fixed mice. *PLOS ONE* **9,** 1–16 (2014).

94. Tucci, V., Hardy, A. & Nolan, P. M. A comparison of physiological and behavioural parameters in C57BL/6J mice undergoing food or water restriction regimes. *Behavioural Brain Research* **173,** 22–29 (2006).

95. Heiderstadt, K. M., McLaughlin, R. M., Wright, D. C., Walker, S. E. & Gomez-Sanchez, C. E. The effect of chronic food and water restriction on open-field behaviour and serum corticosterone levels in rats. *Laboratory Animals* **34,** 20–28 (2000).

96. Melton, A. W. The situation with respect to the spacing of repetitions and memory. *Journal of Verbal Learning and Verbal Behavior* **9,** 596–606 (1970).

97. Urcelay, G. P., Wheeler, D. S. & Miller, R. R. Spacing extinction trials alleviates renewal and spontaneous recovery. *Learning and Behavior* **37,** 60–73 (2009).

98. Commins, S., Cunningham, L., Harvey, D. & Walsh, D. Massed but not spaced training impairs spatial memory. *Behavioural Brain Research* **139,** 215–223 (2003).

99. Sisti, H. M., Glass, A. L. & Shors, T. J. Neurogenesis and the spacing effect: Learning over time enhances memory and the survival of new neurons. *Learning & memory* **14,** 368–375 (2007).

100. Zorrilla, E. P., Schulteis, G., Ormsby, A., Klaassen, A., Ling, N., *et al.* Urocortin shares the memory modulating effects of corticotropin-releasing factor (CRF): Mediation by CRF1 receptors. *Brain Research* **952,** 200–210 (2002).

101. Beck, C. D., Schroeder, B. & Davis, R. L. Learning performance of normal and mutant drosophila after repeated conditioning trials with discrete stimuli. *Journal of Neuroscience* **20,** 2944–2953 (2000).

102. Josselyn, S. A., Shi, C., Carlezon, W. A., Neve, R. L., Nestler, E. J., *et al.* Long-term memory is facilitated by cAMP response element-binding protein overexpression in the amygdala. *Journal of Neuroscience* **21,** 2404–2412 (2001).

103. Aziz, W., Wang, W., Kesaf, S., Mohamed, A. A., Fukazawa, Y., *et al.* Distinct kinetics of synaptic structural plasticity, memory formation, and memory decay in massed and spaced learning. *Proceedings of the National Academy of Sciences of the United States of America* **111,** E194–E202 (2014).

104. Cao, G. & Harris, K. M. Augmenting saturated LTP by broadly spaced episodes of theta-burst stimulation in hippocampal area CA1 of adult rats and mice. *Journal of Neurophysiology* **112,** 1916–1924 (2014).

105. Jarome, T. J., Kwapis, J. L., Werner, C. T., Parsons, R. G., Gafford, G. M., *et al.* The timing of multiple retrieval events can alter GluR1 phosphorylation and the requirement for protein synthesis in fear memory reconsolidation. *Learning and Memory* **19,** 300–306 (2012).

106. Sunsay, C. & Bouton, M. E. Analysis of a trial-spacing effect with relatively long intertrial intervals. *Learning and Behavior* **36,** 104–115 (2008).

107. Kramár, E. A., Babayan, A. H., Gavin, C. F., Cox, C. D., Jafari, M., *et al.* Synaptic evidence for the efficacy of spaced learning. *Proceedings of the National Academy of Sciences of the United States of America* **109,** 5121–5126 (2012).

108. Ajay, S. M. & Bhalla, U. S. A role for ERKII in synaptic pattern selectivity on the time-scale of minutes. *European Journal of Neuroscience* **20,** 2671–2680 (2004).

109. Park, P., Sanderson, T. M., Amici, M., Choi, S. L., Bortolotto, Z. A., *et al.* Calcium-permeable AMPA receptors mediate the induction of the protein kinase a-dependent component of long-term potentiation in the hippocampus. *Journal of Neuroscience* **36,** 622–631 (2016).

110. Philips, G. T., Ye, X., Kopec, A. M. & Carew, T. J. MAPK establishes a molecular context that defines effective training patterns for long-term memory formation. *The Journal of Neuroscience* **33,** 7565–7573 (2013).

111. Jiang, L., Mao, R., Zhou, Q., Yang, Y., Cao, J., *et al.* Inhibition of Rac1 activity in the hippocampus impairs the forgetting of contextual fear memory. *Molecular Neurobiology* **53,** 1247–1253 (2016).

112. Fonseca, R., Nägerl, U. V., Morris, R. G. & Bonhoeffer, T. Competing for memory: Hippocampal LTP under regimes of reduced protein synthesis. *Neuron* **44,** 1011–1020 (2004).

113. Inda, M. C., Muravieva, E. V. & Alberini, C. M. Memory retrieval and the passage of time: From reconsolidation and strengthening to extinction. *Journal of Neuroscience* **31,** 1635–1643 (2011).

114. Landauer, T. K. Reinforcement as consolidation. *Psychological Review* **76,** 82–96 (1969).

115. Silva, A. J., Zhou, Y., Rogerson, T., Shobe, J. & Balaji, J. Molecular and cellular approaches to memory allocation in neural circuits. *Science* **326,** 391–395 (2009).

116. Cai, D. J., Aharoni, D., Shuman, T., Shobe, J., Biane, J., *et al.* A shared neural ensemble links distinct contextual memories encoded close in time. *Nature* **534,** 115–118 (2016).

117. Scharf, M. T., Woo, N. H., Matthew Lattal, K., Young, J. Z., Nguyen, P. V., *et al.* Protein synthesis is required for the enhancement of long-term potentiation and long-term memory by spaced training. *Journal of Neurophysiology* **87,** 2770–2777 (2002).

118. Genoux, D., Bezerra, P. & Montgomery, J. M. Intra-spaced stimulation and protein phosphatase 1 dictate the direction of synaptic plasticity. *European Journal of Neuroscience* **33,** 1761–1770 (2011).

119. Wu, G. Y., Deisseroth, K. & Tsien, R. W. Spaced stimuli stabilize MAPK pathway activation and its effects on dendritic morphology. *Nature Neuroscience* **4,** 151–158 (2001).

120. Akalal, D. B. G., Yu, D. & Davis, R. L. A late-phase, long-term memory trace forms in the γ neurons of Drosophila mushroom bodies after olfactory classical conditioning. *Journal of Neuroscience* **30,** 16699–16708 (2010).

121. Yu, D., Akalal, D. B. G. & Davis, R. L. Drosophila α/β mushroom body neurons form a branch-specific, long-term cellular memory trace after spaced olfactory conditioning. *Neuron* **52,** 845–855 (2006).

122. Farah, C. A., Weatherill, D., Dunn, T. W. & Sossin, W. S. PKC differentially translocates during spaced and massed training in Aplysia. *Journal of Neuroscience* **29,** 10281–10286 (2009).

123. Martin, K. C., Michael, D., Rose, J. C., Barad, M., Casadio, A., *et al.* MAP kinase translocates into the nucleus of the presynaptic cell and is required for long-term facilitation in Aplysia. *Neuron* **18,** 899–912 (1997).

124. Pagani, M. R., Oishi, K., Gelb, B. D. & Zhong, Y. The phosphatase SHP2 regulates the spacing effect for long-term memory induction. *Cell* **139,** 186–198 (2009).

125. Genoux, D., Haditsch, U., Knobloch, M., Michalon, A., Storm, D., *et al.* Protein phosphatase 1 is a molecular constraint on learning and memory. *Nature* **418,** 970–975 (2002).

126. Plaçais, P. Y., Trannoy, S., Isabel, G., Aso, Y., Siwanowicz, I., *et al.* Slow oscillations in two pairs of dopaminergic neurons gate long-term memory formation in Drosophila. *Nature Neuroscience* **15,** 592–599 (2012).

127. Choi, J.-H., Sim, S.-E., Kim, J.-I., Choi, D. I., Oh, J., *et al.* Inter-regional synaptic maps among engram cells underlie memory formation. *Science* **360,** 430–435 (2018).

128. Han, J.-H., Kushner, S., Yiu, A. P., Cole, C. J., Matynia, A., *et al.* Neuronal competition and selection during memory formation. *Science* **316,** 457–460 (2007).

129. Euston, D. R., Gruber, A. J. & McNaughton, B. L. The role of medial prefrontal cortex in memory and decision making. *Neuron* **76,** 1057–1070 (2012).

130. Carlén, M. What constitutes the prefrontal cortex? *Science* **358,** 478–482 (2017).

131. Laubach, M., Amarante, L. M., Swanson, K. & White, S. R. What, if anything, is rodent prefrontal cortex? *eNeuro* **5,** 315–333 (2018).

132. Rose, J. E. & Woolsey, C. N. The orbitofrontal cortex and its connections with the mediodorsal nucleus in rabbit, sheep and cat. *Research Publications-Association for Research in Nervous and Mental Disease* **27,** 210–232 (1948).

133. Uylings, H. B., Groenewegen, H. J. & Kolb, B. Do rats have a prefrontal cortex? *Behavioural Brain Research* **146,** 3–17 (2003).

134. Brodmann, K. *Vergleichende Lokalisationslehre der Grobhirnrinde in ihren Prinzipien dargestellt auf Grund des Zellenbaues* (Johann Ambrosius Barth, Leipzig, 1909).

135. Preuss, T. M. Do rats have prefrontal cortex? The Rose-Woolsey-Akert program reconsidered. *Journal of Cognitive Neuroscience* **7,** 1–24 (1995).

136. Guldin, W. O., Pritzel, M. & Markowitsch, H. J. Prefrontal cortex of the mouse defined as cortical projection area of the thalamic mediodorsal nucleus. *Brain, behavior and evolution* **19,** 93–107 (1981).

137. Rikhye, R. V., Gilra, A. & Halassa, M. M. Thalamic regulation of switching between cortical representations enables cognitive flexibility. *Nature Neuroscience* **21,** 1753–1763 (2018).

138. Marton, T. F., Seifikar, H., Luongo, F. J., Lee, A. T. & Sohal, V. S. Roles of prefrontal cortex and mediodorsal thalamus in task engagement and behavioral flexibility. *Journal of Neuroscience* **38,** 2569–2578 (2018).

139. Deacon, R. M. J., Penny, C. & Rawlins, J. N. P. Effects of medial prefrontal cortex cytotoxic lesions in mice. *Behavioural Brain Research* **139,** 139–155 (2003).

140.   Pinto, L. & Dan, Y. Cell-type-specific activity in prefrontal cortex during goal-directed behavior. *Neuron* **87,** 437–450 (2015).

141.   Otis, J. M., Namboodiri, V. M., Matan, A. M., Voets, E. S., Mohorn, E. P., *et al.* Prefrontal cortex output circuits guide reward seeking through divergent cue encoding. *Nature* **543,** 103–107 (2017).

142.   Spellman, T., Rigotti, M., Ahmari, S. E., Fusi, S., Gogos, J. A., *et al.* Hippocampal-prefrontal input supports spatial encoding in working memory. *Nature* **522,** 309–314 (2015).

143.   Fuster, J. *The prefrontal cortex* (Academic Press, Cambridge, Massachusetts, 2015).

144.   Liu, D., Gu, X., Zhu, J., Zhang, X., Han, Z., *et al.* Medial prefrontal activity during delay period contributes to learning of a working memory task. *Science* **346,** 458–463 (2014).

145.   Fuster, J. M. & Alexander, G. E. Neuron activity related to short-term memory. *Science* **173,** 652–654 (1971).

146.   Schneider, W. X., Owen, A. M. & Duncan, J. *Executive control and the frontal lobe: Current issues* (Springer Science & Business Media, Berlin, 2012).

147.   Juavinett, A. L., Bekheet, G. & Churchland, A. K. Chronically implanted neuropixels probes enable high-yield recordings in freely moving mice. *eLife* **8,** 1–17 (2019).

148.   Tian, L., Hires, S. A., Mao, T., Huber, D., Chiappe, M. E., *et al.* Imaging neural activity in worms, flies and mice with improved GCaMP calcium indicators. *Nature Methods* **6,** 875–881 (2009).

149.   Chen, T. W., Wardill, T. J., Sun, Y., Pulver, S. R., Renninger, S. L., *et al.* Ultrasensitive fluorescent proteins for imaging neuronal activity. *Nature* **499,** 295–300 (2013).

150.   Yang, W. & Yuste, R. In vivo imaging of neural activity. *Nature Methods* **14,** 349–359 (2017).

151.   Helmchen, F. & Denk, W. Deep tissue two-photon microscopy. *Nature Methods* **2,** 932–940 (2005).

152.   Ghosh, K. K., Burns, L. D., Cocker, E. D., Nimmerjahn, A., Ziv, Y., *et al.* Miniaturized integration of a fluorescence microscope. *Nature Methods* **8,** 871–878 (2011).

153.   Harris, K. D., Henze, D. A., Csicsvari, J., Hirase, H. & Buzsáki, G. Accuracy of tetrode spike separation as determined by simultaneous intracellular and extracellular measurements. *Journal of Neurophysiology* **84,** 401–414 (2000).

154.   Holtmaat, A., Bonhoeffer, T., Chow, D. K., Chuckowree, J., De Paola, V., *et al.* Long-term, high-resolution imaging in the mouse neocortex through a chronic cranial window. *Nature Protocols* **4,** 1128–1144 (2009).

155.   Denk, W., Strickler, J. H. & Webb, W. W. Two-photon laser scanning fluorescence microscopy. *Science* **248,** 73–76 (1990).

156. Low, R. J., Gu, Y. & Tank, D. W. Cellular resolution optical access to brain regions in fissures: Imaging medial prefrontal cortex and grid cells in entorhinal cortex. *Proceedings of the National Academy of Sciences of the United States of America* **111,** 18739–18744 (2014).

157. Zong, W., Wu, R., Li, M., Hu, Y., Li, Y., *et al.* Fast high-resolution miniature two-photon microscopy for brain imaging in freely behaving mice. *Nature Methods* **14,** 713–719 (2017).

158. Place, R., Farovik, A., Brockmann, M. & Eichenbaum, H. Bidirectional prefrontal-hippocampal interactions support context-guided memory. *Nature Neuroscience* **19,** 992–994 (2016).

159. Niell, C. M. & Stryker, M. P. Highly selective receptive fields in mouse visual cortex. *Journal of Neuroscience* **28,** 7520–7536 (2008).

160. Skinner, B. *The behavior of organisms: An experimental analysis* (D. Appleton & Company, Boston, 1938).

161. Stone, C., Darrow, C., Landis, C & Heath, L. *Studies in the dynamics of behavior.* (University of Chicago Press, Chicago, 1932).

162. O'Keefe, J. & Dostrovsky, J. The hippocampus as a spatial map. Preliminary evidence from unit activity in the freely-moving rat. *Brain Research* **34,** 171–175 (1971).

163. Harvey, C. D., Collman, F., Dombeck, D. A. & Tank, D. W. Intracellular dynamics of hippocampal place cells during virtual navigation. *Nature* **461,** 941–946 (2009).

164. O'Connor, D. H., Peron, S. P., Huber, D. & Svoboda, K. Neural activity in barrel cortex underlying vibrissa-based object localization in mice. *Neuron* **67,** 1048–1061 (2010).

165. Histed, M. H., Carvalho, L. A. & Maunsell, J. H. Psychophysical measurement of contrast sensitivity in the behaving mouse. *Journal of Neurophysiology* **107,** 758–765 (2012).

166. Sanders, J. I. & Kepecs, A. Choice ball: A response interface for two-choice psychometric discrimination in head-fixed mice. *Journal of Neurophysiology* **108,** 3416–3423 (2012).

167. Abraham, N. M., Guerin, D., Bhaukaurally, K. & Carleton, A. Similar odor discrimination behavior in head-restrained and freely moving mice. *PLOS ONE* **7,** 1–9 (2012).

168. Poort, J., Khan, A. G., Pachitariu, M., Nemri, A., Orsolic, I., *et al.* Learning enhances sensory and multiple non-sensory representations in primary visual cortex. *Neuron* **86,** 1478–1490 (2015).

169. Burgess, C. P., Lak, A., Steinmetz, N. A., Zatka-Haas, P., Bai Reddy, C., *et al.* High-yield methods for accurate two-alternative visual psychophysics in head-fixed mice. *Cell Reports* **20,** 2513–2524 (2017).

170. Aronov, D. & Tank, D. W. Engagement of neural circuits underlying 2D spatial navigation in a rodent virtual reality system. *Neuron* **84,** 442–456 (2014).

171. Dombeck, D. A., Khabbaz, A. N., Collman, F., Adelman, T. L. & Tank, D. W. Imaging large-scale neural activity with cellular resolution in awake, mobile mice. *Neuron* **56,** 43–57 (2007).

172. Harvey, C. D., Coen, P. & Tank, D. W. Choice-specific sequences in parietal cortex during a virtual-navigation decision task. *Nature* **484,** 62–68 (2012).

173. Keller, G. B., Bonhoeffer, T. & Hübener, M. Sensorimotor mismatch signals in primary visual cortex of the behaving mouse. *Neuron* **74,** 809–815 (2012).

174. Andermann, M. M. L., Kerlin, A. M. & Reid, R. C. Chronic cellular imaging of mouse visual cortex during operant behavior and passive viewing. *Frontiers in Cellular Neuroscience* **4,** 1–16 (2010).

175. Makino, H. & Komiyama, T. Learning enhances the relative impact of top-down processing in the visual cortex. *Nature Neuroscience* **18,** 1116–1122 (2015).

176. Allen, W. E., DeNardo, L. A., Chen, M. Z., Liu, C. D., Loh, K. M., *et al.* Thirst-associated preoptic neurons encode an aversive motivational drive. *Science* **357,** 1149–1155 (2017).

177. Toth, L. A. & Gardiner, T. W. Food and water restriction protocols: physiological and behavioral considerations. *Contemporary Topics in Laboratory Animal Science* **39,** 9–17 (2000).

178. Krashes, M. J., Shah, B. P., Madara, J. C., Olson, D. P., Strochlic, D. E., *et al.* An excitatory paraventricular nucleus to AgRP neuron circuit that drives hunger. *Nature* **507,** 238–242 (2014).

179. Jourjine, N., Mullaney, B. C., Mann, K. & Scott, K. Coupled sensing of hunger and thirst signals balances sugar and water consumption. *Cell* **166,** 855–866 (2016).

180. Giles, J. M., Whitaker, J. W., Moy, S. S. & Fletcher, C. A. Effect of environmental enrichment on aggression in BALB/cJ and BALB/cByJ mice monitored by using an automated system. *Journal of the American Association for Laboratory Animal Science* **57,** 236–243 (2018).

181. Ullman-Culleré, M. H. & Foltz, C. J. Body condition scoring: A rapid and accurate method for assessing health status in mice. *Laboratory Animal Science* **49,** 319–323 (1999).

182. Hölscher, C., Schnee, A., Dahmen, H., Setia, L. & Mallot, H. A. Rats are able to navigate in virtual environments. *Journal of Experimental Biology* **208,** 561–569 (2005).

183. Scott, B. B., Brody, C. D. & Tank, D. W. Cellular resolution functional imaging in behaving rats using voluntary head restraint. *Neuron* **80,** 371–384 (2013).

184. Weijnen, J. A. Lick sensors as tools in behavioral and neuroscience research. *Physiology and Behavior* **46,** 923–928 (1989).

185. Slotnick, B. A simple 2-transistor touch or lick detector circuit. *Journal of the Experimental Analysis of Behavior* **91,** 253–255 (2009).

186. Debold, R. C. & Jensen, D. D. Effect of strength of drive determined by a new technique for appetitive classical conditioning of rats. *Learning, Motivation, and Their Physiological Mechanisms* **59,** 492–504 (2017).

187. Li, H., Liang, A., Guan, F., Fan, R., Chi, L., *et al.* Regular treadmill running improves spatial learning and memory performance in young mice through increased hippocampal neurogenesis and decreased stress. *Brain Research* **1531,** 1–8 (2013).

188. Sherwin, C. Voluntary wheel running: A review and novel interpretation. *Animal Behaviour* **56,** 11–27 (1998).

189. Ritter, R. C. & Epstein, A. Saliva lost by grooming: A major item in the rat's water economy. *Behavioral Biology* **585,** 581–585 (1974).

190. Haines, H., Ciskowski, C. & Harms, V. Acclimation to chronic water restriction in the wild house mouse Mus musculus. *Physiological Zoology* **46,** 186–207 (1973).

191. Rowland, N. E. Food or fluid restriction in common laboratory animals: Balancing welfare considerations with scientific inquiry. *Comparative Medicine* **57,** 149–160 (2007).

192. Busse, L., Ayaz, A., Dhruv, N. T., Katzner, S., Saleem, A. B., *et al.* The detection of visual contrast in the behaving mouse. *Journal of Neuroscience* **31,** 11351–11361 (2011).

193. Montijn, J. S., Goltstein, P. M. & Pennartz, C. M. Mouse V1 population correlates of visual detection rely on heterogeneity within neuronal response patterns. *eLife* **4,** 1–31 (2015).

194. Jurjut, O., Georgieva, P., Busse, L. & Katzner, S. Learning enhances sensory processing in mouse V1 before improving behavior. *Journal of Neuroscience* **37,** 6460–6474 (2017).

195. Bekkevold, C. M., Robertson, K. L., Reinhard, M. K., Battles, A. H. & Rowland, N. E. Dehydration parameters and standards for laboratory mice. *Journal of the American Association for Laboratory Animal Science* **52,** 233–239 (2013).

196. Komai, S., Denk, W., Osten, P., Brecht, M. & Margrie, T. W. Two-photon targeted patching (TPTP) in vivo. *Nature Protocols* **1,** 647–652 (2006).

197. Mardinly, A. R., Oldenburg, I. A., Pégard, N. C., Sridharan, S., Lyall, E. H., *et al.* Precise multimodal optical control of neural ensemble activity. *Nature Neuroscience* **21,** 881–893 (2018).

198. Liberti, W. A., Markowitz, J. E., Perkins, L. N., Liberti, D. C., Leman, D. P., *et al.* Unstable neurons underlie a stable learned behavior. *Nature Neuroscience* **19,** 1665–1671 (2016).

199. Betley, J. N., Xu, S., Fang, Z., Cao, H., Gong, R., *et al.* Neurons for hunger and thirst transmit a negative-valence teaching signal. *Nature* **521,** 180–185 (2015).

200. Ziv, Y., Burns, L. D., Cocker, E. D., Hamel, E. O., Ghosh, K. K., *et al.* Long-term dynamics of CA1 hippocampal place codes. *Nature neuroscience* **16,** 264–266 (2013).

201. Kamigaki, T. & Dan, Y. Delay activity of specific prefrontal interneuron subtypes modulates memory-guided behavior. *Nature neuroscience* **20,** 854–863 (2017).

202. Hubel, B. Y. D. H. & Wiesel, A. D. T. N. Receptive fields, binocular interaction and functional architecture in the cat's visual cortex. *Journal of Physiology* **160,** 106–154 (1962).

203. Mank, M., Santos, A. F., Direnberger, S., Mrsic-Flogel, T. D., Hofer, S. B., *et al.* A genetically encoded calcium indicator for chronic in vivo two-photon imaging. *Nature Methods* **5,** 805–811 (2008).

204. Rose, T., Jaepel, J., Hübener, M. & Bonhoeffer, T. Cell-specific restoration of stimulus preference after monocular deprivation in the visual cortex. *Science* **352,** 1319–1322 (2016).

205. Schuett, S., Bonhoeffer, T. & Hübener, M. Mapping retinotopic structure in mouse visual cortex with optical imaging. *Journal of Neuroscience* **22,** 6549–6559 (2002).

206. Grinvald, A. & Bonhoeffer, T. *Optical imaging of electrical activity based on intrinsic signals and on voltage sensitive dyes* 55–97 (Academic Press, Cambridge, Massachusetts, 1996).

207. Leinweber, M., Zmarz, P., Buchmann, P., Argast, P., Hübener, M., *et al.* Two-photon calcium imaging in mice navigating a virtual reality environment. *Journal of Visualized Experiments* **84** (2014).

208. Schindelin, J., Arganda-Carreras, I., Frise, E., Kaynig, V., Longair, M., *et al.* Fiji: An open-source platform for biological-image analysis. *Nature Methods* **9,** 676–682 (2012).

209. Guizar-Sicairos, M., Thurman, S. T. & Fienup, J. R. Efficient subpixel image registration algorithms. *Optics Letters* **33,** 156 (2008).

210. Kerlin, A. M., Andermann, M. L., Berezovskii, V. K. & Reid, R. C. Broadly tuned response properties of diverse inhibitory neuron subtypes in mouse visual cortex. *Neuron* **67,** 858–871 (2010).

211. Zhou, P., Resendez, S. L., Rodriguez-Romaguera, J., Jimenez, J. C., Neufeld, S. Q., *et al.* Efficient and accurate extraction of in vivo calcium signals from microendoscopic video data. *eLife* **7,** 1–37 (2018).

212. Greenberg, D. S., Houweling, A. R. & Kerr, J. N. Population imaging of ongoing neuronal activity in the visual cortex of awake rats. *Nature Neuroscience* **11,** 749–751 (2008).

213. Mazurek, M., Kager, M. & Van Hooser, S. D. Robust quantification of orientation selectivity and direction selectivity. *Frontiers in Neural Circuits* **8,** 1–17 (2014).

214. Ringach, D. L., Shapley, R. M. & Hawken, M. J. Orientation selectivity in macaque V1: Diversity and laminar dependence. *The Journal of neuroscience* **22,** 5639–5651 (2002).

215. Berens, P. CircStat: A MATLAB toolbox for circular statistics. *Journal of Statistical Software* **31,** 1–21 (2009).

216. Klaus, A., Martins, G. J., Paixao, V. B., Zhou, P., Paninski, L., *et al.* The spatiotemporal organization of the striatum encodes action space. *Neuron* **95,** 1171–1180 (2017).

217. Keemink, S. W., Lowe, S. C., Pakan, J. M., Dylda, E., Van Rossum, M. C., *et al.* FISSA: A neuropil decontamination toolbox for calcium imaging signals. *Scientific Reports* **8,** 1–12 (2018).

218. Lu, J., Li, C., Singh-Alvarado, J., Zhou, Z. C., Fröhlich, F., *et al.* MIN1PIPE: A miniscope 1-photon-based calcium imaging signal extraction pipeline. *Cell Reports* **23,** 3673–3684 (2018).

219. Goltstein, P. M., Montijn, J. S. & Pennartz, C. M. Effects of isoflurane anesthesia on ensemble patterns of Ca2+ activity in mouse V1: Reduced direction selectivity independent of increased correlations in cellular activity. *PLOS ONE* **10,** 1–31 (2015).

220. Polack, P. O., Friedman, J. & Golshani, P. Cellular mechanisms of brain state-dependent gain modulation in visual cortex. *Nature Neuroscience* **16,** 1331–1339 (2013).

221. Yu, H., Senarathna, J., Tyler, B. M., Thakor, N. V. & Pathak, A. P. Miniaturized optical neuroimaging in unrestrained animals. *NeuroImage* **113,** 397–406 (2015).

222. Armbruster, B. N., Li, X., Pausch, M. H., Herlitze, S. & Roth, B. L. Evolving the lock to fit the key to create a family of G protein-coupled receptors potently activated by an inert ligand. *Proceedings of the National Academy of Sciences of the United States of America* **104,** 5163–5168 (2007).

223. De Bruin, J. P., Sànchez-Santed, F., Heinsbroek, R. P., Donker, A. & Postmes, P. A behavioural analysis of rats with damage to the medial prefrontal cortex using the Morris water maze: Evidence for behavioural flexibility, but not for impaired spatial navigation. *Brain Research* **652,** 323–333 (1994).

224. Czajkowski, R., Jayaprakash, B., Wiltgen, B., Rogerson, T., Guzman-Karlsson, M. C., *et al.* Encoding and storage of spatial information in the retrosplenial cortex. *Proceedings of the National Academy of Sciences of the United States of America* **111,** 8661–8666 (2014).

225. Gdalyahu, A., Tring, E., Polack, P. O., Gruver, R., Golshani, P., *et al.* Associative fear learning enhances sparse network coding in primary sensory cortex. *Neuron* **75,** 121–132 (2012).

226. Holtmaat, A. & Caroni, P. Functional and structural underpinnings of neuronal assembly formation in learning. *Nature Neuroscience* **19,** 1553–1562 (2016).

227. Lin, A. C., Bygrave, A. M., De Calignon, A., Lee, T. & Miesenböck, G. Sparse, decorrelated odor coding in the mushroom body enhances learned odor discrimination. *Nature Neuroscience* **17,** 559–568 (2014).

228. Maddock, R. J. The retrosplenial cortex and emotion: New insights from functional neuroimaging of the human brain. *Trends in Neurosciences* **22,** 310–316 (1999).

229. Milczarek, M. M., Vann, S. D. & Sengpiel, F. Spatial memory engram in the mouse retrosplenial cortex. *Current Biology* **28,** 1975–1980 (2018).

230. Morrison, D. J., Rashid, A. J., Yiu, A. P., Yan, C., Frankland, P. W., *et al.* Parvalbumin interneurons constrain the size of the lateral amygdala engram. *Neurobiology of Learning and Memory* **135,** 91–99 (2016).

231. Nadel, L. & Moscovitch, M. Memory consolidation, retrograde amnesia and the hippocampal complex. *Current Opinion in Neurobiology* **7,** 217–227 (1997).

232. Pignatelli, M., Ryan, T. J., Roy, D. S., Lovett, C., Smith, L. M., *et al.* Engram cell excitability state determines the efficacy of memory retrieval. *Neuron* **101,** 274–284 (2019).

233. Rashid, A. J., Yan, C., Mercaldo, V., Hsiang, H.-l. L., Park, S., *et al.* Competition between engrams influences fear memory formation and recall. *Science* **353,** 383–387 (2016).

234. Runyan, C. A., Piasini, E., Panzeri, S. & Harvey, C. D. Distinct timescales of population coding across cortex. *Nature* **548,** 92–96 (2017).

235. Sekeres, M. J., Winocur, G. & Moscovitch, M. The hippocampus and related neocortical structures in memory transformation. *Neuroscience Letters* **680,** 39–53 (2018).

236. Vyazovskiy, V. V., Cirelli, C., Pfister-Genskow, M., Faraguna, U. & Tononi, G. Molecular and electrophysiological evidence for net synaptic potentiation in wake and depression in sleep. *Nature Neuroscience* **11,** 200–208 (2008).

237. Keenan, K. P., Hoe, C. M., Mixson, L., McCoy, C. L., Coleman, J. B., *et al.* Diabesity: A polygenic model of dietary-induced obesity from ad libitum overfeeding of Sprague-Dawley rats and its modulation by moderate and marked dietary restriction. *Toxicologic pathology* **33,** 650–674 (2005).

238. Jensen, T. L., Kiersgaard, M. K., Sørensen, D. B. & Mikkelsen, L. F. Fasting of mice: A review. *Laboratory Animals* **47,** 225–240 (2013).

239. Speakman, J. R. & Mitchell, S. E. Caloric restriction. *Molecular Aspects of Medicine* **32,** 159–221 (2011).

240. Méquinion, M., Caron, E., Zgheib, S., Stievenard, A., Zizzari, P., *et al.* Physical activity: Benefit or weakness in metabolic adaptations in a mouse model of chronic food restriction? *American Journal of Physiology - Endocrinology and Metabolism* **308,** E241–E255 (2015).

241. Tye, K. M., Stuber, G. D., De Ridder, B., Bonci, A. & Janak, P. H. Rapid strengthening of thalamo-amygdala synapses mediates cue-reward learning. *Nature* **453,** 1253–1257 (2008).

242. Russell, W. M. S. & Burch, R. L. *The principles of humane experimental technique* (Methuen, London, 1959).

243. Rowland, N. E., Cansler, K., Kim, E., Pawlik, N. & Robertson, K. L. Flavor avoidance induced by LiCl and dexfenfluramine in rats and mice using nondeprivation protocols. *Behavioral Neuroscience* **116,** 777–784 (2002).

244. Urai, A. E., Aguillon-rodriguez, V., Cazettes, F., International, T., Mainen, Z. F., *et al.* Citric acid water as an alternative to water scheduling in behaving mice. *bioRxiv* (2020).

245. Zou, H., Yin, P., Liu, L., Liu, W., Zhang, Z., *et al.* Body-weight fluctuation was associated with increased risk for cardiovascular disease, all-cause and cardiovascular mortality: A systematic review and meta-analysis. *Frontiers in Endocrinology* **10,** 1–9 (2019).

246. Prescott, M. J., Brown, V. J., Flecknell, P. A., Gaffan, D., Garrod, K., *et al.* Refinement of the use of food and fluid control as motivational tools for macaques used in behavioural neuroscience research: Report of a working group of the NC3Rs. *Journal of Neuroscience Methods* **193,** 167–188 (2010).

247. Stafford, A. M., Anderson, S. M., Shelton, K. L. & Brunzell, D. H. Oral operant ethanol self-administration in the absence of explicit cues, food restriction, water restriction and ethanol fading in C57BL/6J mice. *Psychopharmacology* **232,** 3783–3795 (2015).

248. Rose, T., Goltstein, P. M., Portugues, R. & Griesbeck, O. Putting a finishing touch on GECIs. *Frontiers in Molecular Neuroscience* **7,** 1–15 (2014).

249. Dana, H., Sun, Y., Mohar, B., Hulse, B. K., Kerlin, A. M., *et al.* High-performance calcium sensors for imaging activity in neuronal populations and microcompartments. *Nature Methods* **16,** 649–657 (2019).

250. Pologruto, T. A., Yasuda, R. & Svoboda, K. Monitoring neural activity and [Ca2+] with genetically encoded Ca2+ indicators. *Journal of Neuroscience* **24,** 9572–9579 (2004).

251. Yang, Y., Liu, N., He, Y., Liu, Y., Ge, L., *et al.* Improved calcium sensor GCaMP-X overcomes the calcium channel perturbations induced by the calmodulin in GCaMP. *Nature Communications* **9,** 1–18 (2018).

252. Bootman, M. D., Allman, S., Rietdorf, K. & Bultynck, G. Delete-rious effects of calcium indicators within cells; an inconvenient truth. *Cell Calcium* **73,** 82–87 (2018).

253. Kerr, J. N., Greenberg, D. S. & Helmchen, F. Imaging input and output of neocortical networks in vivo. *Proceedings of the National Academy of Sciences of the United States of America* **102,** 14063–14068 (2005).

254. Dana, H., Chen, T. W., Hu, A., Shields, B. C., Guo, C., *et al.* Thy1-GCaMP6 transgenic mice for neuronal population imaging in vivo. *PLOS ONE* **9,** 1–9 (2014).

255. Steinmetz, N. A., Buetfering, C., Lecoq, J., Lee, C. R., Peters, A. J., *et al.* Aberrant cortical activity in multiple GCaMP6-expressing transgenic mouse lines. *eNeuro* **4** (2017).

256. Pnevmatikakis, E. A. Analysis pipelines for calcium imaging data. *Current Opinion in Neurobiology* **55,** 15–21 (2019).

257. Mukamel, E. A., Nimmerjahn, A. & Schnitzer, M. J. Automated analysis of cellular signals from large-scale calcium imaging data. *Neuron* **63,** 747–760 (2009).

258. Friedrich, J., Giovannucci, A. & Pnevmatikakis, E. A. Online analysis of microendoscopic 1-photon calcium imaging data streams. *bioRxiv* (2020).

259. Huang, L., Zhou, X., Liu, Q., MacAulay, C. E. & Tang, S. Minia-turized multimodal multiphoton microscope for simultaneous two-photon and three-photon imaging with a dual-wavelength Er-doped fiber laser. *Biomedical Optics Express* **11,** 624–635 (2020).

260. Zhao, Y., Araki, S., Wu, J., Teramoto, T., Nagai, T., *et al.* An expanded palette of genetically encoded Ca2+ indicators. *Science* **333,** 1888–1891 (2011).

261. Shuman, T., Aharoni, D., Cai, D. J., Lee, C. R., Chavlis, S., *et al.* Breakdown of spatial coding and interneuron synchronization in epileptic mice. *Nature Neuroscience* **23,** 229–238 (2020).

262. Helmchen, F., Denk, W. & Kerr, J. N. Miniaturization of two-photon microscopy for imaging in freely moving animals. *Cold Spring Harbor Protocols* **2013,** 904–913 (2013).

263. Sih, A. Optimal behavior: Can foragers balance two conflicting demands? *Science* **210,** 1041–1043 (1980).

264. Powell, F. & Banks, P. B. Do house mice modify their foraging behaviour in response to predator odours and habitat? *Animal Behaviour* **67,** 753–759 (2004).

265. Morris, D. W. & Davidson, D. L. Optimally foraging mice match patch use with habitat differences in fitness. *Ecology* **81,** 2061–2066 (2000).

266. Orrock, J. L. & Danielson, B. J. Temperature and cloud cover, but not predator urine, affect winter foraging of mice. *Ethology* **115,** 641–648 (2009).

267. Ebersole, J. P. & Wilson, J. C. Optimal foraging: The responses of Peromyscus leucopus to experimental changes in processing time and hunger. *Oecologia* **46,** 80–85 (1980).

268. Mobbs, D., Trimmer, P. C., Blumstein, D. T. & Dayan, P. Foraging for foundations in decision neuroscience: Insights from ethology. *Nature Reviews Neuroscience* **19,** 419–427 (2018).

269. Datta, S. R., Anderson, D. J., Branson, K., Perona, P. & Leifer, A. Computational neuroethology: A call to action. *Neuron* **104,** 11–24 (2019).

270. Maat, A. T., Trost, L., Sagunsky, H., Seltmann, S. & Gahr, M. Zebra finch mates use their forebrain song system in unlearned call communication. *PLOS ONE* **9,** 1–9 (2014).

271. Sarel, A., Finkelstein, A., Las, L. & Ulanovsky, N. Vectorial representation of spatial goals in the hippocampus of bats. *Science* **355,** 176–180 (2017).

272. Luo, L. *Principles of Neurobiology* (Garland Science, Abingdon, 2016).

273. Bast, T. Distinct contributions of hippocampal NMDA and AMPA receptors to encoding and retrieval of one-trial place memory. *Journal of Neuroscience* **25,** 5845–5856 (2005).

274. Wang, B. & Chen, J. Seed size, more than nutrient or tannin content, affects seed caching behavior of a common genus of Old World rodents. *Ecology* **90,** 3023–3032 (2009).

275. Pastro, L. A. & Banks, P. B. Foraging responses of wild house mice to accumulations of conspecific odor as a predation risk. *Behavioral Ecology and Sociobiology* **60,** 101–107 (2006).

276. Chorev, E., Epsztein, J., Houweling, A. R., Lee, A. K. & Brecht, M. Electrophysiological recordings from behaving animals-going beyond spikes. *Current Opinion in Neurobiology* **19,** 513–519 (2009).

277. Jennings, J. H., Ung, R. L., Resendez, S. L., Stamatakis, A. M., Taylor, J. G., *et al.* Visualizing hypothalamic network dynamics for appetitive and consummatory behaviors. *Cell* **160,** 516–527 (2015).

278. Murugan, M., Jang, H. J., Park, M., Miller, E. M., Cox, J., *et al.* Combined social and spatial coding in a descending projection from the prefrontal cortex. *Cell* **171,** 1663–1677 (2017).

279. Remedios, R., Kennedy, A., Zelikowsky, M., Grewe, B. F., Schnitzer, M. J., *et al.* Social behaviour shapes hypothalamic neural ensemble representations of conspecific sex. *Nature* **550,** 388–392 (2017).

280. Gomez-Marin, A., Paton, J. J., Kampff, A. R., Costa, R. M. & Mainen, Z. F. Big behavioral data: Psychology, ethology and the foundations of neuroscience. *Nature Neuroscience* **17,** 1455–1462 (2014).

281. Deisseroth, K. Optogenetics. *Nature Methods* **8,** 26–29 (2011).

282. Mathis, A., Mamidanna, P., Cury, K. M., Abe, T., Murthy, V. N., *et al.* DeepLabCut: Markerless pose estimation of user-defined body parts with deep learning. *Nature Neuroscience* **21,** 1281–1289 (2018).

283. Cepeda, N. J., Pashler, H., Vul, E., Wixted, J. T. & Rohrer, D. Distributed practice in verbal recall tasks: A review and quantitative synthesis. *Psychological Bulletin* **132,** 354–380 (2006).

284. Kogan, J. H., Frankland, P. W., Blendy, J. A., Coblentz, J., Marowitz, Z., *et al.* Spaced training induces normal long-term memory in CREB mutant mice. *Current Biology* **7,** 1–11 (1997).

285. Klapdor, K. & Van Der Staay, F. J. Repeated acquisition of a spatial navigation task in mice: Effects of spacing of trials and of unilateral middle cerebral artery occlusion. *Physiology and Behavior* **63,** 903–909 (1998).

286. Kesner, R. P. & Churchwell, J. C. An analysis of rat prefrontal cortex in mediating executive function. *Neurobiology of Learning and Memory* **96,** 417–431 (2011).

287. Redondo, R. L. & Morris, R. G. M. Making memories last: The synaptic tagging and capture hypothesis. *Nature reviews. Neuroscience* **12,** 17–30 (2011).

288. Lee, S. J. R., Escobedo-Lozoya, Y., Szatmari, E. M. & Yasuda, R. Activation of CaMKII in single dendritic spines during long-term potentiation. *Nature* **458,** 299–304 (2009).

289. Moyer, J. R., Thompson, L. T. & Disterhoft, J. F. Trace eyeblink conditioning increases CA1 excitability in a transient and learning-specific manner. *Journal of Neuroscience* **16,** 5536–5546 (1996).

290. Zhou, Y., Won, J., Karlsson, M. G., Zhou, M., Rogerson, T., *et al.* CREB regulates excitability and the allocation of memory to subsets of neurons in the amygdala. *Nature Neuroscience* **12,** 1438–1443 (2009).

291. Nägerl, U. V., Eberhorn, N., Cambridge, S. B. & Bonhoeffer, T. Bidirectional activity-dependent morphological plasticity in hippocampal neurons. *Neuron* **44,** 759–767 (2004).

292. Nägerl, U. V., Willig, K. I., Hein, B., Hell, S. W. & Bonhoeffer, T. Live-cell imaging of dendritic spines by STED microscopy. *Proceedings of the National Academy of Sciences of the United States of America* **105,** 18982–18987 (2008).

293. Madigan, S. A. Intraserial repetition and coding processes in free recall. *Journal of Verbal Learning and Verbal Behavior* **8,** 828–835 (1969).

294. Hintzman, D. L. in *Theories in Cognitive Psychology: The Loyola Symposium Proceedings* 77–99 (Halsted Press, New York, 1974).

295. Miller, E. K., Li, L. & Desimone, R. A neural mechanism for working and recognition memory in inferior temporal cortex. *Science* **254,** 1377–1379 (1991).

296. Summerfield, C., Trittschuh, E. H., Monti, J. M., Mesulam, M. M. & Egner, T. Neural repetition suppression reflects fulfilled perceptual expectations. *Nature Neuroscience* **11,** 1004–1006 (2008).

297. Feng, K., Zhao, X., Liu, J., Cai, Y., Ye, Z., *et al.* Spaced learning enhances episodic memory by increasing neural pattern similarity across repetitions. *Journal of Neuroscience* **39,** 5351–5360 (2019).

298. Callan, D. E. & Schweighofer, N. Neural correlates of the spacing effect in explicit verbal semantic encoding support the deficient-processing theory. *Human Brain Mapping* **31,** 645–659 (2010).

299. Zhao, X., Wang, C., Liu, Q., Xiao, X., Jiang, T., *et al.* Neural mechanisms of the spacing effect in episodic memory: A parallel EEG and fMRI study. *Cortex* **69,** 76–92 (2015).

300. Hintzman, D. L. & Block, R. A. Memory for the spacing of repetitions. *Journal of Experimental Psychology* **99,** 70–74 (1973).

301. Xue, G., Dong, Q., Chen, C., Lu, Z., Mumford, J. A., *et al.* Greater neural pattern similarity across repetitions is associated with better memory. *Science* **330,** 97–101 (2010).

302. Purpura, D. P. Dendritic spine "dysgenesis" and mental retardation. *Science* **186,** 1126–1128 (1974).

303. Lauterborn, J. C., Schultz, M. N., Le, A. A., Amani, M., Friedman, A. E., *et al.* Spaced training improves learning in Ts65Dn and Ube3a mouse models of intellectual disabilities. *Translational Psychiatry* **9,** 1–16 (2019).

304. Riches, N. G., Tomasello, M. & Conti-Ramsden, G. Verb learning in children with SLI: Frequency and spacing effects. *Journal of Speech, Language, and Hearing Research* **48,** 1397–1411 (2005).

305. Schoephoerster, H. Research into variations of the test-study plan of teaching spelling. *Elementary English* **39,** 460–462 (1962).

306. Settles, B. & Meeder, B. A trainable spaced repetition model for language learning. *Proceedings of the 54th Annual Meeting of the Association for Computational Linguistics* **1,** 1848–1858 (2016).

307. Miyamoto, Y. R., Coleman, C. A., Williams, J. J., Whitehill, J., Nesterko, S., *et al.* Beyond time-on-task: The relationship between spaced study and certification in MOOCs. *Journal of Learning Analytics* **2,** 47–69 (2015).

308. Dumesnil, D. A. *The effects of spaced repetition in online education* PhD thesis (Massachusetts Institute of Technology, 2018), 1–64.

309. Misanin, J. R., Miller, R. R. & Lewis, D. J. Retrograde amnesia produced by electroconvulsive shock after reactivation of a consolidated memory trace. *Science* **160,** 554–555 (1968).

310. Nader, K., Schafe, G. E. & Le Doux, J. E. Fear memories require protein synthesis in the amygdala for reconsolidation after retrieval. *Nature* **406,** 722–726 (2000).

311. Eisenberg, M., Kobilo, T., Berman, D. E. & Dudai, Y. Stability of retrieved memory: Inverse correlation with trace dominance. *Science* **301,** 1102–1104 (2003).

312. Morris, R. G., Inglis, J., Ainge, J. A., Olverman, H. J., Tulloch, J., *et al.* Memory reconsolidation: Sensitivity of spatial memory to inhibition of protein synthesis in dorsal hippocampus during encoding and retrieval. *Neuron* **50,** 479–489 (2006).

313. Przybyslawski, J. & Sara, S. J. Reconsolidation of memory after its reactivation. *Behavioural Brain Research* **84,** 241–246 (1997).

314. Suzuki, A., Josselyn, S. A., Frankland, P. W., Masushige, S., Silva, A. J., *et al.* Memory reconsolidation and extinction have distinct temporal and biochemical signatures. *Journal of Neuroscience* **24,** 4787–4795 (2004).

315. Zhang, Y., Liu, R. Y., Heberton, G. A., Smolen, P., Baxter, D. A., *et al.* Computational design of enhanced learning protocols. *Nature Neuroscience* **15,** 294–297 (2012).

7

Species	Experimental category	Manipulations	Circuits	Spacing protocol	Reference
Cotesia glomerata *C. rubecula* (Parasitoid wasp)	*In vivo*	Behavioral | Ap.C. Pharmacology	N.A.	0 vs 10 min	Smid et al., 2007
Periplaneta americana (American cockroach)	*In vivo*	Behavioral	N.A.	20 sec vs 30 sec vs 2 vs 5 vs 7 vs 10 vs 15 min	Hosono, Matsumoto, & Mizunami, 2016
Lymnaea stagnalis (Pond snail)	*In vivo*	Behavioral Pharmacology	N.A.	0 vs 60 min	Sangha et al., 2003
Hermissenda crassicornis (Sea slug)	*In vivo* *In vitro*	Behavioral | Av.C. Electrophysiology	N.A.	30 vs 60 vs 120 sec	Rogers, Talk, & Matzel, 1994
Xenopus laevis (Clawed frog)	*Ex vivo*	Electrophysiology Pharmacology	Visual system	0 vs 2.5 vs 5 vs 10 vs 15 min	Gong et al., 2011
Canis familiaris (Domestic dog)	*In vivo*	Behavioral	N.A.	1 vs 7 days	Meyer & Ladewig, 2008
C. elegans (Nematode)	*In vivo*	Behavior | Hab.	N.A.	0 vs 60 min	Rose, Kaun, & Rankin, 2002
C. elegans	*In vivo*	Behavior | W.R.	N.A.	0 vs 60 min	Ebrahimi & Rankin, 2007
C. elegans	*In vivo*	Behavior | Av.C Pharmacology	N.A.	0 vs 10 min	Amano & Maruyama, 2011
C. elegans	*In vivo* *Ex vivo*	Behavioral | Ap.C. Molecular	N.A.	0 vs 30 min	Kauffman et al., 2011
C. elegans	*In vivo* *Ex vivo*	Behavioral | Hab. Genetic Molecular	PLM	0 vs 60 min	Li et al., 2013

Species	Method	Approach	Preparation	Time points	Reference	
C. elegans	*In vivo*	Behavioral | Ap.C. Pharmacology	N.A.	0 vs 10 min	Nishijima & Maruyama, 2017	
Aplysia californica (California sea hare)	*In vitro*	Molecular Pharmacology	Tail sensory neurons	0 vs 20 min	Farah, Weatherill, Dunn, & Sossin, 2009	*
A. californica	*In vitro*	Electrophysiology Molecular Pharmacology	Tail motor and sensory neural co-cultures	0 vs 20 min	McCamphill, Farah, Anadolu, Hoque, & Sossin, 2015	
A. californica	*Ex vivo*	Electrophysiology Pharmacology	Siphon withdrawal reflex circuit	0 vs 15 min	Mauelshagen, Sherff, & Carew, 1998	*
A. californica	*In vitro* *Ex vivo*	Behavioral | W.R. Molecular Pharmacology	Siphon withdrawal reflex circuit	15 vs 45 vs 60 min	Philips, Ye, Kopec, & Carew, 2013	*
A. californica	*In vivo* *Ex vivo*	Behavioral | W.R. Morphology	Siphon withdrawal reflex circuit	0.5 vs 24 hrs.	Wainwright, Zhang, Byrne, & Cleary, 2002	*
A. californica	*In vivo*	Behavioral | W.R.	Siphon withdrawal reflex circuit	1 sec vs 15 min	Sutton, Ide, Masters, & Carew, 2002	*
A. californica	*In vivo*	Behavioral Pharmacology	N.A.	0 vs 15 min	Michel, Gardner, Green, Organ, & Lyons, 2013	
A. californica	*In vivo*	Behavioral | Hab.	Siphon withdrawal reflex circuit	0 vs 24 hrs.	Holmes et al., 2015	
Drosophila melanogaster (Fruit fly)	*In vitro*	Electrophysiology Genetic Molecular	N.A.	0 vs 30 min	Lee & O'Dowd, 2000	
D. melanogaster	*Ex vivo*	Behavioral Electrophysiology Morphology	Neuromuscular junction	0 vs 15 min	Martin, Rela, Gelb, & Pagani, 2017	
D. melanogaster	*In vivo*	Behavioral | Av.C. Genetic Pharmacology	N.A.	0 vs 5 vs 10 vs 15	Tully, Preat, Boynton, & Del Vecchio, 1994	

D. melanogaster	*In vivo*	Behavioral | Av.C. Molecular Pharmacology	N.A.	0.5 vs 1 vs 5 vs 10 vs 15 vs 20 vs 30 vs 60 min	Beck, Schroeder, & Davis, 2000	*
D. melanogaster	*In vivo* *Ex vivo*	Behavioral | Av.C. Genetic Molecular	N.A.	0 vs 30 min	Drier et al., 2002	
D. melanogaster	*In vivo* *Ex vivo*	Behavioral | Av.C. Calcium imaging Genetic Molecular	Mushroom body	0 vs 15 min	Yu, Akalal, & Davis, 2006	*
D. melanogaster	*In vivo* *Ex vivo*	Behavioral | Av.C. Genetic Molecular Pharmacology	Mushroom body	45 vs 150 vs 900 sec	Pagani, Oishi, Gelb, & Zhong, 2009	*
D. melanogaster	*In vivo* *Ex vivo*	Behavioral | Av.C. Calcium imaging Genetic Molecular	Mushroom body	0 vs 15 min	Akalal, Yu, & Davis, 2010	*
D. melanogaster	*In vivo* *Ex vivo*	Behavioral | Av.C. Genetic Molecular	Mushroom body Dorsal-anterior-lateral neurons	0 vs 15 min	Chen et al., 2012	*
D. melanogaster	*In vivo* *Ex vivo*	Behavioral | Av.C. Calcium imaging Genetic Molecular	Mushroom body	0 vs 15 min	Plaçais et al., 2012	*
D. melanogaster	*In vivo* *Ex vivo*	Behavioral | Av.C. Genetic Molecular	Mushroom body Dorsal-anterior-lateral neurons	0 vs 15 min	Hirano et al., 2013	
D. melanogaster	*In vivo* *Ex vivo*	Behavioral | Av.C. Genetic	Mushroom body	0 vs 15 min	Zhao et al., 2013	

Species	Preparation	Approach	Region	Interval	Reference	
D. melanogaster	*In vivo*	Behavioral | Av.C. Genetic Molecular	Mushroom body	0 vs 15 min	Miyashita, Kikuchi, Horiuchi, & Saitoe, 2018	
D. melanogaster	*In vivo* *Ex vivo*	Behavioral | Av.C. Genetic Molecular	Mushroom body	0 vs 15 min	Awata et al., 2019	
Apis mellifera (Honey bee)	*In vivo*	Behavioral | Ap.C	N.A.	1 vs 10 min	Bitterman, Menzel, Fietz, & Schäfer, 1983	
A. mellifera	*In vivo*	Behavioral | Ap.C	N.A.	1 vs 10 min	Sandoz, Roger, & Pham-Delegue, 1995	
A. mellifera	*In vivo*	Behavioral | Ap.C Pharmacology	N.A.	30 sec vs 3 min vs 10 min	Menzel, Manz, Menzel, & Greggers, 2001	*
A. mellifera	*In vivo*	Behavioral | Ap.C	N.A.	1 vs 3 vs 5 vs 8 min	Deisig, Sandoz, Giurfa, & Lachnit, 2007	
A. mellifera	*In vivo*	Behavioral | Ap.C Pharmacology	N.A.	30 sec vs 10 min	Williamson & Wright, 2013	
A. mellifera	*In vivo*	Behavioral | Ap.C	N.A.	0.5 vs 30 min	Simcock, Gray, Bouchebti, & Wright, 2018	
A. mellifera	*In vivo*	Behavioral | Ap.C	N.A.	1 vs 10 min	Giurfa et al., 2009	
Bombus impatiens (Bumble bee)	*In vivo*	Behavioral | Ap.C	N.A.	1 vs 3 vs 5 min	Toda, Song, & Nieh, 2009	
Chasmagnathus granulatus (Neohelice crab)	*In vivo*	Behavioral | Hab. Pharmacology	N.A.	4 vs 85 sec	Berón De Astrada & Maldonado, 1999	
C. granulatus	*In vivo*	Behavioral | Hab. Pharmacology	N.A.	0 vs 171 sec	Hermitte, Pedreira, Tomsic, & Maldonado, 1999	
C. granulatus	*In vivo*	Behavioral | Hab.	N.A.	0 vs 171 sec	Pereyra, González Portino, & Maldonado, 2000	
C. granulatus	*In vivo*	Behavioral | Hab. Pharmacology	N.A.	0 vs 171 sec	Locatelli, Maldonado, & Romano, 2002	
C. granulatus	*In vivo* *Ex vivo*	Behavioral | Hab. Pharmacology Molecular	N.A.	0 vs 171 sec	Feld, Dimant, Delorenzi, Coso, & Romano, 2005	

██						
Danio rerio (Zebrafish)	*In vivo*	Behavioral	N.A.	0 vs 5 min	Roberts et al., 2011	
D. rerio	*In vivo*	Behavioral | Hab. Pharmacology	N.A.	0 vs 10 min	Wolman, Jain, Liss, & Granato, 2011	
██						
C. livia	*In vivo*	Behavioral	N.A.	0 vs 10 vs 20 sec	Grant, 2009	
C. livia	*In vivo*	Behavioral	N.A.	6 vs 60 sec	Adams & Santi, 2011	
██						
Mus musculus (House mouse)	*In vivo* *Ex vivo*	Behavioral Electrophysiology Molecular Pharmacology	Hippocampus	20 sec vs 5 min	Scharf et al., 2002	
M. musculus	*In vivo*	Behavioral | Av.C Behavioral | M.W.M. Behavioral Genetic	N.A.	1 vs 60 min 1 vs 10 vs 60 min 1 vs 60 min	Kogan et al., 1997	*
M. musculus	*In vivo*	Behavioral | Av.C Pharmacology	N.A.	6 vs 60 vs 600 sec	Cain, Blouin, & Barad, 2004	
M. musculus	*In vivo*	Behavioral | Av.C	N.A.	1 vs 7 vs 28 days	Matsuda, Matsuzawa, Ishii, Tomizawa, & Shimizu, 2014	
M. musculus	*In vivo* *Ex vivo*	Behavioral | Ap.C. Molecular Pharmacology	Olfactory bulb	15 min vs 24 hrs.	Kermen, Sultan, Sacquet, Mandairon, & Didier, 2010	
M. musculus	*In vivo*	Behavioral | O.R. Lesion	Fornix Amygdala	2 vs 24 hrs.	Aggleton, Kentridge, & Sembi, 1992	
M. musculus	*Ex vivo*	Behavioral | O.R. Genetic Molecular	Hippocampus Neocortex	0 vs 5 vs 15 min	Genoux et al., 2002	*

M. musculus	In vivo Ex vivo	Behavioral ∣ O.R. Genetic Molecular Pharmacology	Hippocampus	20 vs 60 vs 120 min	Seese, Wang, Yao, Lynch, & Gall, 2014	*
M. musculus	In vivo	Behavioral ∣ O.R.	N.A.	30 sec vs 4 min	Whitt & Robinson, 2013	
M. musculus	In vivo	Behavioral ∣ O.R. Behavioral ∣ M.W.M. Pharmacology	Hippocampus	0 vs 60 min 0 vs 60 min	Lauterborn et al., 2019	*
M. musculus	In vivo Ex vivo	Behavioral ∣ Hab. Pharmacology Morphology	Cerebellar cortex	0 vs 0.5 vs 1 vs 24 hrs.	Okamoto, Endo, Shirao, & Nagao, 2011	*
M. musculus	In vivo Ex vivo	Behavioral ∣ Hab. Molecular Morphology	Cerebellar cortex	0 vs 10 vs 20 vs 40 vs 60 min	Aziz et al., 2014	*
M. musculus	In vivo	Behavioral ∣ M.W.M. Pharmacology	N.A.	1 vs 10 min	Upchurch & Wehner, 1990	
M. musculus	In vivo Ex vivo	Behavioral ∣ M.W.M. Lesion	Neocortex	0 vs 90 min	Klapdor & Van Der Staay, 1998	
M. musculus	In vivo	Behavioral ∣ M.W.M. Genetic	N.A.	1 vs 30 min	Steckler, Weis, Sauvage, Mederer, & Holsboer, 1999	
M. musculus	In vivo	Behavioral ∣ M.W.M. Pharmacology	N.A.	0 min vs 3 weeks	Varvel, Anum, & Lichtman, 2005	
M. musculus	In vivo	Behavioral ∣ M.W.M. Electrophysiology Genetic	Hippocampus	1 vs 30 vs 240 min 1 vs 5 min	Zhang, Storm, & Wang, 2011	*
M. musculus	In vivo Ex vivo	Behavioral ∣ M.W.M. Behavioral Genetic Pharmacology	Hippocampus	0 vs 60 min 0 vs 10 vs 60 min	Nomoto et al., 2012	

M. musculus	*In vivo* *Ex vivo*	Behavioral | M.W.M. Molecular	Hippocampus Forebrain	20 min vs 24 hrs.	Stoneham et al., 2017	
R. norvegicus (Brown rat)	*In vitro*	Molecular Pharmacology	Hippocampus	0 vs 5 min	Taylor, Dieterich, Ito, Kim, & Schuman, 2010	*
R. norvegicus	*In vitro* *Ex vivo*	Molecular Pharmacology Morphology	Hippocampus	0 vs 10 min	Wu, Deisseroth, & Tsien, 2001	*
R. norvegicus	*Ex vivo*	Electrophysiology Molecular	Hippocampus	10 vs 20 vs 80 vs 300 vs 600 vs 1800 sec	Ajay & Bhalla, 2004	*
R. norvegicus	*Ex vivo*	Electrophysiology	Hippocampus	0 vs 5 vs 10 sec	Genoux, Bezerra, & Montgomery, 2011	*
R. norvegicus	*Ex vivo*	Electrophysiology Pharmacology	Hippocampus	2 vs 5 vs 10 vs 20 vs 60 min	Park et al., 2016	*
R. norvegicus	*Ex vivo*	Electrophysiology	Hippocampus	0 vs 30 vs 60 vs 90 vs 120 vs 240 min	Cao & Harris, 2014	*
R. norvegicus	*Ex vivo*	Electrophysiology Morphology	Hippocampus	10 vs 30 vs 60 vs 90	Kramár et al., 2012	*
R. norvegicus	*In vivo*	Electrophysiology	Commissural fibers	1 vs 24 hrs.	Froc & Racine, 2004	
R. norvegicus	*In vivo*	Behavioral | Av.C.	N.A.	3 vs 16 vs 60 sec	Fanselow & Tighe, 1988	
R. norvegicus	*In vivo*	Behavioral | Av.C.	N.A.	45 vs 900 sec	Yin, Barnet, & Miller, 1994	
R. norvegicus	*In vivo*	Behavioral | Av.C. Pharmacology	N.A.	1 vs 60 min	Vysotskii, Vysotskii, Gudasheva, Ostrovskaya, & Anokhin, 1999	
R. norvegicus	*In vivo* *Ex vivo*	Behavioral | Av.C. Genetic Molecular	Amygdala	3 sec vs 5 sec vs 10 sec vs 15 sec vs 2 min vs 8 min	Josselyn et al., 2001	*
R. norvegicus	*In vivo*	Behavioral | Av.C. Pharmacology	Insular cortex	2 vs 24 hrs.	Berman, Hazvi, Stehberg, Bahar, & Dudai, 2003	
R. norvegicus	*In vivo*	Behavioral | Av.C.		0 vs 80 min	Christianson, Misanin, Anderson, & Hinderliter, 2005	

R. norvegicus	*In vivo*	Behavioral | Av.C.	N.A.	4 min vs 24 hrs.	Li & Westbrook, 2008	
R. norvegicus	*In vivo* *Ex vivo*	Behavioral | Av.C. Molecular	Amygdala	0 vs 20 min	Perez-Villalba, Mackintosh, & Canales, 2008	
R. norvegicus	*In vivo*	Behavioral | Av.C.	N.A.	6 vs 120 vs 600 sec	Urcelay, Wheeler, & Miller, 2009	
R. norvegicus	*In vivo*	Behavioral | Av.C. Pharmacology	N.A.	10 min vs 24 hrs.	Abdel Baki, Schwab, Haber, Fenton, & Bergold, 2010	
R. norvegicus	*In vivo*	Behavioral | Av.C.	N.A.	45 sec vs 5 min	McConnell, Urushihara, & Miller, 2010	
R. norvegicus	*In vivo* *Ex vivo*	Behavioral | Av.C. Pharmacology Molecular	Basolateral amygdala	1 vs 6 vs 24 vs 168 hrs.	Jarome et al., 2012	
R. norvegicus	*In vivo*	Behavioral | Av.C.	N.A.	20 vs 800 sec	Miguez, Witnauer, Laborda, & Miller, 2014	
R. norvegicus	*In vivo*	Behavioral | Av.C. Pharmacology Molecular	Hippocampus	12 vs 122 vs 600 sec	Jiang, Mao, Zhou, et al., 2016	
R. norvegicus	*In vivo*	Behavioral | Av.C. Pharmacology Molecular	Hippocampus	0 vs 10 vs 30 min	Jiang, Mao, Tong, et al., 2016	
R. norvegicus	*In vivo* *Ex vivo*	Behavioral | Av.C. Molecular	Prefrontal cortex Amygdala	1 vs 7 days	Tapias-Espinosa, Kádár, & Segura-Torres, 2018	
R. norvegicus	*In vivo*	Behavioral | Ap.C.	N.A.	40 vs 960	Stout, Chang, & Miller, 2003	
R. norvegicus	*In vivo*	Behavioral | Ap.C.	N.A.	1 vs 4 vs 16 min	Sunsay, Stetson, & Bouton, 2004	
R. norvegicus	*In vivo*	Behavioral | Ap.C.	N.A.	1 vs 4 min	Moody, Sunsay, & Bouton, 2006	
R. norvegicus	*In vivo*	Behavioral | Ap.C.	N.A.	1 vs 2 vs 3 vs 4 vs 8 vs 16 vs 24 vs 32 min	Sunsay & Bouton, 2008	*
R. norvegicus	*In vivo*	Behavioral | Hab. Pharmacology	N.A.	12 vs 48 hrs.	Kesner & Cook, 1983	
R. norvegicus	*In vivo*	Behavioral | Hab. Lesion	Hippocampus	15 vs 30 sec	Mickley & Ferguson, 1989	

R. norvegicus	*In vivo*	Behavioral | Hab. Molecular	N.A.	30 min vs 24 hrs.	Masini, Day, & Campeau, 2008	
R. norvegicus	*In vivo*	Behavioral | O.C. Electrophysiology	Medial prefrontal cortex	0 vs 24 hrs.	Corbett, Laferriere, & Milner, 1982	
R. norvegicus	*In vivo*	Behavioral | O.C.	N.A.	5 vs 30 sec	Williams, 1992	
R. norvegicus	*In vivo*	Behavioral | O.C. Lesions	Hippocampus	0.5 vs 1 vs 8 min	Han, Gallagher, & Holland, 1998	
R. norvegicus	*In vivo*	Behavioral | O.C.	N.A.	2 vs 30 min	Wheeler & Miller, 2007	
R. norvegicus	*In vivo*	Behavioral Lesions Pharmacology	N.A.	0 vs 60 min	Goldstein & Davis, 1990	
R. norvegicus	*In vivo*	Behavioral | O.R.	N.A.	0 vs 60 min	Anderson, Jablonski, & Klimas, 2008	
R. norvegicus	*In vivo*	Behavioral | O.R.	N.A.	0 vs 24 hrs.	Bello-Medina, Sánchez-Carrasco, González-Ornelas, Jeffery, & Ramírez-Amaya, 2013	
R. norvegicus	*In vivo*	Behavioral | O.R. Pharmacology	Hippocampus	5 min vs 15 min vs 30 min vs 1 hr. vs 4 hrs. vs 7 hrs. vs 9 hrs. vs 24 hrs.	Tintorelli et al., 2020	*
R. norvegicus	*In vivo*	Behavioral | M.T. Lesions	Medial dorsal thalamus	30 sec vs 4 min	Hunt & Aggleton, 1991	
R. norvegicus	*In vivo*	Behavioral | M.T. Pharmacology	N.A.	1.5 min vs 24 hrs.	Meck & Williams, 1999	
R. norvegicus	*In vivo*	Behavioral | M.T.	N.A.	15 sec vs 10 min	Da Silva, Bast, & Morris, 2014	
R. norvegicus	*In vivo*	Behavioral | M.T.	N.A.	30 sec vs 30 min	Wingard, Goodman, Leong, & Packard, 2015	
R. norvegicus	*In vivo* *Ex vivo*	Behavioral | M.T. Molecular Pharmacology	Hippocampus Retrosplenial cortex	30 sec vs 10 min	Nonaka et al., 2017	
R. norvegicus	*In vivo*	Behavioral | M.W.M. Lesion	Nucleus basalis magnocellularis	0 vs 10 min	Mandel, Gage, & Thal, 1989	*
R. norvegicus	*In vivo*	Behavioral | M.W.M.	N.A.	2.5 vs 28 min	Rick, Murphy, Ivy, & Milgram, 1996	

R. norvegicus	*In vivo*	Behavioral | M.W.M.	N.A.	1 hr. vs 24 hrs.	Spreng, Rossier, & Schenk, 2002	*
R. norvegicus	*In vivo*	Behavioral | M.W.M. Pharmacology	N.A.	30 vs 120 sec	Zorrilla et al., 2002	
R. norvegicus	*In vivo* *Ex vivo*	Behavioral | M.W.M.	N.A.	30 sec vs 24 hrs.	Commins, Cunningham, Harvey, & Walsh, 2003	*
R. norvegicus	*In vivo*	Behavioral | M.W.M. Molecular	N.A.	1 vs 24 hrs.	Hoffman, Donato, & Robbins, 2004	
R. norvegicus	*In vivo* *Ex vivo*	Behavioral | M.W.M. Molecular	Hippocampus	0 vs 24 hrs.	Sisti, Glass, & Shors, 2007	
R. norvegicus	*In vivo* *Ex vivo*	Behavioral | M.W.M. Electrophysiology Pharmacology	Hippocampus	1 min vs 2 hrs.	Pandey, Sharma, & Sharma, 2015	*

Abbreviations: Ap.C., appetitive conditioning, Av.C., aversive conditioning, Hab., habituation, M.T., maze task, M.W.M., Morris water maze task, N.A., not applicable, O.C., operant conditioning, O.R., object recognition, W.R., withdrawal reflex. PubMed search terms: [spacing effect AND memory] OR [massed AND spaced] (Filters: Animals: other animals, Year: 1980 – 2020, Language: English), search conducted on 10 February 2020. References that did not contain an internal comparison of multiple interval lengths on memory performance were excluded. References with [September * are of particular interest. When behavioral analysis was performed in blocks of trials, the inter-block time was reported.

8

APPENDIX 2 | *IN VIVO* CALCIUM IMAGING OF
PREFRONTAL CIRCUITRY IN MICE

Illumination method	Mouse characteristics	Implant	Region and / or projections	Construct	Neuronal subtype	Behavioral manipulations	Reference
Two-photon	C57BL/6 (♂)	Microprism	mPFC	AAV2/1-hSyn-GCaMP3-WPRE-SV40	N.A.	N.A.	Low, Gu, & Tank, 2014
Two-photon	C57BL/6 (♂)	Optical cannula	mPFC mPFC—PVT mPFC—NAc	AAVdj-CaMKIIa-GCaMP6s Cav2-Cre & AAVdj-ef1α-DIO-GCaMP6s	N.A.	Appetitive conditioning	Otis et al., 2017
Two-photon	C57BL/6 (♀)	Microprism	mPFC	AAV2/1-hSyn-mRuby2-GSG-P2A-GCaMP6m-WPRE-SV40	N.A.	Operant conditioning	Reinert, Hübener, Bonhoeffer, & Goltstein, *in press*
Epifluorescence	CaMKIIa-Cre PV-Cre SST-Cre VIP-Cre	GRIN lens	PrL	AAV2/1-flex-GCaMP6f	Pyramidal PV-expressing SST-expressing VIP-expressing	Operant conditioning	Pinto & Dan, 2015
Epifluorescence	C57BL/6 (♂)	GRIN lens	mPFC	AAV2/5-hSyn-GCaMP6f	N.A.	Aversive conditioning	Kitamura et al., 2017
Epifluorescence	C57BL/6 (♂ & ♀)	GRIN lens	PrL—NAc	CAV-Cre & AAV2/5-CAG-Flex-GCaMP6f-WPRE-SV40	N.A.	Three chamber sociability test	Murugan et al., 2017
Epifluorescence	C57BL/6	GRIN lens	PrL	AAV2/1-CamKII-GCaMP6f-WPRE-SV40	Pyramidal	Three chamber sociability test	Liang et al., 2018
Epifluorescence	C57BL/6 (♂ & ♀)	GRIN lens	PrL	AAV2/1-Syn-FLEX-GCaMP6s	N.A.	Elevated plus maze exploration	Lee et al., 2019
Epifluorescence	CaMKII-GCaMP6	GRIN lens	ACC	N.A.	Pyramidal	Linear track exploration	Rubin et al., 2019
Epifluorescence	C57BL/6 (♂ & ♀)	GRIN lens	PrL	rAAV2-hSyn-GCaMP7f-wPRE	N.A.	Stress exposure, followed by elevated maze exploration	Marcus et al., 2020

Abbreviations: AAV, adeno-associated virus, C57BL/t, C57 black 6, CaMKII, Ca²⁺/calmodulin-dependent protein kinase II, GRIN, gradient-index, hSyn, human synapsin, mPFC, medial prefrontal cortex, N.A., not applicable, NAc, nucleus accumbens, PV, parvalbumin, PVT, paraventricular nucleus of the thalamus, SST, somatostatin, SV40, simian virus 40, VIP, vasoactive intestinal polypeptide, WPRE, Woodchuck hepatitis virus posttranscriptional regulatory element.

ABBREVIATIONS

a	*Aplysia californica*
AMPA	α-amino-3-hydroxy-5-methyl-4-isoxazole-propionic acid
d	*Drosophila melanogaster*
DBS	Deep brain stimulation
dmPFC	Dorsomedial prefrontal cortex
CaMKII	Ca^{2+}/calmodulin-dependent protein kinase II
cAMP	Cyclic adenosine monophosphate
CNMFe	Constrained nonnegative matrix factorization for endoscopic data
CREB1	cAMP response element binding protein 1
GECI	Genetically encoded calcium indicator
GEVI	Genetically encoded voltage indicator
GFP	Green fluorescent protein
GLM	Generalized linear model
h	*ex vivo* slice preparations of the rodent hippocampus
IEG	Immediate early gene
LTP	Long-term potentiation
m	*Mus musculus*
mPFC	Medial prefrontal cortex
NMDA	N-methyl-d-aspartic acid
MAPK	Mitogen-activated protein kinase
MEK	MAPK/ERK kinase
PKA	Protein kinase A
PP1	Protein phosphatase 1
tDCS	Transcranial direct current stimulation

The well-deserved admiration for such accomplishments would be considerably diminished were we aware of all the time and effort, patience and perseverance, trials, corrections, and even mishaps that worked hand in hand to produce the final success.

Santiago Ramón y Cajal | Advice for a young investigator (1897)

ACKNOWLEDGMENTS

LIST OF PUBLICATIONS

PUBLICATIONS INCLUDED IN THIS THESIS

Glas, A., Hübener, M., Bonhoeffer, T., & Goltstein, P. M. Spaced training enhances memory and prefrontal ensemble stability in mice. *bioRxiv* (2020) *(preprint)*.

Glas, A., Hübener, M., Bonhoeffer, T., & Goltstein, P. M. Benchmarking miniaturized microscopy against two-photon calcium imaging using single-cell orientation tuning in mouse visual cortex. *PLOS ONE* **14**, 1–18 (2019).

Goltstein, P. M.*, Reinert, S.*, **Glas, A.***, Bonhoeffer, T., & Hübener, M. Food and water restriction lead to differential learning behaviors in a head-fixed two-choice visual discrimination task for mice. *PLOS ONE* **13**, 1–19 (2018).

PUBLICATIONS NOT INCLUDED IN THIS THESIS

Glas, A. Join the Lone Kidney Club: Incentivising live organ donation. *Journal of Medical Ethics*, 1–5 (2020).

Riga, D.*, Matos, M. R.*, **Glas, A.**, Smit, A. B., Spijker, S., & Van den Oever, M. C. Optogenetic dissection of medial prefrontal cortex circuitry. *Frontiers in systems neuroscience* **8**, 1–19 (2014).

CHAPTER 2

Goltstein, P. M., Reinert, S.*, **Glas, A.***, Bonhoeffer, T., & Hübener, M. Food and water restriction lead to differential learning behaviors in a head-fixed two-choice visual discrimination task for mice. PLOS ONE **13**, 1–19 (2020).* Authors indicated with an * contributed equally to this work.

All listed authors contributed to this article: Pieter M. Goltstein, Sandra Reinert, Annet Glas, Tobias Bonhoeffer, and Mark Hübener. Funding for the study was acquired by Tobias Bonhoeffer and Mark Hübener. The study was designed by all authors. Data were acquired by Pieter M. Goltstein, Sandra Reinert, Annet Glas, and Mark Hübener. Data were analyzed by Pieter M. Goltstein. All authors drafted the manuscript, revised the manuscript, and approved the final version of the manuscript.

CHAPTER 3

***Glas, A.**, Hübener, M., Bonhoeffer, T., & Goltstein, P. M. Benchmarking miniaturized microscopy against two-photon calcium imaging using single-cell orientation tuning in mouse visual cortex. PLOS ONE **14**, 1–18 (2019).*

All listed authors contributed to this article: Annet Glas, Mark Hübener, Tobias Bonhoeffer, and Pieter M. Goltstein. Funding for the study was acquired by Tobias Bonhoeffer and Mark Hübener. The study was designed by all authors. Data were acquired by Annet Glas. Data were analyzed by Annet Glas and Pieter M. Goltstein. All authors drafted the manuscript, revised the manuscript, and approved the final version of the manuscript.

CHAPTER 4

***Glas, A.**, Hübener, M., Bonhoeffer, T., & Goltstein, P. M. Spaced training enhances memory and prefrontal ensemble stability in mice. bioRxiv (2020) (preprint).*

All authors designed the study. Annet Glas acquired the data. Annet Glas and Pieter M. Goltstein analyzed the data. Tobias Bonhoeffer and Mark Hübener acquired funding. Annet Glas, Mark Hübener, Tobias Bonhoeffer, and Pieter M. Goltstein wrote the manuscript.

SIGNATURES

Annet Glas
München, February 2021

Prof. Dr. Tobias Bonhoeffer
München, February 2021

Dr. Pieter M. Goltstein
München, February 2021

Sandra Reinert
München, February 2021